TLM

TECHNISCHE UNIVERSITÄT MÜNCHEN

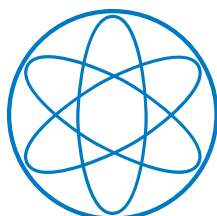# Physics Beyond the Standard Model at all Scales

DISSERTATION

by

TOBIAS THEIL

PHYSIK-DEPARTMENT T75, TUM

TUM

Technische Universität München

TUM School of Natural Sciences

Physics Beyond the Standard Model at all Scales

Tobias Theil

Physics Beyond the Standard Model at all Scales

Physik jenseits des Standardmodells bei allen Skalen

Tobias Theil

Abstract

The observation of phenomena not explainable by the Standard Model calls for new theories, extending our current understanding of Nature. Well motivated extensions populate vast energy ranges. In this thesis, we explore experiments at three benchmark scales and their potential to find or at least constrain new physics: In the first three parts we discuss the effects of physics beyond the Standard model at the LHC and future colliders, its contributions to the lepton and neutron electric dipole moments and finally potential deviations from Newton's law. In the last part, we present a method to efficiently calculate infrared divergences in high-loop amplitudes, which is useful for precision calculations for, among others, the experiments covered in this thesis.

Zusammenfassung

Die Beobachtung von Phänomenen, die nicht durch das bisherige Standardmodell erklärbar sind, verlangt nach neuen Theorien, die unser bisheriges Verständnis erweitern. Gut motivierte Erweiterungen des Standardmodells sagen neue Teilchen bei sämtlichen Energieskalen voraus. In dieser Dissertation untersuchen wir verschiedene Experimente an drei Benchmarkpunkten und ihr Potenzial, neue Physik zu entdecken oder zumindest einzuschränken: In den ersten drei Teilen analysieren wir die Effekte von neuer Physik am LHC und zukünftigen Beschleunigern, ihre Beiträge zu den elektrischen Dipolmomenten der Leptonen und des Neutrons und schließlich mögliche Abweichungen von Newtons Gravitationsgesetz. Im letzten Teil präsentieren wir eine Methode, mit der infrarote Divergenzen in Schleifendiagrammen effizient berechnet werden können, was von hohem Nutzen für Präzisionsrechnungen für die Experimente ist, die in dieser Dissertation betrachtet werden.

Contents

Introduction

The advent of the Standard Model of Particle Physics marks a major milestone in the evolution of modern particle physics. With a rather comprehensible particle content, the accuracy with which it can be used to describe the matter around us and its interactions through all but one of the fundamental forces is astounding. However, it can not explain all observations and this is already a sign of the fact that the Standard Model cannot be the final step in the pursuit of a theory capable of explaining all physical phenomena measurable. Finding this extension of the Standard Model suitable for this task is now the main challenge of particle physics.

In fact, despite the number of predictions of the Standard Model that have been confirmed experimentally — like the measurement of the magnetic dipole moment of the electron as the most accurate verification of such a prediction —, there is a seemingly equal number of problems left unsolved. One main class of these problems contains questions about the large separation between observed scales and the scale of gravity, also known as Hierarchy problems. The two most commonly known members are concerned with the mass of the Higgs boson and the non-zero Cosmological Constant. Neither of these quantities are protected by symmetries, contrary to, e.g., the mass of chiral fermions or the gauge bosons, such that quantum corrections should drive them to be as large as the cut-off of the theory. But this is not what is observed in experiments, and neither has a natural mechanism that protects the Higgs mass or the Cosmological Constant been found so far.

While plenty of proposed solutions for the Hierarchy problems, particularly considering the light Higgs mass, require new degrees of freedom with masses well beyond the weak scale, as in composite Higgs or supersymmetric models, there are further hints for physics beyond the Standard Model at scales below the weak scale. For instance, the Standard Model does not allow for an explanation for why the sector of strong interactions does not violate the combination of charge and parity symmetry, even an operator violating this symmetry can easily be included in the Lagrangian of the Standard Model. To answer this question, it was proposed that the coefficient of this symmetry violating operator is promoted to a dynamical field, the axion, [1–4] whose value dynamically relaxes to zero. Further, it is an irrefutable fact that the visible matter constitutes only a small fraction to the total matter in the universe. The majority is made up from yet unknown dark matter for which no viable candidate exists in the current version of the Standard Model and while theories of dark matter cover an immense mass range, there is also a significant amount that populates masses of around or below the weak scale.

All of this tells us that i) there is a lot of new physics left to discover and ii) new physics does not necessarily have to lie at scales beyond the reach of current experiments, but it could as well be hidden at much lower scales. We use this second insight as the guiding principle of this thesis and investigate how experiments at vastly different energy scales, both current and future ones, can be used to probe, find and at least constrain models of physics beyond the Standard Model: In Part I we explore the potential of the LHC and future colliders to constrain composite Higgs (CH) models through a potentially composite top quark as a representative for

a high-energy search. Next, we significantly reduce the energy in Part II down to the mass of the electron or the neutron, when we investigate the 1-loop effects of higher dimensional operators on their respective electric dipole moments. Even though, these scales are already considerably lower than the ones considered in I, reduce the energy even further, down to the classical, non-relativistic torsion balance experiments in Part III, where we try to probe the contributions of massive higher-spin degrees of freedom to the gravitational potential between two test masses. Finally, in Part IV we change gears and discuss how the energy-momentum tensor can be used as a tool to effectively extract infrared divergences at a priori arbitrarily high orders in massless theories. While this last part does not seem to fit the narrative of testing new physics at all scales, it is nonetheless highly important as it allows for higher-order and therefore more precise calculations used for all of the above experiments. Finally, we conclude in Part V and summarize our main results. We also give an outlook on still ongoing work, open questions and possible future directions.

We start Part I by briefly introducing the Hierarchy problem as well as potential solution in the form of framework of CH models in chapter 2. In this framework, the Higgs arises as a pseudo-Nambu Goldstone Boson (pNGB) associated to the breaking of some large approximate symmetry $G \to H$. This means that the Higgs has to obey an approximate shift symmetry, which in turn protects its mass from large quantum corrections and therefore it can be naturally lighter than the cut-off of the theory. Then, once the Higgs acquires a vacuum expectation value (VEV), the known breaking of the electroweak (EW) symmetry occurs, giving mass to the EW gauge bosons. However, the question on how fermions acquire mass remains open and we adopt the concept of partial compositeness, where the fermions couple linearly to some massive resonances in the new sector, with the mixing angle related to the measured mass or equivalently the Yukawa coupling of the respective fermion. Due to its large mass, this motivates us to assume that the top quark, in particular only its right-handed component, is fully composite. In practice, we will not be interested in the exact dynamics in the new sector, but instead we will take the route of using an effective theory to describe the new physics at energies below the masses of the new resonances. The corresponding power counting of the generated effective operators is presented in Sec. 2.3. Then, in chapter 3, we use the established power counting to identify the dominant operators in the limit of a fully composite right-handed top quark, finding that a dimension-6 operator built from four such quarks is greatly enhanced in the strong coupling regime. While it is not the only operator exhibiting such an enhancement, we find that its growth with energy can easily be exploited in four-top production at hadron colliders. Finally, we discuss the potential of future lepton colliders, where an alternative final state to the four tops has to be found, due to the limited scattering energies.

Then, in Part II we turn to the electric dipole moment (EDM) of the neutron as well as of the leptons and how new physics can contribute in a model-independent effective field theory (EFT) approach. We start by discussing the relevance of the EDMs of elementary particles in chapter 6 and how they arise both in the Standard Model (SM) and beyond. We discuss how flavor symmetries require that EDMs are generated at high loop orders in the SM and how higher dimensional operators can circumvent this. Further, we also explain how the EDM of composite objects can be obtained from those of their elementary constituents, focussing on the case of the neutron. Then in chapter 7, we review the basics of the renormalization of the couplings in a theory. This will be crucial, as the EDMs of the elementary particles can be identified with the Wilson coefficients of certain dimension-5 operators at low energies. In the same chapter, we also see how general helicity and angular momentum arguments can be used to determine the mixing pattern of higher-dimensional operators without any loop calculations, allowing us to reduce the amount of computation necessary. In chapter 8 we perform the full

1-loop calculation of the lepton and neutron EDMs in the dimension-6 Standard Model effective field theory (SMEFT). We discuss all the details of the computations, such as the transition from the gauge to the mass basis, Sec. 8.1, used calculation schemes, 8.2, and how to deal with gauge fixing and redundant operators, 8.3. Finally, we discuss the results in Sec. 8.5, focussing in particular on the effect of non-logarithmic terms compared to the logarithmic ones associated to the renormalization group (RG) running.

In Part III we address the possibility of new, massive higher-spin fields modifying the classical, non-relativistic interaction potential between two massive objects. We start by introducing both the massless and massive spinor helicity variables in chapter 11, which allow for a streamlined calculation of tree-level, on-shell scattering amplitudes, using only the information about the spin or helicity of the external particles, without the need of an Lagrangian and the associated Feynman rules. We then apply this formalism in chapter 12 to scattering amplitudes of four gravitons, computing the full amplitudes generated by an exchange of a particle with arbitrary spin S and mass m_S and we obtain the gravitational EFT upon integrating out these new degrees of freedom at energies $E < m_S$. We also discuss how the higher-spin fields can cure acausalities in the four graviton scattering in the presence of higher-dimensional operators modifying the triple-graviton coupling. Then, in chapter 13, assuming that the higher-spin fields couple directly to matter, we put constraints on these couplings and their masses using a classical torsion-balance experiment by modelling the test mass in the experiment as neutral, massive scalars and computing their non-relativist interaction potential induced by the exchange of the spin-S particle using the aforementioned spinor helicity methods.

Finally, in Part IV, we change topics completely and explore how the energy-momentum tensor can be used to extract the infrared divergences of high-loop amplitudes in massless theories using both modern on-shell techniques as well as the conventional Feynman diagrammatic approach. We start in chapter 16 by extending the concepts of renormalizing couplings, introduced in 7, to the renormalization of Green's functions and scattering amplitudes, obviously including the possibility of infrared divergences. We continue in the chapter 17, where we show explicitly how this renormalization of on-shell amplitudes can be obtained using the optical theorem and on-shell cuts of the renormalized amplitudes instead of the divergences in the bare amplitudes. In chapter 18, we show a physical reason for the appearance of infrared divergences in loop amplitudes, by requiring the cancellation of infrared divergences in total cross-sections or other observables. Then, in chapter 19, we come to the main point of this part and show that conserved currents, among which the energy-momentum tensor resides, do not show any UV renormalization, apart from a few, well understood and therefore easily extractable exceptions. Finally, we apply all this knowledge and formalism to two toy models, varying in complexity: In chapter 20 we consider a theory of a neutral scalar and a Dirac fermion, coupled to each other through a Yukawa-type interaction. For this theory, we show in detail both the on-shell and Feynman diagrammatic calculations. The second theory, discussed in 21, is a toy model for the SM, with its three gauge groups, a Higgs-like scalar and the first generation of quarks. We compute all the building blocks for infrared divergences in this model using only Feynman diagrams and we show how to apply the results by calculating the UV renormalization of the $U(1)$ gauge current.

This thesis is largely based on the following publications,

[5] G. Banelli, E. Salvioni, T. Theil and A. Weiler, *The Present and Future of Four Top Operators*, JHEP **02**, 043 (2021), [`arXiv:2010.05915`].

[6] J. Kley, T. Theil, E. Venturini, and A. Weiler, *Electric dipole moments at one-loop in the dimension-6 SMEFT*, Eur. Phys. J. C 82 (2022) 926, [`arXiv:2109.15085`].

preprint

[7] P. Baratella, S. Maggio, M. Stadlbauer, and T. Theil, *Two-Loop Infrared Renormalization with On-shell Methods*, [`arXiv:2207.08831`],

and work in progress

[8] E. Kaiser, J. Serra, T. Theil and A. Weiler, *Testing Massive Higher Spins with Torsion Balance Experiments*, in preparation.

[9] P. Baratella, M. Stadlbauer, T. Theil and A. Weiler, *The Energy-Momentum Tensor as a Tool for Higher Loop Renormalization*, in preparation.

In particular, some figures and tables contained in this thesis have previously appeared or will soon appear in one of these articles.

Part I

Four-Top Production as a High-Energy Probe of New Physics

Chapter 1

Motivation and Introduction

While the LHC fulfilled one of its main goals, the discovery of the Higgs boson [10, 11], this raised more questions than it actually answered. Out of these, the most important ones are concerned with the origin of the EW symmetry breaking and the smallness of the Higgs mass, both of which cannot be answered by the current SM.

Of course, there are a plethora of proposed answers, leaving it to experiments like the LHC or its successor to decide which one of those portrays Nature the best. One particularly prominent solution is the CH framework [12–14], where the Higgs arises as a composite pNGB of a new strong sector beyond the SM. One of its many appeals comes from the fact that within the CH framework it is straightforward to construct concrete theories just from the symmetry breaking pattern in the new sector, using the CCWZ construction [15,16] established by Callan, Coleman, Wess and Zumino. The minimal ansatz, given by the breaking pattern $SU(3) \to SU(2) \times U(1)$, satisfies the minimal conditions of generating four pNGBs as well as containing the EW part of the SM gauge group as its unbroken subgroup. However, experiments prefer theories where the new sector contains an additional $SO(4) \simeq SU(2) \times SU(2)$, the so-called "custodial symmetry", parts of which will be gauged to become the SM gauge group. This gauging, specifically the U(1) subgroup in one of the SU(2) factors, will then lightly break this symmetry. In fact, the Higgs sector of the SM approximately respects this custodial symmetry, weakly broken by the gauging of the $U(1)_Y$ subgroup, and it can be shown that this fixes the ρ parameter given by the ratio of the heavy gauge bosons masses [17]. Beyond the Higgs sector, the Yukawa interactions of the fermions with the Higgs, in particular the top quark, also explicitly break this custodial symmetry in the SM. Nevertheless, the SM value of this parameter has been confirmed experimentally up to per-mille precision, so any beyond the Standard Model (BSM) models face tight constraints coming from this measurement. Imposing the condition of preserving the custodial symmetry leaves a single choice for a minimal, realistic CH model, $SO(5) \to SO(4)$ [18].

Independent of the precise implementation, all CH models have in common that they, in addition to turning the Higgs into a composite state, generate many more new states. These are heavy resonances similar to the hadrons in low-energy QCD, with masses around the breaking scale in the new sector. Further, for non-minimal models, the symmetry breaking generates more than the four Goldstone modes needed to form the Higgs doublet, which can serve as dark matter candidates [19–22]. These new states can drastically change the phenomenology of experiments like colliders, once they reach energies high enough to produce any of the new particles. While we can expect the heavy resonances to appear beyond the TeV threshold, see e.g., [23, 24] for constraints on colored top partners, their effect on observables can still be captured by employing the EFT language.

In this part of the thesis, we focus on how, in an EFT setting, these new resonances can

impact the top sector of the SM. Being the most massive particle in the SM, the top quark enjoys the strongest coupling to the Higgs, which in turn makes it a natural guess to assume that it also couples more strongly to the new sector than any other particle. In fact, due to their coupling to the strong sector, the fermions can be seen as at least partially composite states [25], with the degree of compositeness being tightly related to the size of their coupling to the Higgs. One can go even further and assign potentially different degrees of compositeness to the chiral components of each fermion individually. They can, however, not be unrelated because the product of the two is fixed by the respective Yukawa coupling, forming a kind of seesaw. Because the left-handed top quark will always be in a non-trivial representation of the new group, it is charged under the EW gauge group of the SM after all, it will always contribute to the Higgs potential and therefore the Higgs mass, where the size of its contribution is controlled by its degree of compositeness [26]. The right-handed top, on the other hand, is already a singlet under the electroweak SM and by choosing it to be also a singlet in the full new sector, one can make its contribution to the Higgs potential to vanish, independent of its degree of compositeness [26]. For this reason, it is highly motivated to consider the limit in which we take the right-handed top quark to be fully composite, leaving the left-handed component with the smallest degree of compositeness possible [26, 27].

We will see, using power counting arguments, that in this limit operators with four right-handed tops can be as parametrically large as ones containing only Higgs fields. In turn, these operators can be tested at current and future colliders, both of the hadronic and leptonic kind, through four top and top quark pair production. We then find that, especially at future colliders, probing top quark production can provide competitive if not superior constraints on CH models compared to precision tests in the Higgs sector itself.

We will start this part of the thesis with an introduction to CH models and how they can give rise to partially composite fermions in chapter 2. In the same chapter, we will also establish the power counting we need to assess the parametric size of various operators appearing in the EFT, such that we can focus on the leading ones. Using this, we will turn to the collider phenomenology in chapter 3, where we will investigate the impact of the leading effective operators both at current and future hadron colliders as well as future lepton colliders.

Chapter 3 is heavily based on [5], from where all figures, tables, and parts of the text have been taken.

Chapter 2

Composite Higgs and Partial Compositeness

In this chapter, we set up the theoretical framework needed for the rest of this chapter. First, we introduce the EW hierarchy problem in Sec. 2.1. Afterward, we introduce one of its most popular solutions, the Composite Higgs framework in Sec. 2.2, where we also discuss how other fields can be made composite in such theories. In the end, we will not use any specific implementation of a CH model, so we will refrain from going into too many details of certain symmetry breaking patterns. We then conclude this chapter by outlining the power counting estimates for strongly coupled theories in Sec. 2.3, which we can use to classify the effective operators generated upon integrating out the heavy resonances in the model.

2.1 The Hierarchy Problem

Discussions about the Higgs hierarchy problem, first formulated in [28–30], are among the most present and controversial topics within high-energy physics. To state the main points and why it is a problem, we will follow [14], for a more recent take on the topic see e.g., [31, 32].

Even though the SM is highly successful in predicting most of the phenomena in Nature, we know that it can only be the EFT of some underlying and more fundamental theory. This fact will be the basis for setting up the hierarchy problem. We even know the latest point at which the SM has to yield in favor of this new theory because of gravity. The current field-theoretical description of gravity is a non-renormalizable theory of a massless spin-2 field, the graviton. This theory can be written as an infinite series of higher and higher dimensional operators, whose size is controlled by the Planck mass M_P. At energies far below this scale, the gravitational operators are highly suppressed compared to the renormalizable part of the SM, however once we reach $E \sim M_\mathrm{P}$ they become effectively strongly coupled, signalling the need for a UV completion that can cure this growth. Of course, it does not have to be that the SM is UV completed only at the Planck scale, there can be one or more intermediate scales at which it is replaced by a new theory.

Nevertheless, at the scales that are currently accessible by experiments, we can therefore write the SM Lagrangian as a series expansion of operators[1]

---

[1]Technically, we could also include a $d = 0$ term, corresponding to the cosmological constant, which comes with a hierarchy problem of its own. However, it is not relevant for the current discussion.

$$\mathcal{L} = \mathcal{L}_{d=2} + \mathcal{L}_{d=4} + \sum_{d>4} \sum_i c_i^{(d)} \frac{O_i^{(d)}}{\Lambda_{\text{SM}}^{d-4}}, \tag{2.1}$$

where d is the mass dimension of the corresponding operator, $c_i^{(d)}$ are constant coefficients and the scale of new physics Λ_{SM} suppressing the higher dimensional operators is necessary purely from dimensional analysis.

The $d = 4$ part of the above Lagrangian is already enough to ensure the aforementioned success of the Standard Model. But the higher dimensional operators can make our description of Nature even more successful. A prime example is given by the neutrino masses, about which experiments tell us that they have to be non-vanishing. If we do not enlarge our field content to accommodate right-handed neutrinos, the only possibility to generate masses is given by the $d = 5$ Weinberg operator,

$$O_\nu^{(5)} = (\bar{L}_L H^c)(L^c H^c), \tag{2.2}$$

with $L^{(c)}$ the (charge conjugate) lepton doublet, H the Higgs doublet and $H^c = i\sigma^2 H^*$. Note, that this operator breaks the lepton symmetry, which is only accidental in the $d = 4$ part of the Lagrangian. In fact, within EFTs it is common for higher dimensional operators to break accidental symmetries respected by the lower dimensional ones. If we assume its coefficient to be of order one, the right size of the neutrino masses can be achieved by setting $\Lambda_{\text{SM}} \sim 10^{14}$ GeV. This immensely large scale suppressing makes it obvious why using only the $d = 4$ part of the Lagrangian is already enough to give predictions that are highly compatible with the current experimental findings, higher order corrections are just too small to observe at low scales. It is interesting to note that for $d = 6$ also the accidental baryon symmetry is broken, rendering proton decay possible, which has yet to be observed. Plugging in the numbers, one finds bounds on Λ_{SM} that are similar in size as the ones we get from neutrino masses, both of which are numerically in the same range as the scale at which a Grand Unified Theory (GUT) is expected to set in, $M_{\text{GUT}} \sim 10^{15}$ GeV. So far, we did concern ourselves with operators with $d > 2$, which are, however, unfazed by the hierarchy problem. The crucial piece is the single $d = 2$ operator we can have in the SM, the Higgs mass term

$$\mathcal{L}_{d=2} = c\, \Lambda_{\text{SM}}^2 |H|^2. \tag{2.3}$$

Since it is a relevant operator, we know its coefficient has to carry a positive mass dimension, which the same scale Λ_{SM} that suppresses the $d > 4$ part takes care of. Consequently, if this scale is large, the Higgs mass term is highly enhanced instead of suppressed. But because we know the Higgs mass from experiments, we know that $\mu^2 \equiv m_H^2/2 = (89 GeV)^2$ and so

$$c = \frac{\mu^2}{\Lambda_{\text{SM}}^2} \sim 10^{-28} \ll 1 \tag{2.4}$$

needs to be highly tuned, which seems very unnatural. In fact, the separation of scales we see lies at the heart of the hierarchy problem. But we can make the notion of naturalness more concrete. If we assume we know the fundamental theory beyond Λ_{SM}, which is valid up to arbitrarily high energies, the Higgs mass is calculable in terms of the parameters $\{p_i\}$ of this fundamental theory, which we can write as [14]

$$m_H^2 = \int_0^\infty dE\, \frac{dm_H^2}{dE}(E; \{p_i\}). \tag{2.5}$$

The integral simply sums up all the contributions to the Higgs mass at various scales. Naturally, we can split it into two contributions, the ones coming from within the SM and the ones from beyond. These two regimes are, by construction, separated by the scale Λ_{SM} and we can calculate the low-energy contribution because we know the SM,

$$m_H^2 = \int_0^{\sim\Lambda_{\text{SM}}} dE \, \frac{dm_H^2}{dE}(E; \{p_i\}) + \int_{\sim\Lambda_{\text{SM}}}^{\infty} dE \, \frac{dm_H^2}{dE}(E; \{p_i\})$$
$$\equiv m_H^2(\delta_{\text{SM}} + \delta_{\text{BSM}}). \tag{2.6}$$

Approximating the low-energy regime using the 1-loop contributions from the top quark and the gauge bosons as well as the Higgs self-interaction, we have [14]

$$m_H^2 \delta_{\text{SM}} = \Lambda_{\text{SM}}^2 \left[\frac{3y_t^2}{8\pi^2} - \frac{3g_W^2}{32\pi^2} \left(1 + \frac{1}{2\cos^2(\theta_W)} \right) - \frac{3\lambda}{8\pi^2} \right]. \tag{2.7}$$

Of course, if we look only at the SM isolated, the above expression mimics the calculation of the quadratic divergences of the respective loop integrals using cut-off regularization. As usual, divergences of this kind are unphysical and have to be subtracted using the appropriate renormalization scheme[2]. However, in the light of calculating the Higgs mass from some UV complete theory, this expression makes sense as a low-energy approximation. Note that, as Eq. (2.3) already suggested, the Higgs mass within the SM is quadratically sensitive to the scale at which new physics sets in. In the end, to get a mass $m_H \ll \Lambda_{\text{SM}}$, as suggested by experiment, the contributions from the theory beyond the SM, δ_{BSM}, has to be tuned in such a way that it cancels the low-energy contribution up to a tiny fraction, and we can, in fact, quantify this tuning by

$$\Delta \geq \frac{\delta_{\text{SM}} m_H^2}{m_H^2} \simeq \left(\frac{\Lambda_{\text{SM}}}{500\,\text{GeV}} \right)^2. \tag{2.8}$$

We want to conclude this section, by stating that there is of course nothing fundamentally wrong with theories that show high degrees of fine-tuning and the solution to the hierarchy problem comes down to just anthropic selection. However, so far, more often than not, it has been the case that Nature tends to be natural and fine-tuning is cured by some underlying principle we have yet to understand. For this reason, it is worthwhile to investigate models that can solve the hierarchy problem without the need for fine-tuning.

2.2 Composite Higgs

The basic idea behind a composite Higgs is, as its name suggests, that the Higgs is not a point-like, elementary particle but instead a bound object of some sorts [33–38]. In practice, this could mean that the Higgs originates from a new strong sector that confines at some scale m_*, in the same way as protons and other hadrons are formed by the confining of QCD at low energies. This can help shield the Higgs mass against large UV effects, by having the picture in mind that the Higgs dissolves into its constituents if probed with energies $E > m_*$, similar to protons deconfining into quarks at energies above the QCD scale. This section loosely follows [14], for further introductory literature and more recent reviews see e.g., [12, 13, 39].

---

[2]In dimensional regularization they do not even appear as quadratic divergences.

2.2.1 The Composite Higgs Framework

To collect all the ingredients that make up a valid CH model, we will make extensive use of analogies to QCD, as we will discover many similarities between the two seemingly unrelated theories.

Obviously, to have composite states, we need some sector that is sufficiently strongly coupled for these states to form in the first place. This composite sector is generated by some new, fundamental theory at a high scale Λ, the concrete definition of which will not matter, after all, the whole point is to desensitize the Higgs mass regarding the UV. The only thing we require is that it generates the composite sector close to a fixed point of its RG running, with no operators with scaling dimension much less than 4. Of course, at tree level, operators with scaling dimension of exactly 4 are marginal and stay at the fixed point indefinitely, but quantum effects will change this by generating an anomalous dimension turning the former marginal coupling into either a relevant or irrelevant one. For marginally relevant operators close to the fixed point, this slight shift of scaling dimension will lead to a logarithmic growth of the coupling g. At some scale, this coupling will formally diverge, signalling the onset of confinement. In fact, the confinement scale m_* can be calculated using

$$m_* = \Lambda \exp\left(-\frac{8\pi^2}{-b_0\, g^2(\Lambda)}\right), \tag{2.9}$$

with $b_0 < 0$ the coefficient of the beta function for the marginally relevant coupling. From this equation, it is obvious that an exponential hierarchy between the UV and the confinement scale can easily be achieved, depending on how close to the fixed point the evolution starts.

Now, if the Higgs would be just any of the composite states, we would naturally expect its mass to be $m_H \sim m_*$. However, we know from experiments that m_* has to sit well beyond the TeV scale. Otherwise, we would have either seen many other resonances of mass m_* directly or they would induce effective operators of sizes that are incompatible with precision measurements. Having such a large confinement scale would reintroduce the problem of a finely tuned Higgs mass.

Luckily, there is a way to keep the setup of a confining sector from a fundamental theory, while still having naturally light scalars; they originate as pNGBs of some spontaneously broken symmetry. But it is not enough to just add a symmetry that is only spontaneously broken; in the broken sector, there will be an exact shift symmetry, making it impossible to generate a potential for the Goldstone modes, keeping them exactly massless. On the other hand, if there is an explicit breaking of the symmetry in the first place, a potential can be generated, leading to mass, whose size is controlled by how severely the symmetry was broken. In practice, the explicit breaking comes from the coupling to an elementary sector, that contains all the SM fields apart from the Higgs and possibly, this is the main point of this part, the right-handed top quark. An additional source of explicit breaking is provided by the gauging of only the $\text{SU}(2) \times \text{U}(1)$ part of the unbroken subgroup H.

To be a bit more concrete, let us assume the new sector respects some symmetry G that, after confining, gets spontaneously broken down to some subgroup H. As mentioned in the introduction, to be phenomenologically viable, the EW gauge group has to be contained in the unbroken group, $H \subseteq \text{SU}(2) \times \text{U}(1)$. Further, to supply at least the four components of the Higgs doublet, there need to be at least four broken generators in the coset G/H. In the following, we will denote the generators of G with T^A, the unbroken ones that span H with T^a and the broken ones in the coset with $T^{\hat{a}}$. Then, we can parametrize the Goldstone modes $\theta^{\hat{a}}$ as fluctuations around some reference vacuum $\boldsymbol{F}$, defined to be orthogonal to the space of H,
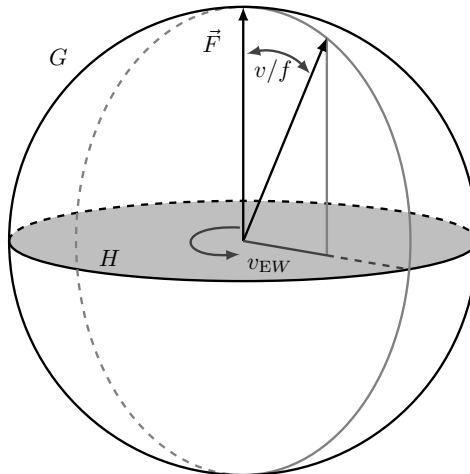
Figure 2.1: Pictorial illustration of the vacuum misalignment mechanism for the breaking pattern SO(3) $\rightarrow$ SO(2). Here $\boldsymbol{F}$ describes the vacuum configuration without any explicit breaking ($\langle\theta\rangle = 0$). $\langle\theta\rangle$ is the pNGB VEV from the explicit breaking characterizing the vacuum misalignment and v is its projection on the subgroup H, corresponding to the EW scale in the SM.

$$\phi(x) = \exp\left[i\theta^{\hat{a}}(x)T^{\hat{a}}\right]\boldsymbol{F}. \tag{2.10}$$

Eventually, we want the Goldstones to acquire a VEV to trigger electroweak symmetry breaking (EWSB). But, if G is exact, there will be no EWSB, since the VEV of the Goldstones are unphysical and can even be set to zero with an appropriate G transformation, using the broken generators, to be more precise. Instead, breaking G is equivalent to choosing a preferred direction in G, which cannot be rotated away by an exact symmetry. This induces a misalignment between the vacuum of the explicitly broken theory, compared to the reference $\boldsymbol{F}$, the angle of which is exactly given by the VEV of the Goldstones, $\langle\theta\rangle$. This angle sets the EWSB scale, which controls the size of the EW breaking effects via

$$v = f\sin(\langle\theta\rangle), \quad f = |\boldsymbol{F}|. \tag{2.11}$$

To obtain a light Higgs, we therefore want $v \ll f$ or equivalently $\sin(\langle\theta\rangle) \ll 1$ and we can parametrize the hierarchy between the two breaking scales as

$$\xi = \left(\frac{v}{f}\right)^2 \ll 1. \tag{2.12}$$

In Fig. 2.1 we show an graphical representation of this vacuum misalignment mechanism for the simple case of the breaking pattern SO(3) $\rightarrow$ SO(2).

2.2.2 Partial compositeness

Until now, we have only considered the composite sector and how the Higgs can arise from it through the spontaneous breaking of an (approximate) global symmetry. This breaking then gives mass to the EW gauge bosons and also produces a massive scalar boson, which we can identify with the SM Higgs boson. It remains, however, the question of how the fermions acquire

their mass. There are various approaches to this, e.g., technicolor models (see [29, 30, 40–42]) or partial compositeness. We will consider the latter here.

In this case, the fermions originating from the elementary sector couple linearly to fermionic, composite resonances from the strong sector [27]

$$\Delta\mathcal{L} = y_L f \bar{q}_L^{\text{el}} \mathcal{P}_q[Q_R] + y_R f \bar{t}_R^{\text{el}} \mathcal{P}_t[T_L] + M_Q \bar{Q}_L Q_R + M_T \bar{T}_R T_L + g_\rho \bar{Q}_L \theta T_R, \tag{2.13}$$

where f denotes the Goldstone decay constant, $Q_{L/R}$ and $T_{L/R}$ are fermionic, composite resonances and $\mathcal{P}_{q/t}$ some projector operators to extract the components of the BSM resonances, such that they can couple to the elementary doublet q_L and singlet t_R. It is obvious that these BSM components have to have the same quantum numbers as the elementary fermions to ensure gauge invariance for the interactions in Eq. (2.13). Here we assumed that the elementary sector couples only to the lowest lying resonances of the strong sector and that the couplings to heavier resonances can be neglected. The last term, the coupling of the heavy resonances to the Goldstone matrix θ with coupling strength g_ρ, will become important once EWSB sets in [27], but for now, we will consider only the bilinear terms.

Diagonalizing these, we get two states that are massless before EWSB,

$$q_L = \cos\theta_L q_L^{\text{el}} + \sin\theta_L \mathcal{P}_q[Q_L], \tag{2.14}$$

$$t_R = \cos\theta_R t_R^{\text{el}} + \sin\theta_R \mathcal{P}_t[T_R], \tag{2.15}$$

which can be identified as the SM fermions, with mixing angles

$$\tan\theta_L = \frac{y_L f}{M_Q}, \tag{2.16}$$

$$\tan\theta_R = \frac{y_R f}{M_T}. \tag{2.17}$$

Additionally, we get states orthogonal to the ones in equations (2.14)-(2.15) with a mass squared $M_Q^2 + y_L^2 f^2$ and $M_T^2 + y_R^2 f^2$, respectively, but these are unimportant for the following discussion.

From equations Eqs. (2.14)-(2.15) we see that the SM fermions are a mixture of the elementary fermions and the composite resonances of the strong sector, which is why they are called *partially composite*. To give them their measured masses after EWSB the last operator in equation (2.13) comes into play. Comparing it with equations (2.14) and (2.15) we see that it is built exactly from the composite components of the SM fermions. Following this line of thought, it is easy to see, that this operator induces the usual Yukawa couplings of the SM states to the Goldstone matrix with coupling strength

$$y = g_\rho \sin\theta_L \sin\theta_R, \tag{2.18}$$

as is illustrated in figure 2.2. Requiring that after θ acquires a non-zero VEV the top mass coincides with the measured value gives constraints on the mixing angles $\sin\theta_{L/R} \gtrsim 0.6/g_\rho$ [27].

The relation in (2.18) makes it clear why the top quark is considered as a mostly composite fermion, as for $y_t \sim \mathcal{O}(1)$ the mixing angles for both chiralities cannot be too small. However, due to the electroweak symmetry that the mixing angles for the left-handed bottom and top quark are forced to be equal, i.e.,

$$\theta_{L,b} = \theta_{L,t}.$$

So, naturally, increasing both mixing angles would also imply a large mixing for the bottom quark which in turn would lead to large corrections to the very precisely known $Z\bar{b}b$ vertex, see
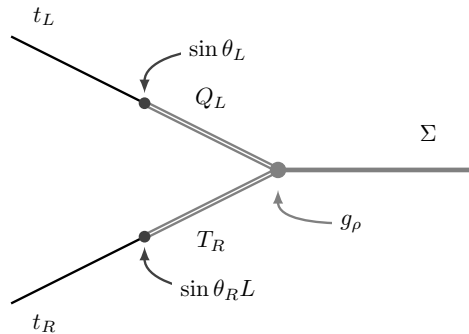
Figure 2.2: Schematic depiction of how the SM Yukawa couplings arise through the elementary-composite mixing of the SM fermions described in the text

e.g., [43]. To circumvent this problem one can then go to the limit, where the top quark is fully composite, i.e., $\sin(\theta_{R,t}) \sim \mathcal{O}(1)$[3]. Another, maybe more robust, argument for considering a fully composite right-handed top is that, assuming it is a singlet under the group G of the new sector, it reduces the amount of fine-tuning needed for the Higgs potential and correspondingly its mass [14, 26]. If the right-handed top quark is to be taken as a singlet, the quadratic Higgs potential can be written as, neglecting subleading gauge boson loops, [14]

$$V(H) \sim \frac{\sin^2 \theta_{L,t}}{16\pi^2} |H|^2. \tag{2.19}$$

While this cannot be made to vanish, numerically it turns out that it is favored for this potential to reach its minimal value. If, on the other hand, t_R does transform non-trivially under G, both chiralities contribute to the above potential, where the leading effect obviously comes from the chirality with the higher degree of compositeness.

To conclude this section, we want to comment briefly on the partial compositeness of other SM states. Previously, we have only considered the possibility that linear couplings between elementary and composite fermions give rise to their respective compositeness. But in fact the same can happen for the gauge bosons. It can be shown that mass mixing terms between the elementary gauge boson and vector resonances of the strong sector respect the SM gauge symmetry, including color [43]. Therefore, after diagonalizing also the gauge part of the Lagrangian, one obtains two linear combinations of gauge and composite bosons, one of which is massless before EWSB, corresponding to the SM gauge boson, and one heavy degree of freedom.

2.3 Power Counting and Effective Operators

In the end, we won't be interested in the precise dynamics of the resonances themselves. Instead, we will use the assumptions that the energies we work at are below the confinement scale, $E < m_*$, so it is vald to work with an EFT built from only SM states. To not having to deal with all effective operators simultaneously, it is nice to have some way of estimating their parametric size. Of course, these estimates cannot always be taken at face value, depending on the observable, operators that are formally subleading can still be more sensitive than leading ones because of the varying experimental precision in the respective processes. Nevertheless, it will be a good guideline.

---

[3]At tree level, this vertex can be protected by a discrete symmetry. However, it is broken at the loop level, which again favors a minimal $\theta_{L,t}$ [27]

The key point to finding such estimates is the assumption that the composite sector can be effectively described by one scale m_* and one coupling g_*, which characterize the typical mass of the composite resonances and coupling strength among them, respectively. Under these assumptions, the Lagrangian can be written as [14, 26]

$$\mathcal{L} = \frac{m_*^4}{g_*^2} \hat{\mathcal{L}} \left[\frac{\partial}{m_*}, \frac{g_* \theta}{m_*} \right], \tag{2.20}$$

with the Goldstone field θ. Of course, there will also be heavy resonances, but they are not relevant here, as they are integrated out in the end.

To be able to use dimensional analysis, we temporarily reintroduce the Planck constant $\hbar$ and the speed of light c.

We know that the action has units of $E \cdot T$, the same as $\hbar$, hence it follows for the Lagrangian

$$[\mathcal{L}] = ET/L^4 = [\hbar]/L^4. \tag{2.21}$$

For canonically normalized bosonic and fermionic fields we can thus derive their dimensions by looking at their kinetic terms (keeping in mind that $[\partial_\mu] = 1/L$) and we find

$$[\theta] = [\hbar]^{1/2}/L \tag{2.22}$$

Now, by looking at terms in Eq. (2.20), we see that

$$[m_*] = L^{-1} \quad \text{and} \quad [g_*] = [\hbar]^{-1/2}. \tag{2.23}$$

Because we know that the symmetry breaking scale f normalizes the Goldstone fields we know $[f] = [\theta]$ and putting together the above relations, dimensional analysis tells us that

$$m_* = g_* f. \tag{2.24}$$

Next, we also need the dimensionality of the elementary fields. Starting with the gauge fields, we notice that they couple to the composite sector through the composite gauge currents J_μ, $g A_\mu J^\mu$. From Noether's theorem, we know that

$$[J] = [\mathcal{L}] \cdot L = [\hbar]/L^3. \tag{2.25}$$

Therefore, given $[A] = [\hbar]^{1/2}/L$, we find that

$$[g] = [\hbar] \quad \text{or} \quad [g \cdot A] = 1/L. \tag{2.26}$$

Finally, we need the dimensions of elementary fermions. For this, we recall the partial compositeness hypothesis, stating that the physical fermions are a mixture of elementary and composite states, characterized by a mixing parameter $\lambda_{L,R} \equiv \sin \theta_{L,R}$ for each of the fermion chiralities. Hence, SM sector fermions have the same dimension as the composite ones, they are, however, accompanied by their respective mixing parameter. So, by introducing the appropriate powers to make each fermion insertion dimensionless, we find

$$\mathcal{L} = \frac{m_*^4}{g_*^2} \hat{\mathcal{L}} \left[\frac{\partial}{m_*}, \frac{g_* \Pi}{m_*}, \frac{g \cdot A_\mu}{m_*}, \lambda_{L,R} \frac{g_* \psi_{L,R}}{m_*^{3/2}} \right], \tag{2.27}$$

The generalization to loop level effects is straightforward.

In the next chapter, we will use this power counting to classify the operators relevant for the phenomenology of composite top quarks at current and future colliders.

Chapter 3

Composite Top Quarks at Colliders

In this chapter, we investigate the implications of a strongly coupled right-handed top quark for the phenomenology at current and future colliders. Because of the power counting arguments given in Sec. 2.3 we expect the operator

$$\frac{c_{tt}}{\Lambda^2}(\bar{t}_R\gamma_\mu t_R)(\bar{t}_R\gamma_\mu t_R) \tag{3.1}$$

to be among the leading ones, with its coefficient scaling like

$$\frac{c_{tt}}{\Lambda^2} \sim \frac{g_*^2}{m_*^2} \equiv \frac{1}{f^2}, \tag{3.2}$$

where we reintroduced the symmetry breaking scale f. Moreover, it induces top scattering with an amplitude of the form

$$|A(t_R t_R \to t_R t_R)| \sim \frac{g_*^4}{m_*^4}(s - 2m_t^2)^2, \tag{3.3}$$

which grows like $s^2 \sim E^4$ at large energies, leading to an enhanced sensitivity compared to the rare SM production [27]. Because of this energy growth, together with its scaling with g_* the main focus of this chapter will be on O_{tt}.

We will start this chapter with introducing the set of effective operators considered in this part, together with their respective power counting estimates, in section Sec. 3.1. We will see that, even though some of them show formally subleading power counting estimates, their different scaling allows them to probe parts of the parameter space the operator O_{tt} cannot reach. Then, in Sec. 3.2 we review the current experimental constraints on the various operators and discuss if these operators are able to explain some of the mild excesses found in the recent $tttt$ and the associated background measurements. Afterward, we will explore the reach achievable at future hadron colliders through $tttt$ production in Sec. 3.3 and top quark pair production at lepton colliders in Sec. 3.4. In the former case, we give a detailed analysis of some multilepton final states, and we also comment on the opportunities and challenges of a fully hadronic decay of the top quarks. We will find that at both future hadron and lepton colliders, this provides a superior probe of CH models with fully composite right-handed top quarks. In fact, future colliders can test, through the top quark, fine-tunings of the electroweak scale at the $\xi \approx 10^{-3}$ level, a hundred-fold that of the LHC and certainly unprecedented in the realm of particle physics. This is a truly exceptional motivation for future discoveries that could await us at the high-energy frontier.

$$O_{tt} = (\bar{t}_R \gamma_\mu t_R)^2$$

$$O_{tq} = (\bar{t}_R \gamma_\mu t_R)(\bar{q}_L \gamma^\mu q_L)$$
$$O_{tq}^{(8)} = (\bar{t}_R \gamma_\mu t^A t_R)(\bar{q}_L \gamma^\mu t^A q_L)$$
$$O_{qq} = (\bar{q}_L \gamma_\mu q_L)^2$$
$$O_{qq}^{(8)} = (\bar{q}_L \gamma_\mu t^A q_L)^2$$

$$O_{Ht} = i(H^\dagger \overset{\leftrightarrow}{D}_\mu H)(\bar{t}_R \gamma^\mu t_R)$$
$$O_{Hq} = i(H^\dagger \overset{\leftrightarrow}{D}_\mu H)(\bar{q}_L \gamma^\mu q_L)$$
$$O_{Hq}^{(3)} = i(H^\dagger \sigma^a \overset{\leftrightarrow}{D}_\mu H)(\bar{q}_L \gamma^\mu \sigma^a q_L)$$
$$O_{y_t} = y_t H^\dagger H \bar{q}_L \widetilde{H} t_R$$

$$O_{tD} = (\partial^\mu B_{\mu\nu})(\bar{t}_R \gamma^\nu t_R)$$
$$O_{tD}^{(8)} = (D^\mu G_{\mu\nu}^A)(\bar{t}_R \gamma^\nu t^A t_R)$$
$$O_{qD} = (\partial^\mu B_{\mu\nu})(\bar{q}_L \gamma^\nu q_L)$$
$$O_{qD}^{(8)} = (D^\mu G_{\mu\nu}^A)(\bar{q}_L \gamma^\nu t^A q_L)$$
$$O_{qD}^{(3)} = (D^\mu W_{\mu\nu}^a)(\bar{q}_L \gamma^\nu \sigma^a q_L)$$

$$O_H = \tfrac{1}{2}(\partial_\mu |H|^2)^2$$
$$O_T = \tfrac{1}{2}(H^\dagger \overset{\leftrightarrow}{D}_\mu H)^2$$
$$O_W = ig \tfrac{1}{2}(H^\dagger \sigma^a \overset{\leftrightarrow}{D}_\mu H) D_\nu W^{a\,\mu\nu}$$
$$O_B = ig' \tfrac{1}{2}(H^\dagger \overset{\leftrightarrow}{D}_\mu H) \partial_\nu B^{\mu\nu}$$
$$O_{2G} = -\tfrac{1}{2}(D^\mu G_{\mu\nu}^A)^2$$
$$O_{2W} = -\tfrac{1}{2}(D^\mu W_{\mu\nu}^a)^2$$
$$O_{2B} = -\tfrac{1}{2}(\partial^\mu B_{\mu\nu})^2$$

$$\widetilde{O}_\gamma = H^\dagger H B^{\mu\nu} \widetilde{B}_{\mu\nu}$$

Table 3.1: Set of dimension-six operators relevant to this part of the thesis, grouped in five different boxes corresponding to the different classes discussed in the main text. Dashed lines within a box separate operators in a given class with a different power counting estimate. We have defined $H^\dagger(\sigma^a)\overset{\leftrightarrow}{D}_\mu H = H^\dagger(\sigma^a)D_\mu H - (D_\mu H)^\dagger(\sigma^a)H$ and $\widetilde{H} = i\sigma^2 H^*$.

3.1 Effective Operators Probing Composite Top Quarks

In this section, we define the dimension-six operators (see Table 3.1) and discuss their expected size in theories with a composite, i.e., a strongly interacting right-handed top quark.

As we will see in the next section, searches for the production of four top quarks at the 13 TeV LHC have provided important constraints on the idea of top quark compositeness. Constraints comparable to the one on c_{tt} are obtained for the full set of four-top operators [44], which also involve the third generation left-handed quark doublet,

$$\frac{c_{tq}}{\Lambda^2}(\bar{t}_R \gamma_\mu t_R)(\bar{q}_L \gamma^\mu q_L), \ \frac{c_{tq}^{(8)}}{\Lambda^2}(\bar{t}_R \gamma_\mu t^A t_R)(\bar{q}_L \gamma^\mu t^A q_L), \ \frac{c_{qq}}{\Lambda^2}(\bar{q}_L \gamma_\mu q_L)^2, \ \frac{c_{qq}^{(8)}}{\Lambda^2}(\bar{q}_L \gamma_\mu t^A q_L)^2, \quad (3.4)$$

where $t^A = \lambda^A/2$ are the generators of SU(3). Then, the generic expectation in scenarios dealing with the generation of the top Yukawa coupling, such as CH models [14], is that operators involving q_L are generated as well, yet with coefficients proportional to y_t, i.e. $c_{tq}, c_{tq}^{(8)}/\Lambda^2 \sim y_t^2/m_*^2$, and $c_{qq}, c_{qq}^{(8)}/\Lambda^2 \sim y_t^2(y_t/g_*)^2/m_*^2$, thus not as enhanced as c_{tt}/Λ^2 for large new-physics couplings $g_* \gg y_t$. We note that the H parameter [45] effectively contributes to four-top production just as the O_{tq} operator does.

Since our main interest is in new-physics scenarios with a strongly interacting Higgs, top-Higgs operators should also be present and in principle with large coefficients. This is the case of

$$\frac{c_{Ht}}{\Lambda^2} i(H^\dagger \overset{\leftrightarrow}{D}_\mu H)(\bar{t}_R \gamma^\mu t_R), \quad (3.5)$$

which leads to a zero-momentum deformation of the Zt_Rt_R coupling. However, we point out that, apart from the fact that the experimental sensitivity on such anomalous couplings has been typically weak (see however Sec. 3.2), this operator turns out to be suppressed by an accidental discrete symmetry [46] in models where the right-handed top does not induce radiative contributions to the Higgs potential, as preferred by fine-tuning considerations. Although such a symmetry is eventually broken, the coefficient of O_{Ht} would be expected to be small in these cases, $c_{Ht}/\Lambda^2 \sim N_c(y_t/4\pi f)^2$. Similar statements can be made for the analogous operators with q_L, namely O_{Hq} and $O_{Hq}^{(3)}$ (see Table 3.1). The combination $c_{Hq} + c_{Hq}^{(3)}$ induces a correction to the Zb_Lb_L coupling which, although constrained at the per-mille level at LEP, is also typically protected by P_{LR} symmetry [46, 47]. Measurements of deviations in the Zt_Lt_L and Wt_Lb_L couplings from the SM, associated with $c_{Hq} - c_{Hq}^{(3)}$ and $c_{Hq}^{(3)}$ respectively, do not reach the level of precision to be competitive with the four-top operator Eq. (3.1), in particular at large m_* because $c_{Hq}/\Lambda^2 \sim y_t^2/m_*^2$. Similarly, for the still poor measurements of the Higgs coupling to the top, which probe the Yukawa-like dimension-six operator O_{y_t}, even if $c_{y_t}/\Lambda^2 \sim g_*^2/m_*^2$.

Even though operators with SM gauge field strengths and top quarks are generated with coefficients that are not enhanced, or are even suppressed at strong coupling,[1] they could be relevant in situations where direct probes of the four-top operators are not feasible, as it is the case of future lepton colliders (see Sec. 3.4). Such operators are

$$\frac{c_{tD}}{\Lambda^2}(\partial^\mu B_{\mu\nu})(\bar{t}_R\gamma^\nu t_R)\,, \qquad \frac{c_{tD}^{(8)}}{\Lambda^2}(D^\mu G_{\mu\nu}^A)(\bar{t}_R\gamma^\nu t^A t_R)\,, \qquad (3.6)$$

with $c_{tD}/\Lambda^2 \sim g'/m_*^2$ and $c_{tD}^{(8)}/\Lambda^2 \sim g_s/m_*^2$, as well as

$$\frac{c_{qD}}{\Lambda^2}(\partial^\mu B_{\mu\nu})(\bar{q}_L\gamma^\nu q_L)\,, \quad \frac{c_{qD}^{(8)}}{\Lambda^2}(D^\mu G_{\mu\nu}^A)(\bar{q}_L\gamma^\nu t^A q_L)\,, \quad \frac{c_{qD}^{(3)}}{\Lambda^2}(D^\mu W_{\mu\nu}^a)(\bar{q}_L\gamma^\nu \sigma^a q_L)\,, \qquad (3.7)$$

with $c_{qD}/\Lambda^2 \sim (y_t/g_*)^2 g'/m_*^2$, $c_{qD}^{(8)}/\Lambda^2 \sim (y_t/g_*)^2 g_s/m_*^2$, $c_{qD}^{(3)}/\Lambda^2 \sim (y_t/g_*)^2 g/m_*^2$ for a strongly coupled right-handed top. These operators are equivalent to a particular combination of four-fermion operators, since by the equations of motion,

$$\partial^\mu B_{\mu\nu} = -g'\left(\tfrac{1}{2}iH^\dagger\overleftrightarrow{D}_\nu H + \tfrac{2}{3}\bar{u}_R\gamma_\nu u_R - \tfrac{1}{3}\bar{d}_R\gamma_\nu d_R + \tfrac{1}{6}\bar{q}_L\gamma_\nu q_L - \bar{e}_R\gamma_\nu e_R - \tfrac{1}{2}\bar{\ell}_L\gamma_\nu \ell_L\right)\,, \qquad (3.8)$$

$$D^\mu G_{\mu\nu}^A = -g_s\left(\bar{u}_R\gamma_\nu t^A u_R + \bar{d}_R\gamma_\nu t^A d_R + \bar{q}_L\gamma_\nu t^A q_L\right)\,, \qquad (3.9)$$

$$D^\mu W_{\mu\nu}^a = -g\tfrac{1}{2}\left(iH^\dagger\sigma^a\overleftrightarrow{D}_\nu H + \bar{q}_L\gamma_\nu\sigma^a q_L + \bar{\ell}_L\gamma_\nu\sigma^a \ell_L\right)\,. \qquad (3.10)$$

For an example of the potential relevance of this class of operators in deciphering the composite nature of the top quark, let us consider probes of $O_{tD}^{(8)}$ at the LHC. This operator affects top-pair production through a $q\bar{q} \to t\bar{t}$ amplitude that grows with energy [49]. Given the expectation $c_{tD}^{(8)}/\Lambda^2 \sim g_s/m_*^2$, one could naively conclude that the new-physics effects do not depend on g_* for fixed m_*. However, renormalization group (see App. I.A) evolution implies that at relevant scale, μ, the coefficient of $O_{tD}^{(8)}$ is [50]

$$c_{tD}^{(8)}(\mu) = c_{tD}^{(8)}(m_*) + c_{tt}(m_*)\frac{g_s}{12\pi^2}\log\left(\frac{m_*^2}{\mu^2}\right)\,. \qquad (3.11)$$

Therefore, one-loop diagrams with one insertion of the four-top contact interaction Eq. (3.1) dominate the amplitude at large g_*, $\mathcal{M}_{q\bar{q}\to t\bar{t}} \sim g_s^2(g_*/4\pi)^2(E/m_*)^2\log(m_*^2/E^2)$. Although current LHC searches in top-pair production yield $c_{tD}^{(8)}/\Lambda^2 < 0.7\,\mathrm{TeV}^{-2}$ at 95% CL [51] and are

---

[1]Interesting exceptions exist, in particular the so-called Remedios power counting [48].

therefore not sensitive enough to yield a relevant constraint on the (m_*, g_*) plane, we show in Sec. 3.4 that this changes at high-energy lepton colliders, due to the superior precision in top-pair production.

The main conclusion of the previous discussion is that probes of the four-top operator Eq. (3.1) are the most relevant ones concerning a strongly interacting (right-handed) top quark.[2] We will discuss the impact of current LHC bounds from four-top production on the (m_*, g_*) parameter space in more detail in Sec. 3.2, where we also present a comparison with the main universal tests of CH models. The latter comprise searches for anomalous Higgs couplings, primarily controlled by $O_H = \frac{1}{2}\left(\partial_\mu |H|^2\right)^2$ and constrained by Higgs and electroweak precision data. Given that $c_H/\Lambda^2 \sim g_*^2/m_*^2$, provides, as we will see, the leading constraint at strong coupling. Note however that such a bound is largely correlated with other contributions to the electroweak parameters, in particular S and T, controlled by the operators O_W, O_B, and O_T respectively (see Table 3.1). These last operators are, in fact, crucial in CH models, giving rise to constraints that are independent of the new-physics coupling, since $c_{W,B}/\Lambda^2 \sim 1/m_*^2$ and $c_T \sim N_c y_t^2(y_t/4\pi)^2/m_*^2$, the latter being of one top-loop size because of custodial symmetry [17]. The other set of relevant bounds are associated with non-standard effects that are largest at weak g_*. They are described in terms of the parameters Z, W, Y [54], or equivalently by the operators O_{2G}, O_{2W}, O_{2B} (see Table 3.1), with coefficients $c_{2G}/\Lambda^2 \sim (g_s/g_*)^2/m_*^2$, $c_{2W}/\Lambda^2 \sim (g/g_*)^2/m_*^2$, $c_{2B}/\Lambda^2 \sim (g'/g_*)^2/m_*^2$, respectively.[3]

Finally, one of the most relevant constraints on CH models, connected as well with the top sector, comes from the CP-violating operator $\widetilde{O}_\gamma = H^\dagger H B^{\mu\nu}\widetilde{B}_{\mu\nu}$, with coefficient of one top-loop size $\tilde{c}_\gamma/\Lambda^2 \sim g'^2 N_c(y_t/4\pi)^2/m_*^2$ and which itself contributes at one loop to the EDM of the electron. The current constraint on m_*, taking the power counting estimate at face value, is $m_* > 20\,\text{TeV}$ at the 95% CL [55, 56]. While this is the strongest bound independent of g_*, let us note that being CP-violating it is of a qualitatively different nature regarding the previous ones; for this reason, we do not further consider it in this part of the thesis. It will reappear, however, in more detail in part II in the context of measurements of EDMs.

3.2   Current Status and BSM Interpretation of Multilepton Excesses

In this section, we review our current knowledge of the corresponding experimental constraints, paying special attention to those operators leading to the largest sensitivity on the parameter space of CH models. The current status is summarized in Fig. 3.1. We will also discuss how the inclusion of the aforementioned EFT operators can at least alleviate some of the tension in four top and top pair production in association with additional weak bosons.

From the absence of significant deviations in the total cross-section in four-top production, which have been searched for using $\approx 36\,\text{fb}^{-1}$ of data in the single-lepton [44, 57, 58], opposite-sign dilepton [44, 58], and same-sign dilepton and multilepton final states [59–61], the combined ATLAS observed (expected) bound on the four-fermion operator Eq. (3.1) is $|c_{tt}|/\Lambda^2 < 1.9\,(1.6)\,\text{TeV}^{-2}$ at 95% CL [58]. A similar bound is obtained by CMS [44]. Besides, very recently both experiments have updated their multilepton searches to $\approx 140\,\text{fb}^{-1}$ [62, 63], observing mild but intriguing excesses with respect to the SM predictions; we will discuss these shortly.

---

[2]See also [52, 53] for previous phenomenological studies at the LHC with a similar spirit.

[3]Since we are considering scenarios with (partial) top quark compositeness, it is implicitly assumed that the new-physics sector features colored states that generate O_{2G} at low energies.
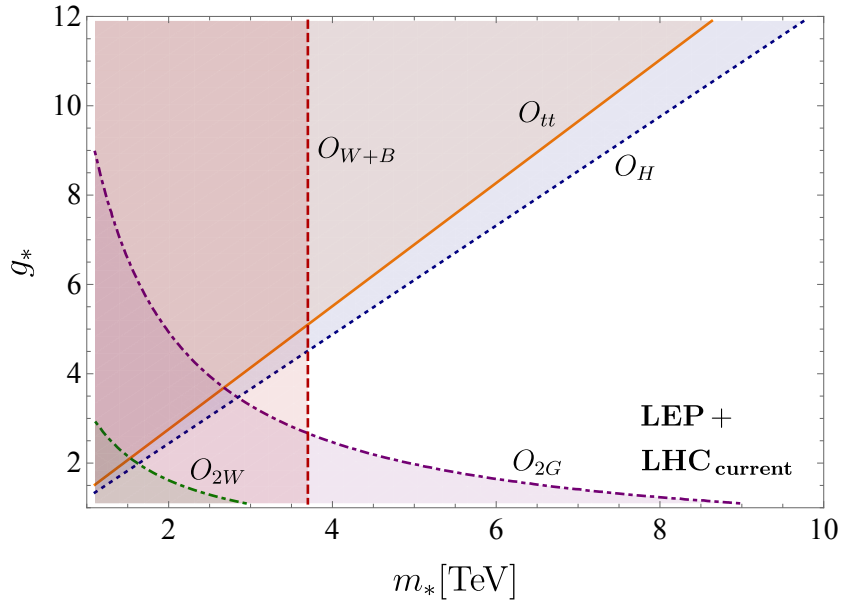
Figure 3.1: Current 95% CL excluded regions in the (m_*, g_*) plane of scenarios featuring a strongly- interacting Higgs and (right-handed) top quark. The different limits are associated with bounds on individual operators, each dominating the corresponding observables in a certain region of parameter space (see main text for details) — this is not a global fit.

The only other operator with the same scaling as O_{tt} is the pure Higgs operator O_H. The current exclusive (one operator at a time) 95% CL bound on its coefficient is $c_H/\Lambda^2 < 1.5\,\mathrm{TeV}^{-2}$ [64]. Including the strong correlation with the operators O_W, O_B, and O_T significantly weakens the bounds, giving $f|_H^{\mathrm{LHC}} \gtrsim 550\mathrm{GeV}$ after marginalizing (i.e., letting the corresponding EW parameters S and T float). As mentioned before, these operators give constraints independent of the new-physics coupling, that is why the region of parameter space covered by the bound $(c_W + c_B)/\Lambda^2 < 0.07\,\mathrm{TeV}^{-2}$ [64, 65], corresponding to $m_* > 3.7$ TeV, is also shown in Fig. 3.1.

Operators with two top quarks also enter top quark pair production at hadron colliders, and we find that the current main sensitivity arises from LHC dijet searches, which lead to the bound $c_{2G}/\Lambda^2 < 0.01\,\mathrm{TeV}^{-2}$ [66–68]. As shown in Fig. 3.1, this is superior to the LEP and LHC limits derived from c_{2W} and c_{2B} [64]. This remains the case at the high-luminosity phase of the LHC, even if with more statistics the constraint on W from $pp \to \ell\nu$ is expected to reach a comparable level to that on Z [69].

Now that we have established the most interesting operators in the context of a strongly coupled top quark, and we saw how well they are currently constrained by experiments, we want to investigate if and how their effects can explain certain tensions in the data. We will focus on the recent measurement of four-top production performed by both the ATLAS [70] and CMS [71] collaborations, as well as the associated measurements of the main backgrounds $t\bar{t}W$, $t\bar{t}Z$, $t\bar{t}h$. At the LHC, these measurements are dominated by final states with multileptons plus jets. After Run 2, an intriguing, generalized pattern of mild excesses has emerged in these final states. We review the latest experimental results here[4]:

1. The CMS four-top analysis [62], in its cut-based version (on which we focus below), finds

---

[4]During writing up this thesis both the CMS and ATLAS collaboration announced the observation of four-top production for the very first time [72, 73]. Both analyses investigate multi-lepton final states and obtain cross-sections which are consistent with each other as well as with the SM prediction.
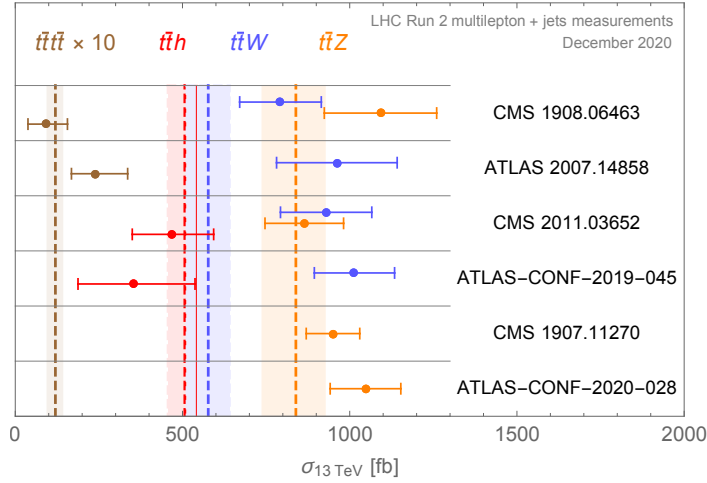
Figure 3.2: Summary of experimental measurements (dots with error bars) compared to theoretical predictions (dashed vertical lines with uncertainty bands).

$\sigma_{t\bar{t}t\bar{t}} = 9.4^{+6.2}_{-5.6}$ fb compared to the SM reference prediction $\sigma^{\mathrm{SM,R}}_{t\bar{t}t\bar{t}} = 12.0$ fb, while letting the normalizations $\mu_{t\bar{t}W} = 1.3 \pm 0.2$ and $\mu_{t\bar{t}Z} = 1.3 \pm 0.2$ float in the fit, with SM reference cross-sections $\sigma^{\mathrm{SM,R}}_{t\bar{t}W} = 610$ fb and $\sigma^{\mathrm{SM,R}}_{t\bar{t}Z} = 840$ fb, respectively.

2. The ATLAS four-top measurement [63] finds $\sigma_{t\bar{t}t\bar{t}} = 24^{+7}_{-6}$ fb, and also observes an excess of $t\bar{t}W$ events relative to the SM reference, with best fit $\mu_{t\bar{t}W} = 1.6 \pm 0.3$ based on $\sigma^{\mathrm{SM,R}}_{t\bar{t}W} = 601$ fb. The normalization of $t\bar{t}Z$ is not left to vary in the fit.

3. The CMS measurement of $t\bar{t}h$, $t\bar{t}W$, and $t\bar{t}Z$ [74],[5] quotes $\mu_{t\bar{t}W} = 1.43 \pm 0.21$ for a reference cross-section $\sigma^{\mathrm{SM,R}}_{t\bar{t}W} = 650$ fb. Interestingly, this analysis included for the first time the $O(\alpha_s \alpha^3)$ contribution to $t\bar{t}W+$jets at the differential level, dominated by tW scattering [75]. In addition, the fit gives $\mu_{t\bar{t}Z} = 1.03 \pm 0.14$ with $\sigma^{\mathrm{SM,R}}_{t\bar{t}Z} = 839$ fb and $\mu_{t\bar{t}h} = 0.92^{+0.25}_{-0.23}$ for $\sigma^{\mathrm{SM,R}}_{t\bar{t}h} = 507$ fb.

4. The ATLAS analysis [76] finds $\mu_{t\bar{t}W} = 1.39^{+0.17}_{-0.16}$ for a SM reference $\sigma^{\mathrm{SM,R}}_{t\bar{t}W} = 727$ fb and $\mu_{t\bar{t}h} = 0.70^{+0.36}_{-0.33}$ for $\sigma^{\mathrm{SM,R}}_{t\bar{t}h} = 507$ fb, when using a single $t\bar{t}W$ normalization factor.

5. A dedicated measurement by CMS of $t\bar{t}Z$ [77] finds a cross-section $\sigma_{t\bar{t}Z} = 950 \pm 80$ fb compared to the SM reference $\sigma^{\mathrm{SM,R}}_{t\bar{t}Z} = 860$ fb.

6. A dedicated measurement of $t\bar{t}Z$ [78] by ATLAS obtains $\mu_{t\bar{t}Z} = 1.19 \pm 0.12$ with $\sigma^{\mathrm{SM,R}}_{t\bar{t}Z} = 880$ fb.

Most measurements [62, 63, 74, 78] are based on $\approx 140\,\mathrm{fb}^{-1}$, whereas [76, 77] use $\approx 80\,\mathrm{fb}^{-1}$. In addition, we mention but do not discuss further the combined analysis of EFT operators in top associated production modes by CMS [71], as well as previous measurements of $t\bar{t}W$, $t\bar{t}Z$ by CMS [79] and ATLAS [80], which are all based on a smaller data set, $\approx 40\,\mathrm{fb}^{-1}$.

The above overview shows that an extensive pattern of 2σ-level excesses with respect to the SM predictions is observed by both ATLAS and CMS. We summarize the status in Fig. 3.2,

---

[5]This analysis also measures the th cross-section, but we omit it since the accuracy is much weaker than for the $t\bar{t}X$ processes.
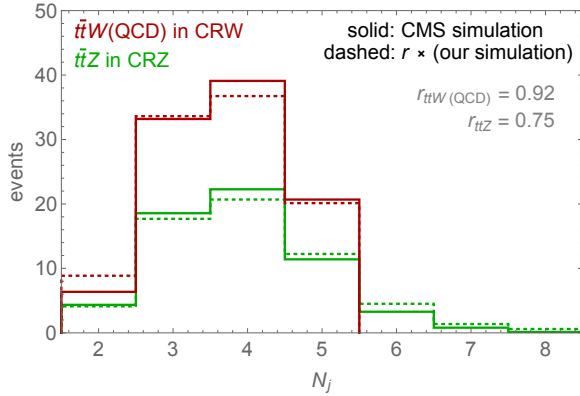
Figure 3.3: Comparison of our MC event yields to the CMS simulation. Once normalized to 544 fb [81], the $t\bar{t}W(\mathrm{QCD})$ sample requires a rescaling factor $r_{t\bar{t}W(\mathrm{QCD})} = 0.92$ to match the total CMS MC yield in CRW. After using 839 fb as normalization [82], the $t\bar{t}Z$ sample is rescaled by $r_{t\bar{t}Z} = 0.75$ to match the total CMS MC yield in CRZ.

where the above-quoted experimental results are compared with the following SM theoretical predictions in femtobarns

$$\sigma_{t\bar{t}t\bar{t}}^{\mathrm{SM}} = 12.0^{+18\%}_{-21\%}, \quad \sigma_{t\bar{t}W}^{\mathrm{SM}} = 577^{+11\%}_{-11\%} \quad [81]; \quad \sigma_{t\bar{t}Z}^{\mathrm{SM}} = 839^{+10\%}_{-12\%}, \quad \sigma_{t\bar{t}h}^{\mathrm{SM}} = 507^{+6.8\%}_{-9.9\%} \quad [82]. \quad (3.12)$$

The discrepancies are mild, yet their somewhat coherent structure hints that they may not be due to mere statistical fluctuations.[6] Recent theoretical studies have focused on pushing the SM predictions to higher accuracy, especially for $t\bar{t}W$ [70, 84–89], which however, still exhibits the strongest disagreement between theory and experiment. For now, a complete NNLO QCD calculation remains unreachable.

Here we take a different standpoint and entertain the possibility that the excesses are due to heavy new physics, described by at least some of the effective operators from the previous section. Since, here, we are interested only in processes with at least two top quarks, the two operators O_{tt} and O_{Ht} are the leading ones according to their power counting (ignoring for now the possible P_{LR} forbidding O_{Ht}). The former mediates $t\bar{t}t\bar{t}$ production, whereas the latter modifies the $Zt_R t_R$ coupling, thereby leading to three distinct effects: it contributes to $t\bar{t}Z$ production at the leading $O(\alpha_s^2 \alpha)$, to $t\bar{t}W+$jets at the formally subleading, but tW scattering-enhanced, $O(\alpha_s \alpha^3)$ [75], and to $t\bar{t}t\bar{t}$ production at $O(\alpha_s^2 \alpha^2)$. We consider these two operators as a motivated first approximation, but note that others should be added in a more general analysis that includes e.g., $t\bar{t}h$ production, notably O_{y_t} given that this modifies the htt coupling (the sensitivity of $t\bar{t}t\bar{t}$ to O_{y_t} was studied in [90]). We concentrate on the CMS four-top analysis [62] because it provides a cut-and-count version and sufficient pre-fit information for us to perform a detailed, if simplified, reinterpretation.

The analysis selects events containing at least two leptons of the same sign, $N_j \geq 2$ and $N_b \geq 2$, $H_T > 300$ GeV and $p_T^{\mathrm{miss}} > 50$ GeV, with complete definitions and list of requirements reported in [62]. The cut-based analysis defines two control regions, CRW (where the contribution of $t\bar{t}W$ is enhanced) and CRZ (where $t\bar{t}Z$ is enhanced), and 14 signal regions. In our reinterpretation, for simplicity, we combine all signal regions into a single one (SR). Signal and background events are generated using MadGraph5_aMC@NLO [91], implementing higher-dimensional operators via FeynRules [92]. The factorization and renormalization scales

---

[6]Note that 8 TeV data only afforded to measure these processes with order 50% uncertainties; see e.g., [83] for $t\bar{t}W$, $t\bar{t}Z$.

are set to the default dynamical value for all processes, the top mass is set to 172.5 GeV, and NNPDF23_lo_as_0130_qed parton distribution functions [93] are used. Parton showering and hadronization are performed by Pythia8 [94] and detector effects are parametrized using the CMS card in Delphes3 [95], but setting $R = 0.4$ for the anti-k_t jet clustering algorithm [96], implemented via the Fast Jet package [97]. As a preliminary check of our simulation tool chain, we reproduce the SM $t\bar{t}W$ ($t\bar{t}Z$) event yields in the CRW (CRZ), obtained by CMS with full detector simulation. The results, reported in Fig. 3.3, show that after application of mild scaling factors to match the overall normalizations, our simulations reproduce reasonably well the results reported by CMS (where it should be kept in mind that we simulate at LO in QCD, whereas the CMS treatment is at NLO). Having thus gained confidence in our setup, we proceed to include the new physics effects.

The impact of O_{Ht} on $t\bar{t}Z$ production is captured by rescaling the CMS yields using the overall factor (note that we set $\Lambda = v$ throughout this section)

$$\mu_{t\bar{t}Z}(c_{Ht}) = \frac{g_{Zt_Lt_L}^2 + g_{Zt_Rt_R}^2 \left(1 + \frac{3c_{Ht}}{4s_w^2}\right)^2}{g_{Zt_Lt_L}^2 + g_{Zt_Rt_R}^2}, \qquad g_{Zff} = g_Z(T_{Lf}^3 - s_w^2 Q_f), \qquad (3.13)$$

which we have checked to be a good approximation by simulating a set of samples with different values of c_{Ht} (see [98, 99] for NLO QCD analyses of the $t\bar{t}Z$ sensitivity to top electroweak couplings). In addition, we consider the impact of c_{Ht} on $t\bar{t}Wj$(EW); this piece was altogether neglected in the CMS simulation of $t\bar{t}W$+jets [62]. For the $t\bar{t}t\bar{t}$ process, our simulation is simplified in two ways: we neglect interference of the O_{tt}-mediated amplitude with the SM,[7] and neglect the contribution of O_{Ht}. We do so because reliably assessing these effects at the hadronic differential level goes beyond our computational resources, and besides it would be best performed by the LHC experiments directly. At the qualitative level, we note that the c_{tt}-SM interference is suppressed at high energies, whereas the impact of c_{Ht} on four-top production is generally expected to be moderate, as the $t\bar{t} \to t\bar{t}$ amplitude does not grow with energy when $c_{Ht} \neq 0$, in contrast with the aforementioned case of tW scattering. We provide an estimate of the expected size and pattern of these effects after presenting the results of our fit.

To shed light on the compatibility of the data with our BSM hypothesis, we form a χ^2 from 18 non-overlapping bins,

$$\chi^2 = \sum_{i_{\text{CRW}}} \left(\frac{\Delta N_i}{\delta_{\text{CMS,i}}}\right)^2 + \sum_{i_{\text{CRZ}}} \left(\frac{\Delta N_i}{\delta_{\text{CMS,i}}}\right)^2 + \sum_{i_{\text{SR}}} \left(\frac{\Delta N_i}{\delta_{\text{CMS,i}}}\right)^2, \qquad (3.14)$$

with $\Delta N_i = N_{\text{SM,i}} - N_i(\{p\})$ the difference between the number of events in each bin in the SM and the predicted number of events dependent on the parameters $\{p\}$ to be estimated. In the above sum i_{CRW} and i_{CRZ} run over all bins given by N_j with the $N_j = 6, 7$ bins in CRZ merged, while i_{SR} enumerates 9 H_T bins with all events with H_T being merged into a single bin. For $\delta_{\text{CMS,i}}$ We use the uncertainties on event counts as read from Figs. 2 and 3 in [62], averaging over positive and negative directions, and neglect theoretical uncertainties. The results of a two-parameter fit to $\{p\} = (c_{Ht}, c_{tt})$ are shown in the upper panels of Fig. 3.4, while in the lower panel we show for comparison a fit where no higher-dimensional operators are introduced,

---

[7]The $O(c_{tt}^2)$ term of the cross-section is normalized by applying a K-factor of 1.24, as derived for SM four-top production using the NLO QCD-only cross-section of 11.1 fb [81]. However, SMEFT@NLO framework [100] has enabled the calculation at full NLO in QCD of the contributions of four-top operators to $t\bar{t}t\bar{t}$ production (including interference with the SM). In particular, $K < 1$ was obtained for the $O(c_{tt}^2)$ piece. Due to the different scale choices, our approximate-NLO cross-section turns out to be numerically very close to the exact-NLO result quoted in [100].
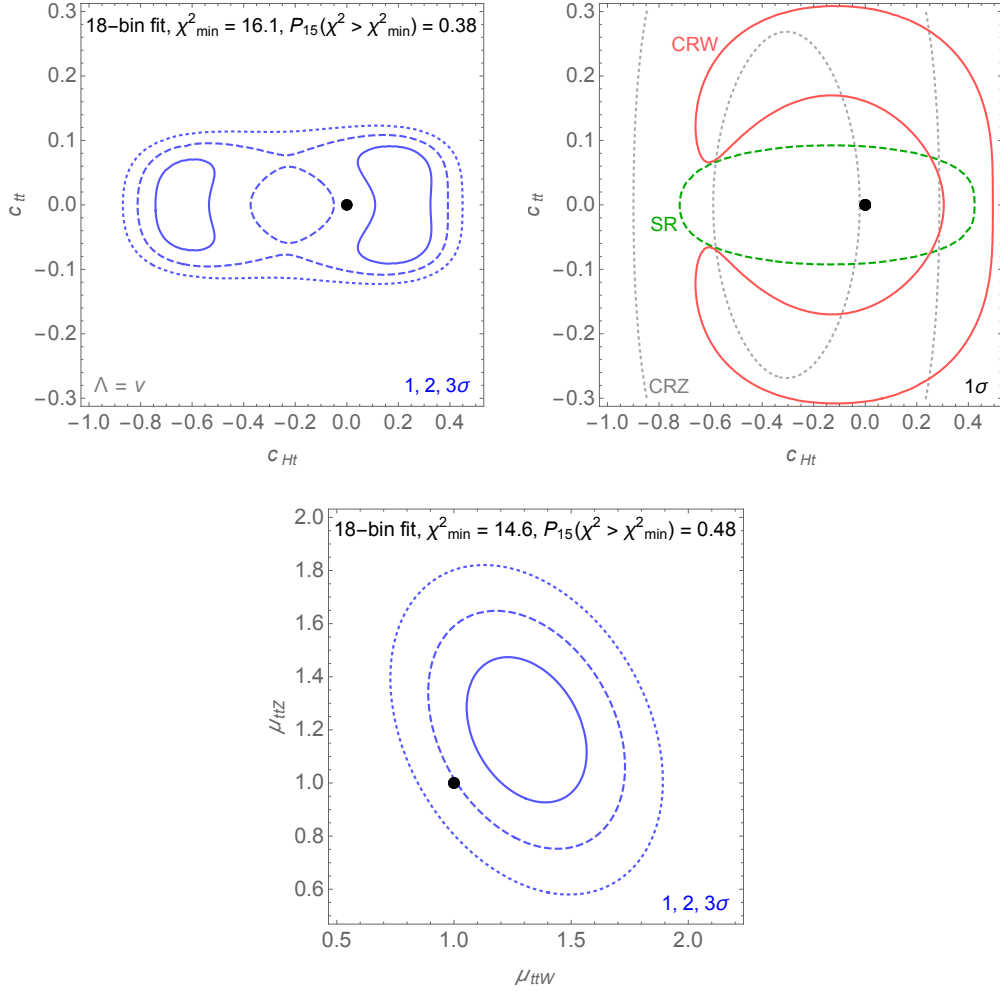
Figure 3.4: Exclusion contours from fits to the CMS data in [62]. *Top:* plane of the EFT coefficients (c_{Ht}, c_{tt}). The contours are invariant under $c_{tt} \to -c_{tt}$ because we neglected interference between the BSM and SM $t\bar{t}t\bar{t}$ amplitudes. The left panel shows the full fit, whereas the right panel displays the 1σ regions when the χ^2 is restricted only to CRW, CRZ, or SR. *Bottom:* plane of the signal strengths $(\mu_{t\bar{t}W}, \mu_{t\bar{t}Z})$. Here $\mu_{t\bar{t}W}$ rescales the total SM rate, including the $t\bar{t}Wj(\text{EW})$ component, which we add to the CMS reference cross-section. In all panels, a black dot indicates the SM point.

but the signal strengths $\{p\} = (\mu_{ttW}, \mu_{ttZ})$ are left floating, which is similar to the treatment performed by CMS. The best-fit point of the latter fit is $(\mu_{t\bar{t}W}, \mu_{t\bar{t}Z}) \approx (1.3, 1.2)$. We note that the two EFT coefficients parametrizing the effects of heavy new physics provide a reasonable fit to the data, with comparable goodness of fit to the ad-hoc signal strengths. The best fit is given by $(c_{Ht}, c_{tt}) \approx (0.21, \pm 0.054)$, corresponding to scales $f|_{Ht} \approx 540\,\text{GeV}$ and $f|_{tt} \approx 1.1\,\text{TeV}$ if the respective coefficients are set to unity. The impact of the BSM contributions to the CRW, CRZ and SR are shown in Fig. 3.5 taking the best-fit values of the coefficients.

Next, to gain some insight on the effects of the approximations we made in our description of the four-top process, we consider parton level $t\bar{t}t\bar{t}$ production (with undecayed tops) including the full LO amplitude for the SM plus O_{tt} and O_{Ht}. We split the cross-section into a low-energy

and a high-energy region according to $M_T = \sum_{i=1}^{4}(m_t^2 + p_T^{i\,2})^{1/2}$,

$$\sigma_{M_T < 1.15\,\text{TeV}}\,[\text{fb}] = 6.1 - 20\,c_{tt} + 410\,c_{tt}^2 + 5.3\,c_{Ht} + 9.3\,c_{Ht}^2 - 63\,c_{Ht}c_{tt}\,, \qquad (3.15)$$

$$\sigma_{M_T > 1.15\,\text{TeV}}\,[\text{fb}] = 3.6 - 6.8\,c_{tt} + 1100\,c_{tt}^2 + 1.4\,c_{Ht} + 2.3\,c_{Ht}^2 - 25\,c_{Ht}c_{tt}\,. \qquad (3.16)$$

The boundary value $M_T = 1.15\,\text{TeV}$ is chosen to roughly match $H_T = 800\,\text{GeV}$ at hadronic level, which we have verified splits the SR into two sub-regions of comparable sensitivity in our fit to CMS data (see the bottom panel of Fig. 3.5). Equation (3.16) confirms the expectation that at high energies, it is reasonable to neglect all BSM terms except for the $O(c_{tt}^2)$ one: for example, plugging in the best fit point, we find $\sigma_>/\sigma_>^{\text{SM}} = 1.79$ whereas our approximation gives 1.86. For the low-energy region, using, Eq. (3.15) we find $\sigma_</\sigma_<^{\text{SM}} = 1.15$ versus the approximate value 1.20. This apparently reasonable agreement is, however, actually, the result of a compensation between different corrections arising from c_{Ht} and c_{tt}, suggesting that the shapes of our fit contours could be somewhat affected by a fully accurate description of BSM effects in the low-H_T bins of SR.

Finally, we remark that O_{Ht} mediates BSM contributions to additional processes, including for instance $pp \to t\bar{t}hj$ at $O(\alpha_s \alpha^3)$ and tZW at $O(\alpha_s \alpha^2)$. The analysis of such subleading effects was initiated in [75] and later expanded in [101]. Based on their findings, we do not expect the O_{Ht} dependence of these and other analogous processes, which is neglected here, to have a significant impact on our results. Nonetheless, a detailed assessment would be of interest to obtain a complete picture of heavy new physics effects in LHC multilepton plus jets final states.

In summary, the main messages we derive from the fit are:

- The $O(\alpha_s \alpha^3)$ $t\bar{t}Wj(\text{EW})$ contribution to $t\bar{t}W$ + jets is important and should be consistently included at the differential level, as originally pointed out in [75] and later analyzed in depth in [81, 86].

- An interpretation of the CMS data [62] in terms of the O_{Ht} and O_{tt} operators gives a goodness of fit comparable to the application of constant rescaling factors to the $t\bar{t}W$ and $t\bar{t}Z$ cross-sections, while having a stronger physical motivation.

- While it is too early to draw any conclusions, it is intriguing that a scale $f \sim 750\,\text{GeV}$ improves the fit to multilepton + jets data, while being roughly consistent both with four-top constraints from the single lepton and opposite-sign dilepton final states [58], and with measurements of the Higgs couplings [64].

A more comprehensive study, including a wider set of signal regions, would be strongly desirable to obtain further insight. Nevertheless, we regard the coincidence of scales suggested by our analysis as an additional motivation to further investigate heavy top-philic new physics.

3.3 Future proton-proton colliders

Let us remark that under well-motivated assumptions, current searches for strong $t\bar{t}t\bar{t}$ production enjoy a higher reach on the compositeness scale $4\pi f$ than probes of the Higgs sector at the LHC. This fact motivates our sensitivity studies at future colliders. We begin in this section with hadron colliders, first discussing shortly the high-luminosity phase of the LHC and then analyzing in detail the 100 TeV FCC-hh [102].

To estimate the HL-LHC sensitivity to c_{tt}/Λ^2, we perform a simple extrapolation of the CMS four-top search in multileptons [62]. We focus on the signal region (bottom panel of Fig. 3.5),
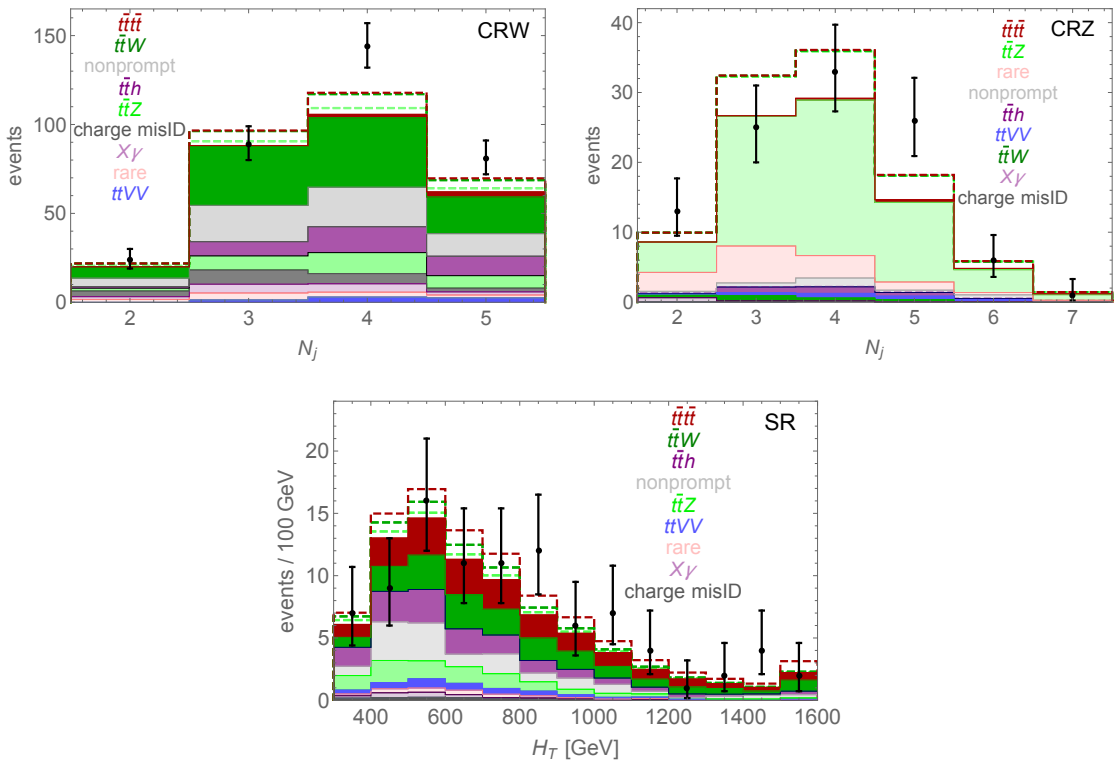
Figure 3.5: The filled histograms show the CMS MC predictions as given in [62]. The stacked, light green [dark green] (dark red) dashed histograms show the BSM contribution to $t\bar{t}Z$ [SM+BSM contribution to $t\bar{t}Wj$(EW)] (BSM contribution to $t\bar{t}t\bar{t}$) at the best-fit point $(c_{Ht}, c_{tt}) \approx (0.21, \pm 0.054)$. Black points show the data with error bars as quoted by CMS. Although in our fit we combine the last two bins of CRZ and the last 5 bins of SR, for illustration here we retain the same binning as chosen by CMS.

adopting the H_T-binning chosen by CMS and rescaling their MC predictions for all SM processes to a luminosity of 3 ab^{-1}. As in the previous section, we include the missing SM $t\bar{t}Wj$(EW) contribution among the backgrounds and simulate the signal, neglecting interference with SM four-top production. Assuming as systematics on the two main backgrounds $(\delta_{t\bar{t}t\bar{t}}, \delta_{t\bar{t}W}) = (8.5\%, 7.5\%)$, which correspond to half the current theoretical uncertainties [81], and applying a mild PDF rescaling factor [103] to account for the increase in collider energy to 14 TeV, we obtain at 95% CL

$$\Lambda/\sqrt{|c_{tt}|} > 1.3 \, \text{TeV} \quad (\text{no syst.: } 1.4 \, \text{TeV}). \qquad (\text{HL-LHC}) \qquad (3.17)$$

We view this as a conservative estimate, as the actual HL-LHC analysis will capitalize on the ≈ 20 times larger statistics by refining the binning at larger H_T, thus increasing slightly the sensitivity.[8] Furthermore, a caveat is that we have assumed agreement of data with the SM predictions, although as discussed in Sec. 3.2 this is somewhat unclear for current multilepton measurements.

We now turn to the analysis of the four-top final state at the FCC-hh. The decays of the four tops give rise to a complex set of possible final states. The same-sign dileptons (SSL) and trileptons (3L) signatures both benefit from suppressed SM backgrounds, while retaining

---

[8]In addition, rescaling the current statistical-only 95% CL bound $\Lambda/\sqrt{|c_{tt}|} > 0.93$ TeV using Collider Reach [103] would give an estimate of 1.7 TeV at the HL-LHC.

not-too-small branching ratios of 4.1% and 2.6%, respectively. These numbers do not include contributions from leptonic τ decays, which are systematically neglected in our FCC analysis (whereas they are always included when we quote LHC results).[9] Conversely, the fully hadronic signature has a large branching ratio of 20%, but suffers from challenging backgrounds. In this section, we thoroughly analyze the SSL and 3L signatures, and perform an exploratory study of the fully hadronic final state.

For the SSL and 3L final states we partly build on the latest LHC searches for four-top production in multilepton + jets [62, 63], and on the LHC study [104] which focused on SM $t\bar{t}t\bar{t}$ production and BSM effects mediated by relatively light new physics (see also [105] for a thorough analysis of resonant signals in the four-top final state at the LHC). Signal and background events are generated using MadGraph5_aMC@NLO [91], using a FeynRules [92] model where O_{tt} is added to the SM. The factorization and renormalization scales are set to $M_T/2$ for all processes, where M_T is the sum of transverse masses. The signal samples only contain the $O(c_{tt}^2)$ contribution, as interference with the SM $t\bar{t}t\bar{t}$ amplitude is a small effect in our signal region; we provide a quantitative assessment of this at the end of the section. The SM four-top production is simulated at full LO, namely $O(\alpha_s^i \alpha^j)$ with $i, j \in \{0, \ldots, 4\}$ and $i + j = 4$, while as normalization we use the complete NLO (QCD+EW) calculation of [81]. The normalization of the signal is rescaled by the ratio of the NLO (QCD+EW) and LO QCD cross-sections as calculated for SM production, which equals 1.8.

Parton showering and hadronization are performed by Pythia8 [94] and detector effects are parametrized using Delphes3 [95] adopting the FCC card. Within Delphes, jets are clustered with the FastJet package [97] using the anti-k_t algorithm [96] with $R = 0.5$. The b-tagging performance is described through the following efficiencies,

$$\epsilon_i(p_T) = \epsilon_i^0 \, \chi_{[10\,\mathrm{GeV},\,15\,\mathrm{TeV}]}(p_T)\Big(1 - \chi_{[500\,\mathrm{GeV},\,15\,\mathrm{TeV}]}(p_T)\,\frac{p_T}{15\,\mathrm{TeV}}\Big), \qquad (3.18)$$

$$\epsilon_{b,c,j}^0 = 0.85, 0.05, 0.01 \ \text{for} \ |\eta| < 2.5, \qquad \epsilon_{b,c,j}^0 = 0.64, 0.03, 0.0075 \ \text{for} \ 2.5 < |\eta| < 4.0,$$

and $\epsilon_{b,c,j}^0 = 0$ for $|\eta| > 4.0$. In Eq. (3.18), χ denotes the characteristic function. As our signals feature highly boosted tops, as well as a generally large amount of hadronic activity, we apply lepton isolation using a variable cone, following the mini-isolation proposal [106]: an electron (muon) ℓ is said to be isolated if $p_T^{\mathrm{cone}}/p_T^\ell < 0.1\,(0.2)$, where p_T^{cone} is the sum of the transverse momenta within a cone of radius $R_{\mathrm{iso}} = \min\left(r_{\min}, p_T^0/p_T^\ell\right)$ around the lepton [the sum excludes the lepton itself], where $r_{\min} = 0.2\,(0.3)$ and $p_T^0 = 8\,(10)\mathrm{GeV}$. These values are very similar to those used in [58, 104]. As input parameters, we take

$$G_F = 1.166 \times 10^{-5}\mathrm{GeV}^{-2}, \quad m_{Z,h,t} = 91.19, 125, 173\,\mathrm{GeV}, \quad \alpha(m_Z) = 1/132.5, \qquad (3.19)$$

and we employ NNPDF23_lo_as_0130_qed parton distribution functions [93].

3.3.1   Same-sign dileptons

In this channel, the main background beyond the irreducible SM $t\bar{t}t\bar{t}$ is the production of $t\bar{t}W$ + jets, which is in fact also primarily measured in the SSL final state. Secondary backgrounds with genuine SSL include $t\bar{t}Z$ and $t\bar{t}h$, as well as some other processes listed in Table 3.2, together with the MC generation-level cross-sections. In all cases, we generate processes giving rise to at least a SSL pair and four jets at the matrix element level; for a few backgrounds, we are able to include additional jets within computing limitations. Some important processes,

---

[9]As taus dominantly originate from W and Z decays, they give approximate equal contributions to both signal and backgrounds, hence neglecting them makes our FCC results slightly conservative.

including SM $t\bar{t}t\bar{t}$ and $t\bar{t}W$ production, are normalized to the best available predictions that include both QCD and EW corrections [81, 107, 108].

In addition, there are important reducible backgrounds: either a jet is misidentified as a "fake" lepton, or one lepton belonging to an opposite-sign pair has its charge mismeasured (Qflip); both of these originate mainly from $t\bar{t}+$jets. The fake lepton component can be estimated by applying a probability for a given jet to be misidentified as a lepton (in general, the probability depends on the jet favor and p_T), and a transfer function relating the properties of the daughter lepton to those of the parent jet [109]. The probability and transfer function parameters need to be tuned against data. Here we follow a simplified approach, assuming a constant probability for both heavy favor and light jets, and that the fake lepton inherits the full four-momentum of the jet it originates from, whereas the lepton charge and favor are assigned randomly and independently. The probability is fixed to $\varepsilon_{\text{fake}} = 3.7 \times 10^{-5}$ by comparing a sample of 13 TeV semileptonic $t\bar{t}+$jets, normalized to a cross-section of 832 pb [110], to the "nonprompt" yields in the control region CRW of the CMS four-top search [62] (see left panel of Fig. 3.5).[10]

The Qflip component is estimated from MC events containing an e^+e^- or $e^\pm\mu^\mp$ pair and applying a constant probability for the charge of each electron with $p_T^e > 10$GeV to be mismeasured (the probability of flipping the charge of a muon is negligible). The probability $\varepsilon_{\text{flip}} = 2.2 \times 10^{-4}$ is taken from [104] and further validated by checking that a 13 TeV fully leptonic $t\bar{t}+$jets sample reproduces the "charge misID" yields in the control region CRW of [62]. The processes we include in our estimates of the fake lepton and Qflip backgrounds at the FCC are listed in Table 3.2.

We now turn to the event selection. First, we identify the lepton and jet candidates satisfying

$$p_T^\ell > 25\text{GeV}\,,\ |\eta_\ell| < 3\,, \qquad p_T^j > 50\text{GeV}\,,\ |\eta_j| < 5\,. \tag{3.20}$$

Next, to prevent assignment of a single detector response to both a lepton and a jet, we apply to the selected candidates an overlap removal procedure, following closely [58]. To avoid the double counting of energy deposits as electrons and jets, for each electron the closest jet within $\Delta R < 0.2$ (if any) is removed; however, if the next-to-closest jet is within $\Delta R < 0.5$ of the electron, then the electron is removed and the previously removed jet is reinstated. For muons, we apply a different criterion, aimed at distinguishing muons arising from hadron decays within proper jets, from muons that undergo bremsstrahlung radiation inside the calorimeter and are accidentally reconstructed as jets, typically characterized by a very small number of matching tracks. If a jet satisfies $\Delta R(\mu, j) < 0.04 + 10\text{GeV}/p_T^\mu$ and it has at least three tracks, the muon is rejected; otherwise, the jet is removed. The baseline selection is completed by the following requirements,

$$\text{exactly two SSL with } p_T^{\ell_1, \ell_2} > 40, 25\text{GeV}\,,$$
$$\geq 5 \text{ jets, of which } \geq 3\ b\text{-tagged}\,, \qquad H_T > 400\text{GeV}\,, \tag{3.21}$$

where ℓ_1 (ℓ_2) denotes the (sub)leading lepton. We expect that the above requirements on the lepton transverse momenta will allow for a high efficiency of an FCC-hh dilepton trigger. At this stage, for a reference BSM scale $\Lambda/\sqrt{|c_{tt}|} = 6$ TeV, we have $S/B \sim 10^{-3}$, as shown in Table 3.3. Therefore, we search for additional cuts tailored to the signal, which is characterized by a hard $t\bar{t} \to t\bar{t}$ scattering. We find as optimal variables the p_T of the leading lepton and S_T, defined as the scalar sum of the transverse momenta of the SSL pair and of all jets. Normalized distributions of these variables after the baseline selection are shown for the signal and the main backgrounds in Fig. 3.6. We apply the cuts $p_T^{\ell_1} > 275$GeV and $S_T > 3$TeV, and divide the

category	processes	decay channel	$\sigma \times \mathrm{BR}$ [fb]
$t\bar{t}t\bar{t}$ (signal)	$t\bar{t}t\bar{t}$ $\Lambda/\sqrt{|c_{tt}|} = 6\,\mathrm{TeV}$	$W_{\ell\pm}\,W_{\ell\pm}\,W_{\mathrm{had}}\,W_{\mathrm{had}}$	0.325
$t\bar{t}t\bar{t}$ (SM)	$t\bar{t}t\bar{t}$	$W_{\ell\pm}\,W_{\ell\pm}\,W_{\mathrm{had}}\,W_{\mathrm{had}}$	144 [81]
$t\bar{t}W$	$t\bar{t}W^{\pm} + 0,1,2$ jets $t\bar{t}W^{\pm}bjj$ $t\bar{t}W^{\pm}jj$	$W_{\ell\pm}\,W_{\ell\pm}\,W_{\mathrm{had}}$ $W_{\ell\pm}\,W_{\ell\pm}\,W_{\mathrm{had}}$ $W_{\ell+}\,W_{\ell-}\,W_{\ell\pm}$	640 [81] 4.11 $63.4^{\dagger}$ [108]
$t\bar{t}Z$	$t\bar{t}Z + 0,1,2$ jets $t\bar{t}Zjj$	$W_{\ell\pm}\,W_{\mathrm{had}}\,Z_{\ell^+\ell^-}$ $W_{\ell+}\,W_{\ell-}\,Z_{\ell^+\ell^-}$	1120 [107] 82.6
$t\bar{t}h$	$t\bar{t}h,\ h \to WW^*$ $t\bar{t}h,\ h \to ZZ^*$ $t\bar{t}h,\ h \to \tau^+\tau^-$	$W_{\ell\pm}\,W_{\ell\pm}\,W_{\mathrm{had}}\,W_{\mathrm{had}}$ $W_{\ell\pm}\,W_{\mathrm{had}}\,Z_{\ell^+\ell^-}\,Z_{\mathrm{had}}$ $W_{\ell\pm}\,W_{\mathrm{had}}\,\tau_{\ell\pm}\,\tau_{\mathrm{had}}$	300 [107] 24.0 [107] 140 [107]
other	$tZbjj$ $t\bar{t}W^+W^-$ $t\bar{t}W^+W^-$	$W_{\ell\pm}\,Z_{\ell^+\ell^-}$ $W_{\ell\pm}\,W_{\ell\pm}\,W_{\mathrm{had}}\,W_{\mathrm{had}}$ $W_{\ell+}\,W_{\ell-}\,W_{\ell\pm}\,W_{\mathrm{had}}$	145 35.3 11.7
fake ℓ	$t\bar{t} + 1,2$ jets $t\bar{t}bjj$	$W_{\ell\pm}\,W_{\mathrm{had}}$ $W_{\ell\pm}\,W_{\mathrm{had}}$	$K_{t\bar{t}}\ 3.45 \times 10^6$ $K_{t\bar{t}}\ 6.13 \times 10^4$
Qflip	$t\bar{t}jj$ $t\bar{t}bjj$	$W_{\ell+}\,W_{\ell-}$ $W_{\ell+}\,W_{\ell-}$	$K_{t\bar{t}}\ 4.63 \times 10^5$ $K_{t\bar{t}}\ 1.06 \times 10^4$

Table 3.2: SSL signal and background processes at $\sqrt{s} = 100\,\mathrm{TeV}$. Samples with different jet multiplicities have been merged using the MLM prescription with a matching scale of 30GeV. The cuts $p_T^j > 50\mathrm{GeV}$ and $|\eta_j| < 5$ are imposed on jets arising from QCD radiation, but no cuts are applied yet to decay products of heavy particles. The subsequent baseline selection, discussed in Sec. 3.3.1, requires ≥ 5 jets, among which ≥ 3 are b-tagged. The higher-order cross-sections we use for normalization always assume $\mu = M_T/2$ (note that in [81] this is not the central choice for $t\bar{t}t\bar{t}$). The † indicates that $p_T^j > 100\mathrm{GeV}$ was exceptionally required, to match [108] (we have checked that this different initial cut has negligible impact on the event yield after the complete selection). Whenever they do not appear in $t\bar{t}$ or $b\bar{b}$ pairs, the symbols t and b refer to either particles or antiparticles. To the $t\bar{t}$ + jets samples used to estimate the fake lepton and Qflip backgrounds, we apply a $K_{t\bar{t}} = 1.4$, calculated for inclusive $t\bar{t}$ production using the NNLO cross-section of 34.7 nb [111].

remaining events into three S_T bins, with S/B ranging from 8×10^{-3} to 5×10^{-2}. To derive a bound on Λ we construct a χ^2, accounting for the systematic uncertainties on the two main SM backgrounds, namely $t\bar{t}t\bar{t}$ and $t\bar{t}W$. For n bins, the χ^2 is defined as

$$\chi^2 = \sum_{i,j=1}^{n} N_i^S (C_{\mathrm{tot}}^{-1})_{ij} N_j^S\,, \qquad C_{\mathrm{tot}} = C_{\mathrm{stat}} + C_{\mathrm{sys}}^{t\bar{t}t\bar{t}} + C_{\mathrm{sys}}^{t\bar{t}W}\,, \qquad (3.22)$$

where the number of signal events $N_i^S \propto c_{tt}^2 \Lambda^{-4}$, and

$$(C_{\mathrm{stat}})_{ij} = (\sigma_i^{\mathrm{stat}})^2 \delta_{ij}\,, \qquad (C_{\mathrm{sys}}^A)_{ij} = \sigma_i^{\mathrm{sys},A} \rho_{ij} \sigma_j^{\mathrm{sys},A} \qquad (A = t\bar{t}t\bar{t},\ t\bar{t}W)\,, \qquad (3.23)$$

with $\sigma_i^{\mathrm{stat}} = \sqrt{N_i^{\mathrm{SM}}}$, $\sigma_i^{\mathrm{sys},A} = \delta_A N_i^A$ and we assume that each systematic uncertainty δ_A is fully correlated across bins, namely $\rho_{ij} = 1$ for all i,j. We have also assumed that the observed number

---

[10]For comparison, $\varepsilon_{\mathrm{fake}} = 7.2 \times 10^{-5}$ was obtained in [104] by matching to an earlier ATLAS analysis.
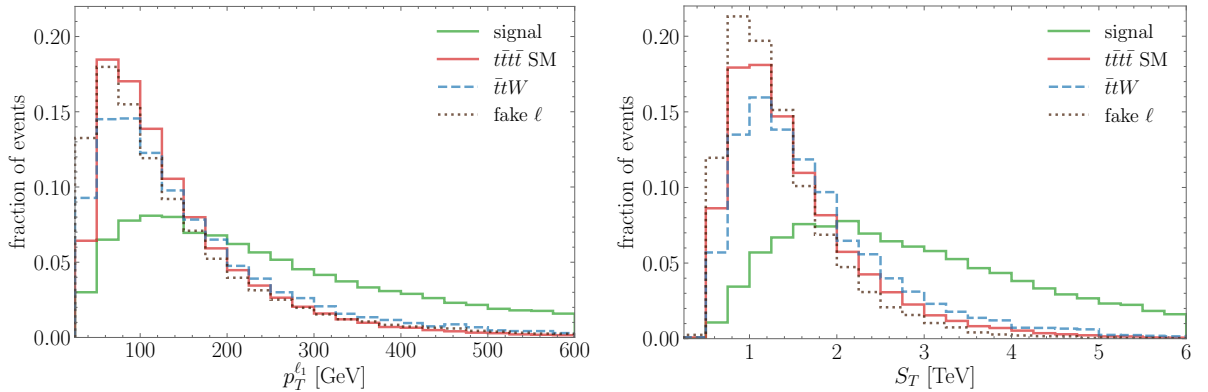
Figure 3.6: Normalized distributions of the leading lepton p_T (left) and the scalar sum of the transverse momenta of all jets and the two leptons (right), after the baseline SSL selection, for the signal and the main backgrounds.

	signal $\Lambda/\sqrt{|c_{tt}|} = 6\,\mathrm{TeV}$	$t\bar{t}t\bar{t}$ SM	$t\bar{t}W$	$t\bar{t}Z$	$t\bar{t}h$	other	fake ℓ	Qflip	$\mathcal{S}$ at 30/ab	S/B $[10^{-2}]$
baseline	43	17000	4200	2900	1800	920	5300	2200	1.3	0.13
$p_T^{\ell_1} > 275\,\mathrm{GeV}$	20	1600	670	300	110	120	590	130	1.8	0.55
$S_T \in [3,4]\,\mathrm{TeV}$	4.2	260	120	90	11	13	47	13	0.99	0.77
$S_T \in [4,5]\,\mathrm{TeV}$	3.1	110	56	1.0	5.4	6.0	15	4.1	1.2	1.6
$S_T > 5\,\mathrm{TeV}$	6.1	67	41	2.1	2.5	2.6	7.3	2.4	2.9	4.9

Table 3.3: Cut flow for the SSL final state, with cross-sections in ab. The (purely statistical) significance is defined as $\mathcal{S} = S/\sqrt{S+B}$, and a two-sided exclusion at $(1-p)$ CL corresponds to $\mathcal{S} = \sqrt{2}\,\mathrm{erf}^{-1}(1-p)$.

of events will match the SM expectation. We take $(\delta_{t\bar{t}t\bar{t}}, \delta_{t\bar{t}W}) = (8.5\%, 7.5\%)$ as reference values, obtained by halving the current theoretical uncertainties on the SM predictions [81]. The resulting 95% CL bound with $L = 30\,\mathrm{ab}^{-1}$ is

$$\Lambda/\sqrt{|c_{tt}|} > 6.1\,\mathrm{TeV}\ (\text{no syst.}: 6.9\,\mathrm{TeV})\,. \qquad \text{(FCC-hh, SSL)} \qquad (3.24)$$

3.3.2 Trileptons

In the trilepton channel the main backgrounds are the irreducible SM $t\bar{t}t\bar{t}$ production and the $t\bar{t}W$, $t\bar{t}Z$, $t\bar{t}h+$ jets processes. The full list of backgrounds we consider is given in Table 3.4, together with the MC generation-level cross-sections. We generate processes giving rise to three leptons and at least four jets at the matrix element level. The fake lepton background is generated using the same method as in the SSL analysis of Sec. 3.3.1, but applied to a different set of processes. The Qflip background is negligible, since no requirement is imposed on the lepton charges. The event selection is analogous to the one for SSL: after lepton and jet candidates are identified as in Eq. (3.20), we apply the same overlap removal procedure. In addition, the baseline selection requires

exactly three leptons with $p_T^\ell > 25\,\mathrm{GeV}\,,$

category	processes	decay channel	$\sigma \times$ BR [fb]
$t\bar{t}t\bar{t}$ (signal)	$t\bar{t}t\bar{t}$ $\Lambda/\sqrt{|c_{tt}|} = 6$ TeV	$W_{\ell^+}\, W_{\ell^-}\, W_{\ell^\pm}\, W_{\text{had}}$	0.206
$t\bar{t}t\bar{t}$ (SM)	$t\bar{t}t\bar{t}$	$W_{\ell^+}\, W_{\ell^-}\, W_{\ell^\pm}\, W_{\text{had}}$	90.9 [81]
$t\bar{t}W$	$t\bar{t}W^\pm jj$	$W_{\ell^+}\, W_{\ell^-}\, W_{\ell^\pm}$	63.4† [108]
$t\bar{t}Z$	$t\bar{t}Z + 0,1,2$ jets	$W_{\ell^\pm}\, W_{\text{had}}\, Z_{\ell^+\ell^-}$	1120 [107]
	$t\bar{t}Zjj$	$W_{\ell^+}\, W_{\ell^-}\, Z_{\ell^+\ell^-}$	82.6
$t\bar{t}h$	$t\bar{t}h, h \to WW^*$	$W_{\ell^+}\, W_{\ell^-}\, W_{\ell^\pm}\, W_{\text{had}}$	190 [107]
	$t\bar{t}h, h \to ZZ^*$	$W_{\ell^\pm}\, W_{\text{had}}\, Z_{\ell^+\ell^-}\, Z_{\text{had}}$	24.0 [107]
	$t\bar{t}h, h \to \tau^+\tau^-$	$W_{\ell^+}\, W_{\ell^-}\, \tau_{\ell^\pm}\, \tau_{\text{had}}$	44.2 [107]
other	$tZbjj$	$W_{\ell^\pm}\, Z_{\ell^+\ell^-}$	145
	$t\bar{t}W^+W^-$	$W_{\ell^+}\, W_{\ell^-}\, W_{\ell^\pm}\, W_{\text{had}}$	11.7
fake ℓ	$t\bar{t}jj$	$W_{\ell^+}\, W_{\ell^-}$	$K_{t\bar{t}}\, 4.63 \times 10^5$
	$t\bar{t}bjj$	$W_{\ell^+}\, W_{\ell^-}$	$K_{t\bar{t}}\, 1.06 \times 10^4$

Table 3.4: 3L signal and background processes at $\sqrt{s} = 100$ TeV. Samples with different jet multiplicities were merged using the MLM prescription with matching scale of 30GeV. The cuts $p_T^j > 50$GeV and $|\eta_j| < 5$ are imposed on jets arising from QCD radiation, but no cuts are applied to decay products of heavy particles. The subsequent baseline selection, discussed in Sec. 3.3.2, requires ≥ 4 jets, among which ≥ 3 are b-tagged. The higher-order cross-sections we use for normalization always assume $\mu = M_T/2$ (note that in [81] this is not the central choice for $t\bar{t}t\bar{t}$). The † indicates that $p_T^j > 100$GeV was exceptionally required, to match [108] (we have checked that this different initial cut has negligible impact on the event yield after the complete selection). Whenever they do not appear in $t\bar{t}$ or $b\bar{b}$ pairs, the symbols t and b refer to either particles or antiparticles. To the $t\bar{t}+$jets samples used to estimate the fake lepton background, we apply a $K_{t\bar{t}} = 1.4$.

	signal $\Lambda/\sqrt{|c_{tt}|} = 6$ TeV	$t\bar{t}t\bar{t}$ SM	$t\bar{t}W$	$t\bar{t}Z$	$t\bar{t}h$	other	fake ℓ	$\mathcal{S}$ at 30/ab	S/B [10^{-2}]
baseline	21	6700	570	1400	680	250	2100	1.1	0.18
$p_T^{\ell_1} > 275$GeV	13	1000	160	180	74	52	310	1.7	0.73
$S_T \in [3,4]$ TeV	2.9	160	35	13	9.4	6.4	33	0.99	1.1
$S_T \in [4,5]$ TeV	2.1	66	19	4.1	1.7	4.0	9.9	1.1	2.0
$S_T > 5$ TeV	3.7	39	16	4.1	1.4	1.9	6.9	2.4	5.3

Table 3.5: Cut flow for the 3L final state, with cross-sections in ab.

$$\geq 4 \text{ jets}\,, \text{ of which } \geq 3\ b\text{-tagged}\,, \qquad H_T > 400\text{GeV}\,, \qquad (3.25)$$

and events, where among the three leptons appears one opposite-sign, same-favor lepton pair satisfying $|m_{\ell_i^+\ell_i^-} - m_Z| < 15$GeV are vetoed, to suppress backgrounds containing a leptonic Z decay. The requirement of three leptons with $p_T^\ell > 25$GeV should allow for a straightforward triggering on these events. Notice that these selection requirements are orthogonal to those of the SSL analysis, which will ease the combination of the results.

After the baseline selection, for a reference BSM scale $\Lambda/\sqrt{|c_{tt}|} = 6$ TeV, we have $S/B \sim 2 \times 10^{-3}$, as shown in Table 3.5. Normalized distributions of $p_T^{\ell_1}$ and S_T at the baseline stage are shown in Fig. 3.7. We adopt the same additional cuts as for the SSL selection, namely
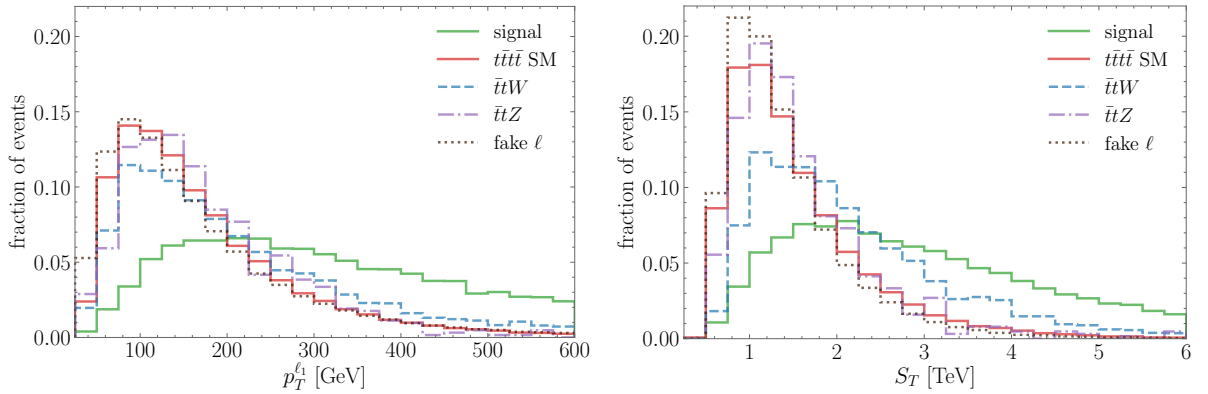
Figure 3.7: Normalized distributions of the leading lepton p_T (left) and the scalar sum of the transverse momenta of all jets and the three leptons (right), after the baseline 3L selection, for the signal and the main backgrounds.

$p_T^{\ell_1} > 275\,\text{GeV}$ and $S_T > 3\,\text{TeV}$, and divide the remaining events into three S_T bins, with S/B in the $(1\text{-}5) \times 10^{-2}$ range. We thus obtain at 95% CL

$$\Lambda/\sqrt{|c_{tt}|} > 5.8\,\text{TeV} \;\; (\text{no syst.:}\; 6.6\,\text{TeV})\,, \qquad (\text{FCC-hh, 3L}) \qquad (3.26)$$

where $L = 30\,\text{ab}^{-1}$ was assumed.

3.3.3 Same-sign dileptons and trileptons combination and discussion

We now combine the results in the SSL and 3L final states, by considering a joint χ^2 with 6 orthogonal bins. We obtain

$$\Lambda/\sqrt{|c_{tt}|} > 6.5\,\text{TeV} \;\; (\text{no syst.:}\; 7.3\,\text{TeV})\,, \qquad (\text{FCC-hh, SSL + 3L}) \qquad (3.27)$$

from $L = 30\,\text{ab}^{-1}$ and with the reference systematic uncertainties $(\delta_{t\bar{t}t\bar{t}}, \delta_{t\bar{t}W}) = (8.5\%, 7.5\%)$. The impact of varying these uncertainties is shown in the left panel of Fig. 3.8; we stress that we assume full correlation of each uncertainty across bins. In the right panel of Fig. 3.8 we display the dependence of the combined bound on the fake lepton probability, whose value at FCC-hh is unknown and which we have fixed based on a fit to LHC data. The Qflip background affects only the SSL analysis and is 3-4 times smaller than the fake lepton background in our benchmark scenario, so its impact remains small for any reasonable choice of the electron charge-flip probability $\varepsilon_{\text{flip}}$.

In addition, we want to ensure that our bounds arise from regions of phase space where the EFT expansion is under control. For this purpose, we show in Fig. 3.9 the combined SSL + 3L bound on $\Lambda/\sqrt{|c_{tt}|}$ obtained by discarding events where the largest parton-level invariant mass of a top quark pair is larger than m_*, which represents the mass of new resonances. Since it is not possible to tell on an event-by-event basis whether the hard scattering involved a $t\bar{t}$, tt, or $\bar{t}\bar{t}$ pair, we make the conservative choice to discard events where the largest invariant mass of *any* such combination is larger than m_*.

We now return to the role of the interference between the signal and SM $t\bar{t}t\bar{t}$ amplitudes. To quantify it, it is enough to work at the parton level, hence as a rough proxy for our signal region we consider the process $pp \to t t\bar{t}\bar{t}$, followed by SSL decays and including the cuts $p_T^{\ell_1} > 200\,\text{GeV}$
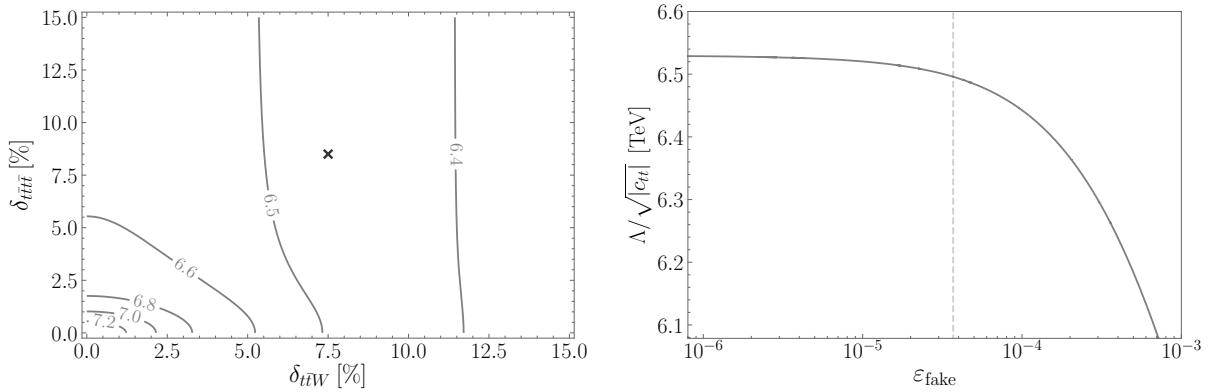
Figure 3.8: *Left:* contours of the 95% CL bound on $\Lambda/\sqrt{|c_{tt}|}$ in TeV, obtained by combining the SSL and 3L analyses, in the plane of systematic uncertainties on the two main SM backgrounds. The cross indicates our reference values. *Right:* Impact on the bound of varying the probability for a jet to give rise to a fake lepton. The dashed line indicates our baseline assumption.
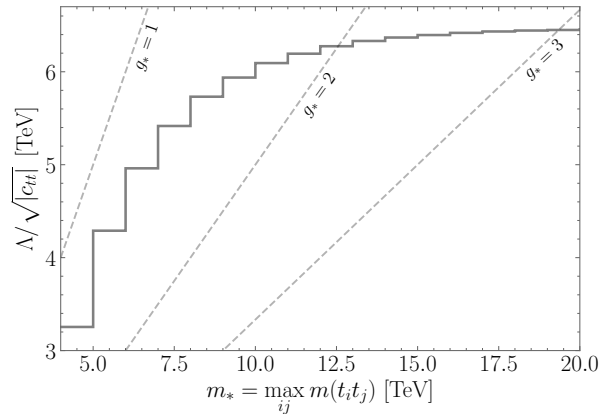
Figure 3.9: Combined SSL + 3L bound as a function of m_*, the maximal allowed parton-level invariant mass of any pair of top or antitop quarks. Dashed lines indicate contours of constant new-physics coupling $g_* = \sqrt{|c_{tt}|}\, m_*/\Lambda$.

and $H_T > 2\,\mathrm{TeV}$.[11] We find the leading order cross-section

$$\sigma(t\bar{t}t\bar{t})\,[\mathrm{fb}] = 1.5 + (0.3 \pm 0.3) \times 10^{-3}\, \frac{(6\,\mathrm{TeV})^2}{\Lambda^2/c_{tt}} + 0.071\, \frac{(6\,\mathrm{TeV})^4}{\Lambda^4/c_{tt}^2}\,, \qquad (3.28)$$

where the coefficients are obtained by fitting to a set of cross-sections calculated for varying c_{tt}/Λ^2, and the uncertainties on the SM and $O(c_{tt}^2)$ terms are negligible compared to the one on the linear term. This result confirms that interference can be safely neglected. The same conclusion applies to the 3L final state.

Finally, in Fig. 3.10 we show the impact of our combined SSL + 3L bound, Eq. (3.27), on the (m_*, g_*) parameter space of CH models, and compare it with other, complementary probes which will become available throughout the development of the FCC program.

Strikingly, four-top production at the FCC-hh provides the dominant sensitivity on the compositeness scale, $f|_{tt}^{\mathrm{FCC}} \gtrsim 6.5\,\mathrm{TeV}$, outperforming tests of Higgs coupling deformations associated

---

[11]For this check we only consider the dominant $O(\alpha_s^2)$ component of the SM amplitude.
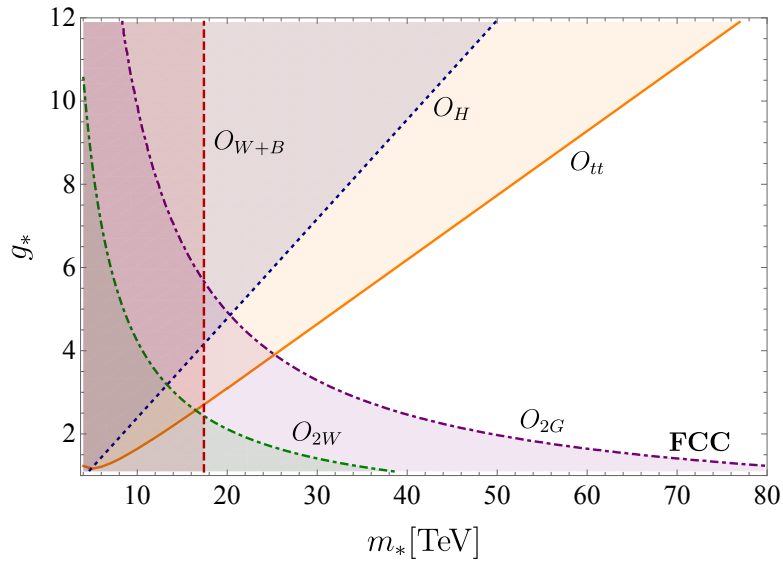
Figure 3.10: Future sensitivity at the FCC, including the ee/eh/hh stages, at 95% CL in the (m_*, g_*) plane of scenarios featuring a strongly interacting Higgs and (right-handed) top quark. The different limits are associated with constraints on individual operators, each dominating the corresponding observables in a certain region of parameter space (see main text for details). The limit on O_{tt} is derived using only FCC-hh.

with O_H, as combined in [112] which includes input from the HL-LHC and the FCC-ee, -eh, and -hh phases, resulting in $f|_H^{\mathrm{FCC}} \gtrsim 4.2\,\mathrm{TeV}$ at 95% CL. In addition, we show the projected constraint on O_W, O_B [112], namely $m_* > 17\,\mathrm{TeV}$ at 95% CL, as well as the expected FCC-hh bounds on O_{2W} and O_{2G}, derived from charged- and neutral-current dilepton production [112] (see also [69]), and high-energy dijet and inclusive jet production [68], respectively. These observables dominate the sensitivity for moderate strength of the new-physics coupling g_*. Finally, we mention that strong constraints are also expected from CP-violating observables: the limit on $\widetilde{O}_\gamma$ from the future measurement of the electron EDM by the ACME III experiment [113] reaches $m_* > 115\,\mathrm{TeV}$ at 95% CL. However, this probe is left out of Fig. 3.10 due to its inherently different nature, as already done in Fig. 3.1.

To conclude the discussion on multilepton final states, we want to note that the presented results would hold in the same way if instead of O_{tt} we had chosen O_{qq} or O_{tq} to generate the signal, since their respective amplitudes all show the same growth with energy (apart from possibly different color factors if the octet operators are chosen). But, of course, they would constrain different parts of the parameter space due to their different power counting behavior. A natural way to extend our analysis in a way that can distinguish between the various operators is to take also the top polarization into account. Because of the definite chirality of the quarks in the operator, this immediately fixes the polarization of all the quarks in the $tttt$ production. This would also increase the discriminating power of the signal with respect to the SM production, which is mostly unpolarized at the LHC because of unpolarized initial state and the vector like coupling of QCD [27].

3.3.4 Fully hadronic final state

Finally, we turn to the signature that arises when all four tops decay hadronically. This channel benefits from a large branching ratio of 20% and is intrinsically interesting because at the FCC-

hh the hadronic tops will frequently possess multi-TeV transverse momenta, entering a kinematic regime that is only marginally accessible at the LHC (for which the fully hadronic signature was discussed in [105], albeit assuming a resonant signal). While this happens already in the SM, the relative importance of ultra-boosted tops increases further in the presence of heavy new physics that generates O_{tt}. To obtain a first estimate of the reach, we perform a crudely simplified analysis that requires four top-tagged jets, relying on the performance of existing hadronic top tagging methods developed for the LHC, as studied by CMS [114]. As a first step, we generate the signal and the main backgrounds, which are $t\bar{t}t\bar{t}$, $t\bar{t}jj$ and $jjjj$ production in the SM, at parton level with a $p_T > 200$ GeV cut on each undecayed top or jet. The interference between the BSM and SM four-top amplitudes is neglected, since we are interested in the high-energy regime. We then include the branching ratios for hadronic top decays and apply, on an event-by-event basis, the p_T-dependent efficiencies and mistag rates extracted from [114].[12] Finally, we select highly energetic events by requiring the total invariant mass of the four final-state objects to be larger than 5.5 TeV and the sum of the transverse momenta to be larger than 4.5 TeV. Demanding $S/\sqrt{B} > 1.96$ for $L = 30 \, \text{ab}^{-1}$ we find the 95% CL bound

$$\Lambda/\sqrt{|c_{tt}|} > 6.0 \, \text{TeV} \, . \qquad \text{(FCC-hh, fully hadronic, estimate)} \qquad (3.29)$$

The corresponding signal cross-section is ≈ 1.0 ab and $S/B \approx 0.13$, which justifies omitting systematic uncertainties in first approximation. The background is dominated by SM four-top production with an $O(10)\%$ contribution from $t\bar{t}jj$, while $jjjj$ is negligible.

The estimate Eq. (3.29), although obtained through rough approximations, indicates a promising potential for the fully hadronic channel. However, requiring a large p_T for all four tops, as necessary to apply the results of [114], severely suppresses the signal rate, ultimately limiting the sensitivity. This motivates pursuing a different strategy, where the two hardest tops are tagged using jet substructure algorithms whereas the two softest tops are identified from their resolved decay-product jets; this is in consonance with the topology of our signal, which is characterized by a high-energy $t\bar{t} \to t\bar{t}$ scattering mediated by O_{tt}. The challenge of this approach is to retain a strong rejection capability against the $t\bar{t}jj$ background, in particular the configuration where the two tops have larger p_T's than the light jets', in which case the signal/background discriminating power must be obtained from the "soft" component of the event.

To study this problem, we generate SM four-top production and $t\bar{t}jj$ with hadronic top decays, using the MadGraph5_aMC@NLO – Pythia8 – Delphes3 chain. All final-state partons are required to have $p_T > 100$GeV, whereas the leading (subleading) jet is required to have $p_T > 900 \, (800)$GeV and the H_T must exceed 2 TeV. The only notable setup differences compared to the multilepton analyses are that we use the default Delphes card and set $R = 0.3$ for the (anti-k_t) jet clustering because using such narrower jets allows for a more efficient matching of the hadron- and parton-level objects, therefore easing the isolation of a $t\bar{t}jj$ sub-sample containing the configuration where the light jets are softer than the tops (which happens for $O(10)\%$ of the events). Two different strategies are investigated to separate this background from SM $t\bar{t}t\bar{t}$ production: one based on top invariant mass reconstruction, and one employing a neural network discriminant.

For the first strategy, we implement an algorithm which first removes the two hard jets that are matched to partonic tops, and then identifies two sets of up to three jets each, whose invariant masses are closest to m_t, with each set required to contain at least one b-tagged jet.

---

[12]For 200GeV $< p_T <$ 600GeV ($p_T > 600$GeV) we use the low-p_T (high-p_T) working point in Fig. 10 (Fig. 11) of [114], assuming the combination of jet substructure algorithms corresponding to the light green points. The efficiency and mistag rate are assumed constant for $p_T > 1.5$ TeV.

This method results in an 8% efficiency per event on SM four-top production and 0.4% on the background. For the second strategy, we use the same MC samples to train a three-layer neural network with 2910 neurons per layer, which takes as input features the p_T, η, ϕ, mass, number of tracks, and b-tag flag of up to 26 jets with $p_T > 50\,\text{GeV}$ in each event (including, in particular, the two hard jets which are matched to tops), as well as information on possible additional particles such as taus and photons, and on missing transverse energy. At the optimal threshold value the efficiency on SM four-top production is 16%, significantly higher than for the mass reconstruction procedure, but this comes at the price of a less effective background suppression of 4%. The above efficiencies are obtained neglecting systematic uncertainties.

Unfortunately, neither approach yields a satisfactory combination of signal efficiency and background rejection, resulting in weaker bounds on $\Lambda/\sqrt{|c_{tt}|}$ than the estimate in Eq. (3.29). Nevertheless, we believe that our attempts have only scratched the surface of the fully hadronic four-top final state, while uncovering some of the main obstacles that need to be overcome. The sensitivity of this channel is thus still waiting to be untapped, for instance through the development and application of FCC-tailored or machine learning-based top tagging algorithms (see e.g., [115–117]) that encompass both the resolved and boosted top regimes. Judging from our preliminary estimates, this channel has the potential to give the strongest constraint on the new-physics scale at the FCC-hh, further improving on our multilepton results.

3.4 Future electron-positron colliders

In this section, we show that future leptonic machines have much to inform on the fate of a strongly interacting top quark. The colliders under consideration are CLIC [118], the International Linear Collider (ILC) [119], and the FCC-ee [102]. We will not be carrying out any new analysis towards the extraction of their sensitivity to the dimension-six effective operators of interest, since this has been the subject of a number of detailed and comprehensive studies. Instead, we merely yet crucially reinterpret the relevant results in terms of the expected effects associated with a strongly interacting (right-handed) top quark, in particular via the four-top operator Eq. (3.1).[13] The different collider specifications can be found in the pertinent works: [121] for what regards the top sector, and [112] concerning universal effects, which we use to draw a comparison of both types of probes in the context of composite Higgs models. The runs from where most of the sensitivity to a composite top comes from are those at the highest energies: $\sqrt{s} = 3\,\text{TeV}$ ($L = 3\,\text{ab}^{-1}$) at CLIC, $\sqrt{s} = 1\,\text{TeV}$ ($L = 1\,\text{ab}^{-1}$) at ILC, and $\sqrt{s} = 365\,\text{GeV}$ ($L = 1.5\,\text{ab}^{-1}$) at FCC-ee.[14] This is because at linear colliders the best process to probe such type of physics is top-pair production, $e^+e^- \to t\bar{t}$. In our new-physics oriented analysis, we find that the largest effects are associated with the four-fermion operators

$$\frac{c_{te}}{\Lambda^2}(\bar{e}_R\gamma_\mu e_R)(\bar{t}_R\gamma^\mu t_R) + \frac{c_{t\ell}}{\Lambda^2}(\bar{\ell}_L\gamma_\mu \ell_L)(\bar{t}_R\gamma^\mu t_R)\,, \tag{3.30}$$

where both e_R and ℓ_L correspond to first-generation leptons. Since we consider a negligible degree of lepton compositeness, as motivated by their small Yukawa couplings, the largest contribution to the coefficients in Eq. (3.30) arises from operators of the form of Eq. (3.6), in particular from O_{tD} which, given the equation of motion Eq. (3.8), yields $c_{te} = g'c_{tD}$ and

---

[13]To some extent, our analysis resembles that of [120]. However, as in previous sections, we focus on a single operator at a time, the one leading to the largest sensitivity in a given region of the (m_*, g_*) parameter space, which is not always the same operator as claimed in that study. Besides, by considering exclusive constraints, we avoid issues associated with cancellations from different operators in a given observable.

[14]Notice the mildly different assumptions made for the luminosities and energies of these machines in [121] and [112].

$c_{t\ell} = g' c_{tD}/2$. What is important to notice is that at the relevant scale, $\mu = \sqrt{s}$, the coefficient of O_{tD} is dominated by the renormalization group evolution (RGE) (see App. I.A) contribution from the four-top operator O_{tt},

$$c_{tD}(\mu) = c_{tD}(m_*) + c_{tt}(m_*) \frac{32}{9} \frac{g'}{16\pi^2} \log\left(\frac{m_*^2}{\mu^2}\right), \tag{3.31}$$

for a mildly strong coupling g_*, since recall $c_{tD}/\Lambda^2 \sim g'/m_*^2$ and $c_{tt}/\Lambda^2 \sim g_*^2/m_*^2$ at the scale m_*, where the coefficients are generated. Therefore, a strongly interacting (right-handed) top quark leads to a new-physics amplitude that scales like

$$\mathcal{M}_{e^+e^- \to t\bar{t}} \sim \frac{g'^2}{16\pi^2} \frac{s}{f^2} \log\left(\frac{m_*^2}{s}\right). \tag{3.32}$$

From the expected 1σ sensitivity to the operator O_{te} at the 3 TeV CLIC, $c_{te}/\Lambda^2 < 1.6 \times 10^{-4}\,\text{TeV}^{-2}$ [121],[15] we arrive at the 95% CL bound on the compositeness scale

$$f|_{tt}^{\text{CLIC}} > 7.7\,\text{TeV}, \tag{3.33}$$

for $m_* = 4\pi f$ (to fix the size of the logarithm in Eq. (3.32)). This is stronger than the expected sensitivity to be achieved in Higgs measurements via the operator O_H, $f|_H^{\text{CLIC}} > 4.3\,\text{TeV}$ [112], also shown in Fig. 3.11 in the (m_*, g_*) plane. At the ILC the sensitivity via the four-top operator is comparatively lower, $f|_{tt}^{\text{ILC}} > 4.1\,\text{TeV}$ ($c_{te}/\Lambda^2 < 7 \times 10^{-4}\,\text{TeV}^{-2}$ [121]), yet similar to that from the Higgs. Finally, the importance of high collision energies for this type of probe is reflected in FCC-ee bounds on c_{te}, $c_{t\ell}$, which are approximately an order of magnitude weaker, yielding a significantly lower sensitivity $f|_{tt}^{\text{FCC-ee}} > 1.6\,\text{TeV}$ ($c_{te} < 4.3 \times 10^{-3}\,\text{TeV}^{-2}$ [121]), see Fig. 3.11.

Let us note at this point that our analysis of one operator at a time must be interpreted with a certain care, particularly in the case where several operators enter a given process. For instance, while the one-loop contribution from O_{tt} gives the leading non-standard effect in $e^+e^- \to t\bar{t}$ at large g_*, for small new-physics couplings other operators become comparable and eventually dominate, in particular the finite contribution to O_{tD} generated at m_*, see Eq. (3.31) (loops from other four-top operators in Eq. (3.4) are not enhanced by the strong coupling and thus always subleading). This implies that, in the transition region, cancellations could take place, reducing the sensitivity to new physics. Fortunately, this is not an issue that prevents us from probing those regions of parameter space, since they are tested in other processes via independent operators; specifically, tests of the operator O_{W+B} in electroweak precision data are expected to provide at CLIC the bound $m_* > 19\,\text{TeV}$ at 95% CL [112], independent of the new-physics coupling. The same holds at ILC and FCC-ee, even though, as shown in Fig. 3.11, the sensitivity to the resonance scale is somewhat lower.

The power of tests of the top sector in covering the parameter space of CH models goes beyond top-pair production. As already noted in [120], production of left-handed bottom pairs at lepton colliders is sensitive to effects that are enhanced at weak coupling, for instance via the operator $O_{qD}^{(3)}$ in Eq. (3.7) with $c_{qD}^{(3)}/\Lambda^2 \sim (y_t/g_*)^2 g/m_*^2$, which from the equations of motion contributes as a contact term to the amplitude for $e^+e^- \to b\bar{b}$. As we show in Fig. 3.11, this is superior to electroweak precision tests in the form of the W parameter, to be measured in e.g., $e^+e^- \to \mu^+\mu^-$ because the coefficient of $O_{qD}^{(3)}$ is enhanced by the top Yukawa coupling, $c_{qD}^{(3)}/(g\,c_{2W}) \sim (y_t/g)^2$, while the experimental precision in the two processes is expected to be comparable. In addition, it is worth noting that at CLIC and ILC, bottom-pair production could

---

[15] The experimental sensitivity to $O_{t\ell}$ is similar, but we neglect it in setting the limit because $c_{t\ell} = c_{te}/2$.
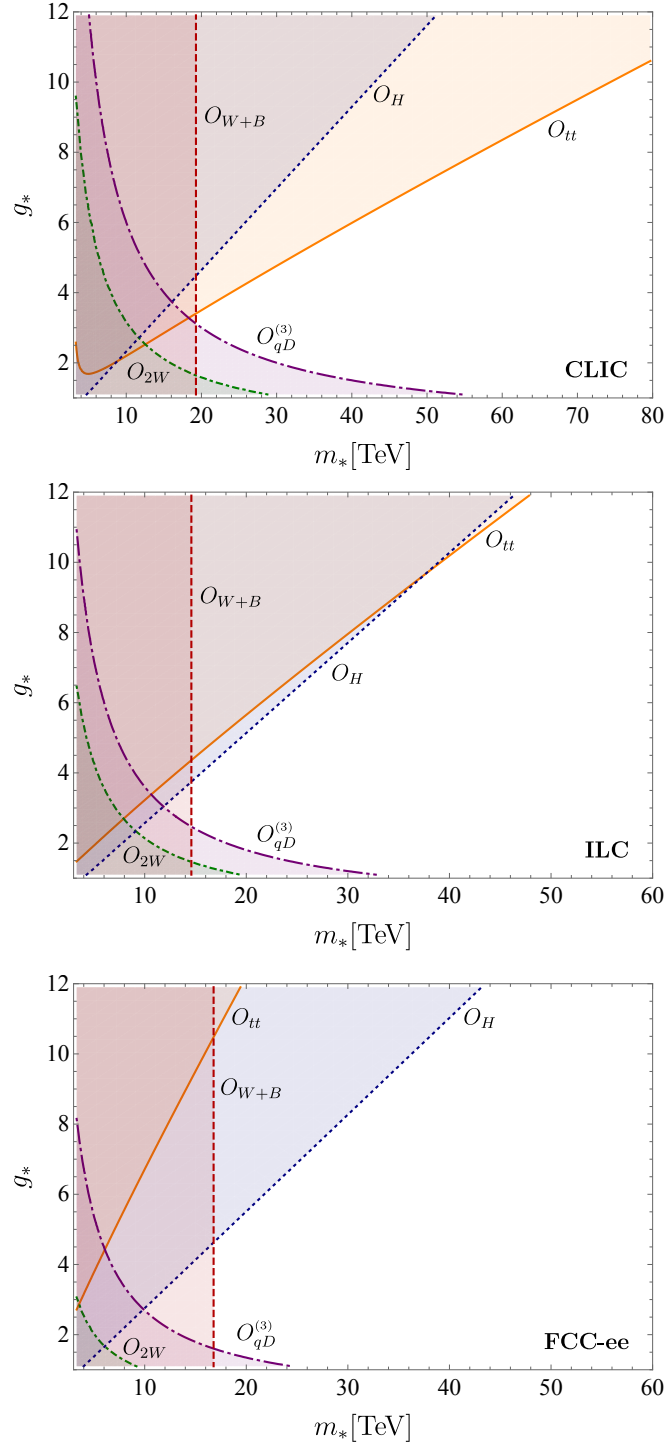
Figure 3.11: Future sensitivities at lepton colliders: CLIC (top), ILC (middle), and FCC-ee (bottom), at 95% CL in the (m_*, g_*) plane of scenarios featuring a strongly interacting Higgs and (right-handed) top quark. The different limits are associated with constraints on individual operators, each dominating the corresponding observables in a certain region of parameter space (see main text for details).

provide a non-negligible sensitivity to the masses of the composite resonances, independently of g_*, because of RGE (see App. I.A) effects associated with the four-top operator O_{tq} in Eq. (3.4),

$$c_{qD}(\mu) = c_{qD}(m_*) + c_{tq}(m_*)\frac{g'}{12\pi^2}\log\left(\frac{m_*^2}{\mu^2}\right). \tag{3.34}$$

Given that $c_{tq}/\Lambda^2 \sim y_t^2/m_*^2$, we find $m_*|_{tq}^{\mathrm{CLIC}} > 6.5\,\mathrm{TeV}$, a significant constraint, yet weaker than the sensitivity to be achieved from the S parameter (O_{W+B}).

Let us finally comment on the potential sensitivity from measurements of anomalous top and bottom couplings to the Z boson. Under our assumptions, both the corrections to the Zt_Rt_R and Zb_Lb_L couplings, dominated by O_{Ht} and $O_{Hq} + O_{Hq}^{(3)}$ respectively, do not receive large tree-level contributions, being protected by a P_{LR} symmetry. This then implies that the dominant contributions arise from the RGE associated with O_{Hq} and $O_{Hq}^{(3)}$ themselves and with the leading four-top operators in g_*, O_{tt} and O_{tq} (see App. I.A),

$$c_{Ht}(\mu) \simeq c_{tt}(m_*)\frac{y_t^2}{2\pi^2}\log\left(\frac{m_*^2}{\mu^2}\right), \tag{3.35}$$

$$c_{Hq}(\mu) + c_{Hq}^{(3)}(\mu) \simeq [3c_{tq}(m_*) + 4c_{Hq}^{(3)}(m_*)]\frac{y_t^2}{16\pi^2}\log\left(\frac{m_*^2}{\mu^2}\right), \tag{3.36}$$

where we set $c_{Hq}(m_*) + c_{Hq}^{(3)}(m_*) \simeq 0$ and neglected gauge coupling terms, which are relatively suppressed by $(g/y_t)^2$ [122]. We find that the expected precision on these couplings [112, 121] is not high enough to give rise to any constraint at the level of those already discussed. In fact, not even measurements of the Zt_Lt_L coupling, which receives relatively large corrections $(c_{Hq} - c_{Hq}^{(3)})/\Lambda^2 \sim y_t^2/m_*^2$ and for which the prospective exclusive 1σ bound is, e.g., at the ILC, $0.075\,\mathrm{TeV}^{-2}$ [121], can compete with universal probes. Dropping P_{LR} symmetry, i.e., for $c_{Ht}/\Lambda^2 \sim 1/f^2$ and $(c_{Hq} + c_{Hq}^{(3)})/\Lambda^2 \sim y_t^2/m_*^2$, the situation at CLIC and ILC is actually not much different. For instance, at the ILC $c_{Ht}/\Lambda^2 < 0.15\,\mathrm{TeV}^{-2}$ at 95% CL [121], which leads to $f|_{Ht}^{\mathrm{ILC}} > 2.6\,\mathrm{TeV}$, a weaker sensitivity than from $e^+e^- \to t\bar{t}$, even though the latter is loop suppressed. Likewise, from $(c_{Hq} + c_{Hq}^{(3)})/\Lambda^2 < 0.019\,\mathrm{TeV}^{-2}$ [112] we find $m_*|_{Hq}^{\mathrm{CLIC}} > 10\,\mathrm{TeV}$, lower than the scale to be reached with electroweak precision data. At the FCC-ee instead, the absence of P_{LR} would make a difference since, as we discussed, the lower $\sqrt{s}$ penalizes the effects of contact interactions. We find $f|_{Ht}^{\mathrm{FCC\text{-}ee}} > 1.8\,\mathrm{TeV}$, which, however, is still below the expected compositeness scale probed with Higgs measurements, while $m_*|_{Hq}^{\mathrm{FCC\text{-}ee}} > 24\,\mathrm{TeV}$, under optimistic assumptions on the systematics of the bottom forward-backward asymmetry [112].

Chapter 4

Conclusions

In this part of the thesis, we have shown that some of the proposed high-energy colliders have an outstanding sensitivity to four-top operators, which constitute telltale signs of a strongly interacting top quark. Focusing on the $O_{tt} = (\bar{t}_R \gamma_\mu t_R)^2$ operator (with coefficient c_{tt}/Λ^2), we have performed realistic analyses of four-top production at the FCC-hh in the same-sign dilepton and trilepton final states, and inspected the fully hadronic final state. We have also reinterpreted previous results to constrain O_{tt} at future high-energy lepton colliders, through its one-loop renormalization group contributions to top-pair production. We have obtained the following 95% CL bounds,

$$
\begin{aligned}
\text{FCC-hh}^{pp \to t\bar{t}t\bar{t}}_{100\,\text{TeV},\ 30\,\text{ab}^{-1}} : \qquad & \Lambda/\sqrt{|c_{tt}|} > 6.5\,\text{TeV}\,, \\
\text{CLIC}^{e^+e^- \to t\bar{t}}_{3\,\text{TeV},\ 3\,\text{ab}^{-1}} : \qquad & \Lambda/\sqrt{|c_{tt}|} > 7.7\,\text{TeV}\,, \\
\text{ILC}^{e^+e^- \to t\bar{t}}_{1\,\text{TeV},\ 1\,\text{ab}^{-1}} : \qquad & \Lambda/\sqrt{|c_{tt}|} > 4.1\,\text{TeV}\,.
\end{aligned}
\tag{4.1}
$$

For context, the 13 TeV LHC limit as derived from a combination of $t\bar{t}t\bar{t}$ final states is $\Lambda/\sqrt{|c_{tt}|} > 0.73\,\text{TeV}$, based on approximately $36\,\text{fb}^{-1}$. Thus, a tantalizing result of our study is that both the FCC-hh and CLIC at its highest-energy run would increase by an order of magnitude the reach on the scale of new physics. Note that to achieve the bound for the FCC-hh, we only exploited the high-energy behavior of O_{tt} and that it could potentially be even improved if its special polarization characteristics are also considered, which could make it easier to distinguish SM from BSM production. In contrast, the lower energy FCC-ee (365GeV, $1.5\,\text{ab}^{-1}$) displays a significantly milder reach of $\Lambda/\sqrt{|c_{tt}|} > 1.6\,\text{TeV}$.

In addition, we have studied the moderate excesses of events observed by ATLAS and CMS in their LHC Run 2 measurements of $t\bar{t}t\bar{t}$, $t\bar{t}W$, $t\bar{t}Z$, and $t\bar{t}h$ in multilepton plus jets final states. We have attempted a first interpretation of these results in the context of heavy physics beyond the SM, examining the latest CMS four-top search in terms of the operators O_{tt} and O_{Ht}, the latter of which modifies the $Zt_R t_R$ coupling with respect to the SM. While far from conclusive, our analysis strongly suggests that a new-physics scale of around $0.75\,\text{TeV}$ could improve the agreement with multilepton + jets data, while remaining consistent with other competing measurements, notably in the Higgs sector. Further studies are warranted, both at the phenomenological level, including a more comprehensive set of measurements, and at the experimental level, where a complete modelling of the impact of higher-dimensional operators can be achieved. A well-motivated set would include, beyond O_{tt} and O_{Ht}, the operator O_{y_t}, which controls non-standard contributions to the htt coupling; these three operators are weakly con-

strained by other measurements, yet their coefficients are expected to be large.[1] In general, the current status of top data provides additional motivation to investigate the new-physics scenarios discussed in this part of the thesis.

Looking ahead, our FCC-hh analysis of O_{tt} in multilepton final states can be repurposed to derive the reach on other four-top operators, which may play a central role under different theoretical assumptions. On the other hand, exploiting the whole potential of the fully hadronic signature requires a targeted study. Furthermore, the indirect sensitivity attainable at a multi-TeV muon collider remains to be explored [123].

Finally, we stress the importance of our results for composite Higgs models, where minimal fine-tuning and electroweak precision data point towards a fully composite right-handed top quark. With the scales of compositeness that we have shown are to be reached, future high-energy colliders will push the concept of naturalness of the electroweak scale to a whole new level, perhaps one where the SM is no longer.

---

[1] A more comprehensive set would incorporate O_H and $O_{Hq}^{(3)}$ (with $c_{Hq} = -c_{Hq}^{(3)}$) as well, which modify respectively the hVV and Wt_Lb_L couplings. The former is of relevance in e.g. th production.

Appendices part I

I.A Running Induced by Four-Fermion Operators

In this appendix, we want to show explicitly how to get the loop contributions shown in Eqs. (3.11), (3.31) and (3.34). The relevant 1-loop diagram is shown in Fig. I.A.1 after choosing the appropriate external states. We will work in the broken phase of the SM; however, we will not rotate the gauge sector to keep the hypercharge boson B^μ. This way, we can calculate the running of operators with an extra Higgs field using the same diagram we use for the renormalization of c_{tD} and $c_{tD}^{(8)}$, while in the unbroken phase diagrams with at least one additional Higgs field would have been necessary.

I.A.1 Loops with external t_R

Starting with the hypercharge boson and writing down the amplitude, we find two independent Lorentz structures with momentum dependent form factors

$$\mathcal{M} = \frac{g'(N_c+1)}{4\pi^2}\frac{c_{tt}}{\Lambda^2}(\bar{t}_R\gamma_\mu t_R)B_\nu\left[F_1(q^2)(q_\mu q_\nu - q^2 g^{\mu\nu}) + m_t^2 F_2(q^2)g^{\mu\nu}\right], \qquad \text{(I.A.1)}$$

with q the momentum of the gauge boson. In the above construction, we chose to name the fermion spinors and gauge boson polarization vector such that it will be easy to match operator structures later, and we suppressed the trivially contracted color indices. Regularizing the loop integral in $D = 4 - 2\epsilon$ space-time dimensions, the form factors turn out to be

$$F_1(q^2) = Y_R \int_0^1 dx\; x(1-x)\left(\frac{1}{\epsilon} - \log\left(\frac{m_t^2 - (1-x)x\,q^2}{\mu^2}\right)\right) + \mathcal{O}(\epsilon) \qquad \text{(I.A.2)}$$

$$F_2(q^2) = (Y_R - Y_L)\int_0^1 dx\left(\frac{1}{\epsilon} - \log\left(\frac{m_t^2 - (1-x)x\,q^2}{\mu^2}\right)\right) + \mathcal{O}(\epsilon), \qquad \text{(I.A.3)}$$

with Y_R and Y_L the U(1) hypercharges of the right- and left-handed top, respectively. Notice that, even though O_{tt} contains only right-handed tops, F_2 picks up a contribution proportional to the left-handed hypercharge. In fact, the form factor F_2 comes with explicit factors of the top mass, or equivalently the top Yukawa in the unbroken phase, signalling the presence of a Higgs field responsible for the needed chirality flip.

Using these results, we can easily match the 1-loop amplitude to the corresponding tree amplitudes after realizing that

$$i(H^\dagger \overset{\leftrightarrow}{D}_\mu H)(\bar{t}_R\gamma^\mu t_R) \supset \frac{g'v^2}{2}(\bar{t}_R\gamma^\mu t_R)B_\mu, \qquad \text{(I.A.4)}$$

if we set the Higgs to its VEV v.
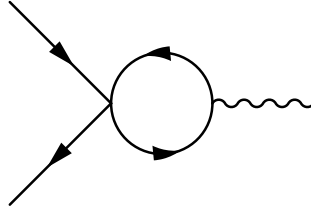
Figure I.A.1: Relevant 1-loop diagram for the renormalization of the two-fermion operators relevant in this part.

To renormalize the UV divergence, we define

$$c_i^{\text{ren}}(q^2) = c_i(q^2) + \delta c_i \tag{I.A.5}$$

and we estimate the counterterm as

$$\delta c_i = -c_i(m_*^2). \tag{I.A.6}$$

Then, putting everything together and plugging in the values for the hypercharges and $N_c = 3$, we arrive at

$$c_{tD}^{\text{ren}} = c_{tD}(m_*) + c_{tt} \; \frac{32}{9} \frac{g'}{16\pi^2} \log\left(\frac{m_*^2}{q^2}\right), \tag{I.A.7}$$

$$c_{Ht}^{\text{ren}} = c_{Ht}(m_*^2) + c_{tt} \; 8\frac{y_t^2}{16\pi^2} \log\left(\frac{m_*^2}{q^2}\right). \tag{I.A.8}$$

The calculation for the gluon is completely analogous, and the form factors are the same as for the hypercharge boson after setting $Y_R = Y_L = 1$ and $g' \to g_s$. We see, immediately, that this sets $F_2(q^2) \equiv 0$, as it should be, since the Higgs field does not couple to the gluon, so no gluonic operator analogous to O_{Ht} exists. In total, we find

$$c_{tD}^{(8),ren} = c_{tD}^{(8)}(m_*) + c_{tt} \; \frac{4}{3} \frac{g_s}{16\pi^2} \log\left(\frac{m_*^2}{q^2}\right). \tag{I.A.9}$$

Note, that technically we only calculated the running of an operator of the form

$$(\partial^\mu G_{\mu\nu}^A)(\bar{t}_R \gamma^\nu t^A t_R). \tag{I.A.10}$$

This is of course not gauge invariant, and we have to replace the ordinary derivative with a covariant one. Therefore, we can, as cross-check, calculate with an additional gluon, which, by gauge invariance, has to give the same result as Eq. (3.11). These diagrams are shown in Fig. I.A.2.

Because of the two ways of contracting both the spinor and color indices in the four-fermion vertex, each diagram Fig. I.A.2 contains two terms with different color structures. Only one of those, the non-trivial contraction of adjoint indices, can be matched onto O_{Ht} and we checked explicitly that the terms with the trivial contraction do not diverge, such that they don't contribute to the running of c_{Ht}.
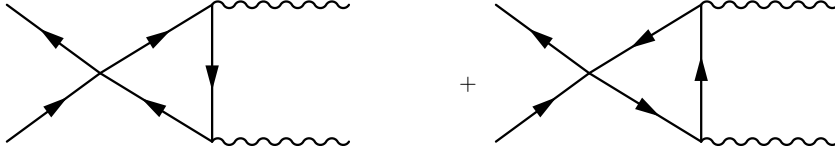
Figure I.A.2: Relevant 1-loop diagrams for the renormalization $c_{tD}^{(8)}$. Note that the calculation of this diagram serves merely as a cross-check for the calculation of the diagram in I.A.1, since gauge-invariance forces them to have the same divergent and logarithmic term for external gluon.

To simplify the calculation, we only calculate the divergent part of the diagram, as this is sufficient to check gauge invariance, and we find

$$i\mathcal{M} = \frac{1}{\epsilon}\frac{4}{3}\frac{g_s^2}{16\pi^2} f^{ABC} T^C G^{\nu A} G^{\mu B} \, \bar{t}_R \left[g_{\mu\nu}(\slashed{k}_1 - \slashed{k}_2) + (2k_2 + k_1)_\mu \gamma_\nu - (2k_1 + k_2)_\nu \gamma_\mu \right] t_R. \tag{I.A.11}$$

After matching to the relevant tree-level expression, we are left with the divergent part

$$c_{tD}^{(8)} = c_{tt}\frac{1}{\epsilon}\frac{4}{3}\frac{g_s^2}{16\pi^2}, \tag{I.A.12}$$

matching the coefficient of the logarithm in Eq. (3.11), as it should be.

I.A.2 Loops with external t_L

Starting with the insertion of O_{tq} we find a structure very similar to the insertion of O_{tt},

$$\mathcal{M} = \frac{g' N_c}{2\pi^2}\frac{c_{tq}}{\Lambda^2}(\bar{t}_L \gamma_\mu t_L) B_\nu \left[F_1(q^2)(q_\mu q_\nu - q^2 g^{\mu\nu}) + m_t^2 F_2(q^2) g^{\mu\nu} \right], \tag{I.A.13}$$

with the form factors defined in Eqs. (I.A.2), (I.A.3). Again subtracting the divergence at $q^2 = m_*^2$ and plugging in the specific values we find for the renormalized coefficients

$$c_{tD}^{\text{ren}} = c_{tD}(m_*) + c_{tq} \frac{2}{3}\frac{g'}{16\pi^2} \log\left(\frac{m_*^2}{q^2}\right), \tag{I.A.14}$$

$$c_{Ht}^{\text{ren}} = c_{Hq}^{\text{ren}}(m_*^2) + c_{tq} \, 3\frac{y_t^2}{16\pi^2} \log\left(\frac{m_*^2}{q^2}\right). \tag{I.A.15}$$

Part II

Electric Dipole Moments as Low-Energy Probes of New Physics

Chapter 5

Motivation and Introduction

The intrinsic angular momentum of a particle couples to external electric and magnetic fields, with strengths characterized by the electric and magnetic dipole moments, respectively. For a spin-1/2 fermion f the non-relativistic Hamiltonian describing these interactions is given by

$$\mathcal{H}_{NR} = \frac{a_f\,eQ_f}{2m_f}\,\boldsymbol{\sigma}\cdot\boldsymbol{B} - d_f\,\boldsymbol{\sigma}\cdot\boldsymbol{E}\,, \tag{5.1}$$

where $\boldsymbol{\sigma}$ is the vector of Pauli matrices (related to the spin operator $\boldsymbol{s} = \boldsymbol{\sigma}/2$), d_f and a_f are the electric and magnetic dipole moments of the fermion and Q_f and m_f are its charge and mass. Already from this classical expression we can deduce the transformation properties of the magnetic and electric dipole moments, respectively, under CP: if the theory is invariant under CP, the only term in Eq. (5.1) which is allowed is the coupling to the magnetic field. The corresponding relativistic Lagrangian is

$$\mathcal{L} = -\frac{a_f eQ_f}{4m_f}\bar{\psi}\,\sigma^{\mu\nu}\psi\,F_{\mu\nu} - \frac{i}{2}d_f\bar{\psi}\,\sigma^{\mu\nu}\gamma_5\psi\,F_{\mu\nu}\,. \tag{5.2}$$

where the second term, barring the factor i, changes sign under a CP transformation due to the presence of the γ_5 matrix.

For this part of this thesis, it is more convenient to use chiral fermions, and we can rewrite the Lagrangian in Eq. (5.2) such that it becomes

$$\mathcal{L} = \frac{c_{f\gamma}}{\Lambda}\,\bar{\psi}_L\,\sigma^{\mu\nu}\psi_R\,F_{\mu\nu} + \text{h.c.}\,. \tag{5.3}$$

In the above equation, we included explicitly a scale Λ for dimensional reasons, such that $c_{f\gamma}$ is dimensionless. By comparing Eqs. (5.2), (5.3) we can relate the coefficient $c_{f\gamma}$ with the dipole moments a_f and d_f and we find

$$a_f = -\frac{4m_f}{eQ_f}\frac{\text{Re}\,[c_{f\gamma}]}{\Lambda}, \qquad d_f = -2\,\frac{\text{Im}\,[c_{f\gamma}]}{\Lambda}\,. \tag{5.4}$$

If not further specified, all operators of the form of Eq. (5.3), i.e., also those built from other vector fields, will be called low-energy dipole operators collectively throughout this work.

While the magnetic moment of the electron has been measured with extraordinary precision [124, 125], there is no experimental evidence for the electric moment of neither the electron nor of all other leptons as well as the neutron. Instead, currently only upper bounds can be given by experiments [126–129],

$$|d_e| < 1.1 \times 10^{-29} \; e \cdot \text{cm} \,,$$
$$|d_\mu| < 1.5 \times 10^{-19} \; e \cdot \text{cm} \,,$$
$$|d_\tau| < 1.6 \times 10^{-18} \; e \cdot \text{cm} \,,$$
$$|d_n| < 1.8 \times 10^{-26} \; e \cdot \text{cm} \,,$$

(5.5)

while the prospected bounds on the electron EDM[1] at the ACME III experiment and on the neutron EDM at n2EDM are [113, 131]

$$|d_e| < 0.3 \times 10^{-30} \; e \cdot \text{cm} \,,$$
$$|d_n| < 10^{-27} \; e \cdot \text{cm} \,.$$

(5.6)

Even though these bounds show incredible sensitivities to electric dipole moments, there is still much room for new physics to hide between the experimental bounds and the estimated SM values. In fact, they are estimated to be [132–136] [2]

$$d_e \sim 10^{-48} \; e \cdot \text{cm} \,,$$
$$d_n \sim 10^{-32} \; e \cdot \text{cm} \,,$$

(5.7)

well below even the proposed future experimental reaches.

Nevertheless, this tiny SM background encourages the usage of EDMs as probes of new physics, simply for the reason that if future experiments measure EDMs of sizes larger than Eq. (5.7), they provide a solid proof of CP violating new physics. As it turns out and depending on the effective operator, the bounds on, e.g., the electron EDM require new physics at very high scales in order for it to be consistent with the experiment, or equivalently, new physics at lower scales would give large contributions to the EDMs. One result presented in this part of the thesis is that the electron EDM acquires, among others, contributions like

$$d_e \simeq -1.1 \times 10^{-29} e \cdot \text{cm} \, \frac{\text{Im}\left[C_{eB}\atop{11}\right]}{g' y_e} \left(\frac{1350\,\text{TeV}}{\Lambda}\right)^2 \,,$$

(5.8)

which does not carry any loop suppression and comes from a tree level Feynman diagram with $O_{eB} = \left(\bar{L}_L \sigma^{\mu\nu} e_R\right) H B_{\mu\nu}$ insertion. In the above expression, we divided the Wilson coefficient by its expected size $g' y_e$ (more on this in Sec. 8.5 and Table 8.2), where g' is the $U(1)_Y$ coupling and y_e the electron Yukawa coupling, and Λ is the scale of new physics. As the formula shows, if $\text{Im}\left[C_{eB}\atop{11}\right] \sim g' y_e$ the scale of the CP violating new physics contributing to the EDMs is bounded to be larger than $\sim 10^3$ TeV.

The constraining power of EDMs has stimulated plenty of different analyses in various UV completions of the SM. There are several studies of the electron and neutron EDMs in SUSY models [138–141], in Composite Higgs models [14, 142, 143], in Leptoquark models [144–147], in complex two-Higgs and three-Higgs doublet models [148–154], in scotogenic models [155] and in the context of dark matter [156]. On the model independent side, Ref. [157] provides an analysis of the electron EDM including some contributions that arise at 2-loop and at dimension-8 level, while Ref. [158] studies the complete 1-loop expression for the lepton magnetic moments.

---

[1]Also the bound on the muon EDM might be improved, by three orders of magnitudes, at a future Muon Collider [130].

[2]Note that the perturbative estimates of the electron EDM could be exceeded by long-distance effects by several orders of magnitude [137].

Ref. [159] studies the neutron EDM in presence of an effective CP violating Higgs-gluon interaction encoded by a dimension-6 SMEFT operator and Ref. [160] analyses the contribution to the neutron EDM induced by chromo-dipoles of second and third generation quarks. Other studies of EDMs in the presence of dimension-6 interactions involving the Higgs boson and fermion fields – in particular related to top physics – are performed in [161–170].

The purpose of the present work is to study the lepton and neutron EDMs to 1-loop accuracy in the presence of new physics at some scale $\Lambda \gg v$, going to $\mathcal{O}(\Lambda^{-2})$. New physics effects are parametrized in a model independent way within the SMEFT, which we expanded in the Warsaw basis [171]. We will provide the complete 1-loop expressions of the low energy EDMs observables, for leptons as well as for the neutron, in terms of the Wilson coefficients of the Warsaw basis, including both RG flow effects and finite terms. In fact, while for extremely large-scale separations the logarithmic contributions are expected to be larger than the corresponding finite terms, for $\Lambda \lesssim 10$ TeV we find them to be comparable. A complete 1-loop result is a step towards a higher accuracy in the theoretical predictions for EDMs observables, which will be measured with increased precision in future experiments. As a matter of fact, having accurate results would turn out crucial in the event of a non-zero measurement of a fermion EDM.

Partial results of these calculations can be found scattered throughout the literature: the derivation of the RGE within SMEFT has been performed in [172–174], both the tree level matching of the SMEFT to the low energy effective field theory (LEFT) as well as the LEFT RGE can be found in [175, 176] and the loop-level matching of the SMEFT to the LEFT has been calculated in [177]. Although these resources are useful in their own right, they cannot be used to obtain the full 1-loop correction to the EDM.

In the context of the loop corrections to the EDMs, we only refer to individual diagrams that appeared in the calculation whenever necessary, the full set of diagrams considered for this chapter can be found in Appendix A of [6].

We will begin this part by discussing the EDM observables in the SM, arguing why they are so highly suppressed using symmetry arguments, as well as defining the relevant set of operators contribution beyond the SM in Chapter 6. In the same chapter, we also define the neutron EDM in terms of the elementary dipole moments of the neutron's constituents. Then, in Chapter 7 we introduce the basics needed to perform renormalization. In particular, we show how to arrive at the RGE for individual Lagrangian parameters. In addition, we introduce selection rules based on both helicity arguments and angular momentum conservation that allow us to determine the pattern of renormalization in an EFT without the need of performing loop integrals. Having defined the necessary ingredients and techniques, we go into the details of the calculations of the full 1-loop expressions of both the electron and the neutron EDM in Chapter 8. We explicitly define all the calculation schemes employed in this part and explain how we perform gauge fixing and how redundant operators, i.e., operators that were not originally part of the operator basis used, are needed to renormalize all appearing divergences. In the same chapter, we also present the results and discuss the origin of non-rational, finite functions in multiscale theories, like the SMEFT in the broken phase. Again, we focus on illustrating the impact of terms not associated with the RG running of the Wilson coefficient, which have largely been overlooked in the literature. As is expected for theories with massless particles, here the photon and the gluon, infrared divergences arise during the calculation and necessitate a different approach than ultraviolet ones. We then conclude this part in Chapter 9.

Chapters 6 and 8 as well as Appendices II.A and II.B are heavily based on [6], from where all figures, tables, results, and large parts of the text have been taken.

Chapter 6

Electric Dipole Moments in the SM and Beyond

In this chapter, we want to discuss the different contributions to both the electron as well as the neutron EDM within the SM and beyond. We start by defining both the electron as well as neutron EDMs in terms of coefficients of higher dimensional operators. For the electron, this will overlap with the discussion presented already in the introduction, due to the electron being an elementary particle. The story is, however, different for the neutron, which we know is a bound state made up of elementary quarks and gluons. Both the electric and chromo-electric, i.e., their coupling to the QCD equivalent to the QED electric field, of the individual constituents combine into the total neutron EDM. In principle, there is also a contribution of the topological QCD θ-term related to the QCD vacuum structure, which can, however, be removed by the well-known Peccei-Quinn mechanism [2] at the cost of introducing the axion field. Then, in Sec. 6.1 and Sec. 6.2, respectively, we will investigate the strong suppression of both the electron and neutron EDM in the SM using symmetry arguments, as well as how contributions from CP violating new physics could dominate over the small SM background.

6.1   Within in the SM

As the dipole operator is an irrelevant operator, it is clear that within the SM these operators cannot be generated through RG effects. Nevertheless, they do acquire finite contributions from loop corrections to the $\bar{\psi}\psi\gamma$ vertex. While the leading contribution to a_f arises already at 1-loop, first calculated by Schwinger in 1948 [178], the EDM d_f receives contributions only starting at three loops, in the quark case, and at four loops, in the electron case, which makes them tiny. The natural question that arises is how such a suppression can arise. For this, it will be instructive to consider the parametric estimate for the electron EDM, which can be estimated to be

$$d_e \sim e \frac{m_e}{m_W^2} \frac{g^6 g_s^2}{(16\pi^2)^4} \left(\frac{v}{m_W}\right)^{12} J_{CP} \,. \tag{6.1}$$

This expression makes the small size explicit. A CP odd physical amplitude, respecting the symmetries of the model, must be a combination of invariants, under (non-physical) changes of basis and field redefinitions, which should be a function of the complex phases responsible for the CP violation. We focus here on the flavor source for CP violating effects; the size of CP odd observables can therefore be estimated exploiting an analysis of the flavor structure

and symmetries of the model. In the absence of Yukawa interactions, the SM, with massless neutrinos, is invariant under the global flavor symmetry [179]

$$G_F = U(3)^5 = U(3)_Q \times U(3)_u \times U(3)_d \times U(3)_L \times U(3)_e, \qquad (6.2)$$

where $i = Q, u, d, L, e$ stands for the left-handed quarks, right-handed up and down quarks and left- and right-handed leptons, respectively, each of them with the corresponding gauge multiplicity. Each of these fermion species transforms as a triplet under its respective $U(3)$ and as a singlet under the remaining ones. Now, the Yukawa interactions break this symmetry explicitly, mixing different fermion species, and assuming this breaking is small due to the small Yukawas[1] we can formally reinstate G_F-invariance by promoting the Yukawa couplings to spurions in flavor space. The assumption that this is the only explicit breaking of G_F is known as Minimal Flavor Violation (MFV) [182–184]; MFV is exact within the SM and can be extended to the full flavor structure of the SMEFT.

In such MFV scenarios, the flavor structure, as well as any flavored CP violation effect, is completely determined by the Yukawa spurions. Ignoring the QCD θ term and neutrino masses, the only source of CP violation in the SM lies in the complex CKM phase in the quark sector; thus, any CP odd quantity must necessarily be built from quark Yukawas. This allows us to estimate the size of the EDMs as functions of $y_{u,d}$ in such a way that the lepton $\bar{L}\sigma_{\mu\nu}d_e y_e e F^{\mu\nu}$ and quark $\bar{Q}\sigma_{\mu\nu}d_{u(d)}y_{u(d)}u(d)F^{\mu\nu}$ dipoles are G_F invariants, where we have factored the y_f Yukawa out of the d_f dipole moments. Since the lepton EDM is a singlet under quark flavor transformations, it must be proportional to the identity matrix times an invariant built from the quark Yukawas. This is the well-known Jarlskog invariant [185]

$$J_{CP} = \frac{1}{2i} \det \left\{ \left[y_u \left(y_u \right)^\dagger, y_d \left(y_d \right)^\dagger \right] \right\} \sim 10^{-22} . \qquad (6.3)$$

which is the single basis independent CP violating quantity in the SM, so it necessarily has to appear in Eq. (6.1). Actually, the Jarlskog invariant is related to the rephasing invariant J of the CKM matrix in the following way: $J_{CP} \approx \frac{m_b^4 m_s^2 m_c^2}{v^8} J$ [184]. The number of Yukawa matrices appearing in Eq. (6.3) can be translated into the the fact that J_{CP}, for the lepton EDM, can only be generated at the 3-loop level or higher. In fact, due to the symmetry properties of the Jarlskog invariant under exchange of up and down quarks an additional gauge loop is needed, such that the lepton EDMs can only be generated at the 4-loop level [184]. This high loop suppression, together with large mass suppression in the Jarlskog invariant, explains the smallness of the lepton EDMs, as seen in Eq. (6.1). A representative Feynman diagram is shown in Fig. 6.1

Similar considerations apply to the quark EDMs, although $d_{u(d)}$ is not a flavor invariant, but rather transforms as an octet of $U(3)_Q$. It should therefore be a non-traced chain of $y_{u(d)}y_{u(d)}^\dagger$ products, and it turns out that it needs to contain at least 8 quark Yukawas and can be generated at the three-loop level (c.f. Fig. 6.1), already including the additional loop needed for amplitude to have the correct symmetries. The imaginary parts of entries of the matrix are again functions of the Jarlskog invariant, which parameterizes all CP violation in the SM, but are less suppressed with respect to the lepton case: they can be 10 orders of magnitudes larger than J_{CP}. For more details, see, e.g., [184].

---

[1]Here we ignore the fact that the top Yukawa is large, $y_t \sim 1$ such that it cannot be considered as a small breaking parameter. One possibility to account for this is to choose the formally unbroken flavor symmetry to act only on the first two generations of fermions [180, 181]
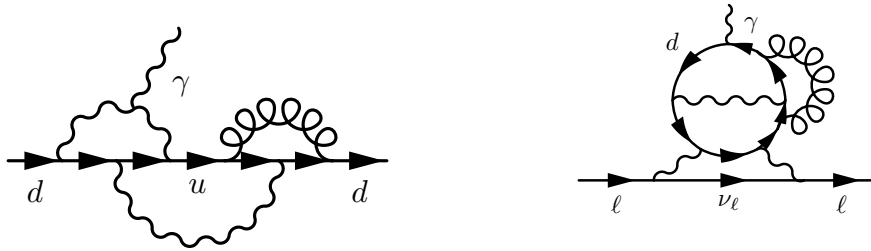
Figure 6.1: Representative Feynman diagrams for the leading SM contributions to the quark *(left)* and the lepton *(right)* EDMs. For the up-quark EDM, the labels d and u have to be exchanged in the left diagram. Unlabeled wiggly lines correspond to W bosons.

6.2 Beyond the SM

The situation explained in the previous section changes drastically in the presence of heavy new physics. The plethora of new, effective operators, in general including CP violating ones, give rise to new phases, which can enter physical observables through other basis invariants than the Jarlskog invariant. In the context of the SMEFT these invariants have been systematically characterized in [186].

In the phase of unbroken EW symmetry, the SMEFT operators relevant for the discussion of EDMs are the ones containing the hypercharge and weak gauge bosons B and W^I, respectively.

To ensure gauge invariance, these operators have to contain an additional Higgs doublet compared to the expression in Eq. (5.2) to compensate for the transformation of the left-handed fermion doublet. They have the form

$$O_{fB} = \left(\bar{\psi}_L \sigma^{\mu\nu} \psi_R\right) \overset{(\sim)}{H} B_{\mu\nu} \quad \text{and} \quad O_{fW} = \left(\bar{\psi}_L \sigma^{\mu\nu} \sigma^I \psi_R\right) \overset{(\sim)}{H} W^I_{\mu\nu}. \tag{6.4}$$

It is easy to see that these reduce to the low-energy dipole operator Eq. (5.3) in the broken phase, by setting the Higgs field to its VEV and performing the appropriate rotation in the gauge sector. This allows us to extract the energy eigenstates and their Wilson coefficients in both phases are related by

$$c_{f\gamma} = \frac{v}{\Lambda} \left(c_w\, c_{fB} + 2T_f^3 s_w\, c_{fW}\right), \tag{6.5}$$

where we defined the trigonometric function of the weak mixing angle $c_w \equiv \cos\theta_w$ and $s_w \equiv \sin\theta_w$ and T_f^3 is the third component of the weak isospin for the respective fermion and is non-zero only for left-handed chiralities.

We already discussed in the previous section, that in the SM the photonic dipole operator can only receive rational contributions at very high loop orders because marginal operators cannot renormalize higher-dimensional ones. If we are, however, in the SMEFT, there are many more dimension-6 operators present, a substantial amount of which can renormalize the dipole operators already at 1-loop. Because the EDMs are low-energy observables, all coefficients have to be evaluated at the scale of the corresponding experiment using the RGE we will discuss in Chapter 7. Then, depending on the scale at which these effective operators are generated by integrating out heavy new physics, the scale separation between the new physics and the electroweak scale solving the RGEs can generate potentially large logarithms, which could easily dominate over the tiny SM value.

$$O^{(3)}_{\underset{abcd}{lequ}} = \left(\bar{L}^{ja}_L \, \sigma_{\mu\nu} e^b_R\right)\epsilon_{jk}\left(\bar{Q}^{kc}_L \, \sigma_{\mu\nu} u^d_R\right)$$

$$O^{(1)}_{\underset{abcd}{quqd}} = \left(\bar{Q}^{ja}_L \, u^b_R\right)\epsilon_{jk}\left(\bar{Q}^{kc}_L \, d^d_R\right)$$

$$O^{(8)}_{\underset{abcd}{quqd}} = \left(\bar{Q}^{ja}_L \, T^A u^b_R\right)\epsilon_{jk}\left(\bar{Q}^{kc}_L \, T^A d^d_R\right)$$

$$O_{\underset{abcd}{le}} = \left(\bar{L}^a_L \gamma_\mu L^b_L\right)\left(\bar{e}^c_R \gamma_\mu e^d_R\right)$$

$$O^{(1)}_{\underset{abcd}{qu}} = \left(\bar{Q}^a_L \gamma_\mu Q^b_L\right)\left(\bar{u}^c_R \gamma_\mu u^d_R\right)$$

$$O^{(8)}_{\underset{abcd}{qu}} = \left(\bar{Q}^a_L \gamma_\mu T^A Q^b_L\right)\left(\bar{u}^c_R \gamma_\mu T^A u^d_R\right)$$

$$O^{(1)}_{\underset{abcd}{qd}} = \left(\bar{Q}^a_L \gamma_\mu Q^b_L\right)\left(\bar{d}^c_R \gamma_\mu d^d_R\right)$$

$$O^{(8)}_{\underset{abcd}{qd}} = \left(\bar{Q}^a_L \gamma_\mu T^A Q^b_L\right)\left(\bar{d}^c_R \gamma_\mu T^A d^d_R\right)$$

$$O^{(1)}_{\underset{abcd}{ud}} = \left(\bar{u}^a_R \gamma_\mu u^b_R\right)\left(\bar{d}^c_R \gamma_\mu d^d_R\right)$$

$$O^{(8)}_{\underset{abcd}{ud}} = \left(\bar{u}^a_R \gamma_\mu T^A u^b_R\right)\left(\bar{d}^c_R \gamma_\mu T^A d^d_R\right)$$

$$O_{\underset{ab}{eB}} = \left(\bar{L}^a_L \sigma^{\mu\nu} e^b_R\right) H B_{\mu\nu}$$

$$O_{\underset{ab}{eW}} = \left(\bar{L}^a_L \sigma^{\mu\nu} \sigma^I e^b_R\right) H W^I_{\mu\nu},$$

$$O_{\underset{ab}{uB}} = \left(\bar{Q}^a_L \sigma^{\mu\nu} u^b_R\right) \widetilde{H} B_{\mu\nu}$$

$$O_{\underset{ab}{uW}} = \left(\bar{Q}^a_L \sigma^{\mu\nu} \sigma^I u^b_R\right) \widetilde{H} W^I_{\mu\nu},$$

$$O_{\underset{ab}{dB}} = \left(\bar{Q}^a_L \sigma^{\mu\nu} d^b_R\right) H B_{\mu\nu}$$

$$O_{\underset{ab}{dW}} = \left(\bar{Q}^a_L \sigma^{\mu\nu} d^b_R\right) H W^I_{\mu\nu}$$

$$O_{\underset{ab}{uG}} = \left(\bar{Q}^a_L \sigma^{\mu\nu} T^A u^b_R\right) \widetilde{H} G^A_{\mu\nu}$$

$$O_{\underset{ab}{dG}} = \left(\bar{Q}^a_L \sigma^{\mu\nu} T^A d^b_R\right) H G^A_{\mu\nu},$$

$$O_{\widetilde{W}} = \epsilon^{IJK} \widetilde{W}^{I\nu}_\mu W^{J\rho}_\nu W^{K\mu}_\rho$$

$$O_{\widetilde{G}} = f^{ABC} \widetilde{G}^{A\nu}_\mu G^{B\rho}_\nu G^{C\mu}_\rho$$

$$O_{H\widetilde{B}} = H^\dagger H B^{\mu\nu} \widetilde{B}_{\mu\nu}$$

$$O_{\widetilde{W}} = H^\dagger H W^{I\mu\nu} \widetilde{W}^I_{\mu\nu}$$

$$O_{HW\widetilde{B}} = (H^\dagger \sigma^I H) W^{I\mu\nu} \widetilde{B}_{\mu\nu}$$

$$O_{H\widetilde{G}} = H^\dagger H G^{A\mu\nu} \widetilde{G}^A_{\mu\nu}$$

$$O_{\underset{ab}{Hud}} = i\left(\widetilde{H}^\dagger D_\mu H\right)\left(\bar{u}^a_R \gamma^\mu d^b_R\right)$$

$$O_{\underset{ab}{dH}} = H^\dagger H \left(\bar{Q}^a_L \, d^b_R \, H\right)$$

$$O_{\underset{ab}{uH}} = H^\dagger H \left(\bar{Q}^a_L \, u^b_R \, \widetilde{H}\right)$$

Table 6.1: Set of dimension-6 SMEFT operators relevant in this part of the thesis, grouped in six different boxes corresponding to the different classes discussed in the main text. The operators $O^{(1,8)}_{ud}$ as well as the $\psi^2 H^3$ type operators can only be probed at the 1-loop level through the neutron EDM. The dashed line separates the 4-fermion operators of the form ψ^4 and those of the form $\psi^2\bar{\psi}^2$. We use the usual definitions $\widetilde{H} = i\sigma^2 H^*$ and $\widetilde{F}_{\mu\nu} = \frac{1}{2}\epsilon_{\mu\nu\alpha\beta} F^{\alpha\beta}$ for F any of the gauge bosons. For the operators $O^{(3)}_{lequ}$ and $O^{(1,8)}_{quqd}$ we show SU(2) indices j, k explicitly. For the vector operators in the 4-fermion class, the only CP violation can arise if the flavors of the fermions in each current are not identical. Hence, we explicitly give the generation indices a, b, c, d.

In practice, one way to determine the effect on the low-energy observable EDM coming from some new physics, that is matched onto the SMEFT at some scale $\Lambda > v$, is to calculate the running of the SMEFT dipole operators, to be introduced in the next section, down to the EW scale, to match these operators onto the respective LEFT operators and finally calculate the loop contributions within the LEFT. To perform the full 1-loop calculation we do not choose

the multi-stage procedure described above, but instead go directly to the phase of broken EW symmetry, with all the SM fields in the (physical) basis of mass and electric charge eigenstates, and calculate all virtual effects at once, expressing our result in terms of the SMEFT coefficients in the Warsaw basis evaluated at the scale Λ above the scale of EW symmetry breaking.

The set of relevant operators contributing to both the electron and neutron EDM is summarized in Table 6.1. To reduce the full Warsaw basis to the ones given in Table 6.1, we used the selection rules explained in Sec. 7.2.

6.3 Dipole moments of non-elementary particles: neutron EDM

So far, we have considered only fundamental particles within the SMEFT. But, as already mentioned in the introduction, another prominent observable apart from the lepton EDMs is the electric dipole moment of the neutron. Being a composite state built from quarks and gluons, we can write the neutron EDM as a function of the constituents' EDMs and chromo-electric dipole moments (cEDMs). The latter are defined as the coefficient of the CP odd operator in Eq. (5.2), but with a gluonic field strength instead of the photonic one. Putting everything together, we find [159, 187–195]

$$
\begin{aligned}
d_n = & -(0.204 \pm 0.011)\, d_u + (0.784 \pm 0.028)\, d_d - (0.0027 \pm 0.0016)\, d_s + \\
& + 0.055(1 \pm 0.5)\, \hat{d}_u + 0.111(1 \pm 0.5)\, \hat{d}_d - 51.2(1 \pm 0.5)\, e \cdot \text{MeV}\, \frac{C_{\tilde{G}}}{\Lambda^2} + \\
& - 9.22(1^{+2.33}_{-0.67})\, e \cdot \text{MeV}\, \frac{\text{Im}[C_{Hud}]}{\Lambda^2} + \\
& - 0.615(1^{+1}_{-0.75})\, e \cdot \text{GeV}\, \left(\frac{\text{Im}[c^{(\text{S1,RR})}_{ud} - c^{(\text{S1,RR})}_{duud}]}{\Lambda^2} + \frac{\text{Im}[c^{(\text{S8,RR})}_{ud} - c^{(\text{S8,RR})}_{duud}]}{\Lambda^2} \right).
\end{aligned}
\tag{6.6}
$$

where the "11" and "1111" subscripts of the Wilson coefficients in the last two lines indicate that the first flavor generation is taken into account.

The first three terms are contributions from the up, down and strange quark EDMs, respectively, the next two terms are the effects of the up and down quark cEDMs and the last term of the second line comes directly from the dimension-6 Weinberg operator [196] built from three gluons,

$$
O_{\tilde{G}} = f^{ABC} G^{A\nu}_\mu G^{B\rho}_\nu \tilde{G}^{C\mu}_\rho,
\tag{6.7}
$$

that can be interpreted as the cEDM of the gluon. The contributions in the third and fourth lines are related to the SMEFT operators

$$
\begin{aligned}
O_{Hud} &= (\bar{u}\gamma_\mu d)(\tilde{H}^\dagger i D^\mu H)\,, \\
O^{(1)}_{quqd} &= (\bar{q}^r u)\epsilon_{rs}(\bar{q}^s d)\,, \\
O^{(8)}_{quqd} &= (\bar{q}^r T^A u)\epsilon_{rs}(\bar{q}^s T^A d)\,.
\end{aligned}
\tag{6.8}
$$

Furthermore, $c^{(\text{S1,RR})}_{ud}$ and $c^{(\text{S1,RR})}_{duud}$ are the Wilson coefficients of the following operators of the low energy effective field theory [175–177]

$$
\begin{aligned}
O^{(\text{S1,RR})}_{ud} &= (\bar{u}_L u_R)(\bar{d}_L d_R)\,, \\
O^{(\text{S1,RR})}_{duud} &= (\bar{d}_L u_R)(\bar{u}_L d_R)\,,
\end{aligned}
\tag{6.9}
$$

which are generated, below the electroweak scale, at tree level by $O^{(1)}_{quqd}$ and at 1-loop level by $O^{(8)}_{quqd}$. The tree level matching conditions are the following,

$$
\begin{aligned}
O^{(\text{S1,RR})}_{\underset{1111}{ud}} &= O^{(1)}_{\underset{1111}{quqd}}, \\
O^{(\text{S1,RR})}_{\underset{1111}{duud}} &= -O^{(1)}_{\underset{1111}{quqd}},
\end{aligned}
\tag{6.10}
$$

where the fermion fields are in the mass basis defined in Sec. 8.1. Analogously, $c^{(\text{S8,RR})}_{ud}$ and $c^{(\text{S8,RR})}_{duud}$ are the Wilson coefficients of

$$
\begin{aligned}
O^{(\text{S8,RR})}_{ud} &= (\bar{u}_L T^A u_R)(\bar{d}_L T^A d_R), \\
O^{(\text{S8,RR})}_{duud} &= (\bar{d}_L T^A u_R)(\bar{u}_L T^A d_R),
\end{aligned}
\tag{6.11}
$$

which are generated at tree level by $O^{(8)}_{quqd}$ and at 1-loop level by $O^{(1)}_{quqd}$, with the following tree level matching conditions

$$
\begin{aligned}
O^{(\text{S8,RR})}_{\underset{1111}{ud}} &= O^{(8)}_{\underset{1111}{quqd}}, \\
O^{(\text{S8,RR})}_{\underset{1111}{duud}} &= -O^{(8)}_{\underset{1111}{quqd}}.
\end{aligned}
\tag{6.12}
$$

All the terms in the third and fourth lines of Eq. (6.6) describe the contributions from CP violating low energy four-fermion interactions. In fact, below the electroweak scale, also O_{Hud} generates four-quark operators through a tree level exchange of a W boson between the right-handed fermion current of the dimension-6 operator and a left-handed current which has an SM coupling with the W. All the coefficients appearing in the above expression should be evaluated at the hadronic scale μ_H that characterizes the neutron EDM. To be more rigorous, in the case of C_{Hud} what is evaluated at energy scales below the EW scale are the coefficients of the four-quark operators generated after integrating out the heavy SM particles from the SMEFT, which is to say $(\bar{u}_L \gamma_\mu d_L)(\bar{d}_R \gamma^\mu u_R)$ at tree level and $(\bar{u}_L \gamma_\mu T^A d_L)(\bar{d}_R \gamma^\mu T^A u_R)$ at 1-loop level. Note that while $C_{\widetilde{G}}$, C_{Hud}, $c^{(\text{S1(8),RR})}_{ud}$ and $c^{(\text{S1(8),RR})}_{duud}$ are dimensionless, the fermionic dipole coefficients have the dimension of an inverse energy ($d_i, \hat{d}_i \sim v/\Lambda^2$).

As we have just discussed, the neutron EDM does not only receive contributions from the EDMs and cEDMs of the quarks. This allows operators to be probed, that would otherwise only be available at higher loop orders, if at all. One example would be the Yukawa type operators $\psi^2 H^3$. At the 1-loop level, they cannot be accessed by EDMs of elementary particles, as they contribute only starting at the 2-loop order. However, as they give 1-loop contributions to O_{Hud}, which enters the neutron EDM also at tree level, one can probe them at a lower order as naively expected.

In the expression of the neutron EDM we implicitly assumed a Peccei-Quinn mechanism [2] to remove the contribution from the well-known QCD $\theta-$term

$$
\mathcal{L}_\theta \sim \bar{\theta} \, \text{Tr} \left[G^{\mu\nu} \widetilde{G}_{\mu\nu} \right],
\tag{6.13}
$$

which otherwise would give the dominant effect on the neutron EDM. Here $\bar{\theta}$ is a linear combination of a bare θ parameter and the argument of the determinant of the quark Yukawa couplings [197]. On top of introducing the usual term that removes the contribution of the QCD θ-term, the Peccei-Quinn mechanism induces a shift on the axion potential due to the presence of the chromo dipole operators. In return, this shift modifies the coefficients for the light quark cEDMs and completely cancels the effect of the strange quark cEDM [189, 198, 199].

At this point, we want to stress that the results presented in this thesis can in principle be used for any function of the neutron EDM in terms of quark (c)EDMs, which might differ from (6.6).

Chapter 7

Renormalization and Operator Mixing

In this chapter, we discuss the renormalization and possible mixing patterns of interaction operators, including also higher-dimensional ones. In particular, we show how the RGE for coupling constant of these operators can be obtained from their respective counterterms, specifically the single pole term, while the higher pole terms arising at higher loop orders have to satisfy certain consistency conditions to ensure the finiteness of the coupling anomalous dimension or, equivalently, the beta function. Further, we investigate general arguments based on both helicity and angular momentum considerations to find and explain zeroes in the one-loop anomalous dimension matrix.

7.1 Coupling renormalization

Given the SM together with some set of higher-dimensional operator (here, we will focus mainly on those of dimension-6), we can write the total Lagrangian as

$$\mathcal{L} = \mathcal{L}_{0,\text{SM}} + \sum_{d>4} \sum_i c_{0,i}^{(d)} \frac{O_{0,i}^{(d)}}{\Lambda_{\text{SM}}^{d-4}}. \tag{7.1}$$

The subscript denotes the fact that we wrote the Lagrangian in terms of bare couplings $c_{0,i}$ and fields Φ_0. When calculating scattering amplitudes using the bare Lagrangian, the results are, in general, not UV finite when going beyond the tree level approximation. However, we can make sense of these divergences by rewriting all the bare quantities in terms of finite, or renormalized, ones, which we denote by simply dropping the subscript "0", and multiplicative divergent constants Z as

$$c_{0,i} = \mu^{n\epsilon} Z_{c_i} c_i, \quad \Phi_0 = Z_\Phi^{1/2} \Phi. \tag{7.2}$$

We introduced an arbitrary renormalization scale μ, which ensures that the renormalized coupling has a constant mass dimension when evaluating loop integrals in $D = 4 - 2\epsilon$ dimensions. The integer n depends on the field content of the operator associated to c_i.

In the weak coupling regime, the renormalization constants Z allow for a perturbative expansion

$$Z_i = 1 + \delta_i, \tag{7.3}$$

where the counterterm δ itself is a power series in the small coupling. Depending on the renormalization scheme, the renormalization constants can contain finite pieces beyond the tree level one, but in this part of the thesis we will exclusively use the $\overline{\text{MS}}$ scheme in which all loop contributions to Z will be purely divergent. This, in turn, lets us write the renormalization constants as a power series in ϵ, which will be useful shortly,

$$Z_i = 1 + \sum_{l=1} \frac{C_i^{(l)}}{\epsilon^l}, \tag{7.4}$$

where each $C^{(l)}$ itself can be written as an perturbative expansion in the coupling.

Plugging Eq. (7.4) into Eq. (7.1), the tree level contribution gives back the original Lagrangian, but now expressed in terms of renormalized objects, while the higher-order terms generate additional vertices, the so-called counterterm Lagrangian. Note that the counterterm Lagrangian will also contain 2-point interactions coming from the expansion of the kinetic terms in the bare Lagrangian. In the end, all of these new vertices are responsible for the cancellation of divergences in correlation functions of renormalized field. In fact, in the $\overline{\text{MS}}$ scheme, the condition to exactly cancel any appearing divergence is how the counterterms are determined in practice.

Since the choice of μ is arbitrary, bare quantities cannot depend on its explicit value, which immediately implies that the renormalized couplings and operators have to depend on μ in such a way that cancels the explicit dependence in Eq. (7.2),

$$\mu \frac{d}{d\mu} c_{0,i} = \mu \frac{d}{d\mu} \big(\mu^{n\epsilon} Z_{c_i} c_i \big) = 0. \tag{7.5}$$

Expanding the derivative using the product rule, we quickly arrive at the RGE for the coupling

$$\mu \frac{d}{d\mu} c_i = -n\epsilon c_i - \gamma_{c_i} c_i, \tag{7.6}$$

where we defined the anomalous dimension γ_c as

$$\gamma_{c_i} = (Z_{c_i})^{-1} \mu \frac{d}{d\mu} Z_{c_i}. \tag{7.7}$$

Note that the entire right-hand side of Eq. (7.6) is often also referred to as the negative of the beta function $\beta = -(n\epsilon + \gamma_{c_i})c_i$. Moreover, in four dimensions, i.e., $\epsilon \to 0$, the first term in Eq. (7.6) vanishes, however, it will be important shortly.

In general, various operators can contribute to each other through renormalization, so the RGE is really a matrix equation and treating the c_i as components of a vector of couplings can write the bare couplings as $c_i^{(0)} = \mu^{n\epsilon}(Z_c)_{ij} c_j$, such that Eq. (7.6) easily generalizes to include the effect of operator mixing

$$\mu \frac{d}{d\mu} c_i = -(\gamma_c)_{ij} c_j,, \tag{7.8}$$

with the anomalous dimension matrix

$$(\gamma_c)_{ij} = (Z_c^{-1})_{ik} \ \mu \frac{d}{d\mu} (Z_c)_{kj}. \tag{7.9}$$

Using, for simplicity, the one-dimensional case, we can now show that the anomalous dimension of a coupling can easily be calculated from the single pole term in the coupling renormalization constant at any order, which is tightly related to the finiteness of γ_{c_i} in the limit $\epsilon \to 0$. First, we plug Eq. (7.4) into the definition of the anomalous dimension and using the fact that the coefficients $C^{(l)}$ depend only implicitly on the scale μ through their dependence on the couplings, we can write

$$\sum_{l=0} \gamma_{c_i} \frac{C^{(l)}}{\epsilon^l} = \sum_{l=1} \frac{\beta}{\epsilon^l} \frac{d}{dc_i} C^{(l)}, \tag{7.10}$$

where we defined $C^{(0)} \equiv 1$ and already used the definition of the beta function as the derivative of the coupling with respect to μ. Then, plugging in the explicit form of β, or equivalently the right-hand side of Eq. (7.6), keeping also seemingly vanishing term linear in ϵ, we find

$$\sum_{l=0} \gamma_{c_i} \frac{C^{(l)}}{\epsilon^l} = -\sum_{l=0} \frac{1}{\epsilon^l} \left[nc_i \frac{d}{dc_i} C^{(l+1)} + \gamma_{c_i} \frac{d}{dc_i} C^{(l)} \right], \tag{7.11}$$

Finally, by comparing powers of ϵ on both sides of the equation, the $n = 0$ term gives us a finite relation between the anomalous dimension and the single pole term in Z_{c_i},

$$\gamma_{c_i} = -nc_i \frac{d}{dc_i} C^{(1)}, \tag{7.12}$$

while the higher-order pole terms have to satisfy a consistency condition which completely determines them in terms of lower-order ones,

$$nc_i \frac{d}{dc_i} C^{(l+1)} = \gamma_{c_i} C^{(l)} - \gamma_{c_i} \frac{d}{dc_i} C^{(l)}. \tag{7.13}$$

Note that Eq. (7.12) is the same for any anomalous dimension defined from other renormalization constant, e.g., the ones for fields and composite operators. Eq. (7.13), on the other hand, has to be slightly modified, by replacing γ_{c_i} in the first term on the right-hand side by the appropriate anomalous dimension, while keeping the coupling anomalous dimension in the second term. The above equations can easily be generalized to the case of multiple couplings that undergo mixing under renormalization by appropriately summing the contributions coming from different couplings.

Now that we know how to calculate the anomalous dimension from the single pole counterterm, the only thing left to do is to determine the counterterm itself. To do so, we make use of the fact that instead of renormalizing couplings and field separately, we can renormalize each term in the Lagrangian as a whole by

$$\mu^{-n\epsilon} c_{0,i} O_{0,i} = Z_{O_i} c_i O_i. \tag{7.14}$$

In the $\overline{\text{MS}}$ scheme, the operator renormalization constant allows for the same series expansion as for the coupling and field renormalization constants. By plugging this expression back into the Lagrangian, it is easy to see that the counterterms in Z_{O_i} capture all divergences appearing in one-particle irreducibe (1PI) diagrams. Then we can relate the renormalization constants of operators to that of their respective coupling,

$$\mu^{-n\epsilon} c_{0,i} O_{0,i} = Z_{O_i} c_i O_i = Z_{c_i} \left(\prod_{j \in \text{fields}} Z_j^{1/2} \right) c_i O_i, \tag{7.15}$$

where the product runs over all fields appearing in the operator. Comparing the two expressions, we can easily identify

$$Z_{c_i} = Z_{O_i} \left(\prod_{j \in \text{fields}} Z_j^{-1/2} \right), \tag{7.16}$$

which can be expanded order by order in perturbation theory.

To summarize, we can calculate the renormalization of any coupling c_i by calculating the Z_{O_i} from the divergences appearing in the loop corrections to the vertex associated to O_i, as well as the field renormalization constants for each field appearing in O_i, and combining them according to Eq. (7.16) to obtain Z_{c_i} at the desired order in perturbation theory.

Coupling renormalization as it was discussed in this section is the method of choice employed for the calculation of the loop corrections to various EDMs discussed in Chapter 8.

Additional care has to be taken if there are particles with the same charge in the theory. In this case, they can mix at the loop level, such that it is not enough to introduce only a renormalization constant for the fields, but also those for the mixing have to be included. An example relevant for this thesis is the EW part of the SM after symmetry breaking, where the photon and the Z boson can mix through loops. To take care of all divergences, we therefore introduce a (non-diagonal) matrix of renormalization constants as

$$\begin{pmatrix} A_0 \\ Z_0 \end{pmatrix} = \begin{pmatrix} Z_{AA}^{1/2} & Z_{AZ}^{1/2} \\ Z_{ZA}^{1/2} & Z_{ZZ}^{1/2} \end{pmatrix} \begin{pmatrix} A \\ Z \end{pmatrix} = \begin{pmatrix} 1 + \frac{1}{2}\delta_{AA} & \frac{1}{2}\delta_{AZ} \\ \frac{1}{2}\delta_{ZA} & 1 + \frac{1}{2}\delta_{ZZ} \end{pmatrix} \begin{pmatrix} A \\ Z \end{pmatrix}. \tag{7.17}$$

We see that this is non-diagonal only beyond tree-level, and plugging this into the bare Lagrangian we find the correct renormalized one.

7.2   Selection Rules

We saw in the previous section that divergences in loop integrals allow different operators to mix, which is governed by the RGE. In fact, not only divergent terms can give contributions to different operators, but also finite terms can induce such shifts. Given a large set of operators, like the *Warsaw* basis [171], it can be quite cumbersome to calculate all possible loop diagrams with all possible operator insertions, just to get the contributions to a single coefficient, even at the 1-loop level. Of course, usually it can be easy to see that many operators cannot contribute to the desired operator, given the fact that there are simply no diagrams possible to draw, but it would still be beneficial to further cut down the set of operators to only those that in the end really do contribute. Fortunately, there exist a few, but still powerful criteria the operators have to satisfy to be able to enter the coefficients of others.

This section will be dedicated to explaining the main ideas behind these criteria, using contributions to the dipole operators as an example. Since there are no conceptual differences regarding the selection rules for the other operators appearing in this chapter, we do not go through them here explicitly.

We summarize the pattern of contributions in Fig. 7.1 allowed by these criteria together with the additional requirement of CP violation, which is crucial for the generation of EDMs.

We want to stress that the selection rules we are going to present in this section are valid only at the 1-loop level.
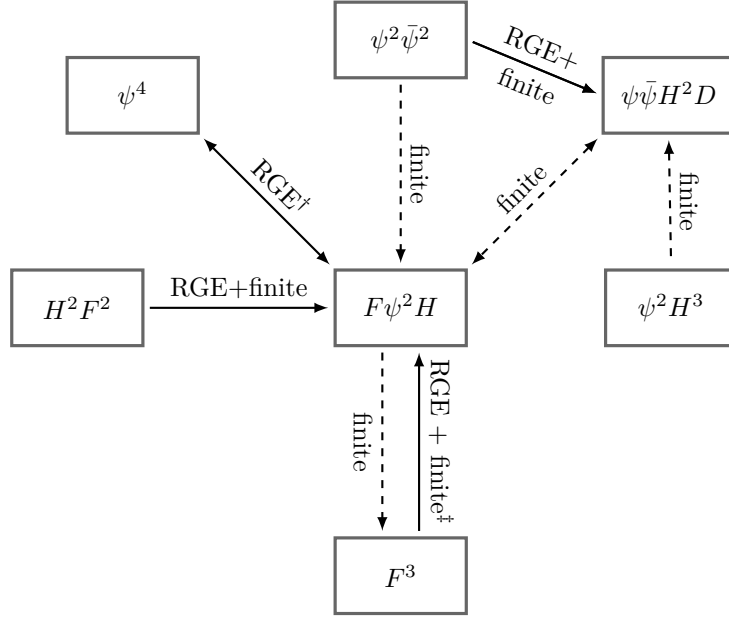
Figure 7.1: The mixing pattern of the operators relevant for this chapter, obtained by using helicity and angular momentum selection rules, as well as the requirement of CP violation. Operators connected with solid arrows enter the RGEs, while dashed arrows describe purely finite effects. The † indicates that the operator $O_{lequ}^{(1)}$ is not included in the ψ^4 class here. Interestingly, we find that the other operators in this class only enter via the RGE, generating no rational terms. The ‡ shows that the operator $O_{\widetilde{W}}$ gives only rational terms.

7.2.1 Helicity Selection Rules

The first set of selection rules relies on the helicity [200, 201] and number of external legs of the amplitudes generated by the effective operators in our set. If one of these operators generates a contact interaction, i.e., an amplitude with no poles or branch cuts, with n external legs and total helicity $\sum h$, it can only be renormalized by another operator with $(n', \sum h')$ if the relations

$$n' \leq n \quad \text{and} \quad \left| \sum h - \sum h' \right| \leq n - n' \tag{7.18}$$

hold [202, 203]. The dipole operators are of the form $F\psi^2 H$, where F and ψ are positive helicity field strength tensor and fermion respectively, so we can characterize them by $(n, \sum h) = (4, 2)$. Using the above relations, we see that the only operators able to renormalize the dipoles within the Warsaw basis of the SMEFT are:

- Operators with $(n, \sum h) = (3, 3)$, i.e., operators of the class F^3;

- Operators with $(n, \sum h) = (4, 2)$. This includes operators of the form $F^2 H^2$, ψ^4 and of course, the dipole operators $F\psi^2 H$ themselves.

Although there is an exception to Eq. (7.18), we can show that it does not change the set of renormalizing operators given above. It is related to the existence of the so-called exceptional, four-dimensional ψ^4 amplitude with $(n, \sum h) = (4, 2)$[1] [202–204]. It can be shown that an insertion of this exceptional amplitude could potentially lead to the renormalization of the dipoles

---

[1]This amplitude is proportional to the product of up and down quark Yukawa couplings and is the only SM 4-point amplitude having total helicity different from zero.

from higher-dimensional operators with $(n, \sum h) = (4, 0)$. Operators with this number of legs and total helicity in the Warsaw basis are of the form $\psi^2 \bar{\psi}^2$, $\psi \bar{\psi} H^2 D$ and $H^4 D^2$. Hence, we see that we cannot build a loop amplitude with the particle content of the dipole in the external states by combining these higher-dimensional contact amplitudes with the four-dimensional exceptional amplitude.

While these helicity selection rules provide a helpful tool when aiming to calculate the RGEs of various operators, they have one major shortcoming if one is interested in a full 1-loop calculation. This is related to the fact that helicity arguments deal only with the renormalization of operators and cannot tell if there are operators that contribute only through rational terms[2].

Interestingly, although the operator $O_{\widetilde{W}}$ belongs to the F^3 class, hence could renormalize the dipole operators, it instead gives only a finite, rational contribution. This was computed using both Feynman diagrams [157, 208, 209] as well as on-shell methods [210]. Its gluonic counterpart, on the other hand, does also enter the dipole operator RGE.

7.2.2 Angular Momentum Selection Rules

We can alleviate the problem of rational terms by augmenting the helicity selection rules with angular momentum considerations [211]. So far, these were used as an alternate way to derive the pattern of renormalization among operators using the conservation of angular momentum of external states, instead of employing the cut-based factorization of loop amplitudes that is used to arrive at the above helicity selection rules. As the name suggests, at the core of this approach lies the conservation of angular momentum during a scattering process. For every scattering amplitude, we find (at least) one scattering channel where the total angular momentum j of the scattering particles is conserved. Given this, operators can renormalize one another if they share at least one such channel. Note that this approach is complementary to the helicity selection rules, in the sense that operators allowed by the former can be forbidden if we additionally use the latter and vice versa. Let us illustrate this with an example relevant for this part of the thesis, the renormalization of the lepton dipole operators by 4-fermion operators. We find two possible scattering channels for the dipoles,

- the $VH \to \psi\psi$ channel, with $j = 1$;

- and the $V\psi \to H\psi$ channel, with $j = 1/2$.

On the other hand, using helicity selection rules, we already know that the only possible 4-fermion operators that can renormalize the dipoles necessarily have to take the form ψ^4, with total helicity $\sum h = 2$. It turns out that in this class of operators, some have $j = 0$ and others $j = 1$ in the $\psi\psi$ scattering channel, while for the dipole operators only the latter is allowed. In the Warsaw basis, the only two operators that could potentially be relevant, concerning the lepton dipole operators, are the semileptonic operator

$$O_{lequ}^{(1)} = \left(\bar{L}_L^j e_R\right) \epsilon_{jk} \left(\bar{Q}_L^k u_R\right) \tag{7.19}$$

and its tensorial cousin $O_{lequ}^{(3)}$ defined in Table 6.1. We see that the former could contribute to the dipole only through a $j = 0$ two-lepton channel, while the latter contributes through a $j = 1$ channel. Since the dipole operators have $j = 1$ in the two-fermion channels, only the tensor operator can, in fact, renormalize the dipole. We want to stress here, that, without actually

---

[2]While there are no helicity selection rules for rational terms, they can still be calculated using helicity amplitudes. However, this would require to perform all possible multi-particle cuts either in D dimensions, see e.g. [205], or using massive loop propagators [206, 207]

performing the loop calculation, we were unable to see this by using only helicity selection rules without the angular momentum conservation. Among the operators mixing with the dipoles through RG flow, the one with $O_{lequ}^{(1)}$ is the only one which would have been allowed by helicity selection rules but is forbidden by angular momentum conservation.

As an example for the opposite relation, we want to mention operators in the class $\psi\bar{\psi}H^2D$, with zero total helicity. By angular momentum arguments these would be allowed to renormalize the dipole, via the ψH channel [211], but they do not satisfy the conditions in Eq. (7.18) and therefore do, in fact, not enter the dipole operators' RGE. Note that these operators cannot give a CP odd contribution with only a single insertion, apart from O_{Hud}. Hence, the latter enters indeed in the 1-loop corrections to (chromo-)dipoles of the quarks, while we can remove the remaining operators of this class from the set of relevant operators with only the condition of CP violation.

Because the angular momentum argument does not rely on performing cuts in the loop integral but only on the angular momentum of external states, it should be possible to extend the procedure to rational terms. While we are not aware of a rigorous proof for this and leave any detailed investigation for later work, we checked a few cases and the procedure worked for all of them. One example would be the $\psi\bar{\psi}H^2D^2$ class of operators, whose renormalization to the dipoles is forbidden by helicity selection rules. Notice, that the only operator in this class that can give CP odd contributions is O_{Hud}, which contributes only to the chromo-dipoles. Looking at the angular momentum structure, we see that O_{Hud} shares the ψH channel with the dipoles [211]. So even though helicity selection rules forbid renormalization, angular momentum conservation allows for rational contributions, which we indeed find.

There is, however, a caveat that is related to the existence of so-called evanescent operators. These are operators that generate non-vanishing amplitudes in $D \neq 4$ space-time dimensions that then vanish in the limit, $D \to 4$ and often arise in the context of 4-fermion operators and Fierz identities that change for $D \neq 4$. In particular, let us look at the operator O_{le} in the Warsaw basis and its counterparts with quarks defined in Table 6.1; the connection of evanescent operators to the dipole through this particular operator was already mentioned in [157]. It lives in the operator class $\psi^2\bar{\psi}^2$, having $j = 0$ in the $\psi\psi$ channel, so by angular momentum conservation it can neither renormalize the dipole nor give only rational contributions. On the other hand, it is straightforward to compute the loop diagram with a single insertion of this operator and see that it, against all odds, does, in fact, give a rational contribution. This apparent contradiction with angular momentum conservation can be resolved by realizing that we can apply a Fierz identity to rewrite this operator as

$$O_{le} = \left(\bar{L}_L\gamma_\mu L_L\right)\left(\bar{e}_R\gamma_\mu e_R\right) \propto \left(\bar{L}_L e_R\right)\left(\bar{e}_R L_L\right). \tag{7.20}$$

Again, we can calculate the corresponding diagram with an insertion of this operator after the Fierzing, and we indeed find a vanishing result, in accordance with angular momentum conservation. At this point, we have to stress that the above Fierzing does only hold in $D = 4$, in a general number of space-time dimensions the identity reads [177]

$$O_{le} = \left(\bar{L}_L\gamma_\mu L_L\right)\left(\bar{e}_R\gamma_\mu e_R\right) = 2\left(\bar{L}_L e_R\right)\left(\bar{e}_R L_L\right) + E_{LR}^{(2)}, \tag{7.21}$$

where $E_{LR}^{(2)}$ is an evanescent operator that vanishes in 4 dimensions. This additional operator then gives a rational term when inserted into the loop integral.

In this chapter we use the Warsaw basis without any Fierzing, so the contribution from this kind of operator appears explicitly in the final result, however, keeping in mind that it is related to the presence of an evanescent operator.

Chapter 8

Electric Dipole Moments at the 1-Loop Order

In this chapter, we provide the details on the calculation of all the 1-loop contributions to the electric and chromo-electric dipole operators and the results thereof. Because we work directly in the broken phase of the SMEFT we start by specifying the procedure we used to translate the Wilson coefficients from the gauge to the mass basis. In section Sec. 8.2, we give the definitions and implications of the different schemes relevant for all calculations. This includes the regularization of divergent loop integrals, the subtraction of both UV and and IR divergences and the treatment of chiral fermions in arbitrary dimensions. Then, in Sec. 8.3, we will discuss the gauge invariance of our calculation and the background field method (BFM) to fix the gauge in a way that simplifies the calculations in practice. We will also explain how redundant operators enter in intermediate steps of our calculations and how gauge invariance can provide a cross-check for their contribution. Before showing the results, we want to briefly discuss the origin of non-rational, but finite functions in multiscale scenarios like the SMEFT in the broken phase in Sec. 8.4. Finally, we conclude this chapter by presenting the results of the calculation in Sec. 8.5, and we will focus on how the inclusion of finite pieces can affect the bounds on various operators compared to just including effects of RG running.

We already want to mention here that we used two independent implementations using the Mathematica package PackageX [212] in one and the FeynRules/FeynArts/FormCalc [213–215] pipeline in the other, finding the same results in both cases. We use the former to obtain explicit analytic expressions of the Passarino-Veltman (PV) loop integrals.

Further, by performing a full 1-loop calculation, we automatically rederived the RGEs in both the SMEFT [172–174] and LEFT [175, 176] and we explicitly verified that our RGEs coincide with the ones in the literature, after performing the respective weak rotations in the case of the SMEFT RGEs.

8.1   Transition from the gauge to the mass basis

As already mentioned, all calculations in this paper were performed directly in the phase of spontaneously broken electroweak symmetry and it is convenient to go from the gauge to the mass basis for fermions, which is necessary to deal with the propagating degrees of freedom. We want to briefly discuss how this basis change affects the Wilson coefficients.

We diagonalise the fermion mass matrices by rotating each chiral fermion, which are triplets

in generation space, using unitary transformations in flavor space,

$$\psi'^{\,i}_{L/R} = U^i_{L/R}\,\psi^i_{L/R} \tag{8.1}$$

with (un)primed fields in the (mass) gauge basis and i denotes any of the fermion flavors. Note, at the order we are working at, it is sufficient to take the SM part from the matrices $U^i_{L/R}$, ignoring their dimension-6 pieces. These rotations can be absorbed by redefining the Wilson coefficients, as shown in Table 8.1.Because the components of the electroweak quark doublets need to be transformed differently to diagonalise all Yukawa matrices, there is no way to redefine the Wilson coefficients such that all rotation matrices are absorbed. This is because the Wilson coefficients are defined in the unbroken phase, where a $U(3)_Q$ flavor transformation acts on the full $SU(2)_L$ doublet. Possible choices, for the gauge basis in which the SMEFT Wilson coefficients are defined in the unbroken phase, are the absorption either of the up-type or of the down-type rotation: we denote them in the following as up- and down-quark bases, in which the up- and down-quark Yukawa matrices are diagonal, respectively. Then, after EW spontaneous symmetry breaking and full rotation to the mass basis, in the quark sector this generates the CKM matrix, defined as

$$V \equiv V_{CKM} = (U^u_L)^\dagger\, U^d_L, \tag{8.2}$$

and the precise terms where it appears are given by the choice of the definition of the Wilson coefficients in the gauge basis[1]. We choose, in our work, to present the final expressions for the EDMs in terms of the Wilson coefficients in the mass basis, defined in Table 8.1, in such a way that the least amount of CKM matrices appear explicitly. Furthermore, also the bounds are set here on the mass basis Wilson coefficients, even if in presenting these constraints in Table II.B.5 and II.B.8, the C' coefficients in the gauge basis are shown explicitly, choosing the up-quark basis and consequently $U^d_L = V$ and $U^u_{L/R} = \mathbf{1}$.

8.2 Scheme definitions

When calculating loop corrections to the various operators appearing in this part, most loop integrals will be divergent, and we regularize them by using dimensional regularization to evaluate all integrals in $D = 4 - 2\epsilon$ space-time dimensions performing the limit $\epsilon \to 0$ at the end of the calculation. In this regularization scheme, 1-loop UV divergences manifest themselves as simple poles in the expansion for small ϵ and we subtract these poles with appropriate counterterms in the $\overline{\text{MS}}$ scheme. The only exception to this procedure are the scalar tadpoles, loop contributions to the Higgs one-point function, that renormalize the Higgs VEV and are present only in the broken phase of the SMEFT. To deal with this type of diagram, we chose the tadpole counterterm such that it cancels the tadpole diagrams completely, analogously to what was done in [216]. The result is that no such diagrams have to be calculated, and the loop contributions to the Higgs VEV are given by the loops in the physical Higgs 2-point function. In addition, due to the photon and gluon being massless, we encounter a few IR divergent diagrams. In the contexts of loop contributions to EDMs, we regularize these by assigning both these bosons an infinitesimally small mass m and keeping only terms that are regular in the limit $m \to 0$. Note, the IR divergences can, of course, be regulated using dimensional regularization, analogous to the UV divergences. Nevertheless, we chose the finite mass regulator to make distinguishing between UV and IR divergences and logarithms straightforward. However, we checked explicitly that the rational terms presented in this chapter are independent of the chosen regulator. In

---

[1]If we would relax our assumption of massless neutrinos the PMNS matrix would be generated accordingly in the lepton sector.

$$C_{dW} = \left(U_L^d\right)^\dagger C'_{dW} U_R^d$$

$$C_{dB} = \left(U_L^d\right)^\dagger C'_{dW} U_R^d$$

$$C_{dG} = \left(U_L^d\right)^\dagger C'_{dW} U_R^d$$

$$C_{dH} = \left(U_L^d\right)^\dagger C'_{dH} U_R^d$$

$$C_{uW} = \left(U_L^u\right)^\dagger C'_{uW} U_R^u$$

$$C_{uB} = \left(U_L^u\right)^\dagger C'_{uW} U_R^u$$

$$C_{uG} = \left(U_L^u\right)^\dagger C'_{uW} U_R^u$$

$$C_{uH} = \left(U_L^u\right)^\dagger C'_{uH} U_R^u$$

$$C_{Hud} = \left(U_R^u\right)^\dagger C'_{Hud} U_R^d$$

$$C^{(3)}_{\substack{lequ \\ abcd}} = \delta_{ia}\delta_{jb} \left(U_L^u\right)^\dagger_{ck} \left(U_R^u\right)_{ld} C'^{(3)}_{\substack{lequ \\ ijkl}}$$

$$C^{(1,8)}_{\substack{quqd \\ abcd}} = \left(U_L^d\right)^\dagger_{ai} \left(U_R^u\right)_{jb} \left(U_L^u\right)^\dagger_{ck} \left(U_R^d\right)_{ld} C'^{(1,8)}_{\substack{quqd \\ ijkl}}$$

$$C^{(1,8)}_{\substack{qu \\ abcd}} = \left(U_L^u\right)^\dagger_{ai} \left(U_L^u\right)_{jb} \left(U_R^u\right)^\dagger_{ck} \left(U_R^u\right)_{ld} C'^{(1,8)}_{\substack{qu \\ ijkl}}$$

$$C^{(1,8)}_{\substack{qd \\ abcd}} = \left(U_L^d\right)^\dagger_{ai} \left(U_L^d\right)_{jb} \left(U_R^d\right)^\dagger_{ck} \left(U_R^d\right)_{ld} C'^{(1,8)}_{\substack{qd \\ ijkl}}$$

$$C^{(1,8)}_{\substack{ud \\ abcd}} = \left(U_R^u\right)^\dagger_{ai} \left(U_R^u\right)_{jb} \left(U_R^d\right)^\dagger_{ck} \left(U_R^d\right)_{ld} C'^{(1,8)}_{\substack{ud \\ ijkl}}$$

Table 8.1: Definitions of Wilson coefficients of fermionic operators used in this work. We suppress flavor indices whenever their contraction is non-ambiguous. (Un)primed coefficients denote the ones in the (mass) gauge basis. The specific form of the U unitary matrices, needed for the transformation to the mass basis, depends on the specific choice for the gauge basis in which the C' coefficients are defined: for example, $U^u_{L/R} = 1$, $U^d_L = V$ ($U^d_{L/R} = 1$, $U^u_L = V^\dagger$) in the up (down) – quark basis. Here we already assumed a diagonal lepton Yukawa, hence $U^e_{L/R} = 1$ and $C_{eV} = C'_{eV}$.

Part IV we will revisit this issue and how to tackle it within dimensional regularization by using matrix elements of UV finite operators.

While dimensional regularization has well-known advantages, like being a mass-independent regulator and preserving gauge invariance and other symmetries, certain theories have to be treated with special care. The SMEFT is one of these theories, since due to its chiral structure and the presence of CP violating, purely bosonic operators, both the fifth Dirac matrix γ_5 as well as the Levi-Civita symbol $\epsilon^{\mu\nu\alpha\beta}$ ($\epsilon^{0123} = +1$) appear explicitly. It is well-known that these two objects are intrinsically defined as four-dimensional, and there exists no generally accepted procedure to consistently extend them to D dimension.

Considering first γ_5, there exist various schemes on how to treat γ_5 in $D \neq 4$ space-time dimensions [217] that all have advantages and disadvantages compared to respective other schemes. For simplicity, we will use the *naive dimensional regularization* (NDR) scheme [218–220]. In this scheme, the anti-commutation property of γ_5,

$$\{\gamma_\mu, \gamma_5\} = 0 \quad \text{for any } \mu, \tag{8.3}$$

is retained for an arbitrary number of space-time dimensions and in particular, we use the definition

$$\gamma_5 = -\frac{i}{4!}\epsilon^{\mu\nu\alpha\beta}\gamma_\mu\gamma_\nu\gamma_\alpha\gamma_\beta, \tag{8.4}$$

making the connection between γ_5 and the Levi-Civita symbol evident.

This leads to obvious inconsistencies in four dimensions by recalling that for $D = 4$ the relation

$$\text{Tr}\left\{\gamma^\mu\gamma^\nu\gamma^\alpha\gamma^\beta\gamma_5\right\} = 4i\epsilon^{\mu\nu\alpha\beta} \tag{8.5}$$

holds. Because of the appearance of the Levi-Civita symbol we can expect this relation to hold strictly only in $D = 4$ dimensions and in fact, preserving the anti-commutation relation of Eq. (8.3), we find

$$\text{Tr}\left\{\gamma^\mu\gamma^\nu\gamma^\alpha\gamma^\beta\gamma_5\right\} = 0 \tag{8.6}$$

in $D \neq 4$ dimensions, which obviously is not smoothly connected to Eq. (8.5) in the limit $D \to 4$. Nevertheless, we will use this scheme for its simplicity and implementation in various computer programs used for evaluating loop integrals, keeping in mind that the finite terms arising in our calculation depend explicitly on this scheme choice and paying attention to possible inconsistencies that could arise in diagrams including traces with an odd number of γ_5 matrices.

The NDR scheme as we use it in this paper also fixes the treatment of the Levi-Civita symbol in an arbitrary number of space-time dimensions, namely, we treat its properties the usual way, pretending as if we are working in four dimensions. This can lead to possible issues for diagrams containing the CP odd operators from the H^2F^2 and F^3 classes. These would arise mainly from contractions of two or more Levi-Civita symbols, but they can be avoided by performing the loop integral before contracting any of the indices of the Levi-Civita symbol, leaving only four four-dimensional indices to be contracted and hence no source of any inconsistencies remain [177]. In fact, we explicitly checked that for the H^2F^2 operators, the result does not change if the indices are contracted from the beginning.

Additional care has to be taken when calculating the contributions of the CP odd F^3 operators to the dipoles, independently of the gauge bosons they are built from. By investigating the respective diagram and performing a power counting we note that its most singular piece is linearly divergent and from the treatment of axial anomalies it is known that such diagrams are not necessarily independent of the choice of momentum routing in the loop. Together with the NDR scheme, this leads to the result for e.g., the W^3 operator,

$$\frac{d_\psi}{e} \times \Lambda^2 \supset \frac{3-A}{32\pi^2}\frac{e\,m_\psi}{s_w}\,C_{\widetilde{W}}. \tag{8.7}$$

Here A is a constant, arbitrary shift of the loop momentum in the convention where the fermion in the loop carries the momentum $q + A\,p_1$, where q is the loop momentum and p_1 the incoming fermion momentum. In this calculation, the choice $A = 0$ corresponds to the known result found in the literature [157, 208, 209]. The same dependence on A appears in the rational part of the gluonic diagram if it is calculated in this naive way, while the divergent structure is independent of the loop momentum routing. To circumvent this issue, we proceed as mentioned above and explained in [177] and keep the Levi-Civita symbol external to the loop integral and contract its indices only after evaluating said integral. However, contrary to [177], we extract the $W^+W^-\gamma$ vertex by treating all the legs of the operator $O_{\widetilde{W}}$ to be on-shell and in $D = 4$, such that we can use properties of the the Levi-Civita symbol to simplify the vertex rule. This procedure reproduces the results in [157, 208, 209], where the authors start from a $W^+W^-\gamma$ operator, but does not capture the the contribution of an evanescent operator, see [177].

8.3 Gauge invariance and redundant operators

8.3.1 Gauge invariance and BFM

Being built upon the SM, the SMEFT is imbued with the same gauge symmetry; hence our results respect this gauge invariance as well.

However, it is a long and well-known fact of QFT that to quantize gauge theories, it is necessary to introduce a gauge fixing term to the Lagrangian to cure the issues arising from the integration over all gauge-related field configurations in the path integral. This explicitly breaks gauge invariance, leaving the theory invariant under the more general BRST transformations [221–223]. For loop calculations, this implies the necessity of gauge-variant, but BRST-invariant, operator structures to account for all the ones appearing in the loops. Allowing for non-renormalizable operators, the usual gauge fixing procedure makes any calculation more tedious because of the large number of such gauge-variant structures needed that did not appear in the original operator basis and hence have to be removed by using field redefinitions. For a calculation of the dipole renormalization using R_ξ gauges with gauge-variant operators, see, e.g., [224].

An alternate way to fix the gauge of a gauge theory lies in the BFM [225–228], which greatly simplifies the calculation and was used for any calculation performed in this paper. The key point is that all the fields are split into a classical background field as well as a quantum field, where the path integral is performed only over field configurations of the latter. By doing so, gauge invariance for the classical fields can be made manifest, such that only gauge-invariant operators have to be considered, greatly simplifying any calculation and the gauge for the quantum fields can be fixed independently of the classical fields. We choose a linear R_ξ gauge and in particular the Feynman gauge ($\xi = 1$) for quantum and unitary gauge ($\xi \to \infty$) for classical fields. We will not go into further detail about the BFM and refer the reader to [225–228] for a more rigorous treatment in general and to [229–231] for the BFM in the context of gauge fixing the SMEFT.

In practice, the classical fields correspond to external fields and tree level propagators while the quantum fields describe fields running in loops and differences to the conventional gauge fixing procedure can arise only in Feynman rules containing both classical and quantum fields. In fact, because we are dealing only with CP odd dimension-6 operators that are not directly affected by gauge fixing, the only modifications we encounter involve only the gauge boson self-interactions, Goldstone-gauge and ghost-gauge vertices within the SM.

Let us remark that, even though Feynman gauge is used for the quantum fields in our calculations, we explicitly checked gauge invariance by leaving the gauge parameter ξ generic in various subsets of diagrams and confirming analytically that every dependence on ξ drops out. Further, as will be illustrated in Sec. 8.3.3, we used the cancellation of various divergences related by gauge symmetry by the same redundant operator as a further check related to gauge invariance.

8.3.2 Redundant operators and choice of basis

As already mentioned, for loop calculations within effective theories one can also use a complete set of operators which are independent under integration by parts (IBP), but possibly redundant under the SM renormalizable equations of motion (EOMs). By applying the latter, this set should then be reduced to an operator basis; this procedure is related to the fact that for theories with non-renormalizable operators there is no unique basis and all different basis choices are related by field redefinitions. In particular, we consider as redundant set the so-called *Green's* basis [232, 233], which is given by all the operators, independent under IBP, which are directly

generated by 1PI Green's functions. In such a way, one can avoid the calculation of reducible diagrams: they correspond indeed, among all the contributions to the operators in the non-redundant basis, to the ones that arise through field redefinitions. So, the procedure is the following:

I Calculate all the relevant, irreducible loop diagrams (see Appendix A in [6]).

II Extend the original, non-redundant operator basis to a redundant set as an intermediate step, such that all operator structures from the previous step can be accounted for. As mentioned, we temporarily extend the *Warsaw* basis [171] to the *Green's* basis, both taken to be in phase of broken EW symmetry.

III Once all operator structures from step I are taken care of, remove the redundant operators by performing the appropriate field redefinitions. This induces shifts of the coefficients of the operators in the non-redundant set as well as those of higher dimensional operators, in terms of the redundant ones, which in turn are fixed by the result of step I. For our purposes, we can neglect the latter, as they would correspond to dimension-8 effects.

Let us note that an alternative to this approach, which avoids the introduction of redundant operators, is to directly compute all reducible diagrams with the desired final states. For our purposes, this would correspond to attaching, e.g., the 1-loop fermion 2-point function to the tree level dipole vertex. But since we are working in the phase of broken EW symmetry with massive particles a cancellation between the 2-point function and the on-shell propagator connecting the loop to the tree level vertex is not obvious and spurious kinematic divergences appear if not treated with care.

8.3.3 Contributions related by gauge invariance

It is well known that due to gauge invariance, certain terms in diagrams with differing numbers of external fields can correspond to the same operator if it contains covariant derivatives or non-Abelian field strength tensors. This allows us to relate terms in different n-point functions coming from the same gauge-invariant operator through the common corresponding Wilson coefficient.

We will explicitly demonstrate this with a situation appearing during our calculations. Consider the loop contributions to the fermion 2-point function, especially the middle and right diagram in Fig. 8.1. The left diagram is not relevant for the discussion to follow, as it is a purely SM diagram, therefore giving contributions only to the fermion wave function and the fermion masses. On the other hand, exchanging one of the SM vertices in this diagram with the electron dipole operator (diagrams on the right) we find that, not only the usual SM structures appear but also one that is proportional to the fermion momentum squared, p^2. Clearly, no operator either within the SM or the Warsaw basis can give rise to such a structure, but there is one in the Green's basis and in the phase of broken EW symmetry it has the form

$$O_{D^2} \sim \bar{\psi} D^2 \psi \,. \tag{8.8}$$

Note that we could have chosen an operator with $\slashed{D}\slashed{D}$ instead of D^2, since these are related by

$$\slashed{D}\slashed{D} = D^2 + \frac{1}{2} e Q_e \sigma_{\mu\nu} F^{\mu\nu} \,, \tag{8.9}$$

and both operators have the same p^2 matrix element. However, we chose the former, as it is easier to relate it to matrix elements with additional gauge bosons, which will be important shortly.
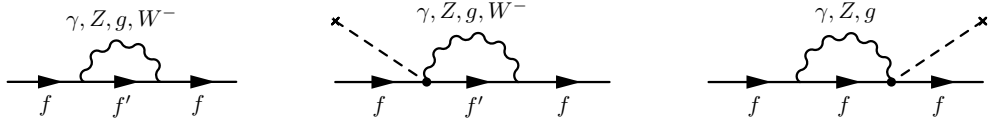
Figure 8.1: The fermionic 2-point function at 1-loop, including both SM and dimension-6 contributions. Dashed lines ending with a crossed endpoint correspond to Higgs fields in the unbroken phase, that are fixed to their VEV in the broken phase.

Note also that Eq. (8.9) is a purely algebraic identity, as it uses only the anti-commutation relation of the Dirac matrices and the definition of the field strength tensor as the commutator of two covariant derivatives: the two operators are indeed equivalent even in the Green's basis, since the above relation does not rely on redefinitions via EOMs.

In the following, we will use the electron field below the weak scale for illustrative purpose, such that the covariant derivative only contains the photon. The reasoning holds for all the other gauge bosons in the same way. The coefficient c_{D^2} of the redundant operator is then given by precisely the 1-loop sized term in the 2-point function proportional to p^2 and, as explained above, we now need to find a field redefinition that removes the D^2 operator at the cost of redefining the coefficients of the other operators appearing in our Warsaw basis. To do so, we summarize the relevant operators for this little exercise,

$$\mathcal{L} \supset i\bar{e}\slashed{D}e + \frac{c_{D^2}v}{\sqrt{2}}\bar{e}D^2 e + \frac{c_{e\gamma}v}{\sqrt{2}}\bar{e}\sigma_{\mu\nu}e F^{\mu\nu} \, . \tag{8.10}$$

The appropriate field redefinition to remove the O_{D^2} operator is

$$e \to e + i\frac{c_{D^2}v}{\sqrt{2}}\,\slashed{D}e \tag{8.11a}$$

and we find that it also induces a shift of the dipole coefficient

$$c_{e\gamma} \to c_{e\gamma} - \frac{1}{2}c_{D^2}, \tag{8.12}$$

which is straightforward to see by plugging the above field redefinition into Eq. (8.10) and neglecting higher dimensional terms.

Accounting for the p^2 term in the 2-point function concerns only the derivative part in the covariant derivatives of the redundant operator. Therefore, investigating the other terms in the covariant derivatives, by gauge invariance, we expect an operator structure in the $ee\gamma$ vertex function that cannot be accounted for by any SM or Warsaw basis operator but instead by the one-photon part of O_{D^2} and is numerically related to the p^2 structure we found above. And we find this exact 1-loop contribution, which serves as another check of our calculations. Taking this reasoning even further, we deduce that there has to be a term in the $ee\gamma\gamma$ 4-point function corresponding to the two-photon part of O_{D^2}, whose coefficient we can predict by gauge invariance from the ones in the 2- or 3-point function, but we have not performed this check explicitly.

For completeness, we also quote the additional redundant operator needed in this chapter, here expressed in the unbroken phase,

$$O_{D^2}^{(2)} = \left(\bar{\psi}_L D_\mu \psi_R \right) D^\mu H \, . \tag{8.13}$$

It appeared in the calculation of the dipole operator contributions to C_{Hud}. We refer to [233] for the coefficients in Warsaw basis in terms of the ones in the Green's basis.

8.4 Non-rational functions

In this section, we want to discuss the presence, in the EDMs expressions, of *finite* but *non-rational* terms, where finite contributions are meant to be the ones that do not contain a logarithmic function of the SMEFT cut-off Λ. Thus, these terms cannot be directly derived from the RGE of the Wilson coefficients in the unbroken phase of the SMEFT and, as we will explain here, they are intrinsically related to the multiscale nature of the SM in the phase of broken EW symmetry.

We see that in App. II.A, in particular in Eqs. (II.A.3) and (II.A.8a)-(II.A.8c), non-rational functions on only SM scales appear. For such functions to appear, at least two massive particles have to take part in one Feynman diagram and because we are working at leading order in m/v, this effectively means that at least two particles with masses of the order of the electroweak scale need to be present. In fact, the equations that we are discussing are the only places in which multiple heavy scales can arise and even though the analytic form of these functions looks very different in (II.A.3) and (II.A.8a)-(II.A.8c) have a very similar origin.

To illustrate this, let us first focus on Eq. (II.A.3), specifically the arctan functions. By looking closely at these expressions, it is not too hard to reconstruct the origin. They come from loop corrections to the scalar 2-point functions, and hence the two heavy scales involved in this amplitude are the external Higgs mass and m_i, with m_i any of the W, Z or top mass from the particles in the loop. It is well-known, this kind of diagrams exhibits a branch cut in the complex s plane starting at $(2\,m_i)^2$, corresponding to the production of a 2-particle state with arbitrary momenta. Then, by setting the external fields to be on-shell and rewriting the complex logarithms appearing in the analytic expression of the discontinuity across this branch cut, we arrive at the arctan functions appearing in (II.A.3).

The non-rational terms in the contributions of the H^2F^2 operators are a bit more involved, as they are 4- instead of 2-point functions with three internal propagators. After the PV decomposition of the loop integrals again, two-propagator bubble integrals are generated with branch cuts, corresponding to either the production of a lepton-Z or lepton-Higgs system, plus additional non-rational functions from three-propagator triangle integrals. Then, keeping leading terms in m/v only the logarithms of ratios of heavy scales survive. And even though they are not related to the divergences of the diagram, they are not completely disconnected from the RG running. In fact, they can be interpreted as the part of the running between the Higgs and the Z boson, that could also be obtained after integrating out only the Higgs boson.

8.5 Results and bounds

Now that we have established all the technical details of our calculation, we will present the results and bounds derived from them in this section. Because the full expressions for all the EDMs are quite long, we will not report them here, but instead refer the reader to App. II.A. The results shown there are taken to be at leading order in the external m/v, where m is the mass of

$$C_{\psi B \atop ii} \to (y_\psi)_{ii}\, g'\, C_{\psi B \atop ii}$$

$$C_{\psi W \atop ii} \to (y_\psi)_{ii}\, g\, C_{\psi W \atop ii}$$

$$C_{qG \atop ii} \to (y_q)_{ii}\, g_s\, C_{qG \atop ii}$$

$$C_{qH \atop ii} \to (y_q)_{ii}\, C_{qH \atop ii}$$

$$C^{(3)}_{lequ \atop iijj} \to (y_\ell)_{ii}\, (y_u)_{jj}\, C^{(3)}_{lequ \atop iijj}$$

$$C^{(1,8)}_{quqd \atop ijji} \to (y_d)_{ii}\, (y_u)_{jj}\, C^{(1,8)}_{quqd \atop ijji}$$

$$C_{H\widetilde{B}} \to g'^2\, C_{H\widetilde{B}}$$

$$C_{H\widetilde{W}} \to g^2\, C_{H\widetilde{W}}$$

$$C_{HW\widetilde{B}} \to g g'\, C_{HW\widetilde{B}}$$

$$C_{H\widetilde{G}} \to g_s^2\, C_{H\widetilde{G}}$$

$$\mathcal{C} \equiv \left\{ C_{Hud}, C^{(1,8)}_{ud}, C^{(1,8)}_{qu}, C^{(1,8)}_{qd}, C_{le} \right\} \to g'^2\, \mathcal{C}$$

Table 8.2: Rescalings of the Wilson coefficients performed throughout this chapter to reflect the natural size we expect them to carry. We assume the operators which are built from vector currents and therefore do not involve a chirality flip to be generated by a heavy vector boson exchange and choose the SM $U(1)_Y$ gauge coupling as a representative.

the external fermion. While this is a good approximation even for the third-generation leptons, this is not applicable for the third generation quarks. Further, due to the sheer amount of Wilson coefficients appearing we also do not present all the bounds we obtained here, rather we quote them in App. II.B. Nevertheless, we will discuss the most interesting points in the following. In particular, one of the main focuses of this chapter lies on the inclusion of finite terms, so we are also interested in quantifying the impact these terms have on the final result. To extract the bounds on various Wilson coefficients from any of the experimental EDM bounds, we neglect the SM contributions, that are many orders of magnitude smaller than the experimental constraints, and turn on only one coefficient at a time, rescaling them by the appropriate combination of SM couplings, reflecting the naturally expected to be carried by the corresponding coefficient, see as well Table 8.2. Using this factorization, we expect, in most of the BSM theories, order one rescaled Wilson coefficients, if the parameters of the UV completion have natural $O(1)$ size. For the new physics scale, we assume $\Lambda = 5$ TeV. Furthermore, we will also set lower bounds on the new physics scale Λ, assuming that the Wilson coefficients have the naturally expected size; we will see that EDMs push Λ to be very large, of the order of 10^3 TeV.

In this section, we define *RG running* contributions to be all terms that explicitly contain a scale dependence, i.e. $\log(\Lambda)$. All remaining terms, both rational and non-rational, are collectively called *finite*.

Note, that we do not use any assumptions on the flavor structure of the dimension-6 operators. For a discussion on the expansion of the coefficients in terms of the needed spurions for different flavor assumptions as well as the bounds obtained with such assumptions can be found in [6].

8.5.1 Lepton EDMs

We will start by investigating the lepton EDMs, where fewer operators appear, compared to the neutron case. In the following, we illustrate the impact of different terms in the contributions to EDMs coming from various class of operators. For the H^2F^2 class, we illustrate the impact of finite terms, showing, in the upper panel of Fig. 8.2, the relative change when using only the RGE versus the full 1-loop result. For illustrative purposes, we use the electron EDM, and while the numerics change due to differing masses, the overall pattern is the same for the other lepton

flavors.

In fact, these, together with the dipole operators themselves, are the only operators that give both RGE and finite contributions, while operators of the ψ^4 class give vanishing rational terms and both the F^3 and $\psi^2\bar{\psi}^2$ class operators enter only through purely rational terms. We want to note that, on the other hand, for the dipole operators finite terms play a negligible role in affecting the result by $\lesssim 1\%$, but this is simply because they enter the EDMs also at tree level, completely dominating over corrections to higher-order terms. This is why, in this case, we do not show the impact of the 1-loop finite terms but rather of the full 1-loop result compared to the tree level term for these operators only, in Fig. 8.2. We see that these higher order effects add destructively to the tree level piece, therefore actually lowering the bound on the scale Λ.

On the contrary, for the H^2F^2 class operators any tree level contribution is obviously absent, which presents a great opportunity to study the size of finite terms. Indeed, we find that the finite terms change the bound by $\sim 10 - 20\%$, however, due to positive relative signs they interfere constructively and consequently increase the bound compared to when using the RG running only. By looking at the corresponding expression, we can also easily explain why the effects of the two operators with only one kind of gauge field appearing are very similar but, on the other hand, quite different from the mixed one. The operators $O_{H\widetilde{B}}$ and $O_{H\widetilde{W}}$ do only get contributions from the photon and Z components of the weak bosons, meaning apart from numerical prefactors coming from different couplings, they give the same contributions. Moreover, the mixed operator, $O_{HW\widetilde{B}}$, also receives contributions from its W component, and it turns out that this piece has the opposite sign of the neutral ones, again reducing the total impact on the lepton EDMs.

Of course, these statements are dependent on the scale Λ, as this changes the energy regime that needs to be swept by the RGE logs. This implies that for new physics sectors well above the TeV, the finite terms will be completely subdominant compared to the large logarithms appearing. On the other hand, the closer the new sector lies to EW scale the smaller the logs and therefore finite terms can have an increasingly big effect. We illustrate this in the lower panel of Fig. 8.2, where we show the dependence on Λ of the relative shift in the electron EDM for the H^2F^2-class operators. We see that because of the slow logarithmic growth, the effect of finite terms does not deteriorate tremendously for e.g., $\Lambda \sim 10$ TeV, while it almost doubles for Λ approaching ~ 1 TeV.

Finally, let us briefly discuss the bounds on the Wilson coefficients from the electron, muon and tau EDM, summarized in Fig. 8.3 and computed assuming $\Lambda = 5$ TeV and applying the rescalings shown in Table 8.2. Here we show the full tree plus loop level result, i.e., including both the RG running and finite terms; in the case of the electron EDM the prospected future bounds are shown as well. Note that for the 4-fermion operators, we chose to show only the component with the most stringent bound for each of the operators. The bounds on other components can easily be obtained from the ones shown in Fig. 8.3 by rescaling them with the appropriate ratio of fermion masses. The most obvious conclusion that can be drawn from this figure, by comparing the upper panel with the lower one (and with the values in Table II.B.1) is that the supreme precision of the eEDM measurement gives by far the most stringent bounds from any of the lepton flavors. One can notice that, for $\Lambda = 5$ TeV, the constraints from the electron EDM can set bounds of order 10^{-5} on the Wilson coefficients of operators with fermions and of $10^{-3} \div 10^{-2}$ in the case of purely bosonic operators. These bounds will further improve by one or two orders of magnitude at ACME III.

Nevertheless, we can make another interesting observation. Even though the experimental sensitivity to the muon EDM is roughly one order of magnitude higher than for the tau EDM, it still happens to be the case that the tau lepton is slightly more constraining than its lighter
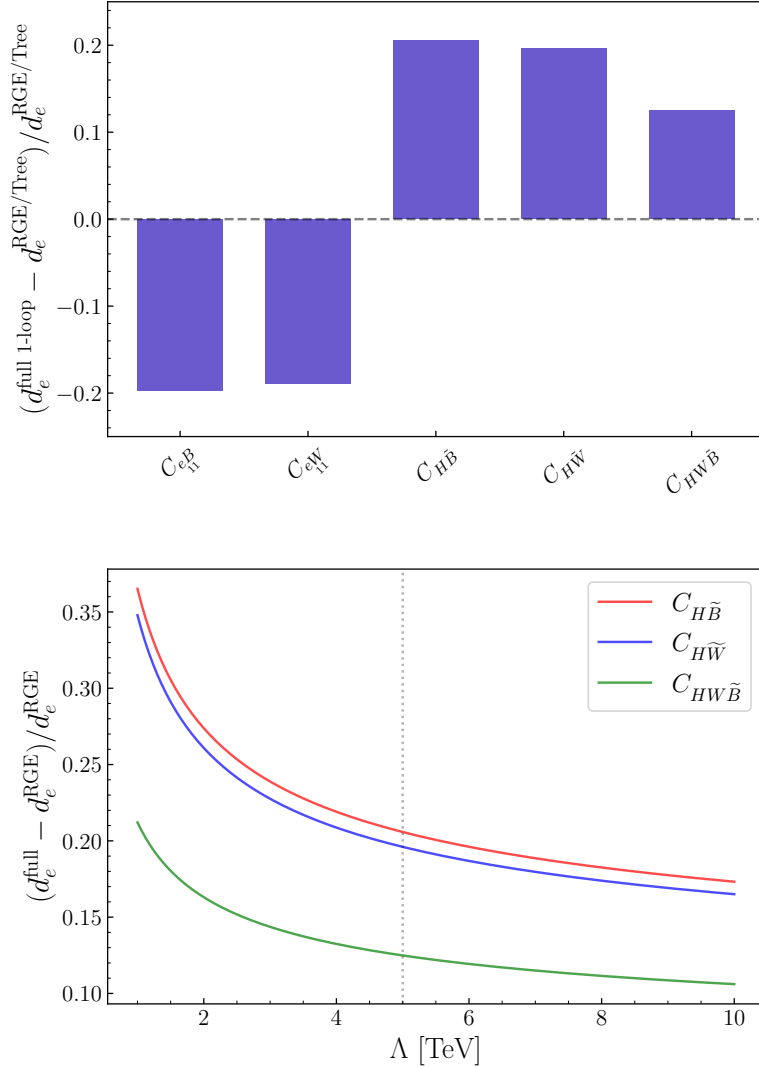
Figure 8.2: *Upper panel:* Relative change of the electron EDM when using the full 1-loop result compared to only the RG running (H^2F^2 operators) and impact of the full 1-loop effects compared to the tree level term ($F\psi^2H$ operators). *Lower panel:* Dependence of the relative shift in the EDMs as a function of the scale Λ. Here the dotted line shows the benchmark value of $\Lambda = 5$ TeV used in this paper.

cousin. Speaking of the different masses of these leptons, this is precisely the reason this happens. For every operator, the contribution is proportional to the lepton Yukawa, either through our rescaling of the Wilson coefficients to their natural size or because the contribution itself is directly proportional to the lepton mass. So it turns out that with the current sensitivities the mass difference between the muon and tau lepton barely overcompensates the lower experimental reach for the latter, such that the tau EDM is indeed more constraining than its muonic counterpart. This argument, however, does not hold for the operator O_{le}. For this operator, we see the inverted situation, where the tau EDM is less constraining than the muon EDM. But this is readily explained by closer examining the corresponding expression in Eq. (II.A.11). Here we see that it is, in fact, not proportional to the mass of the external lepton but of the lepton inside
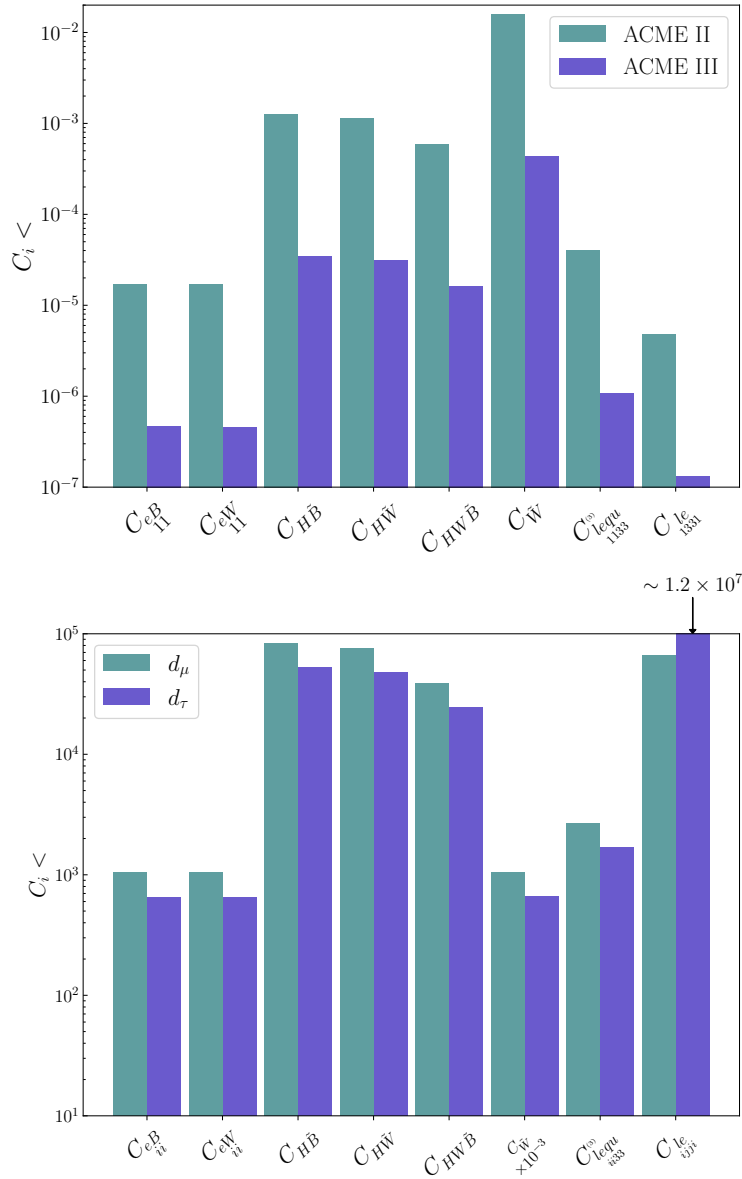
Figure 8.3: Upper bounds on the Wilson coefficients, assuming $\Lambda = 5$ TeV and applying the rescalings shown in Table 8.2, obtained including the full 1-loop expressions, from the experimental bounds on the different lepton EDMs. *Upper panel:* The current constraints (ACME II) coming from the best bounds on the electron EDM, compared to the ones from the projected future bounds (ACME III). *Lower panel:* We compare the bounds of the two heavy lepton flavors with each other. Here $i = 2(3)$ stands for the muon (tau) EDM and j denotes the heavier of the two lepton flavors, different from i in the operator O_{le}.

the loop instead. Because we chose the most constraining component of each Wilson coefficient, this mass is the tau mass for the muon EDM and vice versa, such that the reasoning here is exactly inverted with respect to all the other operators and on top of the weaker experimental bound, the constraint from the tau EDM is further suppressed by the muon mass, contrary to
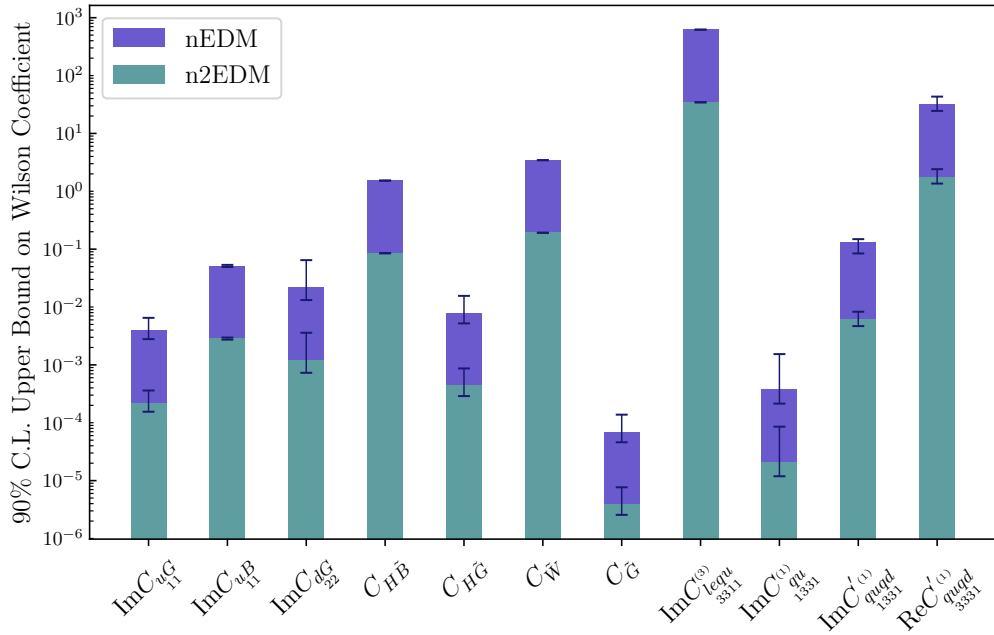
Figure 8.4: Selected upper bounds on the Wilson coefficients, assuming $\Lambda = 5$ TeV and applying the rescalings shown in Table 8.2, obtained including the full 1-loop expressions, from the experimental bounds on the neutron EDM. In addition to the bounds from the central values, we also show the influence of the uncertainties in the determination of the chromo-dipole and Weinberg operator matrix elements. We also show bounds on the Wilson coefficients for the projected accuracy of the n2EDM experiment. Notice that the last two Wilson coefficients are in the up-quark gauge basis, while the others in the mass basis.

the tau mass in the muon EDM. From this perspective, the phenomenal constraining power of the electron EDM is even more impressive, as the mass gap between the electron mass and the other lepton masses spans multiple orders of magnitude, but still, the electron bounds by far overshadow the other ones.

As mentioned before, we also set lower bounds on the new physics scale Λ, assuming that the Wilson coefficients have values corresponding to the natural size indicated in Table 8.2. Turning on one operator at a time, the strongest constraints come from the dipole and the $O^{(3)}_{lequ \atop 1133}$ and

$O_{le \atop 1331}$ contributions and are of the order of 10^3 TeV.

8.5.2 Neutron EDM

We proceed with the neutron EDM, which is composed of the (chromo-)EDMs of the quarks and gluons as well as the operators $O_{Hud \atop 11}$ and $O^{(1,8)}_{quqd \atop 1111}$ which can be matched to operators which have a non-vanishing matrix element on the neutron EDM. There are several differences with respect to the lepton EDMs as we can now have cancellations between the 1-loop contributions of the EDMs and chromo-EDMs of the light quarks, more flavor components of the Wilson coefficients are contributing to the dipole amplitudes (this is all the more true in the gauge basis, due to the non-trivial rotation between gauge and mass basis, see Sec. 8.1) and in general more operators due to the presence of QCD degrees of freedom. We show a selection of bounds in Fig. 8.4

where we have also included a conservative estimate of the influence of the uncertainties in the determination of the matrix elements of all contributing effective operators in the expression of the neutron EDM and a projection for the expected accuracy of the n2EDM experiment [131]. The full set of bounds can be found in App. II.B.2.

Starting with the dipole operators, in addition to the electroweak dipole operators also the gluonic dipole operators contribute to the neutron EDM. There, the effects of including finite terms are much larger than for the electroweak dipoles. This is due to the large rational terms in the wave function renormalization of the gluon. In addition, we can also probe more flavor components of the dipole operators through the appearance of the strange quark dipole in the neutron EDM as well as the appearance of all flavor components of the quark dipole Wilson coefficients in the 3-gluon 1-loop amplitudes. The bounds on these flavor components are suppressed with respect to the dominant up and down quark chromo-dipole operators, since the matrix elements in the expression for the neutron EDM are smaller and some flavor elements only enter through loop corrections. Note also, that the contribution of the dipole operators through effective operators apart from the dipole operators in the expression of the neutron EDM is negligible, since these contributions are suppressed by the much smaller matrix elements of the effective operators and the common loop factor that all dipole contributions receive that are sourced by these additional effective operators. One exception to this is the contribution through the Weinberg operator, as those loop contributions are enhanced by an inverse quark mass.

For the H^2F^2 type operators, we also have to differentiate between the operators with field strengths of electroweak and strong gauge bosons. The bounds on the electroweak operators are less stringent, by around three orders of magnitude, than the ones obtained from the electron EDM, as is expected due to the experimental bound on the neutron EDM being so much weaker. Interestingly, for all three electroweak operators there is a constructive interference between the terms from the different quark EDMs, enhancing the contribution to the neutron EDM, together with the enhancement from the quark Yukawas with respect to the electron case. Therefore, with an experimental bound on the neutron EDM with the same constraining power as the current electron EDM sensitivity, the bounds on the Wilson coefficients would actually be stronger than those obtained from the electron EDM. The neutron EDM receives, through the quark chromo-EDMs, contributions also from the gluonic H^2G^2 operator. Such terms are additionally enhanced by the strong coupling and for this reason, the bound on the corresponding Wilson coefficient is stronger than the constraints obtained for the Wilson coefficients of the electroweak bosonic operators by more than two orders of magnitude, as shown in Fig. 8.4.

For the 4-fermion operators we have the same situation as for the lepton EDMs, only now there are more operators including quarks contributing to the EDM. As for the lepton EDMs, the 4-fermion operators either enter only via RG running or only via rational terms to the dominant contributions that are given by the (chromo-)dipole operators. They can also enter directly with a small hadronic matrix element in the neutron EDM. What is interesting for these 4-fermion operators made from quarks is that the change of basis from the gauge to the mass basis is non-trivial, as discussed in Sec. 8.1. Starting, for example, from an up- or down-quark gauge basis, in the rotation to the mass basis a CKM matrix appears for the down or up component of the operators, respectively. As mentioned above, whenever we use expressions in terms of Wilson coefficients in the gauge basis, we choose the up-basis since more operators with up quarks appear in the final expression of the neutron EDM. In fact, with this choice, a larger number of operators is left unchanged by the basis transformation; for example, this is the case for the $O_{lequ}^{(3)}$ operator already considered in the previous section in the discussion of the lepton EDMs.

However, since both the up and down type dipole appear in the neutron EDM, it is inevitable that CKM matrix elements appear somewhere. Since the CKM matrix contains a CP violating phase, this also enables us to probe the real part of some Wilson coefficients in the gauge basis, in particular of some flavor off-diagonal ones (see the rightmost column in Fig. 8.4). In fact, these real parts contribute to the imaginary parts of the Wilson coefficients in the mass basis, that enter the EDMs expressions. Those constraints are of the same order as the bounds on the corresponding imaginary parts, since the imaginary part of the very off-diagonal part of the CKM matrix is of the same order as its real part.

Another interesting contribution appears through the Weinberg operator. Unlike $O_{\tilde{W}}$, it can also contribute with RG running and in addition to its appearance through the quark chromo-dipoles, it also enters directly in the expression of the neutron EDM, interpreted as the chromo-dipole of the gluon. As can be seen in the analytical expressions of the dipoles with how they enter the neutron EDM, the interference between the different chromo-EDMs is constructive and all effects proportional to the Weinberg Wilson coefficient add up to the comparably strong bound. This, together with the strong coupling enhancement for these contributions, leads to the most stringent among the constraints imposed by the neutron EDM experimental bound, being of order 10^{-4} for $\Lambda = 5$ TeV and for a $C_{\tilde{G}}$ rescaled as in Table 8.2. In addition, there are large finite terms in the self 1-loop contributions of the Weinberg operator, which give corrections of $\sim 45\%$ with respect to only including RG running at the considered scale.

Furthermore, there can be direct contributions of the 4-fermion operators $O_{quqd}^{(1,8)}$, which are however largely suppressed by their small matrix element in the neutron EDM. This leads to an interesting interference where loop suppressed contributions of these 4-fermion operators to the dipole operators, which are further suppressed by small Yukawa couplings, are of the same order as the direct tree level contributions of those operators (see App.II.A and Eq. (6.6)). The dipole contributions to those 4-fermion operators are suppressed by small matrix elements and loop factors, as discussed before.

Finally, there is a small direct contribution to the neutron EDM of the operator O_{Hud}, which also contributes with a finite term to the dipole operators. As can be seen in Fig. 8.4, the Wilson coefficient of these operators gets a significant bound from the neutron EDM, mostly due to the tree level contribution to the neutron EDM. The Yukawa-like operators $O_{uH,dH}$ which appear in the 1-loop contribution to this operator, on the other hand, are largely suppressed by a loop-factor and small Yukawas and therefore only get bounds beyond the perturbative unitarity limit. As mentioned previously, the dipole contributions which also enter this 1-loop expression are negligible when compared to the dominant direct contributions to the neutron EDM. Lastly, there is another 4-fermion operator which enters the 1-loop expression of the operator O_{Hud}, $O_{ud}^{(1,8)}$, which also only receives a bound around the perturbative unitarity limit.

We also show in Fig. 8.4 the error bars associated with the 50% uncertainties of the matrix elements of the quark and gluon chromo-EDMs. Wherever the Wilson coefficients of the chromo-dipole operators enter at tree level, the uncertainties translate directly to the bound. In the case of the electroweak operators, which can only enter at loop level in the chromo-EDMs, the dependence on the uncertainties is much smaller.

Furthermore, we also estimate the bounds on all Wilson coefficients with the projected experimental bound of the n2EDM experiment [131]. With the projected experimental bound of $\sim 10^{-27}e$ cm, we expect an improvement of about one order of magnitude for all Wilson coefficients.

Importantly, we notice that, assuming the Wilson coefficients are of the natural size shown in Table 8.2, the experimental constraint on the neutron EDM sets a bound on the new physics scale of order 10^3 TeV, coming from the Weinberg operator G^3. All the bounds imposed when

any of the other operators is instead turned on are at least one order of magnitude weaker.

Chapter 9

Conclusions

In this part of the thesis, we perform the analysis at 1-loop level of the lepton and neutron electric dipole moments, using the model independent EFT approach. We provide, at this accuracy, the complete expressions of these CP violating low-energy observables as a function of the dimension-6 SMEFT Wilson coefficients in the Warsaw basis, including the RG running effects as well as finite terms. The latter play a fundamental role in the cases of operators that do not renormalize the dipoles, but there are also classes of operators for which they provide an important fraction, $10 - 20\%$, of the total 1-loop contribution, if the NP scale is around $\Lambda = 5$ TeV. In presenting these results, we also discuss the various loop contributions to the EDMs under the light of selection rules, based on helicity, angular momentum and CP arguments.

Furthermore, we compute the full set of bounds that the current and prospected experimental constraints impose on the Wilson coefficients, with one single operator turned on at a time, for a fixed SMEFT cut-off scale. On the other hand, we also provide the lower bounds on the scale of new physics, obtained assuming that the Wilson coefficients values are given by the natural sizes that we expect them to carry. One can see that EDMs provide a powerful probe for deviations from the SM, since the computed bounds are strong and can push the scale of new physics above 10^3 TeV, with the mentioned natural values for the Wilson coefficients. This means that any UV completion of the SM, for which the operators responsible for these strong bounds are generated, should accidentally have a very suppressed CP violation, similar to the SM one, unless some fine-tuning mechanism is present.

Appendices part II

II.A   Analytic expressions of various EDMs

In this appendix, we report the analytic expressions computed in this work. To improve readability, we divide the full expressions into categories defined by the field content of the operators contributing to the dipole. Because we give the expression of the observable EDM we repeat here its relation to the Wilson coefficient $c_{f\gamma}$, of the operator $\bar{f}_L \sigma^{\mu\nu} f_R F_{\mu\nu}$,

$$d_f = -\frac{2}{\Lambda^2} \mathrm{Im}\, c_{f\gamma}, \tag{II.A.1}$$

and similar for the chromo-dipoles.

II.A.1   Universal contributions

Since the full expression of the fermion (c)EDMs is rather long, we will start by providing their universal parts first. Apart from the term proportional to g_s, Eqs. (II.A.2b), (II.A.2d), which is present only for quark dipoles, these are universal in the sense that they correspond to pure SM loops on the external particle 2-point functions and are independent of the fermion species and therefore enter all dipoles in the same way. This includes both the renormalization of the Higgs VEV, which in this work is given by just the loops in the physical Higgs 2-point function, as well as the mixing of the neutral gauge bosons at 1-loop.

All these contributions are:

- Loops on external left-handed (LH) and right-handed (RH) fermions:

$$16\pi^2 \times (\text{LH Fermion 2-pt.})_f = 2\, e^2 Q_f^2 - \frac{e^2}{4 s_w^2} - \frac{e^2}{2 s_w^2 c_w^2}(T_f^3 - Q_f s_w^2)^2 \tag{II.A.2a}$$

$$+ 2\, e^2 Q_f^2 \log\left(\frac{\Lambda}{m_f}\right) + \frac{e^2}{2 s_w^2} \log\left(\frac{\Lambda}{m_W}\right)$$

$$+ \frac{e^2}{s_w^2 c_w^2}(T_f^3 - Q_f s_w^2)^2 \log\left(\frac{\Lambda}{m_Z}\right)$$

$$+ 2\, c_{F,3} g_s^2 + 2\, c_{F,3} g_s^2 \log\left(\frac{\Lambda}{m_f}\right) \tag{II.A.2b}$$

$$16\pi^2 \times (\text{RH Fermion 2-pt.})_f = 2\, e^2 Q_f^2 - \frac{e^2 Q_f^2 t_w^2}{2} + 2\, e^2 Q_f^2 \log\left(\frac{\Lambda}{m_f}\right) \tag{II.A.2c}$$

$$+ e^2 Q_f^2 t_w^2 \log\left(\frac{\Lambda}{m_Z}\right)$$

$$+ 2\, c_{F,3} g_s^2 + 2\, c_{F,3} g_s^2 \log\left(\frac{\Lambda}{m_f}\right) \tag{II.A.2d}$$

- Loop contributions to the Higgs VEV:

$$16\pi^2 \times \text{Higgs 2-pt.} = \frac{4\, N_c m_t^2}{v^2} - \frac{4\, e^2}{s_w^2} - \frac{2\, e^2}{s_w^2 c_w^2} \tag{II.A.3}$$

$$+ \frac{4\, N_c m_t^2}{v^2} \log\left(\frac{\Lambda}{m_t}\right) - \frac{4\, e^2}{s_w^2} \log\left(\frac{\Lambda}{m_W}\right)$$

$$- \frac{2\, e^2}{s_w^2 c_w^2} \log\left(\frac{\Lambda}{m_Z}\right)$$

$$- \frac{2 N_c\, m_t^2}{v^2} \sqrt{\frac{4 m_t^2 - m_h^2}{m_h^2}} \arctan\left(m_h \sqrt{\frac{4 m_t^2 - m_h^2}{\left(2 m_t^2 - m_h^2\right)^2}}\right)$$

$$+ \frac{2\, e^2}{s_w^2} \sqrt{\frac{4 m_W^2 - m_h^2}{m_h^2}} \left[\arctan\left(m_h \sqrt{\frac{4 m_W^2 - m_h^2}{\left(2 m_W^2 - m_h^2\right)^2}}\right) + \pi\right]$$

$$+ \frac{e^2}{s_w^2 c_w^2} \sqrt{\frac{4 m_Z^2 - m_h^2}{m_h^2}} \arctan\left(m_h \sqrt{\frac{4 m_Z^2 - m_h^2}{\left(2 m_Z^2 - m_h^2\right)^2}}\right)\Bigg\}$$

- Loops on external photons:

$$16\pi^2 \times \text{Photon 2-pt.} = -\frac{2\, e^2}{3} - 14\, e^2 \log\left(\frac{\Lambda}{m_W}\right) \tag{II.A.4}$$

$$+ \frac{8}{3} \sum_{\text{fermions}} \left(\delta_{i\ell} + N_c \delta_{iq}\right) e^2 Q_i^2 \log\left(\frac{\Lambda}{m_i}\right)$$

- Photon-Z mixing:

$$16\pi^2 \times \text{Photon-Z Mixing} = -\frac{2e^2}{3 t_w} - \frac{1 + 42 c_w^2}{6 s_w c_w} e^2 \log\left(\frac{\Lambda}{m_Z}\right) \tag{II.A.5}$$

$$+ \frac{4}{3} \frac{e^2}{s_w c_w} \sum_{i \neq t} \left(\delta_{i\ell} + N_c \delta_{iq}\right) Q_i (T_i^3 - 2 Q_i s_w^2) \log\left(\frac{\Lambda}{m_Z}\right)$$

$$+ \frac{4}{3} \frac{N_c e^2}{s_w c_w} Q_u (T_u^3 - 2 Q_u s_w^2) \log\left(\frac{\Lambda}{m_t}\right)$$

- Loops on external gluons:

$$16\pi^2 \times \text{Gluon 2-pt.} = -\frac{67 N_c}{9} g_s^2 - \frac{22}{9} N_c g_s^2 \log\left(\frac{\Lambda}{\mu_H}\right) + \frac{4}{3} g_s^2 \sum_{q=u,d,s,c} \log\left(\frac{\Lambda}{\mu_H}\right) \tag{II.A.6}$$

$$+\frac{4}{3}g_s^2\log\left(\frac{\Lambda}{m_b}\right)+\frac{4}{3}g_s^2\log\left(\frac{\Lambda}{m_t}\right)\biggr\}$$

II.A.2 Lepton EDMs

We start with showing the results for lepton EDMs. Note that the logs arising from the divergent terms of the photon wave function renormalization do not necessarily run down to the mass of the fermion running in the loop, but only to the mass of the external lepton if the latter is heavier than the former.

Contributions from $\psi^2 HF$ operators

$$\frac{d_\ell}{e}\times(4\pi\Lambda)^2\supset$$

$$\mathrm{Im}\left[c_w C_{\underset{11}{eB}}+2\,T_\ell^3 s_w C_{\underset{11}{eW}}\right]\left\{-\frac{16\sqrt{2}\,\pi^2\,v}{e}+4\sqrt{2}\,eQ_\ell^2 v+8\sqrt{2}\,eQ_\ell^2 v\log\left(\frac{\Lambda}{m_\ell}\right)\right. \qquad\text{(II.A.7a)}$$

$$\left.+\frac{v}{\sqrt{2}e}\Big(\text{Eq. (II.A.2a)}_\ell+\text{Eq. (II.A.2c)}_\ell+\text{Eq. (II.A.3)}+\text{Eq. (II.A.4)}\Big)\right\}$$

$$+\mathrm{Im}\left[-s_w C_{\underset{11}{eB}}+2\,T_\ell^3 c_w C_{\underset{11}{eW}}\right]\left\{\sqrt{2}\,eQ_\ell\,v\frac{T_\ell^3-2Q_\ell s_w^2}{s_w c_w}\left[\frac{1}{2}+\log\left(\frac{\Lambda}{m_Z}\right)\right]\right. \qquad\text{(II.A.7b)}$$

$$\left.+\frac{v}{\sqrt{2}e}\Big(\text{Eq. (II.A.5)}\Big)\right\}$$

$$-\mathrm{Im}\left[C_{\underset{11}{eW}}\right]\left\{\frac{ev(5+Q_\ell)}{2\sqrt{2}s_w}-\frac{\sqrt{2}\,ev(3Q_\ell-1)}{s_w}\log\left(\frac{\Lambda}{m_W}\right)\right\}. \qquad\text{(II.A.7c)}$$

Contributions from $H^2 F^2$ operators

$$\frac{d_\ell}{e}\times(4\pi\Lambda)^2\supset-m_\ell\left\{3\left(2\,Q_\ell-T_\ell^3\right)+(8\,Q_\ell-4T_\ell^3)\log\left(\frac{\Lambda}{m_h}\right)\right. \qquad\text{(II.A.8a)}$$

$$\left.+(2s_w^2 Q_\ell-T_\ell^3)\frac{4m_Z^2}{m_Z^2-m_h^2}\log\left(\frac{m_h}{m_Z}\right)\right\}C_{H\widetilde{B}}$$

$$-m_\ell\left\{3\,T_\ell^3+4T_\ell^3\log\left(\frac{\Lambda}{m_h}\right)\right. \qquad\text{(II.A.8b)}$$

$$\left.-(2s_w^2 Q_\ell-T_\ell^3)\frac{4m_Z^2}{m_Z^2-m_h^2}\log\left(\frac{m_h}{m_Z}\right)\right\}C_{H\widetilde{W}}$$

$$+m_\ell\left\{\frac{6\,Q_\ell s_w^2-c_w^2+3\,T_\ell^3 c_{2w}}{2c_w s_w}\right. \qquad\text{(II.A.8c)}$$

$$\left.+\frac{4s_w^2 Q_\ell+2T_\ell^3 c_{2w}}{c_w s_w}\log\left(\frac{\Lambda}{m_h}\right)-\frac{2}{t_w}\log\left(\frac{\Lambda}{m_W}\right)\right.$$

$$-(2s_w^2 Q_\ell - T_\ell^3)\frac{c_{2w}}{c_w s_w}\frac{2m_Z^2}{m_Z^2 - m_h^2}\log\left(\frac{m_h}{m_Z}\right)\Bigg\} C_{HW\widetilde{B}}$$

Contributions from F^3 operators

$$\frac{d_\ell}{e}\times(4\pi\Lambda)^2 \supset -\frac{3}{2}\frac{e\,m_\ell}{s_w}C_{\widetilde{W}} \tag{II.A.9}$$

Contributions from ψ^4 operators

$$\frac{d_\ell}{e}\times(4\pi\Lambda)^2 \supset 16 N_c Q_u \sum_{i\in\{1,2,3\}} m_{u,i}\,\log\left(\frac{\Lambda}{m_{u,i}}\right)\mathrm{Im}\left[C^{(3)}_{\underset{11ii}{lequ}}\right] \tag{II.A.10}$$

Contributions from $\psi^2\bar{\psi}^2$ operators

$$\frac{d_\ell}{e}\times(4\pi\Lambda)^2 \supset -2Q_e \sum_{i\in\{2,3\}} m_{\ell,i}\,\mathrm{Im}\left[C_{\underset{1ii1}{le}}\right] \tag{II.A.11}$$

II.A.3   Quark EDMs

We show here the results for the quark EDMs; for the scale in the logs of the photon 2-point function, the same discussion as in the case of the lepton EDMs applies. Furthermore, $\mu_H \sim \mathcal{O}(\mathrm{GeV})$ denotes the hadronic scale. We define the following frequently used combination,

$$(\text{LH+RH quark WFR})_q = \text{Eq. (II.A.2a)}_q + \text{Eq. (II.A.2b)}_q + \text{Eq. (II.A.2c)}_q + \text{Eq. (II.A.2d)}_q \tag{II.A.12}$$

where the subscript $q = u, d$ denotes the type of quark.

Contributions from $\psi^2 H F$ operators

$$\frac{d_q}{e}\times(4\pi\Lambda)^2 \supset$$

$$\mathrm{Im}\left[c_w C_{\underset{11}{qW}} + 2\,T_q^3 s_w C_{\underset{11}{qW}}\right]\left\{-\frac{16\sqrt{2}\,\pi^2\,v}{e} + 4\sqrt{2}\,eQ_q^2 v + 8\sqrt{2}\,eQ_q^2 v\log\left(\frac{\Lambda}{\mu_H}\right)\right. \tag{II.A.13a}$$

$$\left. +\frac{v}{\sqrt{2}e}\Big(\text{Eq. (II.A.12)}_q + \text{Eq. (II.A.3)} + \text{Eq. (II.A.4)}\Big)\right.$$

$$+\mathrm{Im}\left[-s_w C_{\underset{11}{qB}} + 2\,T_q^3 c_w C_{\underset{11}{qW}}\right]\left\{\sqrt{2}eQ_q v\,\frac{T_q^3 - 2Q_q s_w^2}{s_w c_w}\left[\frac{1}{2} + \log\left(\frac{\Lambda}{m_Z}\right)\right]\right. \tag{II.A.13b}$$

$$\left. +\frac{v}{\sqrt{2}e}\Big(\text{Eq. (II.A.5)}\Big)\right.$$

$$+2T_q^3\mathrm{Im}\left[C_{\underset{11}{qW}}\right]\left\{\frac{ev(5+Q_q)}{2\sqrt{2}s_w} - \frac{\sqrt{2}\,ev(3Q_q - 1)}{s_w}\log\left(\frac{\Lambda}{m_W}\right)\right\} \tag{II.A.13c}$$

$$+\mathrm{Im}\left[C_{\underset{11}{qG}}\right]\left\{2\sqrt{2}v\,c_{F,3}Q_q g_s + 4\sqrt{2}v\,c_{F,3}Q_q g_s\log\left(\frac{\Lambda}{\mu_H}\right)\right\}. \tag{II.A.13d}$$

Contributions from H^2F^2 operators

$$\frac{d_q}{e} \times (4\pi\Lambda)^2 \supset -m_q \left\{ (6\,Q_q - 3T_q^3) + (8\,Q_q - 4T_q^3) \log\left(\frac{\Lambda}{m_h}\right) \right. \tag{II.A.14a}$$

$$\left. + (2s_w^2 Q_q - T_q^3)\frac{4m_Z^2}{m_Z^2 - m_h^2}\log\left(\frac{m_h}{m_Z}\right) \right\} C_{H\widetilde{B}}$$

$$-m_q \left\{ 3\,T_q^3 + 4\,T_q^3 \log\left(\frac{\Lambda}{m_h}\right) \right. \tag{II.A.14b}$$

$$\left. - (2s_w^2 Q_q - T_q^3)\frac{4m_Z^2}{m_Z^2 - m_h^2}\log\left(\frac{m_h}{m_Z}\right) \right\} C_{H\widetilde{W}}$$

$$+m_q \left\{ \frac{12\,Q_q s_w^2 - 2\,c_w^2 + 6\,T_q^3 c_{2w}}{4c_w s_w} \right. \tag{II.A.14c}$$

$$+ \frac{4s_w^2 Q_q + 2T_q^3 c_{2w}}{c_w s_w}\log\left(\frac{\Lambda}{m_h}\right) - \frac{2}{t_w}\log\left(\frac{\Lambda}{m_W}\right)$$

$$\left. - (2s_w^2 Q_q - T_q^3)\frac{c_{2w}}{c_w s_w}\frac{2m_Z^2}{m_Z^2 - m_h^2}\log\left(\frac{m_h}{m_Z}\right) \right\} C_{HW\widetilde{B}}$$

Contributions from F^3 operators

$$\frac{d_q}{e} \times (4\pi\Lambda)^2 \supset 2T_q^3 \frac{3}{2}\frac{e\,m_q}{s_w}\,C_{\widetilde{W}} \tag{II.A.15}$$

Contributions from ψ^4 operators

$$\frac{d_d}{e} \times (4\pi\Lambda)^2 \supset 2\sum_{i\in\{1,2\}} m_{u,i}Q_u \log\left(\frac{\Lambda}{\mu_H}\right)\text{Im}\left[C^{(1)}_{\substack{quqd\\1ii1}} + c_{F,3}\,C^{(8)}_{\substack{quqd\\1ii1}}\right] \tag{II.A.16}$$

$$+2m_t Q_u \log\left(\frac{\Lambda}{m_t}\right)\text{Im}\left[C^{(1)}_{\substack{quqd\\1331}} + c_{F,3}\,C^{(8)}_{\substack{quqd\\1331}}\right]$$

$$\frac{d_u}{e} \times (4\pi\Lambda)^2 \supset 8\sum_{i\in\{1,2,3\}} m_{\ell,i}Q_e \log\left(\frac{\Lambda}{\mu_H}\right)\text{Im}\left[C^{(3)}_{\substack{lequ\\ii11}}\right] \tag{II.A.17}$$

$$+2\sum_{i\in\{1,2\}} m_{d,i}Q_d \log\left(\frac{\Lambda}{\mu_H}\right)\text{Im}\left[C^{(1)}_{\substack{quqd\\i11i}} + c_{F,3}\,C^{(8)}_{\substack{quqd\\i11i}}\right]$$

$$+2m_b Q_d \log\left(\frac{\Lambda}{m_b}\right)\text{Im}\left[C^{(1)}_{\substack{quqd\\3113}} + c_{F,3}\,C^{(8)}_{\substack{quqd\\3113}}\right]$$

Contributions from $\psi\bar{\psi}H^2D$ operators

$$\frac{d_d}{e} \times (4\pi\Lambda)^2 \supset \sum_{i\in\{1,2\}} \frac{4m_i}{\sqrt{2}v}(1 + Q_u)\text{Im}\left[C_{\substack{Hud\\i1}}\right] \tag{II.A.18a}$$

97

$$+ \frac{m_t}{\sqrt{2}v} \left[\frac{m_t^4 - 11m_t^2 m_W^2 + 4m_W^4}{(m_t^2 - m_W^2)^2} \right.$$

$$+ Q_u \frac{m_t^4 + m_t^2 m_W^2 + 4m_W^4}{(m_t^2 - m_W^2)^2}$$

$$\left. + 6m_t^2 m_W^2 \frac{m_t^2 - Q_u m_W^2}{(m_t^2 - m_W^2)^3} \log\left(\frac{m_t^2}{m_W^2}\right) \right] \mathrm{Im}\left[C_{Hud \atop 31} \right] \qquad \text{(II.A.18b)}$$

$$\frac{d_u}{e} \times (4\pi\Lambda)^2 \supset -\frac{2\sqrt{2}}{v} \sum_{i \in \{1,2,3\}} m_{d,i} \, \mathrm{Im}\left[C_{Hud \atop 1i}^\dagger \right] \qquad \text{(II.A.19)}$$

Contributions from $\psi^2 \bar{\psi}^2$ operators

$$\frac{d_d}{e} \times (4\pi\Lambda)^2 \supset -2 \sum_{i \in \{2,3\}} m_{d,i} Q_d \, \mathrm{Im}\left[C_{qd \atop 1ii1}^{(1)} + c_{F,3}\, C_{qd \atop 1ii1}^{(8)} \right] \qquad \text{(II.A.20)}$$

$$\frac{d_u}{e} \times (4\pi\Lambda)^2 \supset -2 \sum_{i \in \{2,3\}} m_{u,i} Q_u \, \mathrm{Im}\left[C_{qu \atop 1ii1}^{(1)} + c_{F,3}\, C_{qu \atop 1ii1}^{(8)} \right] \qquad \text{(II.A.21)}$$

II.A.4 Quark cEDM

Contributions from $\psi^2 H F$ operators

$$\frac{\hat{d}_q}{e} \times (4\pi\Lambda)^2 \supset$$

$$\mathrm{Im}\left[c_w C_{qB \atop 11} + 2T_q^3 s_w C_{qW \atop 11} \right] \left\{ 6\sqrt{2}\, g_s Q_q v + 8\sqrt{2}\, g_s Q_q v \log\left(\frac{\Lambda}{\mu_H}\right) \right\} \qquad \text{(II.A.22a)}$$

$$+\mathrm{Im}\left[-s_w C_{qB \atop 11} + 2T_q^3 c_w C_{qW \atop 11} \right] \left\{ \sqrt{2}\frac{(T_q^3 - 2Q_q s_w^2)}{s_w c_w} g_s v + 4\sqrt{2}\frac{(T_q^3 - 2Q_q s_w^2)}{s_w c_w} g_s v \log\left(\frac{\Lambda}{m_Z}\right) \right\}$$
$$\text{(II.A.22b)}$$

$$+2T_q^3 \mathrm{Im}\left[C_{qW \atop 11} \right] \left\{ \frac{\sqrt{2}\, g_s v}{s_w} + \frac{4\sqrt{2}\, g_s v}{s_w} \log\left(\frac{\Lambda}{m_W}\right) \right\} \qquad \text{(II.A.22c)}$$

$$+\mathrm{Im}\left[C_{qG \atop 11} \right] \left\{ -\frac{16\sqrt{2}\pi^2 v}{e} - 2\sqrt{2}e Q_q^2 v - \frac{v}{\sqrt{2}}\frac{4 + 3N_c^2}{N_c}\frac{g_s^2}{e} \right. \qquad \text{(II.A.22d)}$$

$$- \frac{4\sqrt{2}\, v}{N_c}\frac{g_s^2}{e} \log\left(\frac{\Lambda}{\mu_H}\right)$$

$$\left. + \frac{v}{\sqrt{2}e}\Big(\text{Eq. (II.A.12)}_q + \text{Eq. (II.A.3)} + \text{Eq. (II.A.6)} \Big) \right\}$$
$$\text{(II.A.22e)}$$

Contributions from H^2F^2 operators

$$\frac{\hat{d}_q}{e} \times (4\pi\Lambda)^2 \supset -C_{H\widetilde{G}} \left\{ \frac{6m_q g_s}{e} + \frac{8m_q g_s}{e} \log\left(\frac{\Lambda}{m_h}\right) \right\} \tag{II.A.23}$$

Contributions from F^3 operators

$$\frac{\hat{d}_q}{e} \times (4\pi\Lambda)^2 \supset C_{\widetilde{G}} \left\{ 8N_c m_q \frac{g_s^2}{e} + 6N_c m_q \frac{g_s^2}{e} \log\left(\frac{\Lambda}{\mu_H}\right) \right\} \tag{II.A.24}$$

Contributions from ψ^4 operators

$$\frac{\hat{d}_d}{e} \times (4\pi\Lambda)^2 \supset -2 \sum_{i\in\{1,2\}} \frac{m_{u,i} g_s}{e} \log\left(\frac{\Lambda}{\mu_H}\right) \mathrm{Im}\left[C^{(1)}_{\substack{quqd \\ 1ii1}} - \frac{1}{2N_c} C^{(8)}_{\substack{quqd \\ 1ii1}} \right] \tag{II.A.25}$$

$$- \frac{2m_t g_s}{e} \log\left(\frac{\Lambda}{m_t}\right) \mathrm{Im}\left[C^{(1)}_{\substack{quqd \\ 1331}} - \frac{1}{2N_c} C^{(8)}_{\substack{quqd \\ 1331}} \right]$$

$$\frac{\hat{d}_u}{e} \times (4\pi\Lambda)^2 \supset -2 \sum_{i\in\{1,2\}} \frac{m_{d,i} g_s}{e} \log\left(\frac{\Lambda}{\mu_H}\right) \mathrm{Im}\left[C^{(1)}_{\substack{quqd \\ i11i}} - \frac{1}{2N_c} C^{(8)}_{\substack{quqd \\ i11i}} \right] \tag{II.A.26}$$

$$- \frac{2m_b g_s}{e} \log\left(\frac{\Lambda}{m_b}\right) \mathrm{Im}\left[C^{(1)}_{\substack{quqd \\ 3113}} - \frac{1}{2N_c} C^{(8)}_{\substack{quqd \\ 3113}} \right]$$

Contributions from $\psi\bar{\psi}H^2D$ operators

$$\frac{\hat{d}_d}{e} \times (4\pi\Lambda)^2 \supset \frac{g_s}{e} \sum_{i\in\{1,2\}} \frac{4m_i}{\sqrt{2}v} \mathrm{Im}\left[C_{\substack{Hud \\ i1}} \right] \tag{II.A.27a}$$

$$+ \frac{g_s m_t}{e\sqrt{2}v} \left[\frac{m_t^4 + m_t^2 m_W^2 + 4m_W^4}{(m_t^2 - m_W^2)^2} \right.$$

$$\left. - \frac{6m_t^2 m_W^4}{(m_t^2 - m_W^2)^3} \log\left(\frac{m_t^2}{m_W^2}\right) \right] \mathrm{Im}\left[C_{\substack{Hud \\ 31}} \right] \tag{II.A.27b}$$

$$\frac{\hat{d}_u}{e} \times (4\pi\Lambda)^2 \supset 0 \times \mathrm{Im}\left[C^\dagger_{\substack{Hud \\ ij}} \right] \tag{II.A.28}$$

Contributions from $\psi^2\bar{\psi}^2$ operators

$$\frac{\hat{d}_d}{e} \times (4\pi\Lambda)^2 \supset -2 \sum_{i\in\{2,3\}} \frac{m_i g_s}{e} \mathrm{Im}\left[C^{(1)}_{\substack{qd \\ 1ii1}} - \frac{1}{2N_c} C^{(8)}_{\substack{qd \\ 1ii1}} \right] \tag{II.A.29}$$

$$\frac{\hat{d}_u}{e} \times (4\pi\Lambda)^2 \supset -2 \sum_{i\in\{2,3\}} \frac{m_i g_s}{e} \mathrm{Im}\left[C^{(1)}_{\substack{qu \\ 1ii1}} - \frac{1}{2N_c} C^{(8)}_{\substack{qu \\ 1ii1}} \right] \tag{II.A.30}$$

II.A.5 Gluon cEDM

Contributions from F^3 operators

$$
C_{\widetilde{G}} \times (4\pi\Lambda)^2 \supset \left\{ 2\sqrt{3}\pi^2 N_c - \frac{7N_c}{2} - [8 + N_c] \log\left(\frac{\Lambda}{\mu_H}\right) \right.
$$

$$
\left. - 2\log\left(\frac{\Lambda}{m_b}\right) - 2\log\left(\frac{\Lambda}{m_t}\right) \right\} g_s^2 C_{\widetilde{G}} \tag{II.A.31}
$$

Contributions from $\psi^2 H F$ operators

$$
C_{\widetilde{G}} \times (4\pi\Lambda)^2 \supset \frac{\sqrt{2}\, g_s^2 v}{3} \sum_{\substack{q \in \{u,d\} \\ i \in \{1,2,3\}}} \frac{\mathrm{Im}\left[C_{qG} \atop ii \right]}{m_{q,i}} \tag{II.A.32}
$$

II.A.6 $O_{ud}^{(\mathbf{S1/8,\ RR})}$

Contributions from ψ^4 operators

$$
\mathrm{Im}\left[c_{ud \atop 1111}^{(\mathrm{S1,RR})} \right] \times (4\pi\Lambda)^2 \supset -\frac{c_{F,3} g_s^2}{N_c} \left\{ 3 + 4\log\left(\frac{\Lambda}{\mu_H}\right) \right\} \mathrm{Im}\left[C_{quqd \atop 1111}^{(8)} \right] \tag{II.A.33a}
$$

$$
+ \left\{ (4\pi)^2 - \frac{1}{2}\Big(\text{Eq. (II.A.12)}_u + \text{Eq. (II.A.12)}_d \Big) \right. \tag{II.A.33b}
$$

$$
+ 4c_{F,3} g_s^2 + 2e^2(Q_d^2 - 3Q_d Q_u + Q_u^2) + \frac{5e^2}{4s_w^2}
$$

$$
+ 2e^2 t_w(Q_d^2 - 3Q_d Q_u + Q_u^2) - \frac{5}{2}\frac{T_d^3 T_u^3}{c_w^2 s_w^2} - \frac{5e^2}{c_w^2}
$$

$$
+ 8\left[2c_{F,3} g_s^2 + e^2(Q_d^2 - Q_d Q_u + Q_u^2) \right] \log\left(\frac{\Lambda}{\mu_H}\right) + 2\frac{e^2}{s_w^2}\log\left(\frac{\Lambda}{m_W}\right)
$$

$$
\left. + \frac{4e^2}{s_w^2 c_w^2}\left[2(Q_d^2 - Q_d Q_u + Q_u^2)s_w^4 - 3T_u^3 s_w^2 - T_d^3 T_u^3 \right] \right\} \mathrm{Im}\left[C_{quqd \atop 1111}^{(1)} \right]
$$

$$
+ c_{F,3}\left\{ 3\, g_s^2\, \frac{N_c^2 - 2}{N_c^2} + 3\,\frac{e^2(Q_d + Q_u)^2}{N_c} - \frac{3\, e^2}{2N_c s_w^2} \right. \tag{II.A.33c}
$$

$$
+ \frac{3\, e^2}{N_c s_w^2 c_w^2}\left[(Q_d + Q_u)s_w^2 - T_d^3 \right]\left[(Q_d + Q_u)s_w^2 - T_u^3 \right]
$$

$$
+ \left[4\, g_s^2\, \frac{N_c^2 - 2}{N_c^2} - 4\,\frac{e^2(Q_d + Q_u)^2}{N_c} \right]\log\left(\frac{\Lambda}{\mu_H}\right) - \frac{2\, e^2}{N_c s_w^2}\log\left(\frac{\Lambda}{m_W}\right)
$$

$$
+ \frac{4e^2}{N_c s_w^2 c_w^2}\left[(Q_d + Q_u)s_w^2 - T_d^3 \right]
$$

$$\times \left[(Q_d + Q_u)s_w^2 - T_u^3 \right] \log \left(\frac{\Lambda}{m_Z} \right) \Bigg\} \operatorname{Im} \left[C^{(8)}_{\substack{quqd \\ 1111}} \right]$$

$$+ \left\{ \frac{12 c_{F,3} g_s^2}{N_c} + 3 \frac{e^2 (Q_d + Q_u)^2}{N_c} - \frac{3 e^2}{2 N_c \, s_w^2} \right. \tag{II.A.33d}$$

$$+ 3 \frac{e^2}{N_c \, s_w^2 c_w^2} \left[(Q_d + Q_u)s_w^2 - T_d^3 \right] \left[(Q_d + Q_u)s_w^2 - T_u^3 \right]$$

$$+ \frac{4}{N_c} \left[4 c_{F,3} g_s^2 + e^2 (Q_d + Q_u)^2 \right] \log \left(\frac{\Lambda}{\mu_H} \right) - \frac{2 e^2}{s_w^2} \log \left(\frac{\Lambda}{m_W} \right)$$

$$+ \frac{4 e^2}{N_c \, s_w^2 c_w^2} \left[(Q_d + Q_u)s_w^2 - T_d^3 \right]$$

$$\left. \times \left[(Q_d + Q_u)s_w^2 - T_u^3 \right] \log \left(\frac{\Lambda}{m_Z} \right) \right\} \operatorname{Im} \left[C^{(1)}_{\substack{quqd \\ 1111}} \right]$$

$$\operatorname{Im} \left[c^{(\mathrm{S8,RR})}_{\substack{ud \\ 1111}} \right] \times (4\pi\Lambda)^2 \supset \left\{ (4\pi)^2 - \frac{1}{2} \Big(\text{Eq. (II.A.12)}_u + \text{Eq. (II.A.12)}_d \Big) \right.$$

$$+ \frac{g_s^2 (8 - N_c^2)}{2 N_c} + 2 e^2 (Q_d^2 - 3 Q_d Q_u + Q_u^2) + \frac{5 e^2}{4 s_w^2}$$

$$+ 2 e^2 t_w (Q_d^2 - 3 Q_d Q_u + Q_u^2) - \frac{5}{2} \frac{T_d^3 T_u^3}{c_w^2 s_w^2} - \frac{5 e^2}{c_w^2}$$

$$+ 8 e^2 (Q_d^2 - Q_d Q_u + Q_u^2) \log \left(\frac{\Lambda}{\mu_H} \right) + 2 \frac{e^2}{s_w^2} \log \left(\frac{\Lambda}{m_W} \right)$$

$$+ \frac{4 e^2}{s_w^2 c_w^2} \left[2 (Q_d^2 - Q_d Q_u + Q_u^2)s_w^4 - 3 T_u^3 s_w^2 - T_d^3 T_u^3 \right] \Bigg\} \operatorname{Im} \left[C^{(8)}_{\substack{quqd \\ 1111}} \right]$$

$$- \left\{ 6 g_s^2 + 8 g_s^2 \log \left(\frac{\Lambda}{\mu_H} \right) \right\} \operatorname{Im} \left[C^{(1)}_{\substack{quqd \\ 1111}} \right] \tag{II.A.34a}$$

$$+ \left\{ 3 g_s^2 \frac{2 + N_c^2}{N_c^2} - 3 \frac{e^2 (Q_d + Q_u)^2}{N_c} + \frac{3 e^2}{2 N_c s_w^2} \right. \tag{II.A.34b}$$

$$- \frac{3 e^2}{N_c s_w^2 c_w^2} \left[(Q_d + Q_u)s_w^2 - T_d^3 \right] \left[(Q_d + Q_u)s_w^2 - T_u^3 \right]$$

$$+ \left[4 g_s^2 \frac{2 + N_c^2}{N_c^2} - 4 \frac{e^2 (Q_d + Q_u)^2}{N_c} \right] \log \left(\frac{\Lambda}{\mu_H} \right) + \frac{2 e^2}{N_c s_w^2} \log \left(\frac{\Lambda}{m_W} \right)$$

$$- \frac{4 e^2}{N_c s_w^2 c_w^2} \left[(Q_d + Q_u)s_w^2 - T_d^3 \right]$$

$$\times \left[(Q_d + Q_u)s_w^2 - T_u^3\right] \log\left(\frac{\Lambda}{m_Z}\right)\bigg\} \mathrm{Im}\left[C_{\substack{quqd \\ 1111}}^{(8)}\right]$$

$$+ \left\{-\frac{12g_s^2}{N_c} + 6e^2(Q_d + Q_u)^2 - \frac{3e^2}{s_w^2}\right. \tag{II.A.34c}$$

$$+ 6\frac{e^2}{s_w^2 c_w^2}\left[(Q_d + Q_u)s_w^2 - T_d^3\right]\left[(Q_d + Q_u)s_w^2 - T_u^3\right]$$

$$- 8\left[\frac{2g_s^2}{N_c} - e^2(Q_d + Q_u)^2\right]\log\left(\frac{\Lambda}{\mu_H}\right) - \frac{4e^2}{s_w^2}\log\left(\frac{\Lambda}{m_W}\right)$$

$$+ 8\frac{e^2}{s_w^2 c_w^2}\left[(Q_d + Q_u)s_w^2 - T_d^3\right]$$

$$\left.\times \left[(Q_d + Q_u)s_w^2 - T_u^3\right] \log\left(\frac{\Lambda}{m_Z}\right)\right\} \mathrm{Im}\left[C_{\substack{quqd \\ 1111}}^{(1)}\right]$$

Contributions from $\psi^2 H F$ operators

$$\mathrm{Im}\left[c_{\substack{ud \\ 1111}}^{(\mathrm{S1,RR})}\right] \times (4\pi\Lambda)^2 \supset \frac{\sqrt{2}e\,m_u}{v}\,\mathrm{Im}\left[c_w C_{\substack{dB \\ 11}} - s_w C_{\substack{dW \\ 11}}\right]\left\{\frac{6}{N_c}[Q_d + Q_u - N_c Q_u]\right. \tag{II.A.35a}$$

$$\left. - \frac{8(Q_d + Q_u)}{N_c}\log\left(\frac{\Lambda}{m_W}\right) - 4Q_u\left[\log\left(\frac{\Lambda}{m_Z}\right) + \log\left(\frac{\Lambda}{m_h}\right)\right]\right\}$$

$$+ \frac{\sqrt{2}e\,m_u}{v\,c_w s_w}\,\mathrm{Im}\left[s_w C_{\substack{dB \\ 11}} + c_w C_{\substack{dW \\ 11}}\right]\left\{\frac{2}{N_c}(N_c T_u^3 - 3T_d^3)\right. \tag{II.A.35b}$$

$$+ \frac{2s_w^2}{N_c}(3Q_d + 3Q_u - 2N_c Q_u) + \frac{2}{N_c}(N_c T_u^3 - 4T_d^3)\log\left(\frac{\Lambda}{m_Z}\right)$$

$$+ \frac{2s_w^2}{N_c}(4Q_d + 4Q_u - 2N_c Q_u)\log\left(\frac{\Lambda}{m_Z}\right) + 2(T_u^3 - 2Q_u s_w^2)\log\left(\frac{\Lambda}{m_h}\right)$$

$$- 2(T_u^3 - 2Q_u s_w^2)\frac{m_Z^2}{m_h^2 - m_Z^2}\log\left(\frac{m_h}{m_Z}\right) +$$

$$\left. + 8(T_d^3 - (Q_u + Q_d)s_w^2)\frac{m_W^2}{m_Z^2 - m_W^2}\log\left(\frac{m_Z}{m_W}\right)\right\}$$

$$+ \frac{\sqrt{2}e\,m_u}{v\,s_w}\,\mathrm{Im}\left[C_{\substack{dW \\ 11}}\right]\left\{1 - 6\frac{1 - 2T_d^3}{N_c}\right. \tag{II.A.35c}$$

$$- \frac{16s_w^2(Q_d + Q_u)}{N_c}\frac{m_Z^2}{m_Z^2 - m_W^2}$$

$$+ 4\left[1 + \frac{4(Q_d + Q_u)s_w^2}{N_c}\right]\log\left(\frac{\Lambda}{m_W}\right)$$

$$- 4 \left[\frac{1 - 4T_d^3}{N_c} + \frac{4(Q_d + Q_u)s_w^2}{N_c} \right] \log\left(\frac{\Lambda}{m_Z} \right) - \frac{4}{N_c} \log\left(\frac{\Lambda}{m_h} \right)$$

$$+ 4 \left[1 - 4T_d^3 + 4(Q_d + Q_u)s_w^2 \right] \frac{m_W^2}{m_Z^2 - m_W^2} \log\left(\frac{m_Z}{m_W} \right)$$

$$+ \frac{32\, s_w^2\, m_W^2}{N_c(m_Z^2 - m_W^2)} \left[\frac{T_u^3}{s_w^4} + Q_u + (Q_d + Q_u)\frac{m_Z^2}{m_Z^2 - m_W^2} \right] \log\left(\frac{m_Z}{m_W} \right)$$

$$+ \frac{4}{N_c} \frac{m_W^2}{m_h^2 - m_W^2} \log\left(\frac{m_h}{m_W} \right) \Bigg\}$$

$$+ \frac{4\sqrt{2}g_s m_u}{v} \frac{c_{F,3}}{N_c} \, \mathrm{Im}\left[C_{dG} \atop 11 \right] \left\{ 3 + 4\log\left(\frac{\Lambda}{m_W} \right) \right\} \tag{II.A.35d}$$

$$+ \left(C_{dW} \atop 11 \to -C_{uW} \atop 11, d \leftrightarrow u \right) \tag{II.A.35e}$$

$$\mathrm{Im}\left[c_{\substack{ud \\ 1111}}^{(\mathrm{S8,RR})} \right] \times (4\pi\Lambda)^2 \supset \frac{\sqrt{2}e\, m_u}{v} \, \mathrm{Im}\left[c_w C_{dB} \atop 11 - s_w C_{dW} \atop 11 \right] \left\{ 4(Q_d + Q_u) \left[3 + 4\log\left(\frac{\Lambda}{m_W} \right) \right] \right\} \tag{II.A.36a}$$

$$+ \frac{\sqrt{2}e\, m_u}{v\, c_w s_w} \, \mathrm{Im}\left[s_w C_{dB} \atop 11 + c_w C_{dW} \atop 11 \right] \tag{II.A.36b}$$

$$\times \left\{ 4 \left[(Q_d + Q_u)s_w^2 - T_d^3 \right] \left[3 - \frac{4m_W^2}{m_Z^2 - m_W^2} \log\left(\frac{m_Z}{m_W} \right) + 4\log\left(\frac{\Lambda}{m_W} \right) \right] \right\}$$

$$+ \frac{\sqrt{2}e\, m_u}{v\, s_w} \, \mathrm{Im}\left[C_{dW} \atop 11 \right] \left\{ 12(2T_d^3 - 1) \right. \tag{II.A.36c}$$

$$- 32 s_w^2\, (Q_d + Q_u)\frac{m_Z^2}{m_Z^2 - m_W^2}$$

$$+ 32(Q_d + Q_u)s_w^2 \log\left(\frac{\Lambda}{m_W} \right) - 8\log\left(\frac{\Lambda}{m_h} \right)$$

$$- 8 \left[1 - 4T_d^3 + 4(Q_d + Q_u)s_w^2 \right] \log\left(\frac{\Lambda}{m_Z} \right) + \frac{8m_W^2}{m_h^2 - m_W^2} \log\left(\frac{m_h}{m_W} \right)$$

$$+ \left[1 - 4T_d^3 + 4(Q_d + Q_u)s_w^2 \right] \frac{8m_W^2}{m_Z^2 - m_W^2} \log\left(\frac{m_Z}{m_W} \right)$$

$$+ \frac{64\, s_w^2\, m_W^2}{m_Z^2 - m_W^2} \left[\frac{T_u^3}{s_w^2} + Q_u + (Q_d + Q_u)\frac{m_Z^2}{m_Z^2 - m_W^2} \right] \log\left(\frac{m_Z}{m_W} \right) \right\}$$

$$+ \frac{2\sqrt{2}g_s m_u}{v} \, \mathrm{Im}\left[C_{dG} \atop 11 \right] \left\{ -\frac{3(2 + N_c)}{N_c} - \frac{8}{N_c} \log\left(\frac{\Lambda}{m_W} \right) \right. \tag{II.A.36d}$$

$$-2\log\left(\frac{\Lambda}{m_Z}\right) - 2\log\left(\frac{\Lambda}{m_h}\right)\Big\}$$

$$+\Big(C_{\underset{11}{dW}} \to -C_{\underset{11}{uW}}, d \leftrightarrow u\Big) \tag{II.A.36e}$$

II.A.7 $O_{duud}^{\text{(S1/8, RR)}}$

Contributions from ψ^4 operators

$$\text{Im}\left[c_{\underset{1111}{duud}}^{\text{(S8,RR)}}\right] \times (4\pi\Lambda)^2 \supset \Big\{3g_s^2\frac{2+N_c^2}{N_c^2} - \frac{12e^2Q_dQ_u}{N_c} + \frac{3e^2}{2s_w^2} \tag{II.A.37a}$$

$$-\frac{3e^2}{N_c\,s_w^2c_w^2}(2Q_ds_w^2 - T_d^3)(2Q_us_w^2 - T_u^3)$$

$$+\frac{4}{N_c^2}\left[g_s^2(2+N_c^2) - 4e^2N_cQ_dQ_u\right]\log\left(\frac{\Lambda}{\mu_H}\right) + \frac{2e^2}{N_c\,s_w^2}\log\left(\frac{\Lambda}{m_W}\right)$$

$$-\frac{4e^2}{N_c\,s_w^2c_w^2}(2Q_ds_w^2 - T_d^3)(2Q_us_w^2 - T_u^3)\log\left(\frac{\Lambda}{m_Z}\right)\Big\}\text{Im}\left[C_{\underset{1111}{quqd}}^{(8)}\right]$$

$$+\left\{-\frac{12g_s^2}{N_c} + 24e^2Q_dQ_u - \frac{3e^2}{s_w^2}\right. \tag{II.A.37b}$$

$$+\frac{6e^2}{s_w^2c_w^2}(2Q_ds_w^2 - T_d^3)(2Q_us_w^2 - T_u^3)$$

$$-\frac{16g_s^2}{N_c} + 32e^2Q_dQ_u\log\left(\frac{\Lambda}{\mu_H}\right) - \frac{4e^2}{s_w^2}\log\left(\frac{\Lambda}{m_W}\right) \tag{II.A.37c}$$

$$\left.+\frac{8e^2}{s_w^2c_w^2}(2Q_ds_w^2 - T_d^3)(2Q_us_w^2 - T_u^3)\log\left(\frac{\Lambda}{m_Z}\right)\right\}\text{Im}\left[C_{\underset{1111}{quqd}}^{(1)}\right]$$

$$+\left\{(4\pi)^2 - \frac{1}{2}\Big(\text{Eq. (II.A.12)}_u + \text{Eq. (II.A.12)}_d\Big)\right. \tag{II.A.37d}$$

$$+\frac{g_s^2(8-N_c^2)}{2N_c} - \frac{e^2(Q_d+Q_u)^2}{2} + \frac{5e^2}{4s_w^2}$$

$$-\frac{e^2}{2c_w^2s_w^2}\left[5T_d^3T_u^3 + (Q_d+Q_u)^2s_w^4\right]$$

$$+8e^2Q_dQ_u\log\left(\frac{\Lambda}{\mu_H}\right) + \frac{2e^2}{s_w^2}\log\left(\frac{\Lambda}{m_W}\right)$$

$$\left.+4e^2\left[2Q_dQ_ut_w^2 + \frac{T_u^3}{c_w^2} - \frac{T_u^3T_d^3}{s_w^2c_w^2}\right]\log\left(\frac{\Lambda}{m_Z}\right)\right\}\text{Im}\left[C_{\underset{1111}{quqd}}^{(8)}\right]$$

$$-2g_s^2\left\{3 + 4\log\left(\frac{\Lambda}{\mu_H}\right)\right\}\text{Im}\left[C_{\underset{1111}{quqd}}^{(1)}\right] \tag{II.A.37e}$$

$$\text{Im}\left[c_{\substack{duud \\ 1111}}^{(\text{S1,RR})}\right] \times (4\pi\Lambda)^2 \supset c_{F,3}\left\{3g_s^2\frac{N_c^2-2}{N_c^2} + \frac{12e^2Q_dQ_u}{N_c} - \frac{3e^2}{2s_w^2}\right. \tag{II.A.38a}$$

$$+ \frac{3e^2}{N_c\,s_w^2c_w^2}(2Q_ds_w^2 - T_d^3)(2Q_us_w^2 - T_u^3)$$

$$+ \frac{4}{N_c^2}\left[g_s^2(N_c^2-2) + 4e^2N_cQ_dQ_u\right]\log\left(\frac{\Lambda}{\mu_H}\right) - \frac{2e^2}{N_c\,s_w^2}\log\left(\frac{\Lambda}{m_W}\right)$$

$$\left.+ \frac{4e^2}{N_c\,s_w^2c_w^2}(2Q_ds_w^2 - T_d^3)(2Q_us_w^2 - T_u^3)\log\left(\frac{\Lambda}{m_Z}\right)\right\}\text{Im}\left[C_{\substack{quqd \\ 1111}}^{(8)}\right]$$

$$+ \left\{\frac{12c_{F,3}g_s^2}{N_c} + 12\frac{e^2Q_dQ_u}{N_c} - \frac{3e^2}{2N_c\,s_w^2}\right. \tag{II.A.38b}$$

$$+ \frac{3e^2}{N_c\,s_w^2c_w^2}(2Q_ds_w^2 - T_d^3)(2Q_us_w^2 - T_u^3)$$

$$+ \frac{16}{N_c}\left[g_s^2c_{F,3} + e^2Q_dQ_u\right]\log\left(\frac{\Lambda}{\mu_H}\right) - \frac{2e^2}{N_c\,s_w^2}\log\left(\frac{\Lambda}{m_W}\right) \tag{II.A.38c}$$

$$\left.+ \frac{4e^2}{N_c\,s_w^2c_w^2}(2Q_ds_w^2 - T_d^3)(2Q_us_w^2 - T_u^3)\log\left(\frac{\Lambda}{m_Z}\right)\right\}\text{Im}\left[C_{\substack{quqd \\ 1111}}^{(1)}\right]$$

$$- \frac{c_{F,3}g_s^2}{N_c}\left\{3 + 4\log\left(\frac{\Lambda}{\mu_H}\right)\right\}\text{Im}\left[C_{\substack{quqd \\ 1111}}^{(8)}\right] \tag{II.A.38d}$$

$$+ \left\{(4\pi)^2 - \frac{1}{2}\Big(\text{Eq. (II.A.12)}_u + \text{Eq. (II.A.12)}_d\Big)\right. \tag{II.A.38e}$$

$$+ 4c_{F,3}g_s^2 - \frac{e^2(Q_d+Q_u)^2}{2} + \frac{5e^2}{4s_w^2}$$

$$- \frac{e^2}{2c_w^2s_w^2}\left[5T_d^3T_u^3 + (Q_d+Q_u)^2s_w^4\right]$$

$$+ 8\left[2c_{F,3}g_s^2 + e^2Q_dQ_u\right]\log\left(\frac{\Lambda}{\mu_H}\right) + \frac{2e^2}{s_w^2}\log\left(\frac{\Lambda}{m_W}\right)$$

$$\left.+ 4e^2\left[2Q_dQ_ut_w^2 + \frac{T_u^3}{c_w^2} - \frac{T_u^3T_d^3}{s_w^2c_w^2}\right]\log\left(\frac{\Lambda}{m_Z}\right)\right\}\text{Im}\left[C_{\substack{quqd \\ 1111}}^{(1)}\right]$$

Contributions from ψ^2HF operators

$$\text{Im}\left[c_{\substack{duud \\ 1111}}^{(\text{S1,RR})}\right] \times (4\pi\Lambda)^2 \supset \frac{\sqrt{2}e\,m_u}{v}\text{Im}\left[c_wC_{\substack{dB \\ 11}} - s_wC_{\substack{dW \\ 11}}\right]\left\{\frac{12Q_u}{N_c} - 3(Q_d+Q_u)\right. \tag{II.A.39a}$$

$$+ 2(Q_d + Q_u) \log\left(\frac{\Lambda}{m_W}\right) - \frac{4Q_u}{N_c}\left[\log\left(\frac{\Lambda}{m_Z}\right) + \log\left(\frac{\Lambda}{m_h}\right)\right]$$

$$+ \frac{\sqrt{2}e\,m_u}{v\,c_w s_w}\, \text{Im}\left[s_w C_{dB} + c_w C_{dW}\right]\left\{3T_d^3 - \frac{4T_u^3}{N_c}\right. \tag{II.A.39b}$$

$$+ \frac{8Q_u - 3N_c(Q_d + Q_u)}{N_c}s_w^2$$

$$- 2\left[T_d^3 - \frac{T_u^3}{N_c} - \frac{N_c(Q_d + Q_u) - 2Q_u}{N_c}s_w\right]\log\left(\frac{\Lambda}{m_Z}\right)$$

$$+ \frac{2}{N_c}(T_u^3 - 2Q_u s_w^2)\log\left(\frac{\Lambda}{m_h}\right)$$

$$- (T_u^3 - 2Q_u s_w^2)\frac{4m_Z^2}{m_Z^2 - m_H^2}\log\left(\frac{m_h}{m_Z}\right)$$

$$\left. - ((Q_d + Qu)s_w^2 - T_d^3)\frac{4m_W^2}{m_Z^2 - m_W^2}\log\left(\frac{m_Z}{m_W}\right)\right\}$$

$$+ \frac{\sqrt{2}e\,m_u}{v\,s_w}\, \text{Im}\left[C_{dW}\right]\left\{3 - 6T_d^3 - \frac{2}{N_c}\right. \tag{II.A.39c}$$

$$+ 8s_w^2\,(Q_d + Q_u)\frac{m_Z^2}{m_Z^2 - m_W^2}$$

$$- 8\left[\frac{1}{N_c} + (Q_d + Q_u)s_w^2\right]\log\left(\frac{\Lambda}{m_W}\right)$$

$$- 2\left[4T_d^3 - 1 - 4(Q_d + Q_u)s_w^2\right]\log\left(\frac{\Lambda}{m_Z}\right) + 2\log\left(\frac{\Lambda}{m_h}\right)$$

$$+ \left[4T_d^3 - 1 - 4(Q_d + Q_u)s_w^2\right]\frac{2m_W^2}{m_Z^2 - m_W^2}\log\left(\frac{m_Z}{m_W}\right)$$

$$- \frac{16\,s_w^2\,m_W^2}{m_Z^2 - m_W^2}\left[\frac{T_u^3}{s_w^2} + Q_u + (Q_d + Q_u)\frac{m_Z^2}{m_Z^2 - m_W^2}\right]\log\left(\frac{m_Z}{m_W}\right)$$

$$\left. - \frac{2m_W^2}{m_h^2 - m_W^2}\log\left(\frac{m_h}{m_W}\right)\right.$$

$$+ \frac{4\sqrt{2}g_s m_u}{v}\frac{c_{F,3}}{N_c}\, \text{Im}\left[C_{dG}\right]\left\{3 + 2\log\left(\frac{\Lambda}{m_Z}\right) + 2\log\left(\frac{\Lambda}{m_h}\right)\right\} \tag{II.A.39d}$$

$$+ \left(C_{dW} \to -C_{uW}, d \leftrightarrow u\right) \tag{II.A.39e}$$

$$\text{Im}\left[c_{\substack{duud \\ 1111}}^{\text{(S8,RR)}}\right] \times (4\pi\Lambda)^2 \supset \frac{\sqrt{2}e\,m_u}{v}\,\text{Im}\left[c_w C_{\substack{dB \\ 11}} - s_w C_{\substack{dW \\ 11}}\right]\left\{24 Q_u \right. \tag{II.A.40a}$$

$$\left. +16 Q_u \log\left(\frac{\Lambda}{m_Z}\right) + 16 Q_u \log\left(\frac{\Lambda}{m_h}\right)\right\}$$

$$+ \frac{\sqrt{2}e\,m_u}{v\,c_w s_w}\,\text{Im}\left[s_w C_{\substack{dB \\ 11}} + c_w C_{\substack{dW \\ 11}}\right]\left\{8(2Q_u s_w^2 - T_u^3)\right. \tag{II.A.40b}$$

$$\left. + 8(2Q_u s_w^2 - T_u^3)\left[\log\left(\frac{\Lambda}{m_Z}\right) + \log\left(\frac{\Lambda}{m_h}\right)\right]\right.$$

$$\left. - 8(2Q_u s_w^2 - T_u^3)\frac{m_Z^2}{m_h^2 - m_Z^2}\log\left(\frac{m_h}{m_Z}\right)\right\}$$

$$- \frac{4\sqrt{2}e\,m_u}{v\,s_w}\,\text{Im}\left[C_{\substack{dW \\ 11}}\right]\left\{1 + 4\log\left(\frac{\Lambda}{m_W}\right)\right\} \tag{II.A.40c}$$

$$- \frac{2\sqrt{2}g_s m_u}{v}\,\text{Im}\left[C_{\substack{dG \\ 11}}\right]\left\{\frac{3(2 + N_c)}{N_c} + 4\log\left(\frac{\Lambda}{m_W}\right)\right. \tag{II.A.40d}$$

$$\left. + \frac{4}{N_c}\log\left(\frac{\Lambda}{m_Z}\right) + \frac{4}{N_c}\log\left(\frac{\Lambda}{m_h}\right)\right\}$$

$$+ \left(C_{\substack{dW \\ 11}} \to -C_{\substack{uW \\ 11}}, d \leftrightarrow u\right) \tag{II.A.40e}$$

II.A.8 O_{Hud}

Contributions from $\psi\bar{\psi}H^2 D$ operators

$$\text{Im}\left[C_{\substack{Hud \\ 11}}\right] \times (4\pi\Lambda)^2 \supset \left\{(4\pi)^2 - \frac{1}{2}\left(\text{Eq. (II.A.2c)}_u + \text{Eq. (II.A.2d)}_u + \text{Eq. (II.A.3)}\right.\right. \tag{II.A.41}$$

$$\left.\left. + \text{Eq. (II.A.2c)}_d + \text{Eq. (II.A.2d)}_d\right) - \pi^2 e^2 \right. \tag{II.A.42}$$

$$\left. - \frac{2\pi^2}{3}e^2\frac{m_Z^2}{m_W^2}\left[\frac{Q_d - Q_d\,t_w^2}{4} - Q_d Q_u t_w^2\frac{m_Z^2}{m_W^2}\right]\right.$$

$$\left. - 4e^2 - 4g^2 - 2g^2 c_{2w} - \frac{g^2}{2c_w^2} + e^2 Q_d\frac{c_{2w}}{c_w^2} + \frac{g^2}{12c_w^4} + 2e^2 t_w^2\right.$$

$$\left. - g^2 t_w^2 - 2e^2 Q_d Q_u\frac{t_w^2}{c_w^2} + 2\frac{m_h^2}{v^2} - \frac{m_h^4}{3m_W^2 v^2}\right.$$

$$\left. + 2\left[c_{F,3}g_s^2 + e^2 Q_d Q_u\right]\log\left(\frac{\Lambda}{\mu_H}\right) - 2e^2\log\left(\frac{\Lambda}{m_W}\right)\right.$$

$$- \left[2e^2 + \frac{7}{3}g^2 + 2g^2(c_w^2 - 2s_w^2) - 2e^2(1 + Q_d Q_u)t_w^2 \right] \log\left(\frac{\Lambda}{m_Z} \right)$$

$$- \frac{5g^2}{3} \log\left(\frac{\Lambda}{m_h} \right) - 4e^2 t_w^2 Q_d Q_u \frac{m_Z^4}{m_W^4} \log^2\left(\frac{m_Z}{m_W} \right)$$

$$+ g^2 \left[\frac{1}{3} + \frac{3m_h^2}{v^2} - \frac{2m_h^4}{m_W^2 v^2} + \frac{m_h^6}{3m_W^4 v^2} \right] \log\left(\frac{m_h}{m_W} \right) - \frac{g^2}{3} \log\left(\frac{m_h}{m_Z} \right)$$

$$+ 2e^2 \left[Q_u(3 - t_w^2 + Q_d t_w^2) + \frac{c_{2w}}{c_w^2} - (3 - Q_d Q_u t_w^2)\frac{m_Z^2}{m_W^2} \right] \log\left(\frac{m_Z}{m_W} \right)$$

$$- g^2 \left[\frac{13}{3} + 2c_{2w^2} + \frac{1}{2c_w^2} \right.$$

$$\left. - \left(1 + c_{2w} + \frac{1}{2c_w^2} \right) \frac{m_Z^2}{m_W^2} + \frac{1}{12c_w^2}\frac{m_Z^2}{m_W^2} \right] \log\left(\frac{m_Z}{m_W} \right)$$

$$- \frac{e^2 Q_d}{c_w^2}\frac{m_Z^2}{m_W^2} \left[c_{2w} - 2Q_d Q_u s_w^2 \frac{m_Z^2}{m_W^2} \right] \text{Li}_2\left(1 + \frac{m_Z^2}{m_W^2} \right)$$

$$- \left[g^2 + \frac{4m_h^2}{3v^2} - \frac{m_h^4}{3m_W^2 v^2} \right] F(m_W^2, m_h, m_W)$$

$$+ \left[4e^2 - 2g^2 c_w - \frac{g^2}{3c_w^2} + g^2\frac{m_Z^2}{12m_W^2}\left(\frac{1}{c_w^2} - 12 \right) \right] F(m_W^2, m_W, m_Z)$$

$$+ e^2 \left[2 - \frac{1}{c_w^2} \right] C_0(m_W^2, m_Z, m_W) \bigg\} \text{Im}\left[C_{\underset{11}{Hud}} \right],$$

where we defined

$$F(x, y, z) = \frac{\sqrt{\lambda(x, y^2, z^2)}}{x} \log\left(\frac{y^2 + z^2 - x + \sqrt{\lambda(x, y^2, z^2)}}{2yz} \right), \tag{II.A.43}$$

$$C_0(x, y, \sqrt{x}) = \frac{\pi^2}{6} + \frac{1}{2}\log\left(\frac{\sqrt{y^4 - 4xy^2} - y^2}{2x + \sqrt{y^4 - 4xy^2} - y^2} \right) \tag{II.A.44}$$

$$- \text{Li}_2\left(\frac{2x}{y^2 - \sqrt{y^4 - 4xy^2}} \right) + \text{Li}_2\left(-\frac{2x}{2x + \sqrt{y^4 - 4xy^2} - y^2} \right),$$

with the usual Kallen λ-function and $\text{Li}_2(x)$ denotes the dilogarithm.

Contributions from $\psi^2 HF$ operators

$$\text{Im}\left[C_{\underset{11}{Hud}} \right] \times (4\pi\Lambda)^2 \supset -\frac{5c_{F,3}g_s m_u}{\sqrt{2}v}\text{Im}\left[C_{\underset{11}{dG}} \right] \tag{II.A.45a}$$

$$- \frac{e m_u}{\sqrt{2}v}\text{Im}\left[-s_w C_{\underset{11}{dW}} + c_w C_{\underset{11}{dB}} \right][-1 + 9Q_u$$

$$+ 4Q_u m_h^2 C_0(m_h^2, m_W^2, m_h^2 + m_W^2, 0, 0, 0)] \tag{II.A.45b}$$

$$+ \frac{em_u}{\sqrt{2}s_w c_w v} \text{Im}\left[-s_w C_{dB \atop 11} - c_w C_{dW \atop 11}\right]\left\{-4 + \frac{9}{2}Q_u + 8T_u^3 \right. \tag{II.A.45c}$$

$$+ c_{2w}\left(\frac{1}{2}(1 - 9Q_u) - 4\frac{m_Z^2}{m_W^2} + \pi^2 \frac{2m_Z^4}{3m_W^4}\right) + 2Q_u s_w^2 \log\left(\frac{m_Z^2}{m_h^2}\right)$$

$$+ 2Q_u s_w^2\left[\frac{m_h^4 - m_W^4 + m_h^2 m_Z^2 + 3m_W^2 m_Z^2 - 2m_Z^4}{m_h^2(m_h^2 + m_W^2)}\log\left(\frac{m_Z^2}{m_h^2 + m_W^2 - m_Z^2}\right)\right.$$

$$\left.+ \frac{(m_W^2 - m_Z^2)(m_W^2 - 2m_Z^2 - 4m_h^2)}{m_h^2 m_W^2}\log\left(\frac{m_Z^2}{m_Z^2 - m_W^2}\right)\right]$$

$$+ 2c_{2w}\frac{(m_W^2 + 2m_Z^2)}{m_W^2}\log\left(\frac{m_Z^2}{m_W^2}\right) - 4c_{2w}\frac{m_Z^4}{m_W^4}\text{Li}_2\left(1 - \frac{m_W^2}{m_Z^2}\right)$$

$$\left.+ 2Q_u s_w^2\left(2m_h^2 + m_Z^2\right)C_0(m_h^2, m_W^2, m_h^2 + m_W^2, 0, 0, m_Z)\right\}$$

$$+ \frac{em_u}{\sqrt{2}s_w v}\text{Im}\left[C_{dW \atop 11}\right]\left\{4\left(-3 + 4Q_u s_w^2(3 - \pi^2 + 3s_w t_w^2) + \frac{m_h^2 + m_Z^2}{m_W^2}\right)\right. \tag{II.A.45d}$$

$$- \frac{12m_W^4 + 9m_h^2 m_W^2 - 4m_h^4}{2m_W^2(m_h^2 + m_W^2)}\log\left(\frac{m_W^2}{m_h^2}\right) + \frac{2(m_Z^2 - 4m_W^2)}{m_W^2}\log\left(\frac{m_W^2}{m_Z^2}\right)$$

$$- \frac{4m_h^4 - 12m_h^2 m_W^2 + 8m_W^4}{m_W^4}\log\left(\frac{m_h^2}{m_h^2 - m_W^2}\right)$$

$$- \frac{8m_W^4 - 12m_W^2 m_Z^2 + 4m_Z^4}{m_W^4}\log\left(\frac{m_Z^2}{m_Z^2 - m_W^2}\right)$$

$$- \frac{5m_W^4 - 4m_h^2 m_W^2 + m_h^4}{m_W^4}\log^2\left(\frac{m_W^2}{m_h^2 - m_W^2}\right)$$

$$- \frac{5m_W^4 - 4m_W^2 m_Z^2 + m_Z^4}{m_W^4}\log^2\left(\frac{m_W^2}{m_Z^2 - m_W^2}\right)$$

$$+ \frac{2\sqrt{m_h^4 - 4m_h^2 m_W^2}}{m_h^2}\log\left(\frac{2m_W^2 - m_h^2 + \sqrt{m_h^4 - 4m_h^2 m_W^2}}{2m_W^2}\right)$$

$$+ 4Q_u s_w^2\left[\log\left(\frac{m_Z^2}{m_h^2}\right)\right.$$

$$+\frac{m_h^4 - m_W^4 + m_h^2 m_Z^2 + 3m_W^2 m_Z^2 - 2m_Z^4}{m_h^2(m_h^2 + m_W^2)}\log\left(\frac{m_Z^2}{m_h^2 + m_W^2 - m_Z^2}\right)$$

$$+\frac{(m_W^2 - 2m_H^2 - 2m_Z^2)(m_W^2 - m_Z^2)}{m_h^2 m_W^2}\log\left(\frac{m_Z^2}{m_Z^2 - m_W^2}\right)$$

$$-3s_w^2 t_w\left(\frac{2m_Z^2 - 4m_W^2}{m_W^3 - m_W m_Z^2}\log\left(\frac{m_W^2}{m_Z^2}\right)\right.$$

$$\left.+\frac{4m_Z(m_Z^2 - m_W^2)}{m_W^3}\log\left(\frac{m_Z^2}{m_Z^2 - m_W^2}\right) + \frac{m_Z(m_Z^2 - 2m_W^2)}{m_W^3}\log^2\left(\frac{m_W^2}{m_Z^2 - m_W^2}\right)\right)\Bigg]$$

$$+48 Q_u s_w^2 \mathrm{Li}_2(2) - 2\frac{m_h^4 - 4m_h^2 m_W^2 + 5m_W^4}{m_W^4}\left(\mathrm{Li}_2\left(1 - \frac{m_h^2}{m_W^2}\right) + \mathrm{Li}_2\left(\frac{m_h^2 - 2m_W^2}{m_h^2 - m_W^2}\right)\right)$$

$$-2\frac{m_Z^4 - 4m_W^2 m_Z^2 + 5m_W^4}{m_W^4}\left(\mathrm{Li}_2\left(1 - \frac{m_Z^2}{m_W^2}\right) + \mathrm{Li}_2\left(\frac{m_Z^2 - 2m_W^2}{m_Z^2 - m_W^2}\right)\right)$$

$$-24 Q_u s_w^4 t_w\frac{m_Z(m_Z^2 - 2m_W^2)}{m_W^3}\left(\mathrm{Li}_2\left(1 - \frac{m_Z^2}{m_W^2}\right) + \mathrm{Li}_2\left(\frac{m_Z^2 - 2m_W^2}{m_Z^2 - m_W^2}\right)\right)$$

$$+\left(2m_W^2 - \frac{5}{2}m_h^2\right)C_0\left(m_h^2, m_W^2, m_h^2 + m_W^2, m_W, m_W, 0\right) + 4Q_u s_w^2\Big(\left(2m_h^2 + m_Z^2\right)\times$$

$$\times C_0\left(m_h^2, m_W^2, m_h^2 + m_W^2, 0, 0, m_Z\right) - 2m_h^2 C_0\left(m_h^2, m_W^2, m_h^2 + m_W^2, 0, 0, 0\right)\Big)\Bigg\}$$

$$+\left(C_{dG\atop 11} \to C_{uG\atop 11}^\dagger, C_{dW\atop 11} \to -C_{uW\atop 11}^\dagger, C_{dB\atop 11} \to C_{uB\atop 11}^\dagger, d \leftrightarrow u\right) \tag{II.A.45e}$$

where $C_0(s_1, s_{12}, s_2, m_0, m_1, m_2)$ is the scalar Passarino-Veltman three-point function with kinematic invariants s_1, s_{12}, s_2 and masses m_0, m_1, m_2 which can be evaluated numerically with computer programs like Package-X [212].

Contributions from $\psi^2\bar\psi^2$ operators

$$\mathrm{Im}\left[C_{Hud\atop 11}\right] \times (4\pi\Lambda)^2 \supset 4 \sum_{i,j\in\{1,2,3\}} \frac{m_{d,i} m_{u,j}}{v^2}\mathrm{Im}\left[C_{ud\atop 1ji1}^{(1)} + c_{F,3} C_{ud\atop 1ji1}^{(8)}\right]$$

$$\times\left\{1 + \frac{1}{4}\left[2\,\mathrm{sgn}_{ij} + \frac{m_{u,j}^2}{m_W^2}\right]\log\left(\frac{m_{d,i}^2}{m_{u,j}^2}\right)\right.$$

$$+ 2\log\left(\frac{2\Lambda}{m_{d,i} + m_{u,j} - (m_{d,i} - m_{u,j})\mathrm{sgn}_{ij}}\right)$$

$$\left.+ F(2m_W^2, m_{d,i}, m_{u,j})\right\} \tag{II.A.46}$$

Here we defined

$$\text{sgn}_{ij} = \text{sgn}(m_{d,i} - m_{u,j}). \tag{II.A.47}$$

Contributions from $\psi^2 H^3$ operators

$$\text{Im}\left[C_{H\underset{11}{ud}}\right] \times (4\pi\Lambda)^2 \supset \frac{m_u}{\sqrt{2}\,v} \left\{ 2\pi^2 - 2 - 2\pi^2 \left[\frac{m_h^2}{m_W^2} + \frac{m_h^4}{2m_W^4} \right] \right. \tag{II.A.48a}$$

$$+ \frac{2\pi^2}{3} \left[\frac{m_Z^2}{m_W^2} + \frac{m_Z^4}{2m_W^4} \right] + \frac{3\,m_h^2 - m_Z^2}{m_W^2} +$$

$$+ 6 \left[2 + \frac{m_H^2}{m_W^2} \right] \log\left(\frac{m_h}{m_W} \right)$$

$$- 2 \left[2 + \frac{m_Z^2}{m_W^2} \right] \log\left(\frac{m_Z}{m_W} \right) - 8\,\text{Li}_2(2)$$

$$+ 3 \left[1 + 2\frac{m_h^2}{m_W^2} + \frac{m_h^4}{m_W^4} \right] \left[\text{Li}_2\left(1 + \frac{m_h^2}{m_W^2} \right) + \frac{1}{2} \log^2\left(\frac{m_h^2}{m_W^2} \right) \right]$$

$$- \left[1 + 2\frac{m_Z^2}{m_W^2} + \frac{m_Z^4}{m_W^4} \right] \left[\text{Li}_2\left(1 + \frac{m_Z^2}{m_W^2} \right) \right.$$

$$\left. \left. + \frac{1}{2} \log^2\left(\frac{m_Z^2}{m_W^2} \right) \right] \right\} \text{Im}\left[C_{d\underset{11}{H}} \right]$$

$$+ \left(C_{d\underset{11}{H}} \rightarrow C_{u\underset{11}{H}}^\dagger, d \leftrightarrow u \right) \tag{II.A.48b}$$

Operator	Tree	Tree+Loop
$\mathrm{Im}C_{eB}\atop 11$	$1.37\cdot10^{-5}\lambda_e g^{'}$	$1.70\cdot10^{-5}\lambda_e g^{'}$
$\mathrm{Im}C_{eW}\atop 11$	$1.37\cdot10^{-5}\lambda_e g$	$1.68\cdot10^{-5}\lambda_e g$

Operator	RGE only	RGE + finite
$C_{H\widetilde{B}}$	$5.27\cdot10^{-3}g^{'2}$	$3.08\cdot10^{-3}g^{'2}$
$C_{H\widetilde{W}}$	$1.95\cdot10^{-3}g^{2}$	$1.18\cdot10^{-3}g^{2}$
$C_{HW\widetilde{B}}$	$1.52\cdot10^{-3}gg^{'}$	$2.12\cdot10^{-3}gg^{'}$
$C_{\widetilde{W}}$	—	$1.59\cdot10^{-2}g^{3}$

Operator	RGE only	RGE + finite
$\mathrm{Im}C^{(3)}_{lequ}\atop 1111$	$5.43\cdot10^{4}\lambda_e\lambda_u$	—
$\mathrm{Im}C^{(3)}_{lequ}\atop 1122$	$1.57\cdot10^{-1}\lambda_e\lambda_c$	—
$\mathrm{Im}C^{(3)}_{lequ}\atop 1133$	$4.33\cdot10^{-5}\lambda_e\lambda_t$	—
$\mathrm{Im}C_{le}\atop 1221$	—	$8.15\cdot10^{-5}g^{'2}$
$\mathrm{Im}C_{le}\atop 1331$	—	$4.85\cdot10^{-6}g^{'2}$

Table II.B.1: Upper bounds on the Wilson coefficients contributing to the EDM of the electron, assuming $\Lambda = 5$ TeV and no further assumptions. In the upper left table, the Wilson coefficients which can enter at tree level are presented. The column 'Tree+Loop' presents bounds including the tree level contribution, the RG running and all finite terms. In the other tables one can find all other Wilson coefficients which cannot enter at tree level. The left column shows only RG running, while the right column shows both RG running and finite terms. Above, the parameter λ_i is the ith diagonal entry of the lepton Yukawa matrix.

II.B Bounds on Wilson coefficients and UV scale Λ

In this appendix, we present the bounds on all Wilson coefficients that appear in the expression of the electron and neutron EDM. To give more meaningful bounds, we factor out their naturally expected scaling in the Standard Model couplings. We also obtained bounds on the scale of new physics Λ by rescaling the Wilson coefficients by their natural scaling and demanding the remaining Wilson coefficient to be of order 1.

II.B.1 Electron EDM

Operator	Tree	Tree+Loop
$\text{Im}C_{eB}\atop{11}$	$1.35 \cdot 10^3$	$1.11 \cdot 10^3$
$\text{Im}C_{eW}\atop{11}$	$1.35 \cdot 10^3$	$1.13 \cdot 10^3$

Operator	RGE only	RGE + finite
$C_{H\widetilde{B}}$	$1.03 \cdot 10^2$	$1.2 \cdot 10^2$
$C_{H\widetilde{W}}$	$1.1 \cdot 10^2$	$1.27 \cdot 10^2$
$C_{HW\widetilde{B}}$	$1.62 \cdot 10^2$	$1.46 \cdot 10^2$
$C_{\widetilde{W}}$	—	$3.96 \cdot 10^1$

Operator	RGE only	RGE + finite
$\text{Im}C^{(3)}_{lequ}\atop{1111}$	$1.73 \cdot 10^{-2}$	—
$\text{Im}C^{(3)}_{lequ}\atop{1122}$	$1.30 \cdot 10^1$	—
$\text{Im}C^{(3)}_{lequ}\atop{1133}$	$1.16 \cdot 10^3$	—
$\text{Im}C_{le}\atop{1221}$	—	$5.54 \cdot 10^2$

Table II.B.2: Lower bounds on the UV scale Λ in TeV assuming the natural scaling for all Wilson coefficients as given in the previous table and no further assumptions. The labelling of the tables is the same as for the bounds on the Wilson coefficients.

Operator	Tree	Tree+Loop
$\mathrm{Im}C_{uG \atop 11}$	$1.61 \cdot 10^{-2}\lambda_u g_s$	$3.91 \cdot 10^{-3}\lambda_u g_s$
$\mathrm{Im}C_{uB \atop 11}$	$2.59 \cdot 10^{-2}\lambda_u g'$	$5.12 \cdot 10^{-2}\lambda_u g'$
$\mathrm{Im}C_{uW \atop 11}$	$2.59 \cdot 10^{-2}\lambda_u g$	$4.19 \cdot 10^{-2}\lambda_u g$
$\mathrm{Im}C_{dG \atop 11}$	$3.73 \cdot 10^{-3}\lambda_d g_s$	$1.11 \cdot 10^{-3}\lambda_d g_s$
$\mathrm{Im}C_{dB \atop 11}$	$3.11 \cdot 10^{-3}\lambda_d g'$	$6.48 \cdot 10^{-3}\lambda_d g'$
$\mathrm{Im}C_{dW \atop 11}$	$3.11 \cdot 10^{-3}\lambda_d g$	$5.44 \cdot 10^{-3}\lambda_d g$
$\mathrm{Im}C_{dB \atop 22}$	$4.54 \cdot 10^{-2}\lambda_s g'$	$9.62 \cdot 10^{-2}\lambda_s g'$
$\mathrm{Im}C_{dW \atop 22}$	$4.54 \cdot 10^{-2}\lambda_s g$	$8.95 \cdot 10^{-2}\lambda_s g$

Operator	RGE only	RGE + finite
$\mathrm{Im}C_{dG \atop 22}$	$7.42 \cdot 10^{-2}\lambda_s g_s$	$2.19 \cdot 10^{-2}\lambda_s g_s$
$\mathrm{Im}C_{uG \atop 22}$	—	$1.65 \cdot 10^{-2}\lambda_c g_s$
$\mathrm{Im}C_{dG \atop 33}$	—	$1.65 \cdot 10^{-2}\lambda_b g_s$
$\mathrm{Im}C_{uG \atop 33}$	—	$1.65 \cdot 10^{-2}\lambda_t g_s$

Table II.B.3: Upper bounds on the Wilson coefficients of the dipole operators assuming $\Lambda = 5$ TeV and no further assumptions. On the left-hand side the coefficients are presented which can enter at tree level. The column 'Tree+Loop' presents bounds including the tree level contribution, the RG running and all finite terms. On the right-hand side, one can find all elements which cannot enter at tree level. The left column shows only RG running, while the right column shows both RG running and finite terms. Above, the parameter λ_i is the ith diagonal entry of the corresponding diagonalized quark Yukawa matrix here and in all tables that follow.

Operator	RGE only	RGE + finite
$C_{H\widetilde{G}}$	$9.40 \cdot 10^{-3}g_s^2$	$7.81 \cdot 10^{-3}g_s^2$
$C_{H\widetilde{B}}$	$2.04 \cdot 10^{0}g'^2$	$1.53 \cdot 10^{0}g'^2$
$C_{H\widetilde{W}}$	$2.99 \cdot 10^{-1}g^2$	$2.62 \cdot 10^{-1}g^2$
$C_{HW\widetilde{B}}$	$1.76 \cdot 10^{-1}gg'$	$1.61 \cdot 10^{-1}gg'$
$C_{\widetilde{W}}$	—	$3.46 \cdot 10^{0}g^3$
$C_{\widetilde{G}}$	$4.74 \cdot 10^{-5}g_s^3$	$6.91 \cdot 10^{-5}g_s^3$

Operator	RGE only	RGE + finite
$\mathrm{Im}C_{Hud \atop 11}$	$1.87 \cdot 10^{-2}g'^2$	$2.03 \cdot 10^{-2}g'^2$
$\mathrm{Im}C_{Hud \atop 31}$	—	$1.03 \cdot 10^{-2}g'^2$
$\mathrm{Re}\,C_{Hud \atop 31}$	—	$3.53 \cdot 10^{-3}g'^2$
$\mathrm{Im}C_{uH \atop 11}$	—	$1.33 \cdot 10^{9}\lambda_u$
$\mathrm{Im}C_{dH \atop 11}$	—	$1.33 \cdot 10^{9}\lambda_d$

Table II.B.4: Upper bounds on the Wilson coefficients of the bosonic operators on the left and the $\psi\bar{\psi}H^2D$ and ψ^2H^3 type operators on the right, assuming $\Lambda = 5$ TeV and no further assumptions. The 'RGE + finite' column for $C_{Hud \atop 11}$ also includes the tree level contribution.

II.B.2   Neutron EDM

Operator	RGE only	RGE + finite
$\text{Im}C'^{(3)}_{lequ\,1111}$	$7.54\cdot10^9\lambda_e\lambda_u$	—
$\text{Im}C'^{(3)}_{lequ\,2211}$	$1.76\cdot10^5\lambda_\mu\lambda_u$	—
$\text{Im}C'^{(3)}_{lequ\,2211}$	$6.21\cdot10^2\lambda_\tau\lambda_u$	—
$\text{Im}V_{1i}^\dagger C'^{(1)}_{quqd\,i111}$	$1.88\cdot10^7\lambda_u\lambda_d$	$1.84\cdot10^7\lambda_u\lambda_d$
$\text{Im}V_{1i}^\dagger C'^{(8)}_{quqd\,i111}$	$3.82\cdot10^7\lambda_u\lambda_d$	$3.73\cdot10^7\lambda_u\lambda_d$
$\text{Im}V_{1i}^\dagger C'^{(1)}_{quqd\,i221}$	$7.79\cdot10^2\lambda_c\lambda_d$	—
$\text{Im}V_{1i}^\dagger C'^{(8)}_{quqd\,i221}$	$1.56\cdot10^3\lambda_c\lambda_d$	—
$\text{Im}V_{1i}^\dagger C'^{(1)}_{quqd\,i331}$	$9.86\cdot10^{-2}\lambda_t\lambda_d$	—
$\text{Im}V_{1i}^\dagger C'^{(8)}_{quqd\,i331}$	$1.98\cdot10^{-1}\lambda_t\lambda_d$	—
$\text{Im}V_{2i}^\dagger C'^{(1)}_{quqd\,i112}$	$9.35\cdot10^5\lambda_u\lambda_s$	—
$\text{Im}V_{2i}^\dagger C'^{(8)}_{quqd\,i111}$	$1.03\cdot10^7\lambda_u\lambda_s$	—
$\text{Im}V_{2i}^\dagger C'^{(1)}_{quqd\,i222}$	$2.56\cdot10^4\lambda_c\lambda_s$	—
$\text{Im}V_{2i}^\dagger C'^{(8)}_{quqd\,i222}$	$1.92\cdot10^4\lambda_c\lambda_s$	—
$\text{Im}V_{2i}^\dagger C'^{(1)}_{quqd\,i332}$	$3.24\cdot10^0\lambda_t\lambda_s$	—
$\text{Im}V_{2i}^\dagger C'^{(8)}_{quqd\,i332}$	$2.43\cdot10^0\lambda_t\lambda_s$	—
$\text{Im}V_{3i}^\dagger C'^{(1)}_{quqd\,i113}$	$5.15\cdot10^2\lambda_u\lambda_b$	—
$\text{Im}V_{3i}^\dagger C'^{(8)}_{quqd\,i113}$	$5.65\cdot10^3\lambda_u\lambda_b$	—

Operator	RGE only	RGE + finite
$\text{Im}C'^{(1)}_{qu\,1221}$	—	$5.79\cdot10^{-2}g'^2$
$\text{Im}C'^{(8)}_{qu\,1221}$	—	$4.70\cdot10^{-2}g'^2$
$\text{Im}C'^{(1)}_{qu\,1331}$	—	$3.76\cdot10^{-4}g'^2$
$\text{Im}C'^{(8)}_{qu\,1331}$	—	$4.03\cdot10^{-4}g'^2$
$\text{Im}V_{1i}^\dagger V_{j1}C'^{(1)}_{qd\,ij11}$	—	$7.66\cdot10^{-1}g'^2$
$\text{Im}V_{1i}^\dagger V_{j1}C'^{(8)}_{qd\,ij11}$	—	$6.60\cdot10^{-1}g'^2$
$\text{Im}V_{1i}^\dagger V_{j2}C'^{(1)}_{qd\,ij21}$	—	$3.85\cdot10^{-1}g'^2$
$\text{Im}V_{1i}^\dagger V_{j2}C'^{(8)}_{qd\,ij21}$	—	$3.31\cdot10^{-1}g'^2$
$\text{Im}V_{1i}^\dagger V_{j3}C'^{(1)}_{qd\,ij31}$	—	$8.56\cdot10^{-2}g'^2$
$\text{Im}V_{1i}^\dagger V_{j3}C'^{(8)}_{qd\,ij31}$	—	$7.37\cdot10^{-3}g'^2$
$\text{Im}V_{2i}^\dagger V_{j1}C'^{(1)}_{qd\,ij12}$	—	$3.35\cdot10^3g'^2$
$\text{Im}V_{2i}^\dagger V_{j1}C'^{(8)}_{qd\,ij12}$	—	$2.52\cdot10^3g'^2$
$\text{Im}V_{2i}^\dagger V_{j2}C'^{(1)}_{qd\,ij22}$	—	$1.68\cdot10^2g'^2$
$\text{Im}V_{2i}^\dagger V_{j2}C'^{(8)}_{qd\,ij22}$	—	$1.26\cdot10^2g'^2$
$\text{Im}V_{2i}^\dagger V_{j3}C'^{(1)}_{qd\,ij32}$	—	$3.75\cdot10^0g'^2$
$\text{Im}V_{2i}^\dagger V_{j3}C'^{(8)}_{qd\,ij32}$	—	$2.81\cdot10^0g'^2$
$\text{Im}C'^{(1)}_{ud\,1331}$	$9.30\cdot10^0g'^2$	$7.17\cdot10^0g'^2$
$\text{Im}C'^{(8)}_{ud\,1321}$	$6.98\cdot10^0g'^2$	$5.38\cdot10^0g'^2$

Table II.B.5: Upper bounds on the Wilson coefficients of the 4-fermion operators assuming $\Lambda = 5$ TeV and no further assumptions. Notice that each entry in the table corresponds to one of the mass-basis Wilson coefficients that enter the expression of the neutron EDM. For all of them, however, the corresponding C' Wilson coefficients in the up-quark gauge basis are indicated, together with the CKM transformations needed for the change of basis. Wherever the phase of the CKM matrix enters the bound, the bound is given on the real instead of the imaginary part. If the summation over the CKM elements gives a symmetric contribution for the operator $O_{qd}^{(1,8)}$, they have to be ignored because they are CP even and cannot give rise to an EDM. Note also, that the 'RGE + finite' column for $V_{1i}^\dagger C'^{(1,8)}_{quqd\,i111}$ includes the tree level contribution.

Operator	Tree	Tree+Loop
$\text{Im}C_{uG}\atop{11}$	$3.93 \cdot 10^1$	$8.55 \cdot 10^1$
$\text{Im}C_{uB}\atop{11}$	$3.11 \cdot 10^1$	$1.98 \cdot 10^1$
$\text{Im}C_{uW}\atop{11}$	$3.11 \cdot 10^1$	$2.30 \cdot 10^1$
$\text{Im}C_{dG}\atop{11}$	$8.19 \cdot 10^1$	$1.65 \cdot 10^2$
$\text{Im}C_{dB}\atop{11}$	$8.96 \cdot 10^1$	$4.97 \cdot 10^1$
$\text{Im}C_{dW}\atop{11}$	$8.96 \cdot 10^1$	$5.94 \cdot 10^1$
$\text{Im}C_{dB}\atop{22}$	$2.35 \cdot 10^1$	$1.47 \cdot 10^1$
$\text{Im}C_{dW}\atop{22}$	$2.35 \cdot 10^1$	$1.54 \cdot 10^1$

Operator	RGE only	RGE + finite
$\text{Im}C_{dG}\atop{22}$	$3.26 \cdot 10^1$	$1.99 \cdot 10^1$
$\text{Im}C_{uG}\atop{22}$	—	$3.89 \cdot 10^1$
$\text{Im}C_{dG}\atop{33}$	—	$3.89 \cdot 10^1$
$\text{Im}C_{uG}\atop{33}$	—	$3.89 \cdot 10^1$

Table II.B.6: Lower bounds on the UV scale Λ in TeV, assuming natural scaling of the dipole Wilson coefficients and no further assumptions. On the left-hand side the coefficients are presented which can enter at tree level. The column 'Tree+Loop' presents bounds including the tree level contribution, the RG running and all finite terms. On the right-hand side, one can find all elements which cannot enter at tree level. The left column shows only RG running, while the right column shows both RG running and finite terms.

Operator	RGE only	RGE + finite
$C_{H\widetilde{G}}$	$6.73 \cdot 10^1$	$7.16 \cdot 10^1$
$C_{H\widetilde{B}}$	$3.29 \cdot 10^0$	$3.94 \cdot 10^0$
$C_{H\widetilde{W}}$	$9.97 \cdot 10^0$	$1.06 \cdot 10^1$
$C_{HW\widetilde{B}}$	$1.33 \cdot 10^1$	$1.38 \cdot 10^1$
$C_{\widetilde{W}}$	—	$2.69 \cdot 10^0$
$C_{\widetilde{G}}$	$1.09 \cdot 10^3$	$1.01 \cdot 10^3$

Operator	RGE only	RGE + finite
$\text{Im}C_{Hud}\atop{11}$	$3.67 \cdot 10^1$	$3.53 \cdot 10^1$
$\text{Im}C_{Hud}\atop{31}$	—	$4.93 \cdot 10^1$
$\text{Re}\,C_{Hud}\atop{31}$	—	$8.42 \cdot 10^1$
$\text{Im}C_{uH}\atop{11}$	—	$1.37 \cdot 10^{-4}$
$\text{Im}C_{dH}\atop{11}$	—	$1.37 \cdot 10^{-4}$

Table II.B.7: Lower bounds on the UV scale Λ in TeV, assuming natural scaling for the Wilson coefficients of the bosonic operators and no further assumptions. The 'RGE + finite' column for $C_{Hud}\atop{11}$ also includes the tree level contribution.

Operator	RGE only	RGE + finite
$\text{Im}C'^{(3)}_{\substack{lequ\\1111}}$	$4.02 \cdot 10^{-5}$	—
$\text{Im}C'^{(3)}_{\substack{lequ\\2211}}$	$1.62 \cdot 10^{-3}$	—
$\text{Im}C'^{(3)}_{\substack{lequ\\3311}}$	$1.49 \cdot 10^{-1}$	—
$\text{Im}V^{\dagger}_{1i}C'^{(1)}_{\substack{quqd\\ij111}}$	$5.85 \cdot 10^{-4}$	$6.14 \cdot 10^{-4}$
$\text{Im}V^{\dagger}_{1i}C'^{(8)}_{\substack{quqd\\i111}}$	$6.42 \cdot 10^{-4}$	$6.55 \cdot 10^{-4}$
$\text{Im}V^{\dagger}_{1i}C'^{(1)}_{\substack{quqd\\i221}}$	$1.32 \cdot 10^{-1}$	—
$\text{Im}V^{\dagger}_{1i}C'^{(8)}_{\substack{quqd\\i221}}$	$8.84 \cdot 10^{-2}$	—
$\text{Im}V^{\dagger}_{1i}C'^{(1)}_{\substack{quqd\\i331}}$	$1.88 \cdot 10^{1}$	—
$\text{Im}V^{\dagger}_{1i}C'^{(8)}_{\substack{quqd\\i331}}$	$1.27 \cdot 10^{1}$	—
$\text{Im}V^{\dagger}_{2i}C'^{(1)}_{\substack{quqd\\i112}}$	$1.22 \cdot 10^{-3}$	—
$\text{Im}V^{\dagger}_{2i}C'^{(8)}_{\substack{quqd\\i112}}$	$5.96 \cdot 10^{-4}$	—
$\text{Im}V^{\dagger}_{2i}C'^{(1)}_{\substack{quqd\\i222}}$	$1.64 \cdot 10^{-2}$	—
$\text{Im}V^{\dagger}_{2i}C'^{(8)}_{\substack{quqd\\i222}}$	$1.97 \cdot 10^{-2}$	—
$\text{Im}V^{\dagger}_{2i}C'^{(1)}_{\substack{quqd\\i332}}$	$2.47 \cdot 10^{0}$	—
$\text{Im}V^{\dagger}_{2i}C'^{(8)}_{\substack{quqd\\i332}}$	$2.94 \cdot 10^{0}$	—
$\text{Im}V^{\dagger}_{3i}C'^{(1)}_{\substack{quqd\\i113}}$	$1.58 \cdot 10^{-1}$	—
$\text{Im}V^{\dagger}_{3i}C'^{(8)}_{\substack{quqd\\i113}}$	$3.69 \cdot 10^{-2}$	—

Operator	RGE only	RGE + finite
$\text{Im}C'^{(1)}_{\substack{qu\\1221}}$	—	$2.08 \cdot 10^{1}$
$\text{Im}C'^{(8)}_{\substack{qu\\1221}}$	—	$2.31 \cdot 10^{1}$
$\text{Im}C'^{(1)}_{\substack{qu\\1331}}$	—	$2.50 \cdot 10^{2}$
$\text{Im}C'^{(8)}_{\substack{qu\\1331}}$	—	$2.59 \cdot 10^{2}$
$\text{Im}V^{\dagger}_{1i}V_{j1}C'^{(1)}_{\substack{qd\\ij11}}$	—	$1.81 \cdot 10^{0}$
$\text{Im}V^{\dagger}_{1i}V_{j1}C'^{(8)}_{\substack{qd\\ij11}}$	—	$1.95 \cdot 10^{0}$
$\text{Im}V^{\dagger}_{1i}V_{j2}C'^{(1)}_{\substack{qd\\ij21}}$	—	$8.06 \cdot 10^{0}$
$\text{Im}V^{\dagger}_{1i}V_{j2}C'^{(8)}_{\substack{qd\\ij21}}$	—	$8.69 \cdot 10^{0}$
$\text{Im}V^{\dagger}_{1i}V_{j3}C'^{(1)}_{\substack{qd\\ij31}}$	—	$5.40 \cdot 10^{1}$
$\text{Im}V^{\dagger}_{1i}V_{j3}C'^{(8)}_{\substack{qd\\ij31}}$	—	$5.82 \cdot 10^{1}$
$\text{Im}V^{\dagger}_{2i}V_{j1}C'^{(1)}_{\substack{qd\\ij12}}$	—	$8.63 \cdot 10^{-2}$
$\text{Im}V^{\dagger}_{2i}V_{j1}C'^{(8)}_{\substack{qd\\ij12}}$	—	$9.97 \cdot 10^{-2}$
$\text{Im}V^{\dagger}_{2i}V_{j2}C'^{(1)}_{\substack{qd\\ij22}}$	—	$3.85 \cdot 10^{-1}$
$\text{Im}V^{\dagger}_{2i}V_{j2}C'^{(8)}_{\substack{qd\\ij22}}$	—	$4.45 \cdot 10^{-1}$
$\text{Im}V^{\dagger}_{2i}V_{j3}C'^{(1)}_{\substack{qd\\ij32}}$	—	$2.58 \cdot 10^{0}$
$\text{Im}V^{\dagger}_{2i}V_{j3}C'^{(8)}_{\substack{qd\\ij32}}$	—	$2.98 \cdot 10^{0}$
$\text{Im}C'^{(1)}_{\substack{ud\\1331}}$	$1.26 \cdot 10^{0}$	$1.61 \cdot 10^{0}$
$\text{Im}C'^{(8)}_{\substack{ud\\1321}}$	$1.52 \cdot 10^{0}$	$1.90 \cdot 10^{0}$

Table II.B.8: Lower bounds on the UV scale Λ in TeV, assuming natural scaling of the Wilson coefficients of the 4-fermion operators. Notice that each entry in the table corresponds to one of the mass-basis Wilson coefficients that enter the expression of the neutron EDM. For all of them, however, the corresponding C' Wilson coefficients in the up-quark gauge basis are indicated, together with the CKM transformations needed for the change of basis. Wherever the phase of the CKM matrix enters the bound, the bound is given from the real instead of the imaginary part of the Wilson coefficient. If the summation over the CKM elements gives a symmetric contribution for the operator $O^{(1,8)}_{qd}$, they have to be ignored because they are CP even and cannot give rise to an EDM. Note also, that the 'RGE + finite' column for $V^{\dagger}_{1i}C'^{(1,8)}_{\substack{quqd\\i111}}$ includes the tree level contribution.

Part III

Torsion Balance as a Classical Probe of New Physics

Chapter 10

Introduction and Motivation

While we have not yet encountered any elementary particle of spin > 2, there is a priori nothing preventing them from existing. Just like for any other field, they can be classified in the usual way as representations of the Poincaré group. In fact, higher spins in general are not just of purely academic interest but they exist in nature, e.g., as massive hadronic bound states and their excitations in the low-energy version of QCD.

However, upon closer inspection, it turns out that theories containing fields with higher spins[1] are plagued with theoretical problems and inconsistencies, especially if one aims for implementing massless higher-spin fields. The most commonly known hindrances of writing down theories with massless higher spin fields come in the form of various no-go theorems, which we will briefly summarize here. Using the factorization properties of amplitudes with one bosonic, massless particle of spin S and momentum q, it was shown by Weinberg [234] (see [235, 236] for extension to fermionic and supersymmetric theories), that the unphysical polarization of the spin-S field can decouple in the soft $q \to 0$ limit only if

$$\sum_i g^i p^i_{\mu_1} \cdots p^i_{\mu_{S-1}} = 0, \quad \forall p^i, \tag{10.1}$$

where the p^i denote the momenta of the other external particles and g^i their respective coupling to the spin-S particle. For $S = 1$ and $S = 2$ this reduces to the condition of charge conservation and the requirement that all particles couple universally to the massless spin-2 field, also known as the graviton. But for larger values of S there exists no solution for generic momenta, such that Weinberg's theorem tells us that only field of spin ≤ 2 can interact at low energies and therefore generate long-distance effects. While this does not completely rule out massless higher spin fields, it does put severe constraints on them and it turns out that combining Weinberg's soft theorem with another no-go theorem by Weinberg and Witten [237] and its extension [238] can, in fact, rule out massless higher spins completely in the presence of an universal interaction, which of course exists in nature in the form of gravity. This theorem states that a theory with a gauge-invariant and Lorentz covariant energy-momentum tensor cannot accommodate for the presence of massless fields with spins ≥ 2. While this seems to exclude also the graviton, note that the energy-momentum tensor in a gravitational theory cannot be made both gauge-invariant and Lorentz covariant at the same time and the same is true for theories with massless higher-spin fields[2]. However, the generalization of this theorem, found by Porrati in [238], states that no massless particle with $S > 2$ can consistently be coupled to gravity. Combining Weinberg's

---

[1] If not explicitly stated otherwise, we refer to particles as having "higher spin" if it has spin > 2.

[2] This is equivalent to the spin-1 currents, which cannot be both gauge-invariant and Lorentz covariant for non-Abelian gauge symmetries.

and Porrati's theorem forbids any theory that contains both a universal, i.e., gravitational, interaction and massless fields with $S > 2$. This can be seen as follows: Consider an amplitude with one soft graviton as well as an additional (not necessarily soft) graviton and two fields of spin > 2. Then, Porrati's theorem requires that the soft graviton couples to the higher spin fields with some vanishing coupling, while it couples to the non-soft graviton with some universal coupling. This, however, violates Weinberg's theorem, such that also the full amplitude has to vanish. While the above discussion captures the main point of prohibiting the existence of massless higher-spin fields in the presence of gravity, it, of course, does not cover all the details. For these, we refer the reader to the original literature cited above as well as reviews like, e.g., [239–242].

For massive higher-spin fields, on the other hand, the story is different. There are no no-go theorems ruling out their existence in the first place, so we will focus on massive fields in the rest of this part of the thesis. But even a non-zero mass does not imply that there are no constraints on such theories: A consistent coupling of massive higher-spin fields to either electromagnetism [238] or gravity [243] requires the cut-off of the corresponding EFT to depend on the mass of the higher-spin fields in a way that it vanishes in the massless limit, such that they decouple from the rest of the theory, in accordance to the no-go theorems above. In fact, an upper bound on the cut-off can be found, see [238, 243].

While we do not make explicit use of these bounds in this part of the thesis, it is good to keep them in mind. Instead, we will investigate how an EFT obtained by integrating out higher-spin fields can generate higher dimensional contributions to the usual general relativistic action. Following the discussion in [244], an infinite tower of higher-spin states is said to be able to cure acausalities generated by modified cubic vertices. To see this explicitly using the four graviton amplitude mediated by higher-spin fields is still an open question and we investigate one particular UV-limit of the amplitudes we obtained. Because gravity obviously couples also to ordinary matter, similar causality violations are expected in amplitudes with gravitons and matter, which likely are also cancelled by the very same tower of new degrees of freedom. Taking this approach, it necessitates the fact that the higher-spins directly couple to matter, such that they can be probed through pure matter scattering processes.

We will start this part of the thesis by introducing both massless and massive spinor helicity variables in chapter 11, which streamline the computation of on-shell amplitudes, without the need for a Lagrangian. In fact, the massless variables will also extensively be used in the next part of the thesis. One particularly useful property of using spinor helicity variables is that they allow us to write all the necessary amplitudes for an arbitrary spin S in a closed form. In chapter 12 we then introduce the EFT of gravity and discuss how it can be generated by an infinite tower of massive fields in a low-energy limit. Finally, in chapter 13 we follow the argument presented above and study the possibility of probing the higher-spin fields by looking for deviations from the Newtonian potential generated by the new fields, provided they couple directly to matter.

Chapter 11

Spinor Helicity Variables

We want to devote this chapter to first introducing massless spinor-helicity variables, which allow us to easily write down on-shell scattering amplitudes [245–248]. We will also cover their straightforward extension to massive amplitudes [207]. Our conventions for two-component spinors follow [249]. Unless stated differently, we will assume that all momenta are incoming throughout the remainder of this thesis.

11.1 Massless Particles

The key insight is that the fundamental representations of the complexified Lorentz group, $\mathrm{SO}(1,3) \simeq [\mathrm{SU}(2)_L \times \mathrm{SU}(2)_R]/Z_2$, are given by the spinorial $(1/2, 0)$ and $(0, 1/2)$ spinorial representations. Then, the natural consequence is to use the left- and right-handed spinors $\psi_\alpha \sim (1/2, 0)$ and $\tilde{\psi}_{\dot\alpha} \sim (0, 1/2)$ as basic building blocks for constructing objects in higher representations. Here, dotted and undotted indices denote the $\mathrm{SU}(2)_R$ and $\mathrm{SU}(2)_L$, respectively. This means, we can write any momentum $P \sim (1/2, 1/2)$ as a bispinor instead of a four-vector, by using the four-vector of 2×2 Pauli matrices ($\sigma^0 = \mathbb{1}$),

$$P_{\alpha\dot\alpha} \equiv \sigma^\mu_{\alpha\dot\alpha} P_\mu = \begin{pmatrix} P^0 - P^3 & P^1 + iP^2 \\ P^1 - iP^2 & P^0 + P^3 \end{pmatrix}. \tag{11.1}$$

The on-shell condition then just becomes

$$P^\mu P_\mu = m^2 = \det(P_{\alpha\dot\alpha}), \tag{11.2}$$

as can be easily checked by direct computation. Consequently, for massless momenta $P_{\alpha\dot\alpha}$ has a vanishing determinant and is therefore not of full rank, allowing us to write it as a product of two two-spinors,

$$P_{\alpha\dot\alpha} = \lambda_\alpha \tilde{\lambda}_{\dot\alpha}. \tag{11.3}$$

Note that even though we call these objects spinors, they are not Grassmann numbers. In general, the spinors λ_α and $\tilde{\lambda}_{\dot\alpha}$ are independent, however, imposing the condition of real momenta leads to

$$\tilde{\lambda}_{\dot\alpha} = (\lambda_\alpha)^*. \tag{11.4}$$

For convenience, as it lets us write down scattering amplitudes concisely, we introduce the square and angle bracket notation as follows,

$$\lambda^\alpha = \langle\lambda|^\alpha, \quad \lambda_\alpha = |\lambda\rangle_\alpha, \quad \tilde\lambda_{\dot\alpha} = [\tilde\lambda|_{\dot\alpha}, \quad \tilde\lambda^{\dot\alpha} = |\tilde\lambda]^{\dot\alpha}. \tag{11.5}$$

Indices can be raised and lowered using the antisymmetric epsilon tensor, e.g., $\lambda_\alpha = \epsilon_{\alpha\beta}\lambda^\beta$. Similarly to constructing Lorentz invariants from four-vectors (or objects in higher representations), we can build Lorentz invariants from the spinors λ_α and $\tilde\lambda_{\dot\alpha}$ by contracting all indices,

$$\begin{aligned}
\langle\lambda\chi\rangle &\equiv \epsilon_{\alpha\beta}\lambda^\alpha\chi^\beta = \lambda^\alpha\chi_\alpha = -\chi^\alpha\lambda_\alpha = -\langle\chi\lambda\rangle, \\
[\tilde\lambda\tilde\chi] &\equiv \epsilon^{\dot\alpha\dot\beta}\tilde\lambda_{\dot\alpha}\tilde\chi_{\dot\beta} = \tilde\lambda_{\dot\alpha}\tilde\chi^{\dot\alpha} = -\tilde\chi_{\dot\alpha}\tilde\lambda^{\dot\alpha} = -[\tilde\chi\tilde\lambda],
\end{aligned} \tag{11.6}$$

with the normalization $\epsilon^{12} = \epsilon^{\dot1\dot2} = -\epsilon_{12} = -\epsilon_{\dot1\dot2} = 1$ and from antisymmetry, it follows that $\langle\lambda\lambda\rangle = [\tilde\lambda\tilde\lambda] = 0$[1]. In our convention (again, we follow [249]) undotted indices are always contracted from top to bottom and vice versa for dotted ones.

Let us now present useful relations that can be used to simplify expressions of spinor products. First, we note that we can write Mandelstam invariants as spinor products

$$s_{ij} = (p_i + p_j)^2 = 2p_i p_j = \langle ij\rangle[ji]. \tag{11.7}$$

In an n-particle scattering process, we can also relate various spinor products to each other using momentum conservation, which, in terms of spinors, reads

$$\sum_{j=1}^n p_j = \sum_{j=1}^n \lambda_\alpha^j \tilde\lambda_{\dot\alpha}^j = 0. \tag{11.8}$$

This expression can be sandwiched between two arbitrary spinors i and k, such that

$$\sum_{j=1}^n \langle ij\rangle[jk] = 0. \tag{11.9}$$

The last relations we want to highlight here are the so-called Schouten identities. These make use of the fact that the spinors live in a two-dimensional vector space, such that only two of them can be linearly independent. This implies that we can write every spinor λ_1^α in terms of two others like

$$\lambda_1^\alpha = \frac{\langle 13\rangle}{\langle 23\rangle}\lambda_2^\alpha + \frac{\langle 21\rangle}{\langle 23\rangle}\lambda_3^\alpha. \tag{11.10}$$

This relation can be contracted with a fourth external spinor j to then give the Schouten identities

$$\langle 12\rangle\langle 3j\rangle + \langle 13\rangle\langle j2\rangle + \langle 1j\rangle\langle 23\rangle = 0. \tag{11.11}$$

Obviously, $j \notin \{1, 2, 3\}$ for the above relation to be non-trivial. Equivalent identities, of course, also exist for $SU(2)_R$ spinors.

The real beauty of using the spinor-helicity variables instead of the usual momenta and polarizations to write down scattering amplitudes comes from realizing that Eq. (11.3) does not uniquely determine the spinors λ_α and $\tilde\lambda_{\dot\alpha}$, but instead allows for a rescaling of the form

$$\lambda_\alpha^i \to t_i\lambda_\alpha^i, \quad \tilde\lambda_{\dot\alpha}^i \to t_i^{-1}\tilde\lambda_{\dot\alpha}^i. \tag{11.12}$$

---

[1]This is directly related to the momenta being massless. In the massive case, the spinor contractions of the same spinor do not vanish and are, in fact, proportional to the mass.

Since λ_α and $\tilde{\lambda}_{\dot{\alpha}}$ are independent for complex momenta, t can be any complex number, however, for real momenta it can only be a phase factor because of Eq. (11.4). This freedom of choosing a phase for the spinors is a direct reflection of the U(1) little group, which by definition is the part of the Lorentz group under which the momentum p does not transform, for massless particles.

Then, it can be shown (see, e.g., [245]) that the little group scaling of the spinors Eq. (11.12) can be translated into the scaling behavior of full amplitudes[2] built from these spinors such that

$$\mathcal{A}(1_{h_1}, 2_{h_2}, \ldots, n_{h_n}) \to \prod_{i=1}^{n} t_i^{-2h_i} \mathcal{A}(1_{h_1}, 2_{h_2}, \ldots, n_{h_n}), \tag{11.13}$$

with h_i the helicity of particle i ($h = 1/2$ for fermions, $h = 1$ for vectors, etc.). Thus, we can write any scattering amplitude in the form

$$\mathcal{A}(1_{h_1}, 2_{h_2}, \ldots, n_{h_n}) \propto f(\{s_i j\}) \prod_{i=1}^{n} \lambda_i^r \tilde{\lambda}_i^{\bar{r}}, \quad r - \bar{r} = -2h_i, \tag{11.14}$$

where all spinor indices have to be contracted and $f(\{s_i j\})$ is a scalar function built from only the kinematic invariants. The fact that the little group scaling provides a powerful tool to construct amplitudes is especially true for three-point amplitudes. These are completely fixed by the helicity of the external states, as we will demonstrate now.

For massless external states, all kinematic invariants for on-shell three-point amplitudes have to vanish by momentum conservation, $s_{12} = s_{13} = s_{23} = 0$. Recalling Eq. (11.7), this implies that either $\lambda_1 \propto \lambda_2 \propto \lambda_3$ or $\tilde{\lambda}_1 \propto \tilde{\lambda}_2 \propto \tilde{\lambda}_3$, such that either the square or the angle brackets vanish by antisymmetry of the spinor contractions. In fact, for real momenta, due to Eq. (11.4) all spinor contractions have to vanish, such that all three-point amplitudes are forced to vanish identically. However, temporarily allowing for complex momenta, left- and right-handed spinors are no longer related, and we can choose either the square or the angle brackets to vanish. Demanding a smooth limit to real momenta, where all brackets vanish, any three-point amplitude can then be written as

$$\mathcal{A}(1_{h_1}, 2_{h_2}, 3_{h_3}) = g \begin{cases} \langle 12 \rangle^{h_3 - h_1 - h_2} \langle 23 \rangle^{h_1 - h_2 - h_3} \langle 31 \rangle^{h_2 - h_3 - h_1}, & \sum_i h_i \leq 0 \\ [12]^{h_1 + h_2 - h_3} [23]^{h_2 + h_3 - h_1} [31]^{h_1 + h_3 - h_2}, & \sum_i h_i \geq 0 \end{cases}, \tag{11.15}$$

with some coupling constant g. To conclude this section, we note that because spinor-helicity variables allow us to construct scattering amplitudes from just the external particles, there is no need to worry about details considering gauge redundancies, gauge fixing and so on, contrary to the usual Lagrangian formalism.

One essential property of on-shell amplitudes we will use extensively is that amplitudes factorize into lower point amplitudes for on-shell intermediate states, i.e.

$$\text{Res}_{s_i} \mathcal{A}^{(0)} = \sum_X \mathcal{A}_L^{(0)} \mathcal{A}_R^{(0)*} |_{p_X^2 = m_X^2}, \tag{11.16}$$

where X denotes all possible intermediate states. We will postpone the proof of this relation using the optical theorem to the next part of this thesis.

---

[2]The amplitude is not invariant under little group transformations. However, physical observables depend only on the modulus squared of amplitudes, which is of course invariant under phase transformations.

11.2 Massive Particles

11.2.1 Massive Spinor Helicity Variables

In the last section, we saw how to write down on-shell scattering amplitudes by using only the information about the transformation properties under the little group of the external states. This is particularly easy for massless particles, since the little group contains only scale transformations. Of course, this can be generalized to massive particles, be it at the cost of introducing more complications due to the larger little group.

In this section, we will introduce the formalism for massive spinor helicity variables proposed in [207] and we will closely follow [207,250]. We will start from equation Eq. (11.2) and comment on the connection to the massive little group later.

Now the momenta $P_{\alpha\dot\alpha}$ do not have a vanishing determinant and are therefore of full rank two. Hence, we can write them as a sum of two rank one matrices,

$$P_{\alpha\dot\alpha} = \lambda_\alpha^I \tilde\lambda_{\dot\alpha I}, \tag{11.17}$$

where our spinor helicity variables now carry an additional set of additional indices, $I = 1, 2$, which represent the SU(2) little group of real, massive momenta. These new variables will be the building blocks of massive amplitudes, just as the massless spinor variables in the last section. As we will see, we can also use combinations of massive and massless variables to construct amplitudes containing both kinds of particles. Now, using the fact, that every spin S degree of freedom can be embedded into the symmetric part of a combination of spin $1/2$ representations, every amplitude with n massive external states can be written as [207]

$$\mathcal{A}^{\{I_1\cdots I_{2S_1}\}\cdots\{J_1\cdots J_{2S_n}\}} = \lambda_{1,\alpha_1}^{I_1}\cdots\lambda_{1,\alpha_{2S}}^{I_{2S_1}}\lambda_{n,\beta_1}^{I_1}\cdots\lambda_{n,\beta_{2S}}^{I_{2S_n}}\mathcal{A}^{\{\alpha_1\cdots\alpha_{2S}\}\cdots\{\beta_1\cdots\beta_{2S}\}}, \tag{11.18}$$

where each massive external state contributes its own set of $2S$ indices, which have to be symmetrized individually.[3] Note that all the information about the massive particles is carried by undotted spinors. In fact, as we will see shortly, any dotted spinor can always be transformed into an undotted by the use of the equations of motion and it will turn out convenient to write down massive amplitudes purely in terms of either dotted or undotted massive spinors.

Before we continue with the discussion of the generic structure of (partially) massive three-point amplitudes, we want to briefly introduce the basic identities we need as well as the notation we will use in this part of the thesis, closely following the one in [250].

For the spinor variables, we use the same bracket notation as for the massless ones, with the slight modification that we simply append the additional little group indices. Further, to distinguish them even further from massless spinors, we write them in a bold-faced font, e.g., $\lambda_I^\alpha = \langle\boldsymbol{\lambda}|_I^\alpha$. Obviously, because the little group indices are in the fundamental representation, they can be raised and lowered using the antisymmetric tensor, e.g., $\langle\boldsymbol{\lambda}|_I^\alpha = \varepsilon_{IJ}\langle\boldsymbol{\lambda}J|^\alpha$.

Then, as we saw before, we can write momenta as

$$P_{\alpha\dot\alpha} = |\boldsymbol{\lambda}^I\rangle[\boldsymbol{\lambda}_I|. \tag{11.19}$$

For later convenience we also give the matrix of momenta with the inverse order of dotted and undotted indices by contracting the four-vector with $\bar\sigma^\mu = (\mathbb{1}, -\boldsymbol{\sigma})$, instead of with σ^μ introduced in the last section,

---

[3]Note that we symmetrize as $\{I_1, \cdots I_n\} = 1/n!\sum\sigma(I_1, \cdots I_n)$, where the sum runs over all permutations σ of the objects to be symmetrized. This is different from, e.g., the procedure used in [250] where the appropriate Clebsch-Gordan coefficients are used instead.

$$P^{\dot\alpha\alpha} = -|\boldsymbol{\lambda}^I]\langle\boldsymbol{\lambda}_I|, \tag{11.20}$$

where the minus sign compared to the previous section comes from the fact that the contraction of the little group indices is now inverted. Using these expressions, we can write down the equations of motion for the spinors,

$$\begin{aligned}
P|\boldsymbol{\lambda}^I] = m|\boldsymbol{\lambda}^I\rangle, & \quad P|\boldsymbol{\lambda}^I\rangle = m|\boldsymbol{\lambda}^I], \\
[\boldsymbol{\lambda}^I|P = -m\langle\boldsymbol{\lambda}^I|, & \quad \langle\boldsymbol{\lambda}^I|P = -m[\boldsymbol{\lambda}^I|,
\end{aligned} \tag{11.21}$$

showing that we can trade angle brackets for square ones (and vice versa) by applying the respective momentum and justifying the expression of only undotted spinors in Eq. (11.18). Note also that by taking $m \to 0$ and removing the little group index, we recover the simple massless equations of motion. Using these equations, we can obtain relations for bilinears of the same spinor types

$$\begin{aligned}
[\boldsymbol{\lambda}^I\boldsymbol{\lambda}_J] = m\delta_J^I, & \quad [\boldsymbol{\lambda}^I\boldsymbol{\lambda}^J] = -m\epsilon^{IJ}, & \quad [\boldsymbol{\lambda}_I\boldsymbol{\lambda}_J] = m\epsilon_{IJ} \\
\langle\boldsymbol{\lambda}^I\boldsymbol{\lambda}_J\rangle = -m\delta_J^I, & \quad \langle\boldsymbol{\lambda}^I\boldsymbol{\lambda}^J\rangle = m\epsilon^{IJ}, & \quad \langle\boldsymbol{\lambda}_I\boldsymbol{\lambda}_J\rangle = -m\epsilon_{IJ},
\end{aligned} \tag{11.22}$$

and they also satisfy

$$|\boldsymbol{\lambda}^I\rangle\langle\boldsymbol{\lambda}_I| = -m\delta_\alpha^\beta, \quad |\boldsymbol{\lambda}^I][\boldsymbol{\lambda}_I| = m\delta_{\dot\beta}^{\dot\alpha}, \tag{11.23}$$

for the contraction of little group indices.

These are the main relations we will use in this part and we continue to discuss the general structure of three-point amplitudes. We saw in the previous section that the three-point amplitudes with only massless particles are completely and uniquely fixed by the helicity of the external states, due to the highly constraining three-point kinematics. For massive external states, a case by case study has to be performed, depending on the number of massive external states. The two cases relevant for this part are the all-massive case and amplitudes with only one massive and two massless external states. It turns out that, just as in the all-massless case, the latter amplitude is unique and can be determined from only the helicity of the massless particles [207]. The corresponding stripped amplitude, i.e., without the spinors for the massive particle, reads [207]

$$\mathcal{A}^{h_1 h_2}_{\{\alpha_1\cdots\alpha_{2S}\}} = \frac{g}{\Lambda^{3S+h_1+h_2-1}} \left(\lambda_1^{S+h_2-h_1}\lambda_2^{S+h_1-h_2}\right)_{\{\alpha_1,\cdots,\alpha_{2S}\}} [12]^{S+h_1-h_2}, \tag{11.24}$$

where we introduced the appropriate power of some scale Λ such that the coupling g is dimensionless for any spin S. The all-massive amplitude, on the other hand, is not that heavily constrained. Because there are no massless particles, there are no massless spinors we can use to construct the amplitude and instead a suited set of building blocks is given by

$$\epsilon_{\alpha\beta} \quad \text{and} \quad \mathcal{O}_{\alpha\beta} = \varepsilon^{\dot\beta\dot\gamma} p_{1\{\alpha\dot\beta} p_{2\beta\}\dot\gamma}, \tag{11.25}$$

and the most general, all-massive three-point amplitude can be written as

$$\mathcal{A}_{\{\alpha_1\cdots\alpha_{2S_1}\},\{\beta_1\cdots\beta_{2S_2}\},\{\gamma_1\cdots\gamma_{2S_3}\}} = \sum_{i=0}^{1} \sum_{\sigma_i} g_{\sigma_i} \left(\mathcal{O}^{S_1+S_2+S_3-i}\varepsilon^i\right)^{\sigma_i}_{\{\alpha_1,\cdots,\alpha_{2S_1}\},\{\beta_1,\cdots,\beta_{2S_2}\},\{\gamma_1,\cdots,\gamma_{2S_3}\}}, \tag{11.26}$$

with σ_i labeling, the distinct ways to distribute the $SU(2)$ spinor indices. Note, that this expression contains at most one power of ε due to the relation $\mathcal{O}_{\alpha\beta}\mathcal{O}_{\gamma\delta} - \mathcal{O}_{\gamma\beta}\mathcal{O}_{\alpha\delta} \sim \varepsilon_{\alpha\gamma}\varepsilon_{\beta\delta}$, such that higher powers of ε can be traded for lower powers and products of $\mathcal{O}$. Here we choose not to extract the mass dimension of the coupling, as different terms in the above sum carry different mass dimensions, due to the varying numbers of the $\mathcal{O}$ object.

We will use Eqs. (11.24) and (11.26) to explicitly calculate all the necessary three-point amplitudes needed in this part, see also App. III.A.

11.2.2   High-Energy Limit

Now that we have introduced both the massive and the massless spinor helicity variables, we want to see if they can be related in some way. Naively, we expect that there exists some procedure of taking the limit $m \to 0$ or, alternatively, the limit of large energies, in which the components of massive spinor variables reduce to massless ones. In fact, as we will see, taking this limit then simply decomposes massive amplitudes into their massless helicity components [207]. To take the high-energy limit, we follow the procedure outlined in [207] (see also, e.g., [250] for more details) by expanding the massive spinors in terms of a basis of two-dimensional vectors $\zeta^{\pm I}$ in little group space,

$$\lambda_\alpha^I = \lambda_\alpha \zeta^{-I} + \eta_\alpha \zeta^{+I}, \tag{11.27}$$

$$\tilde{\lambda}_{\dot\alpha}^I = \tilde{\lambda}_{\dot\alpha} \zeta^{+I} + \tilde{\eta}_{\dot\alpha} \zeta^{-I}, \tag{11.28}$$

with

$$\langle \lambda\eta \rangle = m = [\tilde{\eta}\tilde{\lambda}]. \tag{11.29}$$

After plugging this expansion into the amplitude of interest, we can identify the relevant helicity components by counting the numbers of $\zeta^{\pm I}$ appearing. As an example, we will anticipate the result for the amplitude of two scalars coupled to some massive particle of spin S as calculated in App. III.A,

$$\mathcal{A}(\mathbf{1}_{\phi_i}, \mathbf{2}_{\phi_i}, \mathbf{3}_S) = g_S' \langle \mathbf{3}|p_1 p_2|\mathbf{3}\rangle^S, \tag{11.30}$$

where g_S' is not dimensionless here, and calculate its high-energy limit for the first non-trivial cases, $S = 1, 2$. Here and in the following, we use a notation, where we suppress the little group indices on the massive spinors to avoid formulas cluttered with indices. Due to the boldfaced notation, the massive and massless spinors are still easily distinguishable visibly, and the indices can be reinstated unambiguously because they always have to be totally symmetrized.

For simplicity, we will take the scalars to be massless, which is trivial to do, as their respective spinors appear only in the form of momenta. Further, we will drop the little group indices on the $\zeta^\pm$. Starting with $S = 1$ we find

$$\mathcal{A}(1_{\phi_i}, 2_{\phi_i}, \mathbf{3}_{S_1}) = g_S'[(\zeta^-)^2\langle 3|p_1 p_2|3\rangle + (\zeta^+)^2\langle \eta|p_1 p_2|\eta\rangle + \zeta^+\zeta^-(\langle 3|p_1 p_2|\eta\rangle + \langle\eta|p_1 p_2|3\rangle)]. \tag{11.31}$$

We can then read off the $(-, 0, +)$ helicity components of the vector, which should reproduce the well-known coupling of scalars to the photon, as follows (dropping the coupling for brevity),

$$-: \quad \langle 3|p_1 p_2|3\rangle = \langle 31\rangle[12]\langle 23\rangle = g_S' m^2 \frac{\langle 31\rangle\langle 32\rangle}{\langle 21\rangle},$$

$$0: \quad (\langle 3|p_1 p_2|\eta\rangle + \langle\eta|p_1 p_2|3\rangle) = -\frac{g_S'}{m}(\langle 3|p_2 p_1 p_1|3] + [3|p_2 p_1 p_2|3\rangle) = \frac{2g_S'}{m}s_{12}^2 = 2g_S' m^3, \tag{11.32}$$

$$+: \quad g_S'\langle\eta|p_1 p_2|\eta\rangle = \frac{g_S'}{m^2}[3|p_3 p_1 p_2 p_3|3] = \frac{g_S' s_{12}}{m^2}[31][31]\langle 12\rangle = g_S' m^2 \frac{[31][31]}{[21]}$$

To arrive at the final results, we used [250]

$$m\,\eta\rangle = p_3 3], \quad s_{12} = 2p_1 \cdot p_2 = m^2, \tag{11.33}$$

as well as momentum conservation.

Before we go on to the $S = 2$ case, which should recover the known GR amplitudes, let us comment on the results for the $S = 1$ case first. Notice that the spinorial structures of the $+$ and $-$ amplitudes reproduce exactly the well-known result for the coupling of massive scalars to a massless vector. Notice also, that these amplitudes are not supposed to vanish in the $m \to 0$ limit, which can only happen if $g_1' \propto 1/m^2$, or in other words, if the scale Λ is related to the mass of the exchanged spinning particle. Next, notice that the 0 helicity component is just a constant, representing a purely scalar amplitude. This is, of course, expected, since we know that the longitudinal polarization of a vector boson can be seen as an eaten scalar Goldstone boson. Finally, even for $g_1' \propto 1/m^2$, the 0 component still vanishes in the $m \to 0$ limit, again following the expectation, since a massless particle of any spin has only two polarizations.

Let us now continue with the $S = 2$ or graviton amplitude. Plugging in the expansion of the massive spinors, we find

$$\begin{aligned}
M(1_{\phi_i}, 2_{\phi_i}, \mathbf{3}_{S_2}) &= g_2' \langle \mathbf{3}|p_1 p_2|\mathbf{3}\rangle^2 \\
&= g_2' \left[(\zeta^-)^4 \langle 3|p_1 p_2|3\rangle^2 + (\zeta^+)^4 \langle \eta|p_1 p_2|\eta\rangle^2 \right. \\
&\quad + \zeta^+\zeta^- (\langle 3|p_1 p_2|\eta\rangle + \langle \eta|p_1 p_2|3\rangle) \left((\zeta^-)^2 \langle 3|p_1 p_2|3\rangle + (\zeta^+)^2 \langle \eta|p_1 p_2|\eta\rangle \right) \\
&\quad \left. + (\zeta^+\zeta^-)^2 (\langle 3|p_1 p_2|\eta\rangle + \langle \eta|p_1 p_2|3\rangle)^2 \right].
\end{aligned} \tag{11.34}$$

Using the results for the different spinor brackets in the high-energy limit from the $S = 1$ case, we can easily determine the various helicity components:

$$\begin{aligned}
-- : &\quad m^4 \frac{\langle 31\rangle^2 \langle 32\rangle^2}{\langle 21\rangle^2} \\
-0 : &\quad m^5 \frac{\langle 31\rangle \langle 32\rangle}{\langle 21\rangle} \\
00 : &\quad m^6 \\
+0 : &\quad m^5 \frac{[31][31]}{[21]} \\
++ : &\quad m^4 \frac{[31]^2 [31]^2}{[21]^2}
\end{aligned} \tag{11.35}$$

Among these helicity components, we find the known GR amplitudes in the form of the all plus and all minus components. Again, these are non-vanishing in the limit $m \to 0$ if the coupling and the mass are related, in this case $g_2' \propto 1/m^4$. The additional components satisfy the expectation that a massive spin-2 particle has also spin-1 and scalar polarizations, which appear as the vector-scalar and scalar-scalar amplitudes in the ± 0 and the 00 helicity components, respectively. Moreover, as expected, they carry additional factors of the mass compared to the $\pm\pm$ components and vanish for $m \to 0$ even if $g_2' \propto 1/(m^4\Lambda)$, where we introduced the scale Λ to keep the correct mass dimension. In fact, if we choose $\Lambda \sim M_{\text{pl}}$, we recover the gravitational coupling of a massless graviton.

Judging from these two explicit cases as well as the fact that the 3-point amplitude for two scalars and a generic spin S particle is just the vector case to the power S, it is easy to see how it decomposes into its helicity components. Out of these helicity components then all lower

spin components vanish in the limit $m \to 0$, leaving only the ones with helicities $\pm S$, given the coupling scales like

$$g'_S \propto \frac{1}{m^{2S}\Lambda^{S-1}},$$

to cancel spurious powers of the mass, where again the appropriate power of Λ was introduced to keep the correct mass dimension of the 3-point amplitude.

Chapter 12

Graviton Scattering and Higher Spins

12.1 Gravity as an EFT

At long distances, Einstein's theory of general relativity (GR) provides an extraordinarily successful classical theory of gravity. At its heart lies the equation of motion (EOM) of gravity, the Einstein equations,

$$R_{\mu\nu} = \frac{1}{M_{\text{pl}}^2}\left(T_{\mu\nu} - \frac{1}{2}Tg_{\mu\nu}\right),\tag{12.1}$$

with the Ricci tensor $R_{\mu\nu}$ associated with the metric $g_{\mu\nu}$ and the energy-momentum tensor $T_{\mu\nu}$ with its trace $T = g^{\mu\nu}T_{\mu\nu}$ encoding potential contributions from matter fields. The scale $M_{\text{pl}}^2 = 8\pi G$ is the reduced Planck mass, related to the Newton's gravitational constant. Note, we will ignore contributions from a non-vanishing cosmological constant. These equations can be connected to an action of the form

$$S = -\frac{M_{\text{pl}}^2}{2}\int d^4x\sqrt{-g}R + \sqrt{-g}\mathcal{L}_{\text{matter}}\tag{12.2}$$

with the Ricci scalar, $R = g^{\mu\nu}R_{\mu\nu}$, and $g = \det(g_{\mu\nu})$. Minimizing this action, both the Einstein equations as well as the definition of the matter energy-momentum tensor in terms of the matter Lagrangian follow immediately. Because the energy-momentum tensor is the main object of interest in the next part of this thesis, we will postpone showing its definition and we will mainly focus on the purely gravitational terms in this section.

To quantize GR, it turns out to be convenient to separate the metric into some background metric $\bar{g}_{\mu\nu}$ and some fluctuations $h_{\mu\nu}$ around this background, such that

$$g_{\mu\nu} = \bar{g}_{\mu\nu} + \frac{1}{M_{\text{pl}}}h_{\mu\nu},\tag{12.3}$$

where we introduced the Planck mass for dimensional reasons because we will identify the fluctuation $h_{\mu\nu}$ with a bosonic spin-2 field of mass-dimension 1, the graviton. Throughout this entire part, we will take the background to be the flat Minkowski metric, $\bar{g}_{\mu\nu} = \eta_{\mu\nu}$. Note that after using this expansion, only the background metric is used to raise and lower indices, instead of the full one. Plugging this expansion back into the gravitational action Eq. (12.2), it quickly becomes clear that this action corresponds to a non-renormalizable theory,

as we are able to extract higher-dimensional operators at arbitrarily high mass dimensions by expanding the action to the appropriate order, such that the action Eq. (12.2) can only present the leading term in an low energy EFT. In fact, as in any EFT higher-dimensional operators have to be included at latest at the quantum level, to cancel divergences arising from both pure gravitational effects as well as from contributions of matter fields [251–256] order by order in $M_{\rm pl}$. These higher dimensional operators contain higher powers of the Riemann tensor (and its versions with contracted indices) and up to terms with four tensors and mass dimension eight the effective gravitational action can be written as [257,258]

$$
S = \int d^4x \sqrt{-g} \left[-\frac{M_{\rm pl}^2}{2} R + \alpha_2 R^2 + \alpha_2' R_{\mu\nu} R^{\mu\nu} - \frac{1}{3!} \left(\alpha_3 R^{(3)} + \tilde{\alpha}_3 \tilde{R}^{(3)} \right) \right.
$$
$$
\left. + \frac{1}{4} \left(\alpha_4 \left(R^{(2)} \right)^2 + \alpha_4' \left(\tilde{R}^{(2)} \right)^2 + 2\tilde{\alpha}_4 R^{(2)} \tilde{R}^{(2)} \right) + \mathcal{O}(R^5) \right],
$$

(12.4)

where we defined

$$
R^{(2)} = R_{\mu\nu\rho\sigma} R^{\mu\nu\rho\sigma}, \qquad \tilde{R}^{(2)} = R_{\mu\nu\rho\sigma} \tilde{R}^{\mu\nu\rho\sigma},
$$

$$
R^{(3)} = R_{\mu\nu}{}^{\rho\sigma} R_{\rho\sigma}{}^{\alpha\beta} R_{\alpha\beta}{}^{\mu\nu}, \qquad \tilde{R}^{(3)} = R_{\mu\nu}{}^{\rho\sigma} R_{\rho\sigma}{}^{\alpha\beta} \tilde{R}_{\alpha\beta}{}^{\mu\nu}.
$$

(12.5)

with the dual Riemann tensor defined as $\tilde{R}_{\mu\nu\rho\sigma} \equiv \frac{1}{2}\epsilon_{\mu\nu}{}^{\alpha\beta} R_{\alpha\beta\rho\sigma}$ in analogy to the dual field strength tensor in gauge theories. The specific choice of coefficients for the operators with three or more Riemann structures will become clear shortly, when we match these operators to four-graviton amplitudes. Note that in general, we could add a term proportional to just $R^{(2)}$. However, it turns out that in four dimensions it is not independent of the quadratic terms in Eq. (12.4) because the Gauss-Bonnet term $\mathcal{L}_{\rm GB} = R^2 - 4R_{\mu\nu} R^{\mu\nu} + R^{(2)}$ is a total derivative in four dimensions.

Before we turn to the scattering of gravitons induced by this effective action, let us first discuss the quadratic terms separately, as they are interesting in their own right. First notice that that they are formally marginal operators because $[R] = 2$, such that the corresponding coupling constants are dimensionless [1]. In addition, the leading term in their expansion around the flat background is obviously quadratic in the graviton, be it with more derivatives, so they represent contributions to the kinetic term. In fact, as is the case for theories with higher-derivative kinetic terms, they can be rephrased in terms of usual kinetics terms by introducing new, massive degrees of freedom, where their mass is related directly to the coefficient of the higher dimensional term. In the current example of the quadratic gravity terms, this can easily be seen by investigating the propagator [259]

$$
D_{\mu\nu\rho\sigma}(k) = -\frac{i}{(2\pi)^4} \left[\frac{P_{\mu\nu\rho\sigma}^{(2)} - 2P_{\mu\nu\rho\sigma}^{(0)}}{k^2} - \frac{P_{\mu\nu\rho\sigma}^{(2)}}{k^2 + M_{pl}^2/(2\alpha_2')} + \frac{2P_{\mu\nu\rho\sigma}^{(0)}}{k^2 + M_{pl}^2/(4(3\alpha_2 - \alpha_2'))} \right], \quad (12.6)
$$

where $P_{\mu\nu\rho\sigma}^{(2)}$ and $2P_{\mu\nu\rho\sigma}^{(0)}$ are projectors onto massive spin-2 and spin-0 modes of a generic spin-2 field, respectively, the exact form of which is not relevant here. We see that the first term corresponds to the standard propagation of a massless spin-2 degree of freedom. This can be seen from both the location of the pole at $k^2 = 0$, as well as from the fact that in the numerator we

---

[1]Of course, expanding them to sufficiently high order in the graviton generates non-renormalizable interactions. But the leading term is of dimension 4, while already the leading term for all operators with more Riemann tensors is already of dimension higher than 4.

exactly remove the spin-0 modes from the massive spin-2 object, leaving only the massless spin-2. However, the presence of the R^2 terms in Eq. (12.4) generates additional terms, corresponding to the propagation of the aforementioned additional degrees of freedom. We can easily read off their masses from the propagators, finding

$$m_2 = \frac{M_{pl}}{\sqrt{2\alpha_2'}}, \quad m_0 = \frac{M_{pl}}{\sqrt{4(3\alpha_2 - \alpha_2')}}. \tag{12.7}$$

In the non-relativistic limit, these additional massive degrees of freedom generate new contributions to the gravitational potential between two masses already at tree level in the form of Yukawa potentials with their range set by the respective masses. So, in principle, by looking for deviations from the Newtonian inverse-square law (ISL) potential, bounds on the masses of these new fields and therefore on the Lagrangian coefficients can be set. But it turns out that experiments like the torsion-balance experiment of the EötWash group are not very sensitive to these operators. Already in [259] the bounds on the coefficients were estimated to be of order $\alpha_2, \alpha_2' \lesssim 10^{74}$ (see also [260, 261] and even using the newer results of [262] this estimate cannot be pushed down much, giving $\alpha_2, \alpha_2' \lesssim 10^{60}$). But although it seems highly unnatural for these parameters to be much larger than 1, they can be expected to arise in the low-energy ISL experiments. This is because for natural values of $\mathcal{O}(1)$ the effects of the R^2 terms are highly suppressed compared to the leading term in the gravity EFT, due to the additional number of derivatives. So for the ISL experiments, which operate at very low energies, in order for the non-standard pieces to be borderline $\mathcal{O}(1)$ the enormous size of the parameters α_2, α_2' are needed to compensate for the suppression of the additional derivatives.

However, investigating Eq. (12.6) further, there is a glaring issue in the form of the negative sign in front of the massive spin-2 part of the propagator. This signals the presence of a negative-norm state, or in other words, a ghost. But contrary to the ghosts appearing when quantizing a non-Abelian gauge theory, there is nothing preventing these ghosts to appear as external states in scattering processes, making them somewhat physical. One way out of this is to assume that the coefficients α_2, α_2' are small enough (or in other words the masses m_2 and m_0 become large), such that it is possible to go to an EFT in which the new states, including the ghosts, do not appear anymore. In this case, at least in theory, it would still be possible to use ISL type experiments, but the gravitational potential would be generated only at the loop level and would therefore be suppressed by both more powers of M_{pl} and the fact that the potential itself becomes more and more short-ranged. But unfortunately, it was argued in [263] using multiple approaches that operators of the type R^2 do not generate any contributions to the gravitational potential beyond tree-level.

So, in summary, to not have ghosts in our theory, we assume that the coefficients of the quadratic terms are sufficiently small such that we can always integrate out the auxiliary particles. Further, it turns out that the quadratic terms do not contribute to graviton scattering amplitudes, since they can always be traded for pure matter operators using the EOM Eq. (12.1). Then, we can neglect the quadratic operators for our purposes, since all their contributions to both the graviton scattering amplitude as well as the classical potential, the main objects of interest, vanish.

Having said this, we now turn to the terms with three or more Riemann structures. As these are genuine interaction operators, they only modify interaction vertices such that there are no issues of new degrees of freedom needing to be included. We will mainly be interested in the cubic and quartic operators because they are the only ones contributing to the four-graviton scattering amplitude at tree level, the easiest non-trivial, pure graviton amplitude barring the three-point amplitude. Because the gravitons are massless, we can write down the amplitudes

for all possible combinations of their helicities using only the arguments presented in Sec. 11.1. We find, using the same notation as in [258],

$$\mathcal{A}\left(1^{+2}2^{-2}3^{-2}4^{+2}\right) = \langle 23 \rangle^4 [14]^4 f(s,t,u), \tag{12.8}$$

$$\mathcal{A}\left(1^{+2}2^{+2}3^{+2}4^{-2}\right) = ([12][13]\langle 14 \rangle)^4 \, g(s,t,u), \tag{12.9}$$

$$\mathcal{A}\left(1^{+2}2^{+2}3^{+2}4^{+2}\right) = \frac{[12]^2[34]^2}{\langle 12 \rangle^2 \langle 34 \rangle^2} h(s,t,u), \tag{12.10}$$

with $s = (p_1 + p_2)^2$, $t = (p_1 + p_3)^2$ and $u = (p_1 + p_4)^2$. Note the different definitions of the Mandelstam invariants compared to [258]. Amplitudes with more negative helicity gravitons can trivially be obtained from these by complex conjugation. Because the correct helicity weight is already factored, the functions f, g and h can only be functions of the Mandelstam invariants [258],

$$f(s,t) = -\frac{8\pi G}{stu} - \frac{2\pi Gst}{u}|\hat{d}_3|^2 + d_4 - d_5 u + d_6 u^2 - d_6' st + \dots, \tag{12.11}$$

$$g(s,t) = -\frac{4\pi G}{stu}\hat{d}_3 + \frac{1}{2}\hat{d}_6'' + \dots, \tag{12.12}$$

$$h(s,t) = -40\pi G\hat{d}_3 stu + \frac{1}{2}\hat{d}_4\left(s^2 + t^2 + u^2\right)^2$$
$$- 2\hat{d}_5 stu(s^2 + t^2 + u^2) + \hat{d}_6(s^2 + t^2 + u^2)^3 + \hat{d}_6' s^2 t^2 u^2 + \dots, \tag{12.13}$$

ignoring loop effects. The coefficients d_k can be related to the Wilson coefficients of graviton operators with $k/2$ derivatives, in particular

$$\hat{d}_3 = \alpha_3 + i\tilde{\alpha}_3, \quad d_4 = 8\pi G(\alpha_4 + \alpha_4'), \quad \hat{d}_4 = 8\pi G(\alpha_4 - \alpha_4' + i\tilde{\alpha}_4), \tag{12.14}$$

showing why we chose the Wilson coefficient as we did in Eq. (12.4). Notice, that the leading operator in our EFT, i.e., the one corresponding to classical GR, can only contribute to the amplitude with vanishing total helicity, while the effective operators entirely generate the other two. This concludes the discussion about the effective theory of gravity and the corrections to classical GR from higher dimensional operators. In the next section, we investigate a potential theory that can generate the higher-order terms by introducing an infinite tower of massive higher spin fields.

12.2 Gravity EFT from Higher Spins

We want to show how a theory that, apart from universal gravity, contains additional particles of some generic spin > 2 and mass m_S can generate the purely gravitational, higher-dimensional operators once the energy scales are below m_S. To do so, we use the massive spinor helicity formalism introduced in Sec. 11.2. This allows us to write down all the relevant amplitudes in full generality for any generic spin S mediator. Because all gravitons are massless, we can calculate the four-point amplitude by combining two three-point amplitudes with two massless and one massive external leg, which are unique, given the helicities and spin S. Using Eq. (11.24) all relevant amplitudes, turn out to be (see App. III.A)

$$\mathcal{A}(1_{h_+}, 2_{h_+}, \mathbf{3}_S) = \frac{g_S}{m_S^{3S+3}} [12]^4 \langle \mathbf{3} | p_1 p_2 | \mathbf{3} \rangle^S,$$

$$\mathcal{A}(1_{h_-}, 2_{h_-}, \mathbf{3}_S) = \frac{g_S}{m_S^{3S+3}} \langle 12 \rangle^4 \langle \mathbf{3} | p_1 p_2 | \mathbf{3} \rangle^S, \qquad (12.15)$$

$$\mathcal{A}(1_{h_+}, 2_{h_-}, \mathbf{3}_S) = \frac{g_S}{m_S^{3S-1}} [12]^S \langle 13 \rangle^{S-4} \langle 23 \rangle^{S+4}.$$

To calculate the four-point amplitudes from these, we can use Eq. (11.16) to calculate the residues on the poles in all possible channels and put them together with the actual propagators. For gluing amplitudes with massive spinors Eq. (11.16) becomes, e.g., in the s-channel [250]

$$\text{Res}_s(\mathcal{A}(1, 2, 3, 4)) = -\mathcal{A}^{\{I_1 \cdots I_{2S}\}}(1, 2, \mathbf{P}_S) \mathcal{A}_{\{I_1 \cdots I_{2S}\}}(-\mathbf{P}_S, 3, 4). \qquad (12.16)$$

Of course, for massive external states, the amplitude carries little group indices. We do not show them here because they remain unchanged by the gluing procedure, the only indices to be contracted are those associated with the intermediate state. If the mediating particle is of non-zero spin, care has to be taken when treating the spinors with negative momenta in the right amplitude. In fact, it turns out that the relations Eq. (11.23) have to be modified [250],

$$|\boldsymbol{\lambda}^I\rangle\langle-\boldsymbol{\lambda}_I| = m\delta_\alpha^\beta, \qquad |\boldsymbol{\lambda}^I][-\boldsymbol{\lambda}_I| = m\delta_{\dot\beta}^{\dot\alpha}. \qquad (12.17)$$

Technically, also Eq. (11.20) changes sign, but we will not need it because we express our amplitudes in a way that contains only massive spinors of one type.

Before calculating the actual four-point functions, let us note that the three-point amplitudes can be written in a way more convenient for contracting the little group indices, by simply moving around the symmetrization operation. This is possible because, again, the amplitude contains only one type of heavy spinor and in particular only one massive external leg with non-zero spin in total. Then, we can write, e.g., the all-plus three-point as

$$\mathcal{A}(1_{h_+}, 2_{h_+}, \mathbf{3}_S) = \frac{g_S}{m_S^{3S+3}} [12]^4 \lambda_3^{\{I_1\alpha_1} \cdots \lambda_3^{I_{2S}\}\alpha_{2S}}{}_{\alpha_1} |p_1 p_2|_{\alpha_2} \cdots {}_{\alpha_{2S-1}} |p_1 p_2|_{\alpha_{2S}}$$

$$= \frac{g_S}{m_S^{3S+3}} [12]^4 \lambda_3^{I_1\{\alpha_1} \cdots \lambda_3^{I_{2S}\alpha_{2S}\}}{}_{\alpha_1} |p_1 p_2|_{\alpha_2} \cdots {}_{\alpha_{2S-1}} |p_1 p_2|_{\alpha_{2S}} \qquad (12.18)$$

$$= \frac{g_S}{m_S^{3S+3}} [12]^4 \lambda_3^{I_1\alpha_1} \cdots \lambda_3^{I_{2S}\alpha_{2S}}{}_{\{\alpha_1} |p_1 p_2|_{\alpha_2} \cdots {}_{\alpha_{2S-1}} |p_1 p_2|_{\alpha_{2S}\}}.$$

In the first step we used that a symmetrization of the little group indices is equivalent to that of the spinorial indices here and in the last step we used that contracting an tensor with a symmetric tensor just extracts all the symmetric components. Equivalent expressions can similarly be found for the other two three-point functions. Then, using Eq. (12.17) simply turns the contraction of the little group indices into a contraction of the symmetrized spinor indices, e.g.,

$$\text{Res}_s(\mathcal{A}(1_{h_+}, 2_{h_+}, 3_{h_+}, 4_+)) = -\frac{g_S^2}{m_S^{5S+6}} [12]^4 [34]^4{}_{\{\alpha_1} |p_1 p_2|_{\alpha_2} \cdots {}_{\alpha_{2S-1}} |p_1 p_2|_{\alpha_{2S}\}}$$

$$\times {}^{\alpha_1} |p_3 p_4|_{\alpha_2} \cdots {}_{\alpha_{2S-1}} |p_3 p_4|^{\alpha_{2S}}. \qquad (12.19)$$

But this is nothing else than the combinatorial problem of finding all unique contractions of the massless spinors and their respective multiplicities. In fact, it turns out that the contraction

of the stripped amplitudes for the residues can be performed for generic helicities of the external states. For simplicity, we show only the s-channel, but all the other channels can be obtained by appropriate relabelings. We get

$$[12]^{S+h_1+h_2}[34]^{S+h_3+h_4}\left(\lambda_1^{S-h_{12}}\lambda_2^{S+h_{12}}\right)_{\{\alpha_1,\cdots,\alpha_{2S}\}}\left(\lambda_3^{S-h_{34}}\lambda_4^{S+h_{34}}\right)^{\{\alpha_1,\cdots,\alpha_{2S}\}}$$

$$\propto \sum_{a=0}^{\min(S-h_{12},S-h_{34})} c_{h_{12},h_{34}}(a)\ \langle 13\rangle^a\langle 14\rangle^{S-h_{12}-a}\langle 24\rangle^{h_{12}+h_{34}+a}\langle 23\rangle^{S-h_{34}-a}. \tag{12.20}$$

Here we defined $h_{ij} = h_i - h_j$ and the summation index a just counts how often we choose to contract a spinor of momentum p_1 on one side of the cut with a spinor of p_3 on the other side. This also explains the upper limit of the sum, since there cannot be more of these two spinors as the lower amount of each of them. The combinatorial factor turns out to be [207]

$$c_{h_{12},h_{34}}(a) = \frac{(S+h_{12})!(S-h_{12})!(S+h_{34})!(S-h_{34})!}{(2S)!}$$

$$\times \binom{2S}{a,S-h_{12}-a,h_{12}+h_{34}+a,S-h_{34}-a} \tag{12.21}$$

$$= \frac{(S+h_{12})!(S-h_{12})!(S+h_{34})!(S-h_{34})!}{a!(S-h_{12}-a)!(h_{12}+h_{34}+a)!(S-h_{34}-a)!},$$

where the object in the first equation is the multinomial coefficient, defined as

$$\binom{n}{k_1,k_2,\ldots,k_m} = \frac{n!}{k_1!k_2!\cdots k_m!}. \tag{12.22}$$

Let us briefly explain how this factor comes about. We can interpret the problem of combination as sorting an assortment of objects, the spinors, into a set of boxes, the spinor products. The exponents of the spinor products then simply count how many of these objects are put into each box. If all objects were distinct, the number of ways to distribute them among the boxes is precisely given by the multinomial coefficient, with n being the total number of objects, $2S$ in our case, and k_i the multiplicities within each box, the exponents of the spinor products for us. However, not all $2S$ spinors are distinct, so we have to account for this by multiplying with the multiplicity of each spinor, hence the additional factorials in the numerator. Finally, the factor of $(2S)!$ in the denominator simply comes from our choice of symmetrization procedure. Note that summing this coefficient over all values of a just gives $(2S)!$, as it should be.

In the following, we show how to use the above results to calculate the four-point function with vanishing total helicity in some detail. Since there are no conceptual differences for the other two helicity configurations, we will only quote the results. Starting with the s-channel, we need the three-point amplitudes with opposite helicity gravitons, and we have $h_{12} = -h_{34} = 4$. Therefore,

$$\mathrm{Res}_s(\mathcal{A}(1_{h_+},2_{h_-},3_{h_-},4_{h_+})) = -\frac{g_S^2}{m_S^{4S-2}}[12]^S[34]^S\sum_{a=0}^{S-4}c_{4,-4}(a)\ \langle 13\rangle^a\langle 14\rangle^{S-4-a}\langle 24\rangle^a\langle 23\rangle^{S+4-a}$$

$$= -\frac{g_S^2}{m_S^{4S-2}}\frac{\langle 23\rangle^4[14]^4}{t^4}\sum_{a=0}^{S-4}c_{4,-4}(a)\ (-\langle 3|p_2p_1p_4|3])^{S-a}\langle 3|p_4p_2p_1|3]^a$$

$$= -\frac{g_S^2}{m_S^{2S-2}}[23]^4[14]^4 \sum_{a=0}^{S-4} c_{4,-4}(a) \ u^{S-4-a}(-t)^a, \tag{12.23}$$

where we used

$$\langle a|p_b p_c p_d|a] = \mathrm{Tr}\left[P_L \not{p}_a \not{p}_b \not{p}_c \not{p}_d\right] = \frac{1}{2}\mathrm{Tr}\left[(1-\gamma 5)\not{p}_a \not{p}_b \not{p}_c \not{p}_d\right]. \tag{12.24}$$

Because the t-channel is related to the s-channel by a simple exchange of same-helicity gravitons, it can easily be obtained by simply replacing $s \leftrightarrow t$ everywhere, as required by Bose symmetry.

$$\mathrm{Res}_t(\mathcal{A}(1_{h_+}, 2_{h_-}, 3_{h_-}, 4_{h_+})) = -\frac{g_S^2}{m_S^{2S-2}}\langle 23\rangle^4[14]^4 \sum_{a=0}^{S-4} c_{4,-4}(a) \ u^{S-4-a}(-s)^a. \tag{12.25}$$

The u-channel, on the other hand, is different from the previous results because instead of the mixed amplitudes on either side of the cut, we have the same helicity ones. This means

$$\mathrm{Res}_u(\mathcal{A}(1_{h_+}, 2_{h_-}, 3_{h_-}, 4_{h_+})) = -\frac{g_S^2}{m_S^{4S-2}}[23]^{S-4}[14]^{S+4} \sum_{a=0}^{S} c_{0,0}(a) \ \langle 13\rangle^a \langle 12\rangle^{S-a}\langle 42\rangle^a \langle 43\rangle^{S-a}$$

$$= -\frac{g_S^2}{m_S^{2S+6}}[23]^4[14]^4 \sum_{a=0}^{S} c_{0,0}(a) \ (-s)^{S-a}t^a. \tag{12.26}$$

Note the functional differences of the s,t-channel to the u-channel. While, in principle, any spin can contribute to the latter, only spins larger than 4 are able to contribute to the former. Further, by investigating the 3-point amplitudes in more detail (see App. III.A), we can realize that the factor containing the heavy spinors for the same-helicity amplitudes is antisymmetric under an exchange of the two gravitons if S is odd, breaking Bose symmetry. Hence, the only way out is to set $g_S = 0$ for all odd S in these amplitudes. In total, we find

$$\frac{\mathcal{A}(1_{h_+}, 2_{h_-}, 3_{h_-}, 4_{h_+})}{([23][14])^4} = -\sum_S \frac{g_S^2}{m_S^{2S-2}}\left[\sum_{a=0}^{S-4} c_{4,-4}(a)\left(\frac{u^{S-4-a}(-t)^a}{s-m_S^2} + \frac{u^{S-4-a}(-s)^a}{t-m_S^2}\right)\right.$$

$$\left. + \frac{e(S)}{m_S^8}\sum_{a=0}^{S} c_{0,0}(a)\frac{(-s)^{S-a}t^a}{u-m_S^2}\right], \tag{12.27}$$

where we defined

$$e(S) = 1 - S \bmod 2 = \begin{cases} 1 & \text{if } S \text{ is even} \\ 0 & \text{if } S \text{ is odd} \end{cases}, \tag{12.28}$$

to implement the fact of only even spins in the same-helicity three-point functions.

The other amplitudes can be calculated similarly. In fact, since they have to be fully symmetric under any exchange of any two Mandelstam invariants (contrary to the result above, which is only symmetric under $s \leftrightarrow t$), it is sufficient to compute one channel and infer the others by a simple relabelling of invariants. They read

$$\mathcal{A}(1_{h_+}, 2_{h_+}, 3_{h_+}, 4_{h_-}) = -([12][13]\langle 14\rangle)^4 \sum_S \frac{g_S^2}{m_S^{2S-2}} e(S)$$

$$\times \sum_{a=0}^{S-4} c_{0,4}(a)\frac{u^{S-4-a}(-t)^a}{s-m_S^2} + (s \leftrightarrow t) + (s \leftrightarrow u), \tag{12.29}$$

$$\mathcal{A}(1_{h_+}, 2_{h_+}, 3_{h_+}, 4_{h_+}) = -\frac{[12]^2[34]^2}{\langle 12\rangle^2\langle 34\rangle^2}\sum_S \frac{g_S^2}{m_S^{2S-2}}e(S)$$
$$\times\sum_{a=0}^{S} c_{0,0}(a)\frac{(-u^{S-a})t^a}{s-m_S^2} + (s\leftrightarrow t) + (s\leftrightarrow u). \tag{12.30}$$

Now that we have the full four-graviton amplitudes, it is straightforward to determine the effective operators generated upon integrating out the higher spin fields by simply taking the $m_S \to \infty$ limit. Trivially extracting the functions f, g and h and expanding them to the appropriate order, we find

$$f(s,t,u) = 140\frac{\tilde{g}_4^2}{m_4^8} - \frac{14}{5}\left(25\frac{\tilde{g}_4^2}{m_4^{10}} - 99\frac{\tilde{g}_5^2}{m_5^{10}}\right)u + \frac{14}{5}\left(25\frac{\tilde{g}_4^2}{m_4^{12}} - 9\frac{\tilde{g}_5^2}{m_5^{12}} + 335\frac{\tilde{g}_6^2}{m_6^{12}}\right)u^2$$
$$+ \frac{28}{5}\left(25\frac{\tilde{g}_4^2}{m_4^{12}} + 81\frac{\tilde{g}_5^2}{m_5^{12}} + 225\frac{\tilde{g}_6^2}{m_6^{12}}\right)st\dots,$$

$$g(s,t,u) = 210\frac{\tilde{g}_4^2}{m_4^8} + \dots, \tag{12.31}$$

$$h(s,t,u) = 18\frac{\tilde{g}_4^2}{m_4^8}(s^2+t^2+u^2)^2 - \frac{105}{2}\frac{\tilde{g}_4^2}{m_4^{10}}stu(s^2+t^2+u^2)$$
$$+ 3\left(\frac{\tilde{g}_4^2}{m_4^{10}} - 587\frac{\tilde{g}_6^2}{m_6^{10}}\right)s^2t^2u^2 + \frac{1}{4}\left(\frac{\tilde{g}_4^2}{m_4^{12}} + 463\frac{\tilde{g}_6^2}{m_6^{10}}\right)(s^2+t^2+u^2)^3 + \dots,$$

where we defined $\tilde{g}_S = S!\,g_S$ for convenience and we included only particles of spin ≥ 4. Note that at each mass dimension, there is a maximal spin contributing, i.e., there is no need for manually truncating the sum over spins at a fixed mass dimension. This is simply because of the structure of the amplitudes. They are simply polynomials in the Mandelstam invariants, with a degree that increases with the spin of th exchanged particle and by expanding the propagator for large masses this degree cannot be decreased but only increased, giving a maximal contributing spin at each total power of Mandelstams. Using Eq. (12.2) together with Eqs. (12.8) - (12.10), we can easily obtain the EFT parameters by comparing coefficients, giving

$$\hat{d}_3 = 0, \quad d_4 = 140\frac{\tilde{g}_4^2}{m_4^8}, \quad d_5 = \frac{14}{5}\left(25\frac{\tilde{g}_4^2}{m_4^{10}} - 99\frac{\tilde{g}_5^2}{m_5^{10}}\right),$$

$$d_6 = \frac{14}{5}\left(25\frac{\tilde{g}_4^2}{m_4^{12}} - 9\frac{\tilde{g}_5^2}{m_5^{12}} + 335\frac{\tilde{g}_6^2}{m_6^{12}}\right), \quad d_6' = \frac{28}{5}\left(25\frac{\tilde{g}_4^2}{m_4^{12}} + 81\frac{\tilde{g}_5^2}{m_5^{12}} + 225\frac{\tilde{g}_6^2}{m_6^{12}}\right),$$
$$\tag{12.32}$$

$$d_6'' = 420\frac{\tilde{g}_4^2}{m_4^{12}}, \quad \hat{d}_4 = 36\frac{\tilde{g}_4^2}{m_4^8}, \quad \hat{d}_5 = \frac{105}{4}\frac{\tilde{g}_4^2}{m_4^{10}},$$

$$\hat{d}_6 = \frac{1}{4}\left(\frac{\tilde{g}_4^2}{m_4^{12}} + 463\frac{\tilde{g}_6^2}{m_6^{12}}\right), \quad \hat{d}_6' = 3\left(51\frac{\tilde{g}_4^2}{m_4^{12}} - 587\frac{\tilde{g}_6^2}{m_6^{12}}\right).$$

Interestingly, we cannot generate the cubic Riemann operator by simply integrating out the massive degrees of freedom. This is also clear from the structure of the amplitudes. Since the R^3 operators only modify the three-point interaction of gravitons in on-shell amplitudes, their contribution to the four-point amplitude comes with the exchange of an intermediate, massless

graviton. This necessarily has a pole at 0, for when the graviton goes on-shell. The amplitudes from the higher-spin exchange, on the other hand, have, before integrating them out, poles away from 0 at the masses of the mediators and no new poles can be generated by a simple $m_S \to 0$ expansion. We will discuss the R^3 in the context of massive higher spin fields in the next section.

But before we do so, we want to discuss an important consistency check of the results of matching the higher spin theory to the gravity EFT: causality constraints. We will not go into any detail on the derivation of these, instead we just mention that they can be obtained from the requirement of both unitary and causal scattering amplitudes at all energies and they give constraints on EFT coefficients from first principle, independent of any experiment. In [258] such constraints were obtained for the the coefficients in Eqs. (12.11) - (12.13), which we quote here for reference

$$d_4 \geq 0, \quad |\hat{d}_4| \leq d_4, \quad -d_4 \leq d_5 M^2 \leq d_4$$
$$0 \leq d_6 M^4 \leq d_4, \quad -\frac{90}{11} \leq \frac{d_6'}{d_6} \leq 6, \tag{12.33}$$

where M is the EFT cut-off, which we do not further specify here. Note that our results trivially satisfy the first two of these constraints, independently of the parameters of the theory, since

$$140\frac{\tilde{g}_4^2}{m_4^8} \geq 0 \quad \text{and} \quad 140\frac{\tilde{g}_4^2}{m_4^8} \geq 36\frac{\tilde{g}_4^2}{m_4^8}. \tag{12.34}$$

While it is of course crucial for these constraints to be satisfied, the remaining bounds are more interesting since they will establish connections between the couplings and masses of different states. E.g., the third constraint translates to

$$-\frac{25}{99}\frac{\tilde{g}_4^2}{m_4^8 M^2}\left(2 - \frac{M^2}{m_4^2}\right) \leq \frac{\tilde{g}_5^2}{m_5^{10}} \leq \frac{25}{99}\frac{\tilde{g}_4^2}{m_4^8 M^2}\left(2 + \frac{M^2}{m_4^2}\right). \tag{12.35}$$

Note that, assuming real coefficients, the lower bound is trivially satisfied unless $m_4 \leq \sqrt{2}M$, while the the upper bound always represents a non-trivial upper bound on the $S = 5$ particle depending on the $S = 4$ one and the cut-off of the theory.

The third causality constraint then relates the $S = 6$ parameters to the lower ones, in particular we find

$$\frac{10}{737}\frac{\tilde{g}_4^2}{m_4^{10} M^2}\left(1 - \frac{5M^2}{m_4^2}\right) \leq \frac{\tilde{g}_6^2}{m_6^{12}} \leq \frac{10}{737}\frac{\tilde{g}_4^2}{m_4^8 M^4}\left(11 - \frac{M^2}{m_4^2} - \frac{5M^4}{m_4^4}\right), \tag{12.36}$$

where we already used the constraints in Eq. (12.35) to eliminate the $S = 5$ parameters in favor of the $S = 4$ ones. Note that the lower bound can become non-trivial (assuming real coefficients again) for $m_4 \geq \sqrt{5}M$. Finally, note that the final constraint in Eq. (12.33) is trivially satisfied for real couplings, as can be easily seen by simply plugging in the respective matching coefficients.

12.3 Higher Spins in the High-Energy Limit

We have seen in the previous section that the R^3 type operators cannot be generated by integrating out a massive particle with spin $S \geq 4$. However, it was argued in [244] that if such a modification of the the gravitational three-point coupling is present, it leads to causality violation at high energies, which can only be cured by the introduction of an infinite power of massive higher spin particles. As mentioned in the introduction, to our knowledge this still has to be seen explicitly. To address this point, we use the full amplitudes we obtained in the previous

section and take the limit of large energies, which can also be states as $m_S \to 0$ for all $S \geq 4$. This means assuming a rather unique standpoint, in which the effective R^3 operator does not dissolve into new degrees of freedom at high energies, but instead persists at all energies and its dangerous high-energy behavior is cured by the additional inclusion of an infinite tower of higher spin fields. Below the scale at which the R^3 coupling becomes large, the effect of this infinite tower is simply captured by an gravitational EFT, the leading terms of which we already discovered in the last section.

We will focus on the amplitude with vanishing total helicity and in the limit $m_S \to 0$ the corresponding function of Mandelstam invariants can be written as

$$f(s,t,u) = \sum_{S \geq 4} \left[e(S) \sum_{i=1}^{S/2} d_1^{(i)}(S) \, \frac{(st)^i}{u^{2i-1}} + \sum_{i=0}^{S-5} d_2^{(i)}(S) \, \frac{u^{2i+1}}{(st)^i} \right] + \dots, \qquad (12.37)$$

where the ellipses stand for terms of different mass dimension and we find the following closed form for the function $d_1^{(i)}(S)$

$$d_1^{(i)}(S) = \begin{cases} S(1+S)\Gamma(1+S)^2 \, \hat{g}_S^2 & \text{if } i = 1 \\ (-1)^{i+1} \frac{2^{2i+\frac{S}{2}-2}(4i+S-5)!!\Gamma\left(i+\frac{S}{2}-1\right)^2\Gamma(2i+S-3)}{(i!)^2\Gamma\left(\frac{S}{2}-1\right)} \, \hat{g}_{S+2(i-2)}^2 & \text{if } i > 1 \end{cases}, \qquad (12.38)$$

and where we defined $\hat{g}_S^2 = g_S^2/m_S^{10}$. Notice that here we encountered the opposite situation as for the matching coefficient in the sense that instead of a maximal spin contributes at a given order, a minimum spin is needed to generate each of the powers of Mandelstam invariants. We believe that a similarly compact expression can be found for $d_2^{(i)}(S)$, however, we could not find it. Instead, we find that, e.g., the terms originating from odd spins can be written as

$$d_2^{(i)}(S_{\text{odd}}) = \sum_{a=0}^{2i} a_j^{(i)} S^i \times \begin{cases} \sqrt{2}^{-1-i} \frac{\Gamma(1+i+2S)\Gamma(9+i+2S)\Gamma(10+2i+2S)}{\Gamma(2S)} & \text{if } i \text{ is odd} \\ \sqrt{2}^{-i} \frac{\Gamma(i+2S)\Gamma(8+i+2S)\Gamma(9+2i+2S)}{\Gamma(2S-1)} & \text{if } i \text{ is even} \end{cases}, \qquad (12.39)$$

where $a_j^{(i)}$ are some numeric constants and we neglected the coupling dependence.

By comparing this expression with Eq. (12.11), we that the $i = 1$ term in the first sum has the same structure as the one generated by a graviton exchange and the insertion of the R^3 operator. By requiring the cancellation of the two, to recover a well-behaved amplitude, we find the condition

$$|\hat{d}_3|^2 = \frac{1}{2\pi G} \sum_{S=4}^{\infty} \frac{g_S^2}{m_S^{10}} S(1+S)\Gamma(1+2S)^2. \qquad (12.40)$$

Further, it is obvious from Eq. (12.37), that the addition of each new spin contributes not only to Eq. (12.40) but also introduces new terms with larger i, which in term have to be cancelled by including even higher spins, which introduce even higher terms in i and so on. To ensure the cancellation of these spurious terms, we require that

$$\sum_{S=4}^{\infty} \frac{2^{2i+\frac{S}{2}-2}(4i+S-5)!!\Gamma\left(i+\frac{S}{2}-1\right)^2\Gamma(2i+S-3)}{(i!)^2\Gamma\left(\frac{S}{2}-1\right)} \frac{g_{S+2(i-2)}^2}{m_{S+2(i-2)}^{10}} = 0 \quad \forall i > 1, \qquad (12.41)$$

which, in principle, allows us to relate the couplings and masses of higher spin fields with that of lower ones, down to $S = 4$, which can in turn be used to relate the R^3 coupling to a single higher spin coupling using (12.40). Then, provided a closed expression for $d_2^{(i)}$ is obtained, further relations between all the odd and even spin couplings can be derived by requiring the vanishing of all terms in the second sum in 12.37, fixing the full spectrum of the higher spin sector in terms of the lowest spin.

Note that the fact that $d_1^{(i)}$ is generated only by even spins is consistent with the fact that the amplitudes with different helicity configurations are generated by only even spins, such that the respective term arising from R^3 can only be cancelled by even spins in these amplitudes in the first place. In summary, the odd spins are only necessary for cancelling the spurious terms with more Mandelstam invariants after the odd spins have taken care of the R^3 operator. To conclude this section, we want to mention that the results presented in this section represent only a first step towards mapping out the full pattern of the higher spin spectrum and we leave the full determination of $d_2^{(i)}$ as well as discussion about the other helicity configurations for future work.

We want to conclude this section by commenting on the particular limit we chose. By having a closer look at Eq. (12.41), we see that every term in this sum is non-negative, such that the naive limit $m_S \to 0$, or equivalently $E \to \infty$, would imply that all couplings have to vanish identically. However, to avoid issues of non-perturbativity in the high-energy regime, one should rather take the limit while keeping the impact parameter finite, which is currently under investigation.

Chapter 13

Testing Higher Spins with Torsion Balance

We have seen in the previous chapter how the introduction of massive higher spin states can cure the bad energy growth behavior in pure graviton scattering amplitudes, in particular from R^3 type operators. Since this operator also enters the scattering of gravitons with matter through the modified triple graviton vertex, we expect the same behavior for large energies, which needs to be tamed to have in a sensible theory. In fact, since we already included the massive higher spin states to cure problems arising from R^3 contributions in the graviton four-point function, these new degrees of freedom will be able to also cure the matter-graviton amplitudes, once we allow for a coupling to matter directly.

However, in this chapter we will not further investigate this cancellation of the high-energy growth, but instead we will focus on experimental probes of these new higher spin degrees of freedom, provided their direct coupling to matter. In particular, given the fact that new mediating particles contribute to the potential between two sources as a fifth force, we will show how torsion-balance experiments like the EötWash experiment (see e.g., [262]) can be used to use as a classical and therefore very low-energy probe of these new particles.

13.1   Interaction potential from Higher Spins

Before we go into details about the actual experiments and how to extract constraints on the higher spin states, we first need to calculate the main object of interest: The four-point scattering amplitude of massive matter fields mediated by the new fields, hence modifying the interaction potential. For simplicity, we will model the matter fields ϕ_{12}, which later we will associate with the macroscopic test bodies used in the torsion balance experiment, as two scalars with masses m_1 and m_2, respectively, such that we can neglect any spin-dependent or electromagnetic interactions.

To actually calculate the needed amplitudes, we want to exploit the advantages of the massive spinor helicity formalism introduced in Chapter 17. This allows us to calculate all amplitudes for a generic spin S in a relatively straightforward way, which would become exponentially difficult even for single-digit values of S in the Lagrangian approach, due to the enormous gauge redundancies and introduction of many Goldstone-like particles. As shown in App. III.A, it turns out the the three-point interaction between two massive scalars and a generic, massive spin S particle can be written in two very compact but equivalent ways

$$M(\mathbf{1}_{\phi_i}, \mathbf{2}_{\phi_i}, \mathbf{3}_S) = \frac{g_S}{\Lambda^{2S-1}} \langle \mathbf{3}|p_1 - p_2|\mathbf{3}]^S = \frac{g_S'}{\Lambda^{3S-1}} \langle \mathbf{3}|p_1 p_2|\mathbf{3}\rangle^S, \tag{13.1}$$

where we again suppressed the little group indices on the massive spinors, as they are trivial to reinstate because they are fully symmetrized. Notice that the the expression with fewer momenta, i.e., the one proportional to g_S, looks a lot like the result obtained from a Lagrangian approach using the usual Feynman diagrams, by realizing that it can also be written as

$$\mathcal{A}(\mathbf{1}_{\phi_i}, \mathbf{2}_{\phi_i}, \mathbf{3}_S) = \frac{g_S}{\Lambda^{2S-1}} \epsilon(\mathbf{3})_{\mu_1 \mu_2 \cdots \mu_S} (p_1 - p_2)^{\mu_1} (p_1 - p_2)^{\mu_2} \cdots (p_1 - p_2)^{\mu_S}, \tag{13.2}$$

with

$$\epsilon(\mathbf{3})_{\mu_1 \mu_2 \cdots \mu_S} \propto \langle \mathbf{3}|\sigma^{\mu_1}|\mathbf{3}] \langle \mathbf{3}|\sigma^{\mu_2}|\mathbf{3}] \cdots \langle \mathbf{3}|\sigma^{\mu_S}|\mathbf{3}] \tag{13.3}$$

the polarization tensor of the spin S particle (see [264] for the $S = 2$ case). However, since it contains both dotted and undotted massive spinors, the contraction of the little group indices when calculating the four-point function becomes much more involved. Therefore, we use the expression with more momenta, i.e., the one proportional to g_S' because it contains only undotted spinors, ignoring the couplings for now, reinstating them in the end. We can easily transform the symmetrization of the little group indices into a symmetrization of the spinorial indices

$$\begin{aligned}
\mathcal{A}(1_{\phi_i}, 2_{\phi_i}, 3_S) &= \lambda_3^{\{I_1 \alpha_1} \lambda_3^{I_2 \alpha_2} \cdots \lambda_3^{I_{2S}\}\alpha_{2S}}{}_{\alpha_1} |p_1 p_2|_{\alpha_2 \alpha_3} |p_1 p_2|_{\alpha_4} \cdots {}_{\alpha_{2S-1}} |p_1 p_2|_{\alpha_{2S}} \\
&= \lambda_3^{I_1 \alpha_1} \lambda_3^{I_2 \alpha_2} \cdots \lambda_3^{I_{2S}\alpha_{2S}}{}_{\{\alpha_1} |p_1 p_2|_{\alpha_2 \alpha_3} |p_1 p_2|_{\alpha_4} \cdots {}_{\alpha_{2S-1}} |p_1 p_2|_{\alpha_{2S}\}},
\end{aligned} \tag{13.4}$$

where we also used that contracting a symmetric tensor with an arbitrary tensor picks out exactly the symmetric component of this latter tensor.

Then, we can use Eq. (12.16) to calculate the four point function, or rather the residues on its poles, by gluing two three-point amplitudes together and contracting all little group indices. As for the graviton amplitude, we can directly use Eq. (11.22) to transform the contraction of the little group indices into a contraction of spinor indices. Since we later we will be interested only in the long-range effects of the amplitude once transformed into position space, the only relevant channel will the the $t = (p_1 + p_3)^2$ channel. Nevertheless, all the other channels can be calculated in the same way by the gluing procedure. Alternatively, we can just use the fact that an amplitude of four real scalars has to be Bose symmetric under any exchange of external states, such that e.g., the $s = (p_1 + p_2)^2$ channel result can be obtained from the t-channel one by simply exchanging $s \leftrightarrow t$ and equivalently of the other channels. Having said this, one possible complication might arise because we are considering fully massive amplitudes, but since we are dealing only with external scalars, we know that the dependence on their momenta can only appear in the form of spinors that are contracted into actual momenta, i.e., there are no open little group indices. This helps the computation tremendously, since we can temporarily demote the momenta in Eq. (13.4) to massless ones, which allows us to easily split them into spinors and use the relations of the massless spinor helicity formalism, knowing that in the end they all have to recombine into momenta again. We then have

$$\text{Res}_t(\mathcal{A}(\mathbf{1}_{\phi_1}, \mathbf{2}_{\phi_2}, \mathbf{3}_{\phi_1}, \mathbf{4}_{\phi_2})) = m_S^{2S} [13]^S [24]^S \lambda_{1\{\alpha_1} \lambda_{3\alpha_2} \cdots \lambda_{1\alpha_{2S-1}} \lambda_{3\alpha_{2S}\}} \lambda_2^{\beta_1} \lambda_4^{\beta_2} \cdots \lambda_2^{\beta_{2S-1}} \lambda_4^{\beta_{2S}}. \tag{13.5}$$

As was the case for the graviton amplitudes, what remains is the combinatorial problem of finding all the possible contractions of the spinors and their respective multiplicities. For the

case that all helicities are zero, Eq. (12.21) just reduces to the square of a binomial coefficient and the residue in the t-channel simply reads

$$\text{Res}_t(\mathcal{A}(\mathbf{1}_{\phi_1}, \mathbf{2}_{\phi_2}, \mathbf{3}_{\phi_1}, \mathbf{4}_{\phi_2})) = m_S^{2S}[13]^S[24]^S(S!)^2 \sum_{a=0}^{S}(-1)^a\binom{S}{a}^2\langle 12\rangle^{S-a}\langle 14\rangle^a\langle 23\rangle^a\langle 34\rangle^{S-a}.$$

(13.6)

Note that this result matches the one for the s-channel exchange in [207] after making the $2 \leftrightarrow 3$ exchange. In fact, in the s-channel, this amplitude reproduces the well-known result that the four-scalar amplitude reduces to a Legendre polynomial in the center of mass frame. To quickly check this, we first do $2 \leftrightarrow 3$ to go from a t-channel to an s-channel exchange and then we go to the center of mass frame in which we can relate the spinors $\lambda_{3/4}$ with $\lambda_{1/2}$ by using

$$\begin{pmatrix}|3\rangle \\ |4\rangle\end{pmatrix} = \begin{pmatrix} c_{\theta/2} & -s_{\theta/2}e^{i\phi} \\ s_{\theta/2}e^{i\phi} & c_{\theta/2} \end{pmatrix}\begin{pmatrix}|1\rangle \\ |2\rangle\end{pmatrix},$$

(13.7)

as well as the conjugate relation for the $\tilde{\lambda}$ spinors. Here θ is the scattering angle. Plugging this in we find

$$\begin{aligned} \text{Res}_t(\mathcal{A}(\mathbf{1}_{\phi_1}, \mathbf{2}_{\phi_2}, \mathbf{3}_{\phi_1}, \mathbf{4}_{\phi_2})) &= m_S^{2S}[12]^S[34]^S(S!)^2 \sum_{a=0}^{S}\binom{S}{a}^2\langle 13\rangle^{S-a}\langle 14\rangle^a\langle 23\rangle^a\langle 24\rangle^{S-a} \\ &= m_S^{2S}s^{2S}\frac{1}{2^S}(S!)^2 \sum_{a=0}^{S}\binom{S}{a}(\cos\theta - 1)^a(\cos\theta + 1)^{S-a} \\ &= m_S^{2S}s^{2S}(S!)^2 P_S(\cos\theta), \end{aligned}$$

(13.8)

where we used the definition of the Legendre polynomials in the last step,

$$P_n(x) = \frac{1}{2^n}\sum_{a=0}^{n}\binom{S}{a}(x-1)^a(x+1)^{S-a}.$$

(13.9)

We would have arrived at a very similar result if we had used massive spinors throughout the entire computation, the only difference being we would have to carry around the contracted little group indices. But these are trivial to reinstate because we know that they all have to be contracted in such a way that momenta can be formed. So we just need to assign each pair of square and angle brackets with the same argument the same index. This is unambiguous since there is the same number of both square and angle brackets, so we can always find a counterpart to construct momenta. Nevertheless, we keep the spinors to be massless for now, such that we do not have to carry these indices, but writing Eq. (13.6), we find

$$\begin{aligned} \text{Res}_t(\mathcal{A}(\mathbf{1}_{\phi_1}, \mathbf{2}_{\phi_2}, \mathbf{3}_{\phi_1}, \mathbf{4}_{\phi_2})) &= m_S^{2S}(S!)^2 \sum_{a=0}^{S}(-1)^a\binom{S}{a}^2\langle 1|243|1]^{S-a}\langle 1|423|1]^a \\ &= \left(\frac{m_S^2}{2}\right)^S \sum_{a=0}^{S}\binom{S}{a}^2(2m_1^2m_2^2 - st)^{S-a}(tu - 2m_1^2m_2^2)^a \\ &= \left(\frac{m_S^2}{2}\right)^S [(2m_1^2 + t)(2m_2^2 + t)]^S P_S\left(\frac{t(s-u)}{(2m_1^2 - t)(t - 2m_2^2)}\right). \end{aligned}$$

(13.10)

Of course, when evaluating the Dirac traces, we now can no longer treat the scalars to be massless, hence the appearances of the masses $m_{1/2}$. Finally, because to calculate the t-channel residue we go to the limit $t \to m_S^2$, we can replace every t with the mediator mass and using Bose symmetry, we can easily find for the full four-scalar amplitude induced by a generic spin S exchange

$$\mathcal{A}(\mathbf{1}_{\phi_1}, \mathbf{2}_{\phi_2}, \mathbf{3}_{\phi_1}, \mathbf{4}_{\phi_2}) = 2^{-S}(S!)^2 \frac{\left[m_S^2 \left(m_S^2 - 2m_1^2 \right) \left(m_S^2 - 2m_2^2 \right) \right]^S}{t - m_S^2}$$
$$\times P_S \left(\frac{m_S^2(s - u)}{\left(m_S^2 - 2m_1^2 \right) \left(m_S^2 - 2m_2^2 \right)} \right) + (t \leftrightarrow s) + (t \leftrightarrow u),$$
(13.11)

where we used $P_S(-x) = (-1)^S P_S(x)$ and we ignored all factors of $(-1)^S$ because we know from the 3-point amplitude that S has to be even.

We are now in the position to calculate the contribution to the interaction potential between the two scalars arising from the mediating higher spin field.

Since we are eventually interested in the position space potential, calculated from a $2 \to 2$ scattering amplitude, between the two scalars, we need to change the particles (3,4) from being incoming to outgoing states. Employing a slight abuse of notation this does not change the form of the amplitude, keeping the change of sign of the momenta implicit in the definition of the Mandelstam invariants, which are now the usual ones for $2 \to 2$ scattering. We will see shortly that it will be convenient to express it only in terms of the Mandelstam invariants s, related to the scattering energy $(s = (E_1 + E_2)^2)$, and t, related to the momentum transfer $(t = -|\boldsymbol{q}|^2)$. Thus, we use

$$s + t + u = 2m_1^2 + 2m_2^2$$

to arrive at the final expression for the four-scalar amplitude

$$\mathcal{A}(\mathbf{1}_{\phi_1}, \mathbf{2}_{\phi_2} \to \mathbf{3}_{\phi_1}, \mathbf{4}_{\phi_2}) = 2^{-S}(S!)^2 \frac{\left[m_S^2 \left(m_S^2 - 2m_1^2 \right) \left(m_S^2 - 2m_2^2 \right) \right]^S}{t - m_S^2}$$
$$\times P_S \left(\frac{m_S^2(2s - 2m_1 - 2m_2^2 - |\boldsymbol{q}^2|)}{\left(m_S^2 - 2m_1^2 \right) \left(m_S^2 - 2m_2^2 \right)} \right)$$
(13.12)

where we ignored the other two channels, as they will contribute only through short-ranged contact terms to the total potential, which is not what we are interested in. To calculate the potential we Fourier-transform the amplitude to move from the momentum-exchange-space to distance-space

$$V(r, s) = \frac{1}{4E_1 E_2} \int \frac{d^3 q}{(2\pi)^3} e^{i\boldsymbol{q}\cdot\boldsymbol{r}} \mathcal{A}(\mathbf{1}_{\phi_1}, \mathbf{2}_{\phi_2} \to \mathbf{3}_{\phi_1}, \mathbf{4}_{\phi_2}),$$
(13.13)

where the factor in front of the integral is needed to account for the different normalization of states in non-relativistic quantum mechanics with respect to the one used in the QFT framework. Using the residue theorem, the integral is easily performed and we arrive at

$$V(r, s) = \frac{2^{-S}}{16\pi}(S!)^2 \frac{\left[m_S^2 \left(m_S^2 - 2m_1^2 \right) \left(m_S^2 - 2m_2^2 \right) \right]^S}{E_1 E_2}$$
$$\times P_S \left(\frac{m_S^2(2s - 2m_1^2 - 2m_2^2 + m_S^2)}{\left(m_S^2 - 2m_1^2 \right) \left(m_S^2 - 2m_2^2 \right)} \right) \times \frac{1}{r} e^{-m_S r},$$
(13.14)

finding that the functional dependence on the distance is the same as the Yukawa potential. This could have been expected already from the form of the $2 \to 2$ scattering amplitude (13.12).

For different choices of S, only the degree S polynomial in the numerator changes. When performing the contour integral arising in the Fourier transformation, the functional dependence on the distance r is set only by the pole in the denominator, while the numerator just becomes a constant, namely the polynomial evaluated at the pole. The only way to change the functional form is if the pole would lie on the real axis, i.e., if the spin S particle is massless, but it is well-known that there is no consistent theory of massless particles with spin $S > 2$.

Finally, we take the non-relativistic limit, since the experiment we want to test the potential with works at such low energies by setting

$$E_1 \sim m_1, \quad E_2 \sim m_2 \quad s \sim (m_1 + m_2)^2. \tag{13.15}$$

Then the non-relativistic potential between two scalar masses reads

$$
V_{\mathrm{NR}}(r) = -\frac{2^{S-4}}{\pi}(S!)^2 \left(\frac{g_S}{m_S \Lambda^{S-1}}\right)^2 \frac{\left[(m_S^2 - 2m_1^2)(m_S^2 - 2m_2^2)\right]^S}{m_1 m_2}
$$
$$
\times P_S \left(\frac{m_S^2(m_S^2 - 4m_1 m_2)}{(m_S^2 - 2m_1^2)(m_S^2 - 2m_2^2)}\right) \times \frac{1}{r}e^{-m_S r}, \tag{13.16}
$$

where we reinstated the coupling dependence and used (III.A.15) to rewrite it in terms of the lower dimensional, unprimed coupling, as well as the results of the discussion on the high-energy limit in Sec. 11.2.2.

Before going to the experimental constraints set on the higher spin fields using the above potential, we want to comment on the expression for specific values of S, namely $S = 1, 2$, which are well known in the literature.

Considering first the case of $S = 1$, the Eq. (13.16) reduces to

$$
V_{\mathrm{NR}}^{S=1}(r) = \frac{g_S^2}{2\pi}\left(1 - \frac{m_S^2}{4m_1 m_2}\right) \times \frac{1}{r}e^{-m_S r} \simeq \frac{g_S^2}{2\pi}\frac{1}{r}e^{-m_S r}, \tag{13.17}
$$

where in the last step assumed that $m_S \ll m_{1,2}$, which is a good approximation for classical experiments like EötWash.

At this point, we note that the above potential vanishes for real scalars, as the three point function of two identical scalars and a vector has to vanish due to Bose symmetry. However, if we take the scalars to be complex this obstruction can be avoided since now the scalars in the 3-point function are distinguishable by their charge Q_i. This means that the coupling now depends on the charge of the scalars and we have

$$
V_{\mathrm{NR}}^{S=1}(r) = \frac{\alpha_S^2 Q_1 Q_2}{2\pi}\frac{1}{r}e^{-m_S r}, \tag{13.18}
$$

recovering the known potential between charged objects, generated by a massive vector field, see, e.g., [265].

For $S = 2$, however, things look different and the potential reduces to

$$
V_{\mathrm{NR}}^{S=2}(r) = \frac{1}{8\pi}\left(\frac{g_S}{m_S^2 \Lambda}\right)^2 \frac{3(4m_1 m_2 - m_S^2)^2 m_S^4 - (m_S^2 - 2m_1^2)^2(m_S^2 - 2m_2^2)^2}{m_1 m_2} \times \frac{1}{r}e^{-m_S r}
$$
$$
\simeq -\frac{2}{\pi}\left(\frac{g_S}{\Lambda}\right)^2 \frac{m_1^2 m_2^2}{m_S^4} \times \frac{m_1 m_2}{r}e^{-m_S r}, \tag{13.19}
$$

which does not reproduce the usual potential from a massive spin-2 exchange, see e.g., [260, 266],

$$V_{\text{lit}}^{S=2}(r) = -\frac{4}{3}\frac{1}{8\pi}\frac{1}{m_S^2} \times \frac{m_1 m_2}{r}e^{-m_S r}, \tag{13.20}$$

due to the additional, dimensionless fraction of masses. Although we believe that our result is correct, in the end it reproduces the results presented in [207], it is still curious that such a discrepancy arises, but finding the origin is left for future work. But, to conclude this section, we want to give a possible explanation that might be worth further investigation. One possible source where the difference between our expression for the massive $S = 2$ and the literature might originate from is the prescription we use for symmetrizing the little group indices for the massive spinors. This implies that, even though the three-point amplitudes are correct, differences in higher point functions might arise, since there the symmetrization prescription is relevant for the contracted little group indices. Recall that we use a global factor of $1/n!$ dividing the sum of all possible permutations of a given set of indices. An alternative way, which allows for a straightforward identification of the scalar polarizations, would be to use the appropriate Clebsch-Gordan coefficients, as explained in [250]. Another point in favor of this theory is that, using Eq. (13.2), we can strip the massive polarization tensor from the amplitude and use the resulting vertex rule together with the appropriate propagator to calculate the four point amplitude. We explicitly checked that this reproduces the usual massive $S = 2$ potential, however, recalling the previous point, using already the propagator implicitly assumes a sum over massive polarizations using the symmetrization with the Clebsch-Gordan coefficients [250]. Nevertheless, we will use our results for the potential obtained with our symmetrization prescription here and in the following.

13.2 The Torsion Balance Experiment

In the last section, we calculated the non-relativistic potential between two massive scalars generated by the exchange of a new particle with arbitrary spin S. Of course, this is not the total potential between the scalars, but only a new contribution to the omnipresent Newtonian potential mediated by a massless graviton. Hence, one way to probe these new degrees of freedom is by employing experiments that search for deviations from the Newtonian potential generated by new fith-forces. In particular, we focus on the EötWash experiments using the results presented in [262] and the associated supplementary material.

Before presenting the constraints set by this experiment, we want to first want to discuss how it works in the first place. At its core, the experiment is simply constructed from objects of different masses which are put in very close proximity to each other, such that the force between these two objects generated by their interaction potential can be measured. In practice, this, of course, requires a far more sophisticated setup to be able to test the potential at microscopic distances. Further, all other possible interactions, such as electromagnetic or spin interactions, need to be eliminated as thoroughly as possible, to effectively isolate the gravitational contribution as well as effects from new physics. Therefore, these objects can be modelled as some neutral scalar. Further, we will assume that the higher-spin fields couple to all constituents with the same strength and that the entirety of the macroscopic objects coherently contributes to the interaction potential.

In the case of the EötWash experiment [262] (see also [267, 268] for details on the current and previous implementations of the experiment, respectively) the two test masses are thin metal plates aligned vertically. These plates feature an inner 120-fold and outer 18-fold pattern of
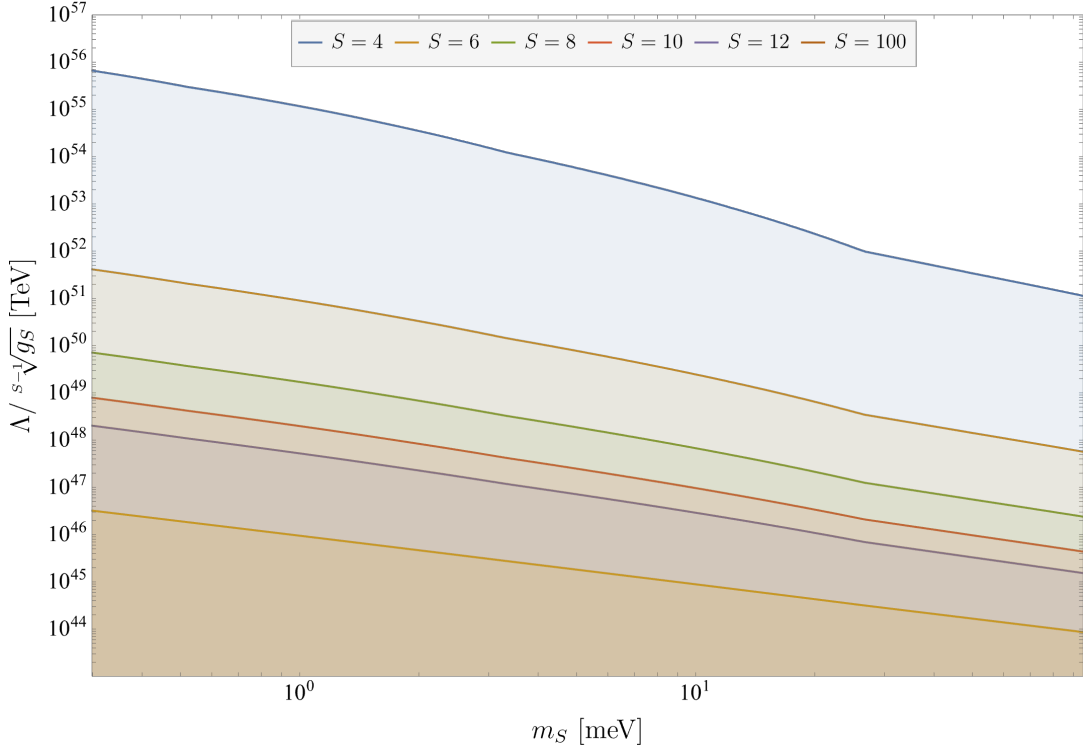
Figure 13.1: Constraints on the higher-spin fields set by the EötWash experiment in the $m_S-\Lambda$ plane.

alternating wedges, with every other wedge being a cut-out of filled with glue. When rotating one of these plates, called the attractor, with respect to the other, the pendulum, this periodic change of the mass density a fixed point on the pendulum sees, induces a periodic torque which can be read out and related to the gravitational interactions between the two plates. This periodic mass distribution, together with the (approximate) cylindrical symmetry of the whole setup, allows for a Fourier decomposition of the measured torque function in terms of mode functions [269], making an extraction of the signal generated by the individual wedge patterns straightforward. For a Yukawa type potential of the form

$$V(r) = \frac{\alpha m_1 m_2}{r} e^{-\lambda r} \tag{13.21}$$

the torque induced on the pendulum by the rotating attractor can be calculated as [269]

$$T_{h,N}(\theta) = 128hN^2\frac{\alpha\rho^2}{\pi}\sin(hN\theta) \times \int_0^\infty dk \, \frac{\sinh(t_1\gamma/2)\sinh(t_2\gamma/2)}{k\gamma^3} \exp\left[-\gamma\left(s + \frac{t_1+t_2}{2}\right)\right]$$

$$\times \left[\sum_{j=0}^\infty \frac{hN+2j+1}{(hN+2j)(hN+2j+2)}\left(r_1 J_{hN+2j+1}(r_1 k) - r_2 J_{hN+2j+1}(r_2 k)\right)\right]^2, \tag{13.22}$$

with $J_i(x)$ the Bessel function of the first kind. Here ρ is the mass density of the two objects, where we assumed that they both have the density, which is a valid approximation for the experiment at hand. The variables $t_{1/2}$ denote the thickness of the two objects, $r_{1/2}$ are the radii of the inner and outer wedge patterns respectively and $\gamma = \sqrt{k^2 + \lambda^2}$. Finally, h and N

149

are the h-th harmonic of the N-th multiple of the attractor eigenfrequency, $N = 18, 120$, and θ denotes the relative angle between the two plates with respect to some initial reference position. Obviously, this expression reduces to the torque in a Newtonian potential in the limit $\lambda \to 0$. Then, from Eq. (13.22), it is clear that the measured torques can easily be compared to the predicted values by decomposing them into Fourier modes and comparing the amplitudes of the sine terms of the appropriate frequency.

Then, by using a χ^2 we can find constraints on the masses and couplings of the higher spin fields to the matter fields using Eq. (13.16) and we show the results in Fig. 13.1 for various values of S. We want to conclude this section by discussing the main features in Fig. 13.1. First, we see the bounds for all values of S shown are extremely strong for light new states with masses below of order of a few milli-electronvolts. Here the mass range is limited by the physical separation between the test bodies that can be achieved in the experiments and which is of the order of at leas a few microns in the current setup of the EötWash experiment. The large values for the suppression scale then come from the macroscopically large external masses $m_{1/2}$ which appear to the power of some multiple of S in Eq. (13.16), such that a large value of Λ is necessary to compensate for them. Recalling the discussion on the $S = 2$ potential from the last section, they might become significantly less restrictive once the situation with additional mass fractions is resolved. The qualitative features of the exclusion regions, however, are not expected to change notably. Further, for increasing values of S the bounds become weaker and while there is still some non-trivial structure observable for the boundary curve of the lower spins, it flattens out more and more for higher values. Both these features arise from the fact that for higher spins a higher power of Λ is needed to keep the correct mass dimension of the potential, such that, ultimately, a lower value is necessary for the same compensation of the remaining terms in the potential. Finally, while not shown explicitly in Fig. 13.1, we observed that for spins $S \gtrsim 100$ the bounds become stronger again, exactly when the global $(2S!)^2$ factor overtakes the suppression by the high powers of Λ.

Chapter 14

Conclusions

In this part of the thesis, we have investigated effects on both gravitational as well as matter scattering induced by new, massive degrees of freedom of spin $S \geq 4$. We have shown how integrating them out generates an EFT of purely gravitational, higher dimensional operators and we give the the matching coefficients for operators with at most four Riemann tensors and up to dimension eight in Eq. (12.32). As a result of this matching, we also find that no contributions to cubic operators are generated. We can easily convince ourselves of this fact, by realizing that the four-point amplitude generated by such operators still has poles due to the necessary graviton exchange, while no such non-localities can remain after the massive propagator is expanded to give local interactions.

However, following the argument presented in [244], we investigated how an infinite tower of higher-spin fields can cure acausalities in the four-point function generated in the presence of the cubic operator at high energies. To do so, we took the high-energy limit of the four-graviton amplitude with a massive mediator and isolated the structure matching that from the R^3 operator. In particular, we focused on the graviton configuration with vanishing total helicity and we were able to find closed a closed expression for a large part of the amplitude in the high-energy limit at the relevant mass dimension, see Eq. (12.37). While a full closed expression still needs to be determined, our results already show interesting features. First, we showed that the correct structure to cancel contributions of the cubic operator can only be generated by particles of even spin. Further, we saw that by adding the lowest spin possible, $S = 4$, additional terms with higher powers of the Mandelstam invariants are generated. This can be cancelled by adding the next higher spin, $S = 6$, however, it also generates contributions to the R^3 structure as well as even higher powers in the Mandelstam invariants. These will be cancelled by the $S = 8$ particle and so on such that in the end we arrived at an expression of the Wilson coefficient of the R^3 operator in terms of a linear combination of the couplings and masses of all the even higher spins and additionally a set of relations between these couplings and masses from requiring the cancellation of these higher-power terms. In the end, we could, in principle, use to express everything in terms of the lowest spin coupling and mass. Of course, upon expanding around the high-energy limit, also terms with entirely different combinations of the Mandelstam invariants are generated, e.g., the second sum in Eq. (12.37). In the case of the amplitude with vanishing total helicity, this is where the odd spins come into play, which are able to cancel these terms. But, we also found that the conditions for cancellation of these spurious terms in the naive $E \to \infty$ imply that all couplings necessarily need to vanish in this regime. An alternate limit, which is still under investigation, keeps the impact parameter to be finite, such that non-perturbatively large couplings at high-energy can be avoided. In summary, we see that investigating different limits and finding the full closed expression of Eq. (12.37)

and equivalently for other limits for all spins as well as finding the equivalent expression for the other two helicity configurations can provide interesting insights in the necessary insights on the pattern of the the higher-spin sector. We leave this for a future work.

Finally, assuming that the higher-spin fields also directly couple to matter, we present a way to probe them using classical experiments like fith-force experiments looking for deviations from the Newtonian potential at short distances. To do so, we modelled the experimental test masses as point-like massive scalars, that universally couple to the higher-spin degrees of freedom, independently of their constituents. This allowed us to calculate the four-point amplitude of only scalars mediated by these new fields and compute the interaction potential between by isolating the long-range contributions. While our result does show discrepancies to other results for the potential found in the literature (which might originate from our choice of symmetrization prescription of the little group indices in the massive amplitudes, as discussed below (13.19)), we still use it to set constraints on the higher-spin parameter space, as it passes cross-checks with the literature on massive on-shell scattering amplitudes [207], see also Appendix A of [258], shown in (13.1). We also leave the resolution of this issue for future work. Coming back to the constraint, we found that the classical EötWash experiment has the potential of being an excellent probe of the higher-spin sector for light new states, even if the explicit form of the potential might change as a consequence of a different choice of the symmetrization procedure during the calculation, where future iterations of the experimental setup can potentially lead to a significant increase in both the reach on the mass as well as the effective coupling strength.

Appendices part III

III.A   Calculation of Massive Amplitudes

We devote this appendix to the calculation of the massive three-point amplitudes necessary for this part of the thesis using Eqs. (11.24) and (11.26).

III.A.1   All-massive Amplitude with Two Scalars

We start by calculating the amplitude of two massive scalars coupled to an massive state of arbitrary spin S. We start with Eq. (11.26) and for $S_1 = S_2 = 0$ and $S_3 = S$ we find

$$\mathcal{A}_{\{\alpha_1,\cdots,\alpha_{2S}\}} = \sum_{i=0}^{1} \sum_{\sigma_i} g_{\sigma_i} \left(\mathcal{O}^{S-i}\varepsilon^i\right)^{\sigma_i}_{\{\alpha_1,\cdots,\alpha_{2S}\}}. \tag{III.A.1}$$

It will be instructive to calculate the amplitude for the first few explicit values of S, to see how it generalizes to arbitrary S. We find

S=0:

$$\mathcal{A} = \sum_{i=0}^{1} \sum_{\sigma_i} g_{\sigma_i} \left(\mathcal{O}^{-i}\varepsilon^i\right)^{\sigma_i} \tag{III.A.2}$$

Because there can be no negative powers, the only term contributing in the outer sum is $i = 0$, trivially giving

$$\mathcal{A}(\mathbf{1}_{\phi_i}, \mathbf{2}_{\phi_i}, \mathbf{3}_{S_0}) = const, \tag{III.A.3}$$

as expected for a purely scalar amplitude.

S=1:

$$\mathcal{A}_{\{\alpha\beta\}} = \sum_{i=0}^{1} \sum_{\sigma_i} g_{\sigma_i} \left(\mathcal{O}^{1-i}\varepsilon^i\right)^{\sigma_i}_{\{\alpha,\beta\}} = g_0\, p_{1\{\alpha\dot\beta}p_{2\beta\}}{}^{\dot\beta} + g_1\, \varepsilon_{\{\alpha\beta\}} \tag{III.A.4}$$

Obviously, the second term drops out after explicitly expanding the symmetrization of the indices. After contracting with the external massive spinors, we find

$$\mathcal{A}(\mathbf{1}_{\phi_i}, \mathbf{2}_{\phi_i}, \mathbf{3}_{S_1}) = g_0\, \lambda_{\mathbf{3}I}^\alpha \lambda_{\mathbf{3}J}^\beta\, p_{1\{\alpha\dot\beta}p_{2\beta\}}{}^{\dot\beta} = g_0\, \langle\mathbf{3}|p_1 p_2|\mathbf{3}\rangle. \tag{III.A.5}$$

Here we used that the symmetrization in the indices $SU(2)$ Lorentz indices, α, β, is equivalent to the symmetrization of the $SU(2)$ little group indices, which is, however, left implicit in our choice for notation of massive spinors. Using momentum conservation, $p_1 + p_2 + p_3 = 0$, as well as the equations of motion (11.21) we can write the amplitude as

$$\mathcal{A}(\mathbf{1}_{\phi_i}, \mathbf{2}_{\phi_i}, \mathbf{3}_{S_1}) = -g_0 m_i^2 \langle \mathbf{33} \rangle + g_0 m_S \langle \mathbf{3}|p_2|\mathbf{3}], \tag{III.A.6}$$

which, after using momentum conservation once more, as well as

$$\langle \mathbf{3}^{\{I}\mathbf{3}^{J\}}\rangle = m_S \varepsilon^{\{IJ\}} = 0,$$

and redefining the arbitrary coupling constant, we finally arrive at

$$\mathcal{A}(\mathbf{1}_{\phi_i}, \mathbf{2}_{\phi_i}, \mathbf{3}_{S_1}) = g_0 \langle \mathbf{3}|p_1 - p_2|\mathbf{3}]. \tag{III.A.7}$$

This result reproduces the spinor structure in [250] for a fully massive scalar-scalar-vector amplitude. Note, this amplitude, having all the correct transformation properties, is antisymmetric under the exchange $\mathbf{1} \leftrightarrow \mathbf{2}$, while it has to be symmetric for identical scalars, forcing us to set $g_0 = 0$.

S=2:

$$\mathcal{A}_{\{\alpha\beta\mu\nu\}} = \sum_{i=0}^{1} \sum_{\sigma_i} g_{\sigma_i} \left(\mathcal{O}^{2-i}\varepsilon^i \right)^{\sigma_i}_{\{\alpha,\beta\}} = g_0 \, \mathcal{O}_{\{\alpha\beta}\mathcal{O}_{\mu\nu\}} + g_1 \, \mathcal{O}_{\{\alpha\beta}\varepsilon_{\mu\nu\}} \tag{III.A.8}$$

Again, symmetrizing the $SU(2)$ Lorentz indices is equivalent to symmetrizing the $SU(2)$ little group indices, so after contracting the above expression with the external spinors, we find

$$\mathcal{A}(\mathbf{1}_{\phi_i}, \mathbf{2}_{\phi_i}, \mathbf{3}_{S_2}) = \lambda^{\alpha}_{\mathbf{3}\{I}\lambda^{\beta}_{\mathbf{3}J}\lambda^{\mu}_{\mathbf{3}K}\lambda^{\nu}_{\mathbf{3}L\}} \left(g_0 \, \mathcal{O}_{\alpha\beta}\mathcal{O}_{\mu\nu} + g_1 \, \mathcal{O}_{\alpha\beta}\varepsilon_{\mu\nu} \right)$$

$$= g_0 \langle \mathbf{3}|p_1 p_2|\mathbf{3}\rangle^2 + g_1 \langle \mathbf{3}|p_1 p_2|\mathbf{3}\rangle\langle \mathbf{33}\rangle. \tag{III.A.9}$$

Using the results from the $S = 1$ case and defining new arbitrary coefficients, this can be written in the form

$$\mathcal{A}(\mathbf{1}_{\phi_i}, \mathbf{2}_{\phi_i}, \mathbf{3}_{S_2}) = g_0 \langle \mathbf{3}|p_1 - p_2|\mathbf{3}]^2 + g_1 \langle \mathbf{3}|p_1 - p_2|\mathbf{3}]\langle \mathbf{33}\rangle + g_2 \langle \mathbf{33}\rangle^2. \tag{III.A.10}$$

After making the symmetrization of the little group indices explicit, it is easy to see that the g_1 and g_2 term vanish, as there will always be pairs of permutations related by only a single index exchange for one of the antisymmetric tensors arising from $\langle \mathbf{3}^{\{I}\mathbf{3}^{J\}}\rangle \sim \varepsilon^{\{IJ\}} = 0$, e.g.

$$\begin{aligned}
\varepsilon^{\{IJ}\varepsilon^{KL\}} &= \varepsilon^{IJ}\varepsilon^{KL} + \varepsilon^{IJ}\varepsilon^{LK} \quad (= 0) \\
&+ \varepsilon^{KJ}\varepsilon^{LI} + \varepsilon^{KJ}\varepsilon^{IL} \quad (= 0) \\
&+ \cdots = 0.
\end{aligned} \tag{III.A.11}$$

Since this does not rely on exchanging indices of both tensors, but only one, the same argument holds also for the g_1 term.

In summary, we find

$$\mathcal{A}(\mathbf{1}_{\phi_i}, \mathbf{2}_{\phi_i}, \mathbf{3}_{S_2}) = g_0 \langle \mathbf{3}|p_1 - p_2|\mathbf{3}]^2. \tag{III.A.12}$$

Note, this spinor structure precisely matches the one in [264]. By comparing the $S = 1$ and $S = 2$ terms, there is an apparent pattern emerging where the amplitude for an arbitrary spin S is simply the $S = 1$ expression taken to the power S (keeping in mind that all indices have still to be symmetrized, i.e., the symmetrization procedure is obviously not exponentiated). Indeed, we find that this pattern emerges, as we will show now.

With the previous results, we can make the ansatz

$$\mathcal{A}(\mathbf{1}_{\phi_i}, \mathbf{2}_{\phi_i}, \mathbf{3}_S) = \tilde{g}_0 \langle \mathbf{3}|p_1 p_2|\mathbf{3}\rangle^S + \tilde{g}_1 \langle \mathbf{3}|p_1 p_2|\mathbf{3}\rangle^{S-1} \langle \mathbf{33}\rangle = \sum_{i=0}^{S} g_i \langle \mathbf{3}|p_1 - p_2|\mathbf{3}]^{S-i} \langle \mathbf{33}\rangle^i. \quad \text{(III.A.13)}$$

Using the antisymmetry of the ε tensor as before, we see that all terms with $i > 0$ vanish after symmetrizing all the little group indices, so we find for general (bosonic) spin

$$\mathcal{A}(\mathbf{1}_{\phi_i}, \mathbf{2}_{\phi_i}, \mathbf{3}_S) = \frac{g_S}{\Lambda^{2S-1}} \langle \mathbf{3}|p_1 - p_2|\mathbf{3}]^S = \frac{g_S'}{\Lambda^{3S-1}} \langle \mathbf{3}|p_1 p_2|\mathbf{3}\rangle^S, \quad \text{(III.A.14)}$$

where we introduced the appropriate power of some scale Λ such that g_S (g_S') is dimensionless. Note that Bose symmetry demands $g_S = 0 = g_S'$ if S is odd. In fact, the two couplings are related by

$$g_S' = \left(\frac{m_S}{2}\right)^S g_S. \quad \text{(III.A.15)}$$

Since scalars do not have spin, we know that all spinors corresponding to their momenta have to combine into momenta, such that all the little group transformation becomes trivial. Since it is trivial to go from massive to massless momenta and vice versa, taking the massless limit for the scalar is just as trivial, we just treat all appearing momenta to be massless instead of massive. In fact, this leads to an easier and shorter way to derive the needed 3-point amplitudes by using (11.24), such that one can use the simpler tricks of the massless spinor-helicity formalism at least for two out of the three particles in the amplitude. For the case of two massless scalars, the general expression for such an amplitude reduces to just

$$\mathcal{A}_{\{\alpha_1, \cdots, \alpha_{2S}\}} = \left(\lambda_1^S \lambda_2^S\right)_{\{\alpha_1, \cdots, \alpha_{2S}\}} [12]^S, \quad \text{(III.A.16)}$$

where we ignored the coupling dependence for simplicity. Let us use this formula in a few cases before considering general spin.

S=0: This case is trivial, all powers are 0 and therefore

$$\mathcal{A}(1_{\phi_i}, 2_{\phi_i}, \mathbf{3}_{S_0}) = const \quad \text{(III.A.17)}$$

S=1: As before, symmetrizing in the $SU(2)$ Lorentz indices is equivalent to symmetrizing the $SU(2)$ little group indices, which is left implicit in the notation we use here. Therefore

$$\begin{aligned}
\mathcal{A}(1_{\phi_i}, 2_{\phi_i}, \mathbf{3}_{S_1}) &= \lambda_{\mathbf{3}}^{\alpha\{I} \lambda_{\mathbf{3}}^{\beta J\}} \lambda_{1\alpha} \lambda_{2\beta} [12] \\
&= \langle \mathbf{31}\rangle \langle \mathbf{32}\rangle [12] \\
&= \langle \mathbf{3}|p_1 p_2|\mathbf{3}\rangle.
\end{aligned} \quad \text{(III.A.18)}$$

After taking the same steps as in the all massive case, one can arrive at the same final form of the amplitude.

S=2:

$$\begin{aligned}
\mathcal{A}(1_{\phi_i}, 2_{\phi_i}, \mathbf{3}_{S_2}) &= \lambda_{\mathbf{3}}^{\alpha\{I} \lambda^{\beta J} \lambda_{\mathbf{3}}^{\mu K} \lambda_{\mathbf{3}}^{\nu L\}} \lambda_{1\alpha} \lambda_{1\beta} \lambda_{2\mu} \lambda_{2\nu} [12]^2 \\
&= \langle \mathbf{31}\rangle \langle \mathbf{31}\rangle \langle \mathbf{32}\rangle \langle \mathbf{32}\rangle [12]^2 \\
&= \langle \mathbf{3}|p_1 p_2|\mathbf{3}\rangle^2,
\end{aligned} \quad \text{(III.A.19)}$$

which again matches the result of the all massive amplitude after performing the same manipulations.

General S:

$$
\begin{aligned}
\mathcal{A}(1_{\phi_i}, 2_{\phi_i}, \mathbf{3}_S) &= \lambda_{\mathbf{3}}^{\alpha_1\{I_1} \cdots \lambda^{\alpha_S I_S} \lambda_{\mathbf{3}}^{\alpha_{S+1} I_{S+1}} \cdots \lambda_{\mathbf{3}}^{\alpha_{2S} I_{2S}\}} \lambda_{1\alpha_1} \cdots \lambda_{1\alpha_S} \lambda_{2\alpha_{S+1}} \lambda_{2\alpha_{2S}} [12]^S \\
&= \langle \mathbf{3}^{\{I_1} 1 \rangle \cdots \langle \mathbf{3}^{I_S} 1 \rangle \langle \mathbf{3}^{I_{S+1}} 2 \rangle \langle \mathbf{3}^{I_{2S}\}} 2 \rangle [12]^S \qquad\qquad \text{(III.A.20)} \\
&= \langle \mathbf{3} | p_1 p_2 | \mathbf{3} \rangle^S.
\end{aligned}
$$

Again, we recover the same amplitude as in the fully massive case.

Notice, that this particular form of the amplitude could also have been obtained by considering all particles to be massless and bolding all the spinors only at the end. Of course, when simplifying the amplitude, the massless limit, especially for the spin S particle, cannot be used further and its non-zero mass has to be reintroduced.

III.A.2 Two-massless One-massive Amplitude with Two Gravitons

Because the two gravitons are massless, we can directly use Eq. (11.24) to calculate its coupling to a generic spin S particle. However, since they carry non-vanishing helicity, there are three different amplitudes, corresponding to the three helicity combinations. We will start by presenting the calculation for the case that both gravitons have the same helicity, as this is very similar to the scalar computation shown in the previous section.

For two positive helicity gravitons, Eq. (11.24) reduces to

$$
\mathcal{A}_{\{\alpha_1, \cdots, \alpha_{2S}\}} = \frac{g}{\Lambda^{3S+3}} \left(\lambda_1^S \lambda_2^S \right)_{\{\alpha_1, \cdots, \alpha_{2S}\}} [12]^{S+4}. \qquad\qquad \text{(III.A.21)}
$$

Since the only difference to the scalar case is the power of the already contracted massless spinors, contracting this expression with the massive spinors is completely analogous and we find

$$
\mathcal{A}(1_{h_+}, 2_{h_+}, \mathbf{3}_S) = \frac{g}{\Lambda^{3S+3}} [12]^4 \langle \mathbf{3} | p_1 p_2 | \mathbf{3} \rangle^S = \frac{g}{\Lambda^{3S+3}} [12]^4 \langle \mathbf{3} | p_1 - p_2 | \mathbf{3} \rangle^S \qquad \text{(III.A.22)}
$$

The amplitude for two negative helicity gravitons can be calculated in a very similar manner, since the the only difference is again only the power of the already contracted spinors. We find

$$
\mathcal{A}(1_{h_-}, 2_{h_-}, \mathbf{3}_S) = \frac{g}{\Lambda^{3S-5}} [12]^{-4} \langle \mathbf{3} | p_1 p_2 | \mathbf{3} \rangle^S = \frac{g}{\Lambda^{3S-5} m_S^8} \langle 12 \rangle^4 \langle \mathbf{3} | p_1 p_2 | \mathbf{3} \rangle^S, \qquad \text{(III.A.23)}
$$

where we used $\langle 12 \rangle [21] = (p_1 + p_2)^2 = m_S^2$ in the last equality to trade the square brackets for angular ones. Since we want the change of helicity of the gravitons to correspond to a complex conjugation of the respective spinors, we choose $\Lambda = m_S$.

Finally, we present the amplitude with opposite helicity gravitons. Already contracting with the external massive spinors, the amplitude reads

$$
\begin{aligned}
\mathcal{A}(1_{h_+}, 2_{h_-}, \mathbf{3}_S) &= \frac{g}{m_S^{3S-1}} \lambda_{\mathbf{3}}^{\alpha_1\{I_1} \cdots \lambda^{\alpha_S I_S} \lambda_{\mathbf{3}}^{\alpha_{S+1} I_{S+1}} \cdots \lambda_{\mathbf{3}}^{\alpha_{2S} I_{2S}\}} \lambda_{1\alpha_1} \cdots \lambda_{1\alpha_{S-4}} \lambda_{2\alpha_{S-3}} \lambda_{2\alpha_{2S}} [12]^S \\
&= \frac{g}{m_S^{3S-1}} \langle \mathbf{3}^{\{I_1} 1 \rangle \cdots \langle \mathbf{3}^{I_{S-4}} 1 \rangle \langle \mathbf{3}^{I_{S-3}} 2 \rangle \langle \mathbf{3}^{I_{2S}\}} 2 \rangle [12]^S \\
&= \frac{g}{m_S^{3S-1}} [12]^S \langle 13 \rangle^{S-4} \langle 23 \rangle^{S+4}.
\end{aligned}
$$

$$
\text{(III.A.24)}
$$

Note that here, we cannot factor the dependence on the heavy spinors and the helicity of the external states due to the potentially negative exponents of the $\langle 13 \rangle$ factor. While inverse powers of spinor contractions are well-defined for massless momenta, as they are simply numbers, this is not the case if it at least one massive spinor is involved, due to the resulting contraction not being a scalar object.

Part IV

IR divergences from the Renormalization of the Energy-Momentum Tensor

Chapter 15

Motivation and Introduction

We have already seen in previous parts of this thesis that for the running of couplings, it is not sufficient to calculate only the running of the corresponding vertex, but also effects from the external states have to be considered and contributions of UV and IR divergent terms have to be disentangled. While the former can easily be done using the usual methods for loop calculations of two-point functions, the latter is more involved. However, both these contributions are universal in the sense that they are a characteristic property of the external states in a theory, such that it suffices to calculate them once for the simplest possible cases. In practice, there are different ways of regularizing divergences in loop amplitude and, in general, independent regulators can be used for UV and IR divergences. One possibility was already presented in Part II, namely to introduce an auxiliary mass for the massless fields in the amplitude, serving as a lower cut-off for the loop integral. An alternative, which is favored from a computational perspective, is to use dimensional regularization, such that all divergences are treated in the same way. One disadvantage, however, is that both types of divergences appear as poles in the limit $d \to 4$, leaving the possibility of cancellation between different types of divergences. Obviously, this makes it difficult to disentangle different dynamics, creating the need for methods to do so. In this part of the thesis, we tackle this by using matrix elements of UV finite operators, such that the divergences can be attributed to only the external states and possible additional IR divergences. In the following, we will collectively denote these two contributions as IR divergences. We do so, since we will see that, to calculate the UV renormalization of non-finite operators, exactly their combined associated anomalous dimension has to be subtracted from the total anomalous dimension. In particular, we use the matrix elements of conserved currents because it can be shown on general grounds to be finite, up to a small and well-understood set of exceptions. While it is not the simplest such tensor, we will use the energy-momentum tensor for a given field Φ as the conserved Noether current of the space-time translations,

$$T^{\mu\nu} = \frac{\partial \mathcal{L}}{\partial(\partial_\mu \Phi)} \partial^\nu \Phi - g^{\mu\nu} \mathcal{L}, \tag{15.1}$$

with $\mathcal{L}$ the Lagrangian as usual. Note that, in general, this is not symmetric in the Lorentz indices, but it is well-known that it can be made symmetric by adding the divergence of a fully antisymmetric 3-tensor, which does not affect the current conservation. The reason, we use the energy-momentum tensor is that we can find one for every propagating degree of freedom in a theory, and in some cases it is even the only conserved current, as in the case of a real scalar field. Of course, for charged particles, a possibly easier current can be found and we will come back to this later.

Instead, we can directly derive a symmetric energy momentum tensor by temporarily treating

the metric tensor $g_{\mu\nu}$ to be non-Minkowskian and calculate the variation of the action with respect to it,

$$T^{\mu\nu} = \frac{-2}{\sqrt{-g}} \frac{\delta S}{\delta g_{\mu\nu}} = -2\frac{\delta \mathcal{L}}{\delta g_{\mu\nu}} + g^{\mu\nu}\mathcal{L}, \qquad (15.2)$$

where $g = \det(g_{\mu\nu})$ and we used $S = \int \sqrt{-g}\mathcal{L}$. Since this expression is manifestly symmetric, we can further split it into a symmetric and traceless part, as well as a term corresponding to the trace. Both of these terms transform irreducibly like a 2-tensor and a scalar under Lorentz transformation, such that we can assign them an angular momentum of $J = 2$ and $J = 0$ [270], respectively. This separation is immensely useful, as it allows us to calculate matrix elements of only one of the two components, by utilizing the appropriate projection operator, as we will see in the rest of this part.

We will start this part by briefly reviewing the renormalization of Green's functions with operator insertions and explicitly giving RGEs up to the two-loop order in Chapter 16. Then, since we will consider only massless theories in this part, we introduce the spinor helicity variables as a powerful tool to write down on-shell amplitudes, without the need of intensive computations, especially at tree level in Chapter 17. In the same chapter, we also discuss the optical theorem for on-shell amplitudes as a direct consequence of the unitarity of the S matrix. We will see that, at tree level, it implies that we can build up amplitudes as simple products of on-shell amplitudes with fewer legs, which, again, can easily be written down using the spinor helicity variables. We also go beyond tree level, where the optical theorem tells us that the imaginary part of loop amplitudes is calculable by performing on-shell cuts between simpler amplitudes of lower loop orders and different numbers of external legs according to the Cutkosky rules [271]. Further, by using the analytical properties of the logarithms contained in loop amplitudes, we can directly relate these on-shell cuts to the RGE, enabling us to extract the anomalous dimensions. In Chapter 19 we then show why conserved currents are, up to very few exceptions, UV finite and we discuss the aforementioned exceptions. Finally, we apply all these techniques to a simple theory of a real scalar coupled to a Dirac field through a Yukawa interaction in Chapter 20. There, we first perform the calculation of the IR anomalous dimension of the scalar using the on-shell methods described in Chapter 17, as well as by calculating the full two-loop expressions as a non-trivial consistency check finding perfect agreement between the two methods. Then, we repeat the calculations for the fermion in the theory using again both the on-shell as well as Feynman diagrammatic methods, finding agreement once more. Moreover, since the fermion is a complex field, we can assign it a conserved charge with an associated conserved current. As an additional, non-trivial consistency check, we calculate amplitudes with an insertion of this charge current instead of the energy momentum tensor, finding the same result, as it should be. Finally, we conclude in Chapter 22.

This part of the thesis IV is heavily based on [7], from which most of the results and some figures have been taken.

Chapter 16

Renormalization of Green's Functions

Instead of calculating RGEs for parameters appearing in the Lagrangian, as presented in Chapter 7, we can directly renormalize the Green's functions obtained from the Lagrangian. This approach is more general than just the renormalization of couplings because it allows for insertions of operators which do not appear in the Lagrangian and hence do not have to satisfy momentum conservation at the operator vertex.

We define bare Green's functions with an additional insertion of some operator O as the correlator,

$$\langle O \rangle_0 \equiv \langle \Omega | O_0(y) \Phi_0(x_1) \Phi_0(x_2) \cdots | \Omega \rangle, \tag{16.1}$$

where time ordering and the amputation of external legs is implied. For Green's functions without any sources, we can just take $O = \mathbb{1}$. Here we did not restrict ourselves to some order in the couplings and take the Green's function as an all-order object, which can be expanded in perturbation theory.

As is usually the case for bare quantities, the bare Green's function is, in general, divergent beyond tree level. Therefore, we define the renormalized Greens's function by renormalizing fields, couplings, and the operator O itself[1]. A slight caveat arises in the presence of infrared divergences. These cannot be cancelled by the the renormalization above because these only deal with the UV behavior, so an additional constant Z_{IR} has to be included. We define

$$\langle O \rangle_0 = Z_{\mathrm{IR}} Z_O \langle O \rangle \equiv Z_G \langle O \rangle, \tag{16.2}$$

where the renormalization of couplings is implicit in $\langle O \rangle$ and we defined Z_G as the total multiplicative renormalization constant. Notice that we can calculate anomalous dimensions for each of the Z_i factors individually, as well as for Z_G, using Eq. (7.12), and the consistency condition Eq. (7.13) has also to be obeyed by all the Z_i^2 separately and by the total Z_G. Note also that Z_{IR} contains the renormalization of the external fields, but can, in general, contain additional pieces, associated to infrared divergences. Often times it is more convenient to calculate the

---

[1]Note that even though O is built from fields it is not enough to renormalize just the fields, but instead a new renormalization constant has to be included. A simple example illustrating this fact is given by the renormalization of the operator ϕ^2 in a ϕ^4 theory at 1-loop. The field is not renormalized at 1-loop, but the 2-point function with insertions of ϕ^2 still contains divergences, which have to be cancelled by the operator renormalization.

[2]This is true only in the absence of IR divergences. With IR divergences, Z_G can depend explicitly on μ, see, e.g., [272–274]. However, there will be additional higher pole terms to ensure the finiteness of the anomalous dimension.

renormalized Green's function using the inverted relation,

$$\langle O \rangle = Z_G^{-1} \langle O \rangle_{0|g_0 \to g},\tag{16.3}$$

where we made explicit that the coupling in the bare Green's function has to be replaced by the renormalized one. Upon expanding in powers of couplings, we trivially find

$$\langle O \rangle = (1 + \delta_G^{(1)} + \delta_G^{(2)} + \ldots)^{-1} \langle O \rangle_{0|g_0 \to g}^{(0)} - \delta_G^{(1)} \langle O \rangle_{0|g_0 \to g}^{(1)} + \ldots.\tag{16.4}$$

At this point, we want to comment on the last term containing only one-loop objects. Obviously, it is of two-loop order, but it is not a genuine two-loop term, as it can be predicted after doing just the one-loop calculation. Nevertheless, it is important as it takes care of cancelling one-loop sub-divergences, which is particularly obvious in the absence of IR divergences. In this case, bare two-loop Green's functions contain non-local divergences, which cannot be cancelled by local counterterms alone. Instead, this last term, is responsible for removing them, since it is just a local counterterm multiplied by a non-local one-loop amplitude. While this procedure of renormalizing can easily be done by just replacing all couplings by their renormalized counterparts and multiplying by counterterms obtained from only overall divergences, we can also follow the textbook approach to cancel subdivergences and explicitly calculate Green's functions with insertions of counterterm vertices. As it turns out, using the field and coupling counterterms from the renormalized Lagrangian accounts for replacing the bare with renormalized coupling in the above equation, as well as as the field counterterm contained in δ_G. The remaining divergences in δ_G can be accounted for by adding counterterm vertices for all possible loop amplitudes absorbing the remaining divergences. In this part of the thesis, we will use both methods for two different models.

Given Eq. (16.3), we can easily derive the RGE for the renormalized Green's function by requiring that the bare one does not depend on any scale choice,

$$0 = \mu \frac{d}{d\mu} \langle O \rangle_0 = Z_G \left(\mu \frac{d}{d\mu} \langle O \rangle \right) + \left(\mu \frac{d}{d\mu} Z_G \right) \langle O \rangle.\tag{16.5}$$

We can rewrite this equation to arrive at the well-known RGE for Green's functions

$$(\mu \partial_\mu + \beta \partial + \Delta \gamma) \langle O \rangle = 0,\tag{16.6}$$

where we defined the anomalous dimension $\Delta \gamma$ in analogy to Eq. (7.7) and we used

$$\mu \frac{d}{d\mu} = \mu \partial_\mu + \mu \frac{dc_i}{d\mu} \frac{\partial}{\partial c_i} = \mu \partial_\mu + \beta \frac{d}{dc_i} \equiv \mu \partial_\mu + \beta \partial.\tag{16.7}$$

Here, $\Delta \gamma$ accounts for the fact that the running of Green's functions is not only generated by UV effects, but also IR ones. We defined it such that

$$\Delta \gamma = \gamma_{\text{UV}} - \gamma_{\text{IR}}.\tag{16.8}$$

Eq. (16.6) is valid to all orders in perturbation theory, but the all order expression is not very useful, as we cannot calculate the Green's function at all orders. Instead, we can expand it and since we will be interested in the 2-loop equation later, this will be the highest order we will be working at. Collecting terms of the same size, we find the 1- and 2-loop RGEs,

$$0 = \mu \partial_\mu \langle O \rangle^{(1)} + (\gamma^{(1)} + \beta^{(1)} \partial) \langle O \rangle^{(0)},\tag{16.9}$$

$$0 = \mu \partial_\mu \langle O \rangle^{(2)} + (\gamma^{(1)} + \beta^{(1)} \partial) \langle O \rangle^{(1)} + (\gamma^{(2)} + \beta^{(2)} \partial) \langle O \rangle^{(0)},\tag{16.10}$$

where the superscript denotes the loop order at which the various objects are evaluated.

We will extensively use these equations to calculate the anomalous dimension of the energy-momentum tensor up to the 2-loop order, making use of different ways of rewriting them.

Chapter 17

Amplitudes and Unitarity

17.1 Tree-Level Factorization

We have seen in the previous section how we can use spinor-helicity variables to efficiently determine the structure of (massless) on-shell scattering amplitudes and that their behavior under little group transformations uniquely and completely determines all three-point amplitudes purely in terms of the helicity of the external states. In this section, we want to establish how these can be used to construct higher point amplitudes as well as determine the renormalization of loop amplitudes, based only on their analytic properties as well as the condition for the S-matrix to be unitary.

We can use this constraint on the S-matrix to derive the optical theorem, which in turn can be used to calculate the factorization of higher point tree-level amplitudes as well as anomalous dimensions at a priori arbitrary orders in perturbation theory.

Starting with the S-matrix, we can split it up into a trivial piece and the T-matrix, which captures all the non-trivial scattering information,

$$S = 1 + iT. \tag{17.1}$$

Then, using that the S-matrix is unitary, $SS^\dagger = 1$, we arrive at the relation

$$iT^\dagger - iT = TT^\dagger. \tag{17.2}$$

Sandwiching this expression between initial and final states i and j and inserting a complete set of states on the right-hand side, we already arrive at the optical theorem.

$$\mathcal{A}_{if} - \mathcal{A}_{fi}^* = i \sum_X \int \mathrm{dLIPS}_X \mathcal{A}_{iX} \mathcal{A}_{Xf}^*. \tag{17.3}$$

with $\mathcal{A}_{if} \equiv \langle f|T|i\rangle$ describing the amplitude for scattering an initial state i into a final state j and dLIPS_X the Lorentz-invariant phase space of the (multi-)particle state X, defined as

$$\mathrm{dLIPS}_X = \prod_i \frac{d^4 p_i}{(2\pi)^4} (2\pi)\delta^+(p_i^2)(2\pi)^4\delta^4(p_i - p_X), \tag{17.4}$$

where the superscript on the delta function means that only solutions with positive energy contribute to the phase space. Here we leave the inclusion of appropriate symmetry factors needed in the presence of indistinguishable particles implicit

For the cases we are interested in, f is the vacuum state, such that exchanging initial and final states amounts to simply flipping the signs of all the external momenta. Provided time

reflection invariance is obeyed, the scattering amplitude is invariant under such a transformation such that we can write the optical theorem as

$$2\text{Im}(\mathcal{A}) = \sum_X \int \text{dLIPS}_X \mathcal{A}_L \mathcal{A}_R^*. \tag{17.5}$$

Here we changed the subscripts of the amplitudes in a way that reflects the fact that they can be seen on the left and right side of propagators that are cut in the sense of the Cutkosky cutting rules [271], i.e., they are joined by on-shell propagators.

Before we go on, there are a few, but important comments at order. By definition, the left-hand side of the above equation is entirely real, implying the same also for the phase space integral. Then, by complex conjugation, it is easy to see that it does not matter which of the amplitudes in the integral has to be complex conjugated, as long as one of them is. We also want to stress the relevance of the above equation. It tells us how to calculate the imaginary part of any loop amplitude and from a product of two easier amplitudes integrated over the phase space of some on-shell intermediate state and it is at the heart of the factorization properties of amplitudes.

Insert, for example, a tree level amplitude into the left-hand side. Restoring the Feynman prescription in the propagators, any tree amplitude has the structure

$$\mathcal{A}^{(0)} = \sum_i \frac{\text{Res}_i(\mathcal{A}^{(0)})}{s_i + i\epsilon} + \text{contact} = \sum_i \text{Res}_i(\mathcal{A}^{(0)}) \frac{s_i - i\epsilon}{s_i^2 + \epsilon^2} + \text{contact}, \tag{17.6}$$

where $\text{Res}_i(\mathcal{A}^{(0)})$ is the residue of the amplitude at the i-th pole, i.e., when $s_i = 0$ and the last term collects all potential regular pieces and it is purely real. The number in the superscript denotes the loop order at which the amplitude is evaluated.

Using this last expression, we trivially get the imaginary part of the amplitude,

$$\text{Im}(\mathcal{A}^{(0)}) = -\sum_i \text{Res}_i(\mathcal{A}^{(0)}) \frac{\epsilon}{s_i^2 + \epsilon^2}. \tag{17.7}$$

This seems to be vanishing in the limit $\epsilon \to 0$ (which is implicit here), but this is true only off-shell, i.e., $s_i \neq 0$, consistent with the fact, that the Feynman prescription becomes important only on the poles. On the other hand, for general momentum configurations, one has to realize that

$$-\lim_{\epsilon \to 0} \frac{\epsilon}{x^2 + \epsilon^2} = \pi\delta(x), \tag{17.8}$$

such that

$$-\sum_i \text{Res}_i(\mathcal{A}^{(0)})\delta(s_i) = \sum_X \delta(p_X^2)\mathcal{A}_L^{(0)}\mathcal{A}_R^{(0)*}|_{p_X=p_i}, \tag{17.9}$$

where we used on the right-hand side that X can only be a single-particle state such that the momentum-conserving delta function trivializes the integral, leaving only the on-shell condition for X times 2π, which, however, cancels with the left-hand side. To make it easier to read off the factorization property, we focus only on one particular factorization channel, i.e. $p_i^2 = s_i$. Then,

$$\text{Res}_i(\mathcal{A}^{(0)}) = \sum_X \mathcal{A}_L^{(0)}\mathcal{A}_R^{(0)*}|_{p_X^2=s_i}. \tag{17.10}$$

This equation pretty clearly states, that the residue of an amplitude at any pole can be calculated as the product of lower point amplitudes summed over all possible on-shell intermediate single-particle states with momenta corresponding to the respective factorization channel. To make the formula even more familiar, recall that we can extract any residue from the full amplitude by

$$\lim_{s_i \to 0} s_i \mathcal{A}^{(0)} = \lim_{s_i \to 0} \left[\sum_j \text{Res}_j(\mathcal{A}^{(0)}) \frac{s_i}{s_j + i\epsilon} + s_i \times \text{contact} \right] = \text{Res}_i(\mathcal{A}^{(0)}), \qquad (17.11)$$

such that we finally arrive at the well-known expression

$$\lim_{s_i \to 0} s_i \mathcal{A}^{(0)} = \sum_X \mathcal{A}_L^{(0)} \mathcal{A}_R^{(0)*}|_{p_X^2 = s_i}. \qquad (17.12)$$

17.2 Renormalization from the Optical Theorem

In addition to simple poles, which are captured by the discussion above, the pole structure of loop amplitudes contains branch cuts, which, as the optical theorem will tell us, arise from the propagation of on-shell multi-particle states. In the following, we will use that the scale dependence of amplitudes appears only as powers of logarithms. This can be easily seen from the fact that to keep the mass dimension of an n-loop integral constant for any number of dimensions, we multiply it by $\mu^{-2n\epsilon}$ with some integer n. In the limit $\epsilon \to 0$, this generates only polynomials of logarithms. The loop integral itself depends solely on external and loop momenta, so no additional dependence on μ can be generated by solving the integral itself. Defining the branch cut of the complex logarithm via

$$\log\left(-\frac{s_i}{\mu^2}\right) \equiv \log\left(\frac{s_i}{\mu^2}\right) - i\pi, \quad s_i > 0, \qquad (17.13)$$

where we implicitly restored Feynman's ϵ prescription by setting $s_i \to s_i + i\epsilon$ in the limit $\epsilon \to 0$, we can relate the imaginary part of any power of logarithms to a series of derivatives by

$$2\text{Im}\left[\log^n\left(-\frac{s_i}{\mu^2}\right)\right] = i\left(e^{-i\pi\mu\partial_\mu} - 1\right)\log^n\left(-\frac{s_i}{\mu^2}\right). \qquad (17.14)$$

We explicitly prove this relation for an arbitrary choice of branch of the logarithm in App. IV.C.1.

Since the derivative is linear, this relation obviously also holds for linear combinations of different powers of logarithms such that

$$2\text{Im}\left[\mathcal{A}\right] = i\left(e^{-i\pi\mu\partial_\mu} - 1\right)\mathcal{A}, \qquad (17.15)$$

which, after plugging it back into the optical theorem, immediately yields

$$\left(e^{-i\pi\mu\partial_\mu} - 1\right)\mathcal{A} = -i\sum_X \int d\text{LIPS}_X \mathcal{A}_L \mathcal{A}_R^*. \qquad (17.16)$$

Notice that, if we had used the expressions for the conjugated amplitude, we would recover the main formula in [275][1],

---

[1]Technically, the equation in [275] is given for form factors. However, it holds equivalently for the scattering amplitudes, as form factors and the T-matrix can be treated on equal footings. We will come back to this shortly.

$$e^{i\pi D}A^* = SA^*,\tag{17.17}$$

after identifying $D = -\mu\partial_\mu$.

Eq. (17.16) is an exact equation, but it will be more useful to investigate its perturbative expansion order by order. But before we do so, an important comment is in order. The form of the optical theorem we use is heavily reliant on the choice of the branch cut of the logarithm, Eq. (17.13), simply because for other choices the relation between the imaginary part of the logarithm and its derivatives is no longer given by Eq. (17.14), as explicitly seen in IV.C.1.

It turns out that for evalauating Eq. (17.16) up to the two-loop order, it suffices to expand the exponential to fourth order[2], all higher derivatives of the amplitude will necessarily correspond to higher loop effects,

$$\left[\mu\partial_\mu - \frac{i\pi}{2}(\mu\partial_\mu)^2 - \frac{\pi^2}{6}(\mu\partial_\mu)^3 + \frac{i\pi^3}{24}(\mu\partial_\mu)^4\right]\mathcal{A} = \frac{1}{\pi}\sum_X \int \mathrm{dLIPS}_X \mathcal{A}_L \mathcal{A}_R^*.\tag{17.18}$$

Moreover, up to this loop order, X can be either a two- or three-particle state[3] If $\mathcal{A}$ is renormalized, we can use the RGE Eq. (16.6) to rewrite the derivatives in terms of anomalous dimensions and beta functions,

$$\begin{aligned}(\gamma + \beta\partial)\,\mathcal{A} &- \frac{i\pi}{2}\mu\partial_\mu\left[(\gamma + \beta\partial)\,\mathcal{A}\right] \\ &= -\frac{1}{\pi}\sum_X \int \mathrm{dLIPS}_X \mathcal{A}(i \to X)\mathcal{A}^*(X \to 0).\end{aligned}\tag{17.19}$$

This equation still contains both one- and two-loop pieces, which we can separate because the optical theorem has to be satisfied order by order. Starting at one-loop, the higher order derivatives are seemingly irrelevant. While this is true for the third and fourth derivative, it is not for the second derivative in the presence of IR, specifically soft divergences. In this case, the anomalous dimension can explicitly depend on the renormalization scale [272–275], due to the presence of higher order poles before renormalization or equivalently higher order logarithms in the renormalized amplitude. Schematically, we can write

$$\gamma \supset -2ag^2 \log\left(-\frac{s}{\mu^2}\right),\tag{17.20}$$

with some numerical factor a. With this, the left-hand side of Eq. (17.19) can be written as

$$(\gamma + \beta\partial)\,\mathcal{A}^{(0)} - \frac{i\pi}{2}\mu\partial_\mu\left[(\gamma + \beta\partial)\,\mathcal{A}^{(0)}\right] \supset -2ag^2\left[\log\left(-\frac{s}{\mu^2}\right) + i\pi\right]\mathcal{A}^0.\tag{17.21}$$

Using our choice of the branch cut, Eq. (17.13), we see that the second derivative term is responsible for cancelling the imaginary part of the anomalous dimension in the presence of soft divergences. This is exactly as expected in the light of the above discussion.

Then, in total, we find the well-known result [275]

---

[2]At an arbitrary loop order n, the highest divergence the amplitude can have is of order ϵ^{-2n}, which implies that the highest power of logarithms is $2n$ after expanding around $\epsilon = 0$. In the end, terms up to the $2n$'th derivative are needed at loop order n.

[3]We saw before that for X to be a one-particle state, the amplitude $\mathcal{A}$ needs to be a tree-amplitude. But tree-amplitudes do not contain logs, they have only simple poles. These are not captured by Eq. (17.18), which explicitly uses the branch cuts of logarithms.

$$\left(\mathrm{Re}\left[\gamma^{(1)}\right] + \beta^{(1)}\partial\right)\mathcal{A}^{(0)} = -\frac{1}{\pi}\sum_X \int \mathrm{dLIPS}_2 \mathcal{A}_L^{(0)}\mathcal{A}_R^{(0)} = -\frac{2}{\pi}\mathrm{Im}\left[\mathcal{A}^{(1)}\right], \qquad (17.22)$$

where we dropped the complex conjugate because tree amplitudes are real. We also ignored the second derivative at the cost of explicitly introducing the real part of the anomalous dimension to account also for soft divergences.

In App. IV.C.2, we show how to express this integral in terms of only two angular integrals, corresponding to the polar and azimuthal angles between initial and final states in $2 \to 2$ scattering in the center-of-mass frame,

$$\left(\gamma^{(1)} + \beta^{(1)}\partial\right)\mathcal{A}^{(0)} = -\frac{1}{8\pi^3}\sum_X \int_0^{2\pi} d\phi \int_0^{\frac{\pi}{2}} d\theta \; \cos\theta\sin\theta\mathcal{A}_L^{(0)}\mathcal{A}_R^{(0)}. \qquad (17.23)$$

Finally, to also write the amplitudes in terms of these angular variables it is best to express them in terms of spinor-helicity variables and relate the loop momenta, l_i, to the external ones, p_i [275–277],

$$\begin{pmatrix} \lambda_{l_1} \\ \lambda_{l_2} \end{pmatrix} = \begin{pmatrix} \cos\theta & -\sin\theta e^{i\phi} \\ \sin\theta e^{-i\phi} & \cos\theta \end{pmatrix}\begin{pmatrix} \lambda_1 \\ \lambda_2 \end{pmatrix} \qquad (17.24)$$
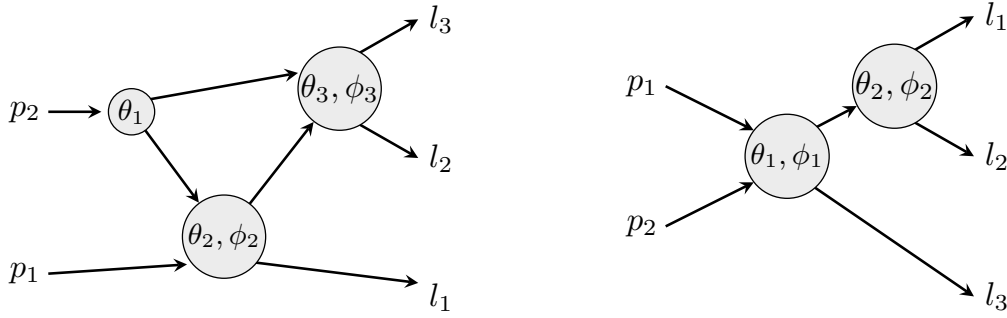
and the analogous relation for the complex conjugate variables. Note that this relation obeys momentum conservation, $l_1 + l_2 = p_1 + p_2$.

Next, we tackle the two-loop pieces. Again, the higher derivative terms are there to ensure the realness of the equation. As for the one-loop case, the presence of soft divergences generates an explicit dependence on μ for γ. The higher derivatives generate extra terms from the derivative of the anomalous dimension, with the purpose of cancelling its imaginary part. As in the one-loop discussion, we ignore these at the cost of explicitly taking the real part of γ. But starting at this loop order, they will also introduce corrections to the real part in the presence of soft divergences. Carefully expanding the exponential above and using the RGE repeatedly, keeping track of any imaginary parts, and assuming that the anomalous dimension contains at most linear logarithms [273, 274] then yields

$$\left(\mathrm{Re}\left[\gamma^{(2)}\right] + \beta^{(2)}\partial\right)\mathcal{A}^{(0)} + \left(\mathrm{Re}\left[\gamma^{(1)}\right] + \beta^{(1)}\partial\right)\mathrm{Re}\left[\mathcal{A}^{(1)}\right] - \frac{\pi}{6}\beta^{(1)}\left(\partial\mathrm{Im}\left[\gamma^{(1)}\right]\right)\mathcal{A}^{(0)}$$
$$= -\frac{1}{\pi}\sum_X \int \left[\mathrm{dLIPS}_2\left(\mathcal{A}_L^{(0)}\mathcal{A}_R^{(1)*} + \mathcal{A}_L^{(1)}\mathcal{A}_R^{(0)}\right) + \mathrm{dLIPS}_3\mathcal{A}_L^{(0)}\mathcal{A}_R^{(0)}\right]$$
$$(17.25)$$

The first two terms in the second line in this equation are equivalent to the one-loop expression, taking one of the amplitudes in the cut to be higher order. Hence, the phase-space integral can be brought to the same form as in Eq. (17.23). Note that because the RGE is written for renormalized amplitudes, all one-loop objects in Eq. (17.25) have to be renormalized, including the ones appearing in on-shell cuts. The last term, however, gives new contributions, not present at lower orders, since it contains the phase-space of three intermediate, on-shell particles. Pictorially, we can write the second line in Eq. (17.23) as

$$\sum_X \int \left[\mathrm{dLIPS}_2\left(\mathcal{A}_L^{(0)}\mathcal{A}_R^{(1)*} + \mathcal{A}_L^{(1)}\mathcal{A}_R^{(0)}\right) + \mathrm{dLIPS}_3\mathcal{A}_L^{(0)}\mathcal{A}_R^{(0)}\right]$$

$$(17.26)$$

Figure 17.1: Illustrations of the physical interpretation of the various parameterizations used for the three-particle phase space as different scattering processes. Grey circles indicate the origin of integration variables in the phase space measure. *Left:* First, one of the external momenta splits into a collinear pair, with subsequent $2 \to 2$ scatterings. *Right:* The initial momenta scatter into a massless and a massive momentum, with the latter further decaying into two massless final states.

where (un)holed ellipses denote (tree-)loop-level amplitudes, respectively, and complex conjugation of $\mathcal{A}_R$ is left implicit on the right-hand side.

For the three-particle phase space, we use two different but equivalent parametrizations, whose physical interpretations are shown schematically in Fig. 17.1. In practice, this can be useful because we can choose the parameterization in a way that makes solving the phase-space integrals as easy as possible.

The first one leads to a differential phase-space of the form [275–277]

$$\int \mathrm{dLIPS}_3 = \frac{p_X^2}{4^3 \pi^5} \int_0^{\pi/2} d\theta_1 d\theta_2 d\theta_3 \int_0^{2\pi} d\phi d\rho \, \sin\theta_1 \cos\theta_1 \sin^3\theta_2 \cos\theta_2 \sin\theta_3 \cos\theta_3, \quad (17.27)$$

corresponding to relating the spinors of the internal momenta l_i to the external ones p_1 via

$$
\begin{pmatrix} \lambda_{l_1} \\ \lambda_{l_2} \\ \lambda_{l_3} \end{pmatrix} =
\begin{pmatrix} c_2 & -s_2 e^{i\phi} & 0 \\ s_2 c_3 & c_2 c_3 e^{i\phi} & -s_3 e^{i(\rho+\phi)} \\ s_2 s_3 & c_2 s_3 e^{i\phi} & c_3 e^{i(\rho+\phi)} \end{pmatrix}
\begin{pmatrix} \lambda_1 \\ c_1 \lambda_2 \\ s_1 \lambda_2 \end{pmatrix}
$$
$$
= \begin{pmatrix} 1 & 0 & 0 \\ 0 & e^{i\phi} & 0 \\ 0 & 0 & e^{i(\phi+\rho)} \end{pmatrix}
\begin{pmatrix} 1 & 0 & 0 \\ 0 & c_3 & -s_3 e^{i\rho} \\ 0 & s_3 e^{-i\rho} & c_3 \end{pmatrix}
\begin{pmatrix} c_2 & -s_2 e^{i\phi} & 0 \\ s_2 e^{-i\phi} & c_2 & 0 \\ 0 & 0 & 1 \end{pmatrix}
\begin{pmatrix} \lambda_1 \\ c_1 \lambda_2 \\ s_1 \lambda_2 \end{pmatrix},
$$

$$(17.28)$$

where we used to notation $s_i \equiv \sin\theta_i$ and equivalently for c_i.

By splitting the 3×3 matrix, as we did in the second line of Eq. (17.28), we make the physical interpretation, modulo the phases in the first matrix, of this parametrization explicit. As depicted on the left of Fig. 17.1, we can interpret the momentum p_2 to split collinearly into two daughters with momentum fractions $\sin\theta_1$ and $\cos\theta_1$, respectively. Then, the momenta l_i are reached by scattering one of those daughters with p_1 according to Eq. (17.24). One of the final states of this first scattering is then rescattered with the second, so far unchanged, daughter of p_2, where the scattering is characterized by (θ_2, ϕ_2), while the other is already identified with one of the l_i. The reaming two l_i are then identified with the products of this second scattering, characterized by (θ_3, ϕ_3).

An alternative parametrization can be found by using a different physical interpretation [278]. We will first present the result and explain the physical reasoning afterward. The parametrization is given by

$$\begin{pmatrix} \lambda_{l_1} \\ \lambda_{l_2} \\ \lambda_{l_3} \end{pmatrix} = \begin{pmatrix} e^{-i\phi_2}c_1s_2 - e^{i\phi_1}\sqrt{\lambda}\,c_2s_1 & c_1c_2 + e^{i(\phi_1+\phi_2)}\sqrt{\lambda}\,s_1s_2 \\ \sqrt{\lambda}\,c_1c_2 + e^{-i(\phi_1+\phi_2)}s_1s_2 & e^{-i\phi_1}c_2s_1 - e^{i\phi_2}\sqrt{\lambda}\,c_1s_2 \\ \sqrt{1-\lambda}\,c_2 & e^{i\phi_2}\sqrt{1-\lambda}\,s_2 \end{pmatrix} \begin{pmatrix} \lambda_1 \\ \lambda_2 \end{pmatrix}, \tag{17.29}$$

leading to the phase space integral

$$\int \mathrm{dLIPS}_3 = \frac{p_X^2}{128\pi^5} \int_0^1 d\lambda \,(1-\lambda) \int_0^{2\pi} d\phi_1 d\phi_2 \int_0^{\frac{\pi}{2}} d\theta_1 d\theta_2 \; \sin\theta_1\cos\theta_1\sin\theta_2\cos\theta_2. \tag{17.30}$$

We explicitly show how to arrive at the above phase space integral in App. IV.C.2.

Let us briefly discuss the physical reasoning behind these expressions. The full process described in the following is shown diagrammatically on the right in Fig. 17.1. First, we can treat again the problem as a $2 \to 3$ scattering of the p_i into the l_i. Further, we can treat it as a two-step process, where p_i scatter into a massless and a massive momentum, l_3 and $p_{12} = l_1 + l_2$. We also introduce two auxiliary, massless momenta p_α and p_β along the direction of p_{12} and l_3, respectively. Note that even though l_3 is already massless, l_3 and p_β are only equal up to a proportionality constant κ to be determined later, $p_3 = \kappa p_\mu$. We then use Eq. (17.24) to relate

$$\begin{pmatrix} \lambda_\beta \\ \lambda_\alpha \end{pmatrix} = \begin{pmatrix} \cos\theta_2 & -\sin\theta_2 e^{i\phi_2} \\ \sin\theta_2 e^{-i\phi_2} & \cos\theta_2 \end{pmatrix} \begin{pmatrix} \lambda_1 \\ \lambda_2 \end{pmatrix}. \tag{17.31}$$

Further, we can parametrize any massive momentum as a linear combination of two massless ones, which we choose to be p_β and p_α. Momentum conservation, $p_{12} + l_3 = p_1 + p_2$, implies that

$$\begin{aligned} p_{12} &= \lambda\, p_\beta + p_\alpha \\ p_3 &= (1-\lambda)\, p_\beta. \end{aligned} \tag{17.32}$$

But we also know that $\lambda\, p_\mu + p_\alpha = l_1 + l_2$, so we can use Eq. (17.24) one more time to get

$$\begin{pmatrix} \lambda_{l_1} \\ \lambda_{l_2} \end{pmatrix} = \begin{pmatrix} \cos\theta_1 & -\sin\theta_1 e^{i\phi_1} \\ \sin\theta_1 e^{-i\phi_1} & \cos\theta_1 \end{pmatrix} \begin{pmatrix} \sqrt{\lambda}\lambda_\beta \\ \lambda_\alpha \end{pmatrix}, \tag{17.33}$$

where we used that spinors get rescaled by the square root of the momentum rescaling by the virtue of Eq. (11.3). Putting everything together and eliminating the auxiliary momenta gives Eq. (17.29).

So far, we only considered on-shell cuts between amplitudes, so now we will argue that the above relations are also valid for form factors $\mathcal{F}$, which are amplitudes with additional insertions of momentum through off-shell operators. This will become important in the following sections. Physically, they can be seen as a perturbation of the S matrix [275], $\delta S = i\mathcal{F}$. Then, unitarity of the S-matrix implies

$$\mathcal{F} = S\mathcal{F}^\dagger S. \tag{17.34}$$

Now, because the S-matrix leaves the vacuum invariant, this relation can be simplified by sandwiching it between one vacuum state and one state with only incoming stats. Then,

$$\langle\Omega|\mathcal{F}|i\rangle = \langle\Omega|S\mathcal{F}^\dagger S|i\rangle = \langle\Omega|\mathcal{F}^\dagger S|i\rangle. \tag{17.35}$$

Inserting a complete set of states on the right-hand side and writing $S = 1 + i\mathcal{M}$, we see that

$$2\text{Im}\,[F] = \sum_X \int \text{dLIPS}_X \, F\mathcal{A}^*, \tag{17.36}$$

where we used the regular font to denote the matrix elements of $\mathcal{F}$. We also used the realness of the equation to move the complex conjugation from the form factor to the amplitude. This equation is in complete analogy with Eq. (17.5) and because form factors depend only logarithmically on the renormalization scale, just like amplitudes do, we can use the very same relations to rewrite the imaginary part in terms of derivatives and consequently use the RGE Eq. (16.6).

To conclude this section, we want to mention the issue of fermion signs in this formalism. Using the conventional Feynman diagrammatic approach, it is well known that, e.g., a minus sign has to be introduced for each closed fermion loop. However, in the on-shell approach, it is not always clear how to assign signs, as it is not always obvious if a fermion loop is cut or not. Further, when using spinor-helicity formalism to write down amplitudes, it is convenient to have all momenta either incoming or outgoing. But, as we saw above, one of the amplitudes in the cut describes a scattering of particles, i.e., with both incoming and outgoing states. Even though we can use crossing symmetry to cross everything into either the final or initial states, this introduces issues of the right fermion ordering and how to deal with spinors of negative momenta. We will cover each of these issues in order. First, using crossing symmetry to write everything in terms of incoming states, we have

$$\langle p_1^{h_1}, p_2^{h_2} | T | p_3^{h_3}, p_4^{h_4} \rangle = \langle \Omega | T | -p_2^{-h_2}, -p_1^{-h_1}, p_3^{h_3}, p_4^{h_4} \rangle = \mathcal{A}(-p_2^{-h_2}, -p_1^{-h_1}, p_3^{h_3}, p_4^{h_4}). \tag{17.37}$$

Note that not only the sign of the momenta, but also the corresponding helicities have to be inverted and we reversed the order of the crossed momenta to take care of minus signs from fermion loops [275].

Then, note that there is no unique way to deal with spinors of negative momenta, since the only condition they need to satisfy is

$$-p_1^{\alpha\dot{\alpha}} = \lambda_{-p_1}^{\alpha} \tilde{\lambda}_{-p_1}^{\dot{\alpha}}. \tag{17.38}$$

We choose the convention where

$$(|-p_i\rangle, |-p_i]) = i(|p_i\rangle, |p_i]). \tag{17.39}$$

This, however, introduces additional factors of i, as can be seen using helicity scaling arguments of the amplitudes in the cut. To account for these, we introduce a correction factor to the phase space integral, such that [279, 280]

$$\text{dLIPS}_X \to i^{F(\{X\})}\text{dLIPS}_X, \tag{17.40}$$

where $F(\{X\})$ is the number of fermions in the intermediate state X. Note that this holds only if the negative momentum is chosen on the right side of the cut. If we assign the negative momentum to the other side, the correction factor $(-i)^{F(\{X\})}$ has to be used instead. This accounts for all possible signs that can arise from cutting through intermediate states.

Chapter 18

Infrared Divergences from Real Radiation

In general, and especially in the presence of massless particles, it happens that loop amplitudes show more than one type of divergence. First, there are the UV divergences which require the machinery of renormalizing field, couplings, and composite operators to be tamed, as we discussed thoroughly in previous sections. They are sensitive to modes with large energies and are therefore depended on the details of the scattering process itself. On the other hand, there also exist IR divergences, which can be further split into soft and collinear ones and depend only on the types of external states. These names are somewhat self-explanatory, and we will come back to their physical interpretation shortly. While we cannot get rid of such divergences by the means of renormalization, using dimensional regularization, which conveniently regularizes both UV and IR divergences, we can still remove them from amplitudes similarly, see Eq. (16.2). The corresponding divergent factors allow for an renormalization group equation similar to the UV one, which is why we can combine both UV and IR effects into a single equation, such that both the UV and IR anomalous dimensions appear in Eq. (16.6). In fact, the running of IR divergent terms can be associated with the renormalization of Wilson coefficients in a soft-collinear effective field theory (SCET), obtained after integrating out hard and non-collinear modes. The UV behavior of the corresponding operators is then directly linked to the IR part of the full theory. We will not go into any details on SCET, but for an introduction see, e.g., [281].

Instead, to interpret IR singularities, we will adopt another, possibly more physical approach. As it turns out, IR divergences do not only appear when integrating over some internal loop momenta, but also in processes with additional external states, whenever some corresponding momenta become soft, i.e., they have vanishing energy, collinear, i.e., their opening angle is small, or both. While tree-amplitudes are finite, even in the soft or collinear limit, the cross-section calculated from them can be infinite because of the phase-space integration. This seems problematic because cross-sections, being the observables they are, cannot be infinite. However, it was realized by Bloch and Nordsieck that in QED cross-sections are finite if on top of higher-loop virtual corrections also contributions from processes with more and more additional photons in the final state are included [282]. Of course, these are different processes, because of the different external states, however, in the soft and collinear limit the additional photons cannot be resolved by experiment with a finite resolution, such that they *look* like the same process in any measurement. Schematically, we can write this as

$$\sigma \sim |M_0 + M_1 + \ldots|^2 = |M_0^{(0)}|^2 + |M_1^{(0)}|^2 + 2\text{Re}\left[M_0^{(0)} M_0^{(1)*}\right]\cdots, \qquad (18.1)$$

where the subscript and superscript denote the number of additional photons in the final state and the loop order, respectively, and a sum over polarization and spins is implied. At this point we want to stress that the amplitudes in Eq. (18.1) are required to be UV renormalized, in the sense that all couplings appearing are the renormalized ones. Even though this removes all infrared divergences in observables in QED, it happens that it is not enough in more complicated theories like QCD. Here, also additional external states radiated from the initial states have to be included such that all divergences cancel, as shown by Kinoshita, Lee and Nauenberg [283,284]. While this is, in general, not very useful for practical calculations, it still gives a clear interpretation of the IR divergences appearing in loop amplitudes. They come from regions of the integration over loop momenta where some momenta are either soft, collinear or both and they are such that they cancel the ones coming from processes with additional, indistinguishable radiation, rendering observables finite in the process. We will also use this interpretation as a physical cross-check of the IR anomalous dimension we calculate using the RGE, Eq. (16.6). To do so, we focus on a specific processes in which initial state radiation is not present, leaving only the sum over final state radiation, as is the case in the Bloch-Nordsieck theorem in QED.

In the context of infrared divergences, there is a particularly convenient way to parametrize the phase space integrals appearing in the calculation, where we will work in the center-of-mass frame of the momentum P, such that $P = (\sqrt{P^2}, \mathbf{0})$. Further, because we want to calculate spin-summed and squared matrix elements, we can express everything in terms of scalar products of momenta, which, if at all, depend only on polar angles θ_i. To calculate infrared divergences up to the two-loop level, we need phase space integrals over the momenta of up to $n = 4$ particles.

For $n = 2$, the situation is trivial, as momentum conservation forces the momenta $p_{1/2}$ to be back to back in the center-of-mass frame. Therefore, all appearing scalar products are independent of any angles, rendering all possible squared matrix element trivial under integration against the measure given by Eq. (IV.C.13) in the limit $m \to 0$.

For $n = 3$, this becomes slightly more involved, as not the entire angular dependence can be made trivial. After using momentum conservation to express p_3 in terms of p_1 and p_2, we are left with two independent momenta. Then we again assume, the center of mass frame of P, such that the momentum p_1 points along the z-direction. Further, the kinematics of such a system allow it for p_1 and p_2 to always lie in the same plane, such that the polar angle of p_2 (or equivalently the angle between p_1 and p_2) is, together with energies E_1 and E_2, enough to parameterize the full phase space. Finally, we can relate these three variables to the Mandelstam invariants $s_{ij} = 2p_i \cdot p_j$ to get a phase space of the form [285]

$$\int \mathrm{dLIPS}_3^{(D)} = \frac{2^{1-2D}\pi^{1-D}}{\Gamma(D-2)}(P^2)^{1-D/2}\int_0^\infty ds_{12}ds_{13}ds_{23}\,\frac{\delta(P^2 - s_{12} - s_{13} - s_{23})}{(s_{12}s_{13}s_{23})^{2-D/2}}, \qquad (18.2)$$

where the remaining delta function is the on-shell condition for p_3.

Choosing the Mandelstam invariants as integration variables makes the physical origin of infrared divergences obvious. Soft singularities arise whenever, any momentum goes to 0, leading to the simultaneous vanishing of two invariants, e.g., $s_{12} \to 0$ and $s_{13} \to 0$ for $p_1 \to 0$. Collinear divergences, on the other hand, have their origin in two momenta becoming parallel, such that only one invariant vanishes at a time, e.g., $s_{12} \to 0$ for $p_1 || p_2$. Then, using these considerations, it is easy to identify the terms giving divergences once the squared matrix element is written in terms of the s_{ij}. In particular, it is easy to check by direct computation the squared matrix element has to contain negative powers of any Mandelstam. In fact, there have to be more negative powers than positive ones in total, to generate divergences. But these naturally arise in diagrams with additional radiation due to additional propagators, leading us to yet another

physical interpretation: infrared divergences arise whenever intermediate propagators go on-shell, signalled by $s_{ij} \to 0$ in the massless limit, where one on-shell propagator is enough for collinear divergences, while we need to simultaneously on-shell propagators to generate soft ones.

Note also that if we start with a two-particle final state, the real radiation contribution can have at most one additional propagator, such that the squared amplitude can have at most two powers of Mandelstam invariants in the denominator. With the previous considerations, it is then easy to see that the 3-particle phase space for such processes can develop at most quadratic poles in ϵ; one from the soft region, where both vanish at the same time, and one from the collinear region, where only one at a time vanishes. To simplify the integration, we eliminate the delta function and define the new integration variables z_i via

$$s_{12} = P^2(1 - z_1), \quad s_{13} = P^2 z_1 z_2, \quad s_{23} = P^2 z_1(1 - z_2), \tag{18.3}$$

such that the integral becomes

$$\int \mathrm{dLIPS}_3^{(D)} = \frac{2^{1-2D}\pi^{1-D}}{\Gamma(D-2)}(P^2)^{D-3} \int_0^1 dz_1 dz_2 \, z_1^{D-3}[z_2(1-z_1)(1-z_2)]^{D/2-2}. \tag{18.4}$$

Finally, the case for $n = 4$ is again more involved, as more particles and therefore a stronger angular dependence appear. However, we can follow the strategy from before, where we assume that p_1 points along the z-direction. Then we parametrize p_2 and p_3 in terms of the angles θ_1 and θ_2 with p_1 (or equivalently their respective polar angles), while p_4 is fully determined by momentum conservation. These are, however, only five variables and not enough to specify all six Mandelstam invariants. The crucial point we are missing so far is that three independent vectors can, in general, not be defined to lie in the same plane. So the final variable is the azimuthal angle ϕ of p_3. Expressing all energies and angles in terms of the Mandelstam invariant yields [285]

$$\int \mathrm{dLIPS}_4^{(D)} = \frac{16^{1-D}\sqrt{\pi}^{1-3D}}{\Gamma(D-3)\Gamma(\frac{d-1}{2})}(P^2)^{3-D/2} \int_0^\infty ds_{12}ds_{13}ds_{14}ds_{23}ds_{24}ds_{34}$$
$$\frac{\delta(P^2 - s_{12} - s_{13} - s_{14} - s_{23} - s_{24} - s_{34})}{\sqrt{-\Delta}^{5-d}}\theta(-\Delta), \tag{18.5}$$

where we defined $\Delta = s_{12}^2 s_{34}^2 + s_{13}^2 s_{24}^2 + s_{14}^2 s_{23}^2 - 2(s_{12}s_{34}s_{13}s_{24} + s_{12}s_{34}s_{14}s_{23} + s_{14}s_{23}s_{13}s_{24})$.

Extracting the infrared divergences follows the same argument as in the previous case: Squared amplitudes come with extra propagators, manifesting themselves as inverse powers of Mandelstam invariants. Whenever the integration hits regions where one or more invariants vanish, divergences are generated. However, for four final states, there are now more divergent configurations on top of the single-collinear and single-soft in the $n = 3$ case. These are the double-collinear region, where two distinct momenta become collinear to others, the double-soft region with two soft momenta and the mixed region with one pair of collinear momenta as well as one soft momentum. Whenever all these regions, together with the single-collinear region, overlap, up to four invariants vanish simultaneously, which is the maximal number of propagators in squared matrix elements at this level, generating up to quartic divergences. While the above integral allows for a direct computation of the four particle phase space, solving it in practice is highly non-trivial, see [285]. Instead, we will employ another technique, the so called reversed unitarity [286], making use of the fact that phase-space integrals are nothing else than just multiparticle, on-shell cuts of higher loop amplitudes. We go into more details about this

in section Sec. 20.1.3, when we actually apply the method to compute four-particle phase space integrals.

While the approach to calculating infrared divergences highlights the physical origin of infrared divergences, it also requires a lot of calculational effort. Assuming a two-particle final state at leading order, at the two-loop level, e.g., we need tree-level objects with up to four final states and one-loop objects with up to three final states, integrating the appropriate phase space measures introduced above, which in itself can become highly non-trivial. Then, to check the cancellation of the infrared divergences, the two-final-state two-loop object is necessary.

On the other hand, exploiting the RGE for form factors or amplitudes of UV safe operators, as explained in the previous sections, greatly reduces the amount of computation necessary. Using on-shell methods, one-loop objects are the highest order necessary and the phase space integrals have to be performed only over two- and three-particle particle states, where the latter contains only tree-level objects.

Nevertheless, we use the calculation of real emission contributions to have an additional check of our RGE calculations and help to understand them in more detail.

Chapter 19

(Non-)Renormalization of Conserved Currents

If we transform all fields in our theory according to

$$\Phi \to \Phi' = \Phi + \epsilon F[\Phi'] + \mathcal{O}(\epsilon^2), \tag{19.1}$$

with $F[\Phi']$ such that the transformation is a symmetry under which the action is invariant, $S[\Phi'] = S[\Phi]$. Then, the reparametrization invariance of the path integral leads to the Ward identity, the quantum-mechanical equivalent of current conservation [287–291],

$$\frac{\partial}{\partial x_\mu} \left\langle T \left\{ j^\mu(x) \prod_{i=1}^{m} \Phi_i(x_i) \right\} \right\rangle = (-i) \sum_{k=1}^{m} \delta(x - x_k) \left\langle T \left\{ F_k[\Phi(x_k)] \prod_{i \neq k}^{m} \Phi_i(x_i) \right\} \right\rangle. \tag{19.2}$$

The conserved current j^μ associated to the symmetry is given by

$$j^\mu = \frac{\delta \mathcal{L}}{\delta(\partial_\mu \Phi_n)} F_n[\Phi] - K^\mu, \tag{19.3}$$

where K^μ accounts for a possible transformation of the Lagrangian itself, $\mathcal{L} \to \mathcal{L} + \partial_\mu K^\mu$.

So far, we did not specify if the Green's functions in Eq. (19.2) are bare or renormalized. In fact, Eq. (19.2) can be derived using either the bare or renormalized Lagrangian in the same way, such that it holds in both cases by just replacing bare objects with renormalized ones. On the other hand, we can always express bare operators in terms of renormalized ones using divergent renormalization constants, see, e.g., Eq. (7.2). This leads to the identification of renormalized Green's function (we do not explicitly denote renormalized quantities here for simplicity)

$$Z_j \frac{\partial}{\partial x_\mu} \left\langle T \left\{ j^\mu(x) \prod_{i=1}^{m} \Phi_i(x_i) \right\} \right\rangle = \frac{\partial}{\partial x_\mu} \left\langle T \left\{ j^\mu(x) \prod_{i=1}^{m} \Phi_i(x_i) \right\} \right\rangle, \tag{19.4}$$

or equivalently $Z_j = 1$. From this, we could infer that Green's functions with the insertion of a conserved current, and consequently also the current itself, do not require any renormalization on top of the renormalization of fields and couplings. For a more detailed derivation of the non-renormalization of conserved currents, we refer the reader to [289–291].

Note, however, the non-renormalization implied by Eq. (19.4), holds strictly only for the divergence of the Green's functions. In fact, conserved currents can mix with a special class of counter-term operators O_μ whose divergence vanishes identically, $\partial_\mu O^\mu \equiv 0$, without the use of the equations of motion. If those were necessary, the divergent counterterm would introduce

new, divergent terms to the right-hand side of Eq. (19.2) by the virtue of the equation of motion for Green's functions

$$\left\langle T\left\{ \frac{\delta S}{\delta \Phi_j} \prod_{i=1}^{m} \Phi_i(x_i) \right\} \right\rangle = i \sum_{k=1}^{m} \delta(x-x_k)\delta_{jk} \left\langle T\left\{ \prod_{i\neq k}^{m} \Phi_i(x_i) \right\} \right\rangle, \qquad (19.5)$$

spoiling the finiteness of Eq. (19.2).

It turns out that identically conserved counterterms exist only in the context of gauge theories, as well as for the energy-momentum tensor [291, 292], the conserved tensor current of space-time translations. An example of the former is the electron number current $j_\mu = \bar{\psi}\gamma_\mu\psi$ in QED with its counterterm of the form $O_\mu = \partial_\nu F^{\nu\mu}$, whose divergence vanishes trivially by the antisymmetry of the field strength tensor. For more details on the renormalization of the vector current and a discussion on accompanying problems as well as their solution, we refer the reader to [293].

In this thesis, we are more interested in the case of the energy-momentum tensor. If we assume gravity to be non-dynamical, there exists only a single possible operator. We will show this explicitly now, employing a rather brute force approach. We start by listing all conditions possible counterterms have to satisfy:

i) a symmetric Lorentz-tensor carrying two indices, $O^{\mu\nu} = O^{\nu\mu}$,

ii) of mass dimension 4, $[O^{\mu\nu}] = 4$,

iii) identically conserved, $\partial_\mu O^{\mu\nu} \equiv 0$, without the usage of any EOMs.

While, in general, the energy-momentum tensor calculated from Noether's theorem Eq. (19.3) itself does not obey condition i), we can always add the divergence of an antisymmetric three-tensor to make it symmetric without changing any of its physical properties. Given these conditions, we can check whether it is impossible to build counterterms from fermions (ψ), scalars (ϕ) or vectors (A) in theories with at most marginal couplings. Further, note that condition iii) implies that here it is sufficient to consider only operators with the same field content because the only way to mix operators with different field contents is by the equations of motion.

Fermions:

Their transformation under the Lorentz group tells us that fermions must always come in pairs, $\bar{\psi}\psi$, which have mass dimension $[\bar{\psi}\psi] = 3$. The remaining mass dimension can then be obtained by either a relevant coupling λ, a bosonic field or one derivative.

For a relevant coupling or a scalar, the situation is easy, as in this case, the only symmetric, two index structure we can have is the metric, which is obviously not identically conserved,

$$\partial_\mu O^{\mu\nu} \sim \partial^\nu \begin{cases} (\phi\bar{\psi}\psi) \\ (\bar{\psi}\psi) \end{cases} \neq 0. \qquad (19.6)$$

The case of additional derivatives and a vector field can be combined by using the covariant derivative. There are two independent possible structures

$$g^{\mu\nu}\bar{\psi}\slashed{D}\psi, \qquad\qquad \bar{\psi}\gamma^{\{\mu}D^{\nu\}}\psi, \qquad (19.7)$$

neither of which are traceless or identically conserved on their own. (Note we defined the symmetrization without symmetry factor, e.g., $\gamma^{\{\mu} D^{\nu\}} = \gamma^\mu D^\nu + \gamma^\nu D^\mu$)

But, of course, it may be possible to construct suitable operators from linear combinations of the above. The most general symmetric operator we can then write reads

$$O_F^{\mu\nu} = a \, g^{\mu\nu} \bar{\psi} \slashed{D} \psi + b \, \bar{\psi} \gamma^{\{\mu} D^{\nu\}} \psi, \tag{19.8}$$

with a priori arbitrary coefficients a, b. However, because the two operators are independent by construction, the same holds for their divergences, so the only possibility to satisfy condition iii) is the trivial solution $a = b = 0$. So we conclude that it is not possible to construct a suitable counterterm from operators containing fermions.

Scalars:

In theories with scalars, there is the well-known counterterm term, see e.g., [292], built from scalars and derivatives only,

$$O^{\mu\nu} = \left(\partial^\mu \partial^\nu - g^{\mu\nu} \partial^2\right) \phi^2. \tag{19.9}$$

Obviously, operators built from four scalars are not identically conserved and from above, we know that also fermions are not a viable option. This leaves only the inclusion of vector bosons, which, due to gauge invariance, can only appear in field strength tensors $F^{\mu\nu}$. It turns out that the only possibility is to have one field strength without additional derivatives. It can be checked, that otherwise we would either need a non-zero trace of the field strength or condition i) cannot be satisfied. So one is left with

$$O^{\mu\nu} \sim F^{\mu\nu} \phi^n \qquad n \in \{1, 2\} \,. \tag{19.10}$$

This is obviously not conserved identically, we conclude that no suitable counterterm containing scalars can be constructed. Note that all operators of the form Eq. (19.9) with ϕ^2 replaced by any other Lorentz scalar are valid counterterms as well, however, all gauge invariant combinations of non-scalar fields are necessarily of higher order.

Vectors:

From the above, we know that operators with fermions and scalars cannot give rise to counterterms, so the only option left are vectors and derivatives thereof.

For operators with only field strength tensors and no additional derivatives, we again have two possibilities for a symmetric two-index tensor,

$$F^{\mu\alpha} F^\nu_\alpha, \qquad\qquad g^{\mu\nu} F^{\alpha\beta} F_{\alpha\beta}, \tag{19.11}$$

neither of which are conserved identically. As in the fermionic case, we can construct no identically conserved linear combination because of the linear independence of the operators.

If we chose to have additional derivatives instead of a second field strength tensor and the only possible structure is,

$$\partial_\alpha \partial^{\{\mu} F^{\nu\}\alpha}, \tag{19.12}$$

which is not identically conserved because of pieces in which two derivatives are contracted.

In the end, we find that any possible counterterm cannot contain scalars, vectors, or fermions up to marginal interactions, implying that the energy momentum tensor cannot be renormalized at any order in such theories.

This is, however, not the case once gravity is turned and the graviton is allowed to propagate. In this case, the operator [294]

$$O^{\mu\nu} = \partial_\rho \partial_\sigma C^{\rho\mu\sigma\nu} \tag{19.13}$$

is identically conserved. Here $C^{\rho\mu\sigma\nu}$ is the Weyl tensor, the traceless part of the Riemann tensor. Since the Weyl tensor inherits all the symmetries of the Riemann tensor, conservation of the above operator follows trivially from antisymmetry. In this thesis, we will not consider the renormalization induced by this operator, and focus only on marginal couplings instead.

As discussed in [210], form factors of the energy-momentum tensor can be split into pieces corresponding to different angular momenta of the external states using a partial wave decomposition. This corresponds to decomposing the tensor itself into its irreducible representations under the Lorentz group. Then the symmetric and traceless piece corresponds to an angular momentum $J = 2$, while the trace has $J = 0$. Now, the crucial point is that the operator Eq. (19.9) lives entirely in the $J = 0$ region and can as such be completely associated with the trace. Thus, since there are no other possible counterterms, it follows immediately that the $J = 2$, or in other words, the symmetric and traceless part, is not renormalized at any loop order.

At this point, we want to stress, that this is the main point of this part of the thesis. Due to the all-order non-renormalization of the $J = 2$ component, we know that $\gamma_{\mathrm{UV}} = 0$ exactly. In turn, this immediately implies that by considering the renormalization of form factors of the $J = 2$ component, we directly calculate the universal infrared anomalous dimension, without the need of separating UV and IR contributions first. Once this has been done for all particles in a given theory at a given loop order, this reduces the computational effort when calculating the renormalization of any other amplitude in the theory, as any IR anomalous dimension can easily be subtracted without any additional computation, leaving only the UV piece.

Chapter 20

Infrared Divergences in a Yukawa Theory

Now that we introduced and explained the main computational methods to calculate infrared divergences using form factors of the traceless energy-momentum tensor, we want to explicitly perform them in a simple toy model. The model contains a Dirac fermion ψ, which we split into its left- and right-handed components ψ_L and ψ_R, respectively, as well as a real, conformally coupled scalar ϕ. The interactions included are a Yukawa type interaction of strength y between the fermions and scalar together with a scalar quartic coupling λ, which is necessary for the renormalizability of the theory. The energy-momentum tensor of such a theory is given by

$$
\begin{aligned}
T_{\mu\nu} = \partial_\mu\phi\partial_\nu\phi - \frac{1}{2}\eta_{\mu\nu}\partial_\alpha\phi\partial^\alpha\phi + \frac{D-2}{4(D-1)}(\partial_\mu\partial_\nu - \eta_{\mu\nu}\partial^2)\phi^2 \\
+ i\frac{1}{4}\sum_{i=L,R}\bar{\psi}[\gamma_\mu\overleftrightarrow{\partial}_\nu + \gamma_\nu\overleftrightarrow{\partial}_\mu - 2g_{\mu\nu}\gamma_\alpha\overleftrightarrow{\partial}^\alpha] + \dots,
\end{aligned}
\tag{20.1}
$$

where the ellipsis stands for terms with more than two fields. These are irrelevant for the present purpose, simply because their index structure is trivially given by the metric and therefore they vanish once projected according to the method we will explain later. The last term in Eq. (20.1) is generated by the conformal coupling of the scalar and originates, in the Lagrangian picture, from a term of the form $R\phi^2$, with R being the Ricci scalar. We also kept it to depend explicitly on D such that $T = \eta^{\mu\nu}T_{\mu\nu} = 0$ in all dimensions. In $D = 4$, it reduces to the known factor of $1/6$.

To set up the notation for this section, we define

$$
T_{\mu\nu}(\{j\}) \equiv \langle\Omega|T_{\mu\nu}|1, 2, \dots, j\rangle.
\tag{20.2}
$$

Since we can always write the energy momentum tensor in a symmetric form, also the corresponding Green's function will be a symmetric two-tensor. Hence, we can always decompose it as

$$
T_{\mu\nu}(\{j\}) = T_{2,i}(q^2)\, T_{\mu\nu,2}(\{j\}) + T_{0,i}(q^2)\, T_{\mu\nu,0}(\{j\}),
\tag{20.3}
$$

where $T_{\mu\nu,2}(\{j\})$ is the symmetric and traceless component, which transforms like a two-tensor under rotations and can therefore be associated with an angular momentum of $J = 2$. $T_{\mu\nu,0}(\{j\})$, on the other hand, is the trace part, which transforms like a scalar under a rotation, with an corresponding angular momentum of $J = 0$. The scalar functions $T_{2,i}$ and $T_{0,i}$ are form factors, in full analogy to the electric and magnetic form factors of the QED vertex function. For a two-particle final state, the i in the subscript is given by the difference of their helicities, $i = h_1 - h_2$.

To efficiently extract the scalar form factors, it is convenient to define some projection procedure, effectively removing all open Lorentz indices. We present the procedure used for two-particle states of particle-antiparticle pairs in App. IV.D. Throughout the rest of this part of the thesis, we will make extensive use of the projection techniques presented in that appendix.

To obtain the infrared anomalous dimension, we first use on-shell methods to directly calculate it. We then confirm the results of the on-shell calculation by using the full two-loop form factor and extract the anomalous dimension from both the imaginary part of the UV renormalized form factor, as well as the single pole divergence.

Finally, we calculate squared matrix elements to check if the divergences we find cancel against real emission contributions in physical observables. To do so, we temporarily restore the graviton and couple it the the the vertex of the $T^{\mu\nu}$ insertion. When squaring the amplitude, the only ingredient needed is the polarization sum for the spin-2 polarization tensor, for which we use

$$\sum_k \epsilon_k^{\mu\nu} \epsilon_k^{\rho\sigma} = \frac{1}{2} \left(g^{\mu\rho} g^{\nu\sigma} + g^{\nu\rho} g^{\mu\sigma} - g^{\mu\nu} g^{\rho\sigma} \right). \tag{20.4}$$

This choice of initial state allows us to consider only corrections from initial-state radiation, as any radiation from the initial gluon would contribute only at higher orders in the gravitational coupling, which is not what we are interested in.
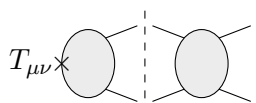
20.1   Scalar Field

We start by calculating the infrared divergences associated to the scalar of the theory, i.e., we fix the external states to be a pair of scalars. The relevant angular momentum component we project on is $T_{2,0}(1_\phi, 2_\phi)$. This also implies that at tree-level, the form factor is the minimal one, meaning it does not depend on any couplings in the theory. Hence, the derivative with respect to the coupling in Eq. (16.6) vanish whenever they act on the tree-level form factor.

20.1.1   On-shell Methods

Starting with the on-shell approach, we use the relevant tree- and one-loop form factors and amplitudes [7] to calculate all the on-shell cuts as dictated by the RGE. It turns out that in the theory at hand, all two-particle phase-space integrals up to the two loop order can straightforwardly be evaluated in four dimensions. This will not be the case, in general, in the presence of soft divergences, where the phase space integral itself is divergent in four dimensions.

Starting at one-loop, there are in principle on-shell cuts with both fermion chiralities as well as the scalar as intermediate particles. The latter, however, vanishes, as can be seen by using angular momentum arguments. Projecting onto the $J = 2$ component, this obviously fixes the angular momentum of the legs in the form factor. Angular momentum conservation then forces the $J = 2$ to be transmitted to the amplitude. Now, since the external states are fixed to be scalars, we need a four-scalar amplitude in this channel. In our theory, the only such amplitude at tree level is given by the contact interaction generated by λ, which, however, has only a $J = 0$ component. This implies that the phase space integral has to vanish. Thus, at one-loop only intermediate fermions contribute to the infrared divergences and being careful with fermion signs, we find

$$T_{\mu\nu} \!\!\! \begin{array}{c} \end{array} = \frac{y^2}{4\pi} T_{2,0}^{(0)}(1_\phi, 2_\phi). \tag{20.5}$$

Plugging this into Eq. (17.23) and using both $\Delta\gamma = -\gamma_{\text{IR}}$ and $\partial T_{2,0}^{(0)}(1_\phi, 2_\phi) = 0$ we find

$$\gamma_{\text{IR}}^{(\phi,1)} = \frac{y^2}{4\pi^2}. \tag{20.6}$$

This is the well-known result of twice (once for each external scalar field) the collinear anomalous dimension of a scalar coupled with a Yukawa term to a Dirac fermion. Note, that we also explicitly reproduced the fact there are no infrared divergences in a quartic scalar theory at all, as our result does not depend on λ. We will see why this is indeed the case, using the cancellation of infrared divergences between real and virtual corrections in cross-sections. Further, it does not contain logarithms, implying the absence of soft divergences, such that the correction term from the higher derivative terms in Eq. (17.25) is absent for the scalar in this theory.

But first, we continue with the two-loop calculation. As already mentioned, also at this order the two-particle phase space can straightforwardly be evaluated in four dimensions, however, now also the scalar channel contributes. For the tree-insertions of the energy-momentum tensor we find, also the scalar channel contributes because at one-loop, the four-scalar amplitude is no longer constrained to contain only $J = 0$ pieces, and in total we find

$$T_{\mu\nu} \times \quad = \left[\frac{y^4}{128\pi^3} \left(5\log\left(\frac{s_{12}}{\mu^2}\right) - 30 - i\pi \right) - \frac{\lambda^2}{1536\pi^3} \right] T_{2,0}^{(0)}(1_\phi, 2_\phi), \tag{20.7}$$

where we already extracted the imaginary part, keeping in mind that the loop amplitude has to be complex conjugated, and explicitly see the contribution from the scalar quartic. Calculating the missing two-particle cuts with one-loop insertions of $T_{\mu\nu}$ we find

$$T_{\mu\nu} \times \quad = -\frac{y^4}{128\pi^3} \left[\log\left(\frac{s_{12}}{\mu^2}\right) - 3 - i\pi \right] T_{2,0}^{(0)}(1_\phi, 2_\phi). \tag{20.8}$$

Here, the scalar channel, or equivalently, terms proportional to λ vanish because of the same angular momentum argument as at one-loop. Adding these two results, we easily see that the imaginary parts cancel each other, as required by the optical theorem, explicitly highlighting the importance of the complex conjugation of the appropriate loop amplitudes.

This leaves us with only the three-particle cuts left to compute. As usual, the necessary form factors and amplitudes are given in [7]. It turns out, these are quite a bit more involved and we will make full use of our freedom of choosing a parameterization for the phase-space integral to make the computation as easy as possible. We will briefly explain, why it can be so useful to have different ways of expressing the same integral. Take for example the spinor expression $\langle l_1 p_1\rangle\langle l_2 p_2\rangle$, which appears at some point of the calculation of the 3-particle cuts: Using the parameterization given in Eq. (17.28), we find

$$\langle l_1 1\rangle\langle l_2 2\rangle = e^{i\phi}\cos\theta_1 \sin^2\theta_2 \cos\theta_3 \langle 12\rangle, \tag{20.9}$$

i.e., we get an expression where all phases can be factored out. To obtain expressions with definite powers of phases is particularly helpful if they appear in denominators, such that all phases can just be factored out. Because of the structure of the phase-space integral, only terms with a trivial dependence on any phase survive the integration (provided, again, all terms contain only definite powers). On the other hand, it can be easily shown by direct computation, that using Eq. (17.29), it is impossible to reach something with definite phases starting from $\langle l_1 1\rangle\langle l_2 2\rangle$, even after possible relabelings of the l_i. On the other hand, e.g., the expression

$s_{l_2 l_3} \langle l_2 1 \rangle \langle l_1 l_3 \rangle$ can only be turned into something with a definite phase by using Eq. (17.29) and not Eq. (17.28). So, whenever, the denominator in a certain parameterization does not look to be easily integrable, there is the possibility that a different one does. However, we will encounter a few cases, where neither of the two can give a denominator of definite phase. We will come back to them shortly.

Another subtlety, as we will see, is given by the fact that some integrals appearing cannot be solved in four dimensions, they exhibit a divergence, that needs to be treated using, e.g., dimensional regularization. We will come back to the origin of this divergence when discussing the calculation of the full two-loop form factor. So in total, we can split the calculation of the three-particle cuts into three categories: (i) finite integrals, that can easily be solved using the appropriate parameterization, (ii) finite integrals with denominators with no definite phase and (iii) divergent integrals. We give the result for the first category without going into the details of the computation

$$
T_{\mu\nu} \!\!\! \left.\raisebox{-1em}{}\right|_{(i)} = \frac{9y^4}{128\pi^3} T_{2,0}^{(0)}(1_\phi, 2_\phi). \tag{20.10}
$$

For category (iii) we can use Eq. (17.29)[1] to find expressions of definite phase and the D-dimensional phase space measure Eq. (IV.C.18), evaluating to

$$
T_{\mu\nu} \!\!\! \left.\raisebox{-1em}{}\right|_{(iii)} = \frac{y^4}{64\pi^3}\left[2\log\left(\frac{s_{12}}{\mu^2}\right) - \frac{1}{\epsilon} - \frac{37}{6}\right] T_{2,0}^{(0)}(1_\phi, 2_\phi), \tag{20.11}
$$

such that we last missing ingredient is given by category (ii). Choosing again Eq. (17.29), the integrand, not including the measure, can be written in form

$$
F^{(0)}\mathcal{A}^{(0)} = s_{12}\left(-\frac{(1-\lambda)^2}{2\sqrt{\lambda}}(1 + 3c_{4\theta_2})\right)
$$
$$
\left(-\frac{1}{\left(\sqrt{\lambda}c_{\theta_1}c_{\theta_2} - e^{i(\phi_1 - \phi_2)}s_{\theta_1}s_{\theta_2}\right)\left(c_{\theta_1}c_{\theta_2} - \sqrt{\lambda}e^{-i(\phi_1-\phi_2)}s_{\theta_1}s_{\theta_2}\right)}\right). \tag{20.12}
$$

We see that the term in the first bracket depends only on one angular variable, so we can focus on the second one. To start, we mention that it is easiest to solve the integration over (θ_1, ϕ_1) first, treating all other integration variables as constants for now. By doing so, we can bring it to an easily calculable form using the residue theorem. Reinstating the relevant part integration measure, but dropping all constant factors for now, we find

$$
\int \mathrm{dLIPS}_3 F^{(0)}\mathcal{A}^{(0)} \propto \frac{e^{i\phi_2}}{c_{\theta_2}s_{\theta_2}}\int_0^\pi d\theta_1 \oint_{S^1}\frac{dz}{i}\frac{1}{(z - \eta t)(z - \eta/t)}, \tag{20.13}
$$

where we defined $\eta = \sqrt{\lambda}\exp(i\phi_2)$, $t = t_{\theta_1}t_{\theta_2}$ and $z = \exp(i\phi_1)$. The integrand has two distinct poles, which, however, can only contribute to the integral if $|\eta t| < 1$ or $|\eta/t| < 1$ or both, such that they lie within the integration contour. Using the residue theorem yields

---

[1]When performing the integration in D dimensions, we have to change $\phi_i \to 2\phi_i$ in the exponentials. This accounts for the fact, that in $D \neq 4$ the ϕ_i are not the azimuthal angles and have only half of the integration range, $\phi_i \in [0, \pi]$, compared to $d = 4$, where $\phi_i \in [0, 2\pi]$.

$$\int \mathrm{dLIPS}_3 F^{(0)} \mathcal{A}^{(0)} \propto \frac{1}{c_{\theta_2} s_{\theta_2}} \frac{2\pi}{\sqrt{\lambda}} \int_0^\pi d\theta_1 \, \frac{t}{t^2-1} \left[\theta\left(\frac{1}{\sqrt{\lambda}} - t\right) - \theta(t - \sqrt{\lambda}) \right], \qquad (20.14)$$

with the Heaviside functions encoding the conditions for the poles to lie within the integration contour. Then, changing the integration variable from θ_2 to $y = t^2$, we arrive at an integral that can straightforwardly be evaluated,

$$\begin{aligned}
\int \mathrm{dLIPS}_3 F^{(0)} \mathcal{A}^{(0)} &\propto \frac{1}{c_{\theta_2} s_{\theta_2}} \frac{\pi}{\sqrt{\lambda}} \left(\int_0^{\frac{1}{\lambda}} - \int_\lambda^\infty \right) \frac{dy}{(y-1)(y/t_{\theta_1}^2 + 1)} \\
&= \frac{\pi}{\sqrt{\lambda}} \log \left(\frac{(\lambda-1)^2 t_{\theta_1}^2}{(\lambda + t_{\theta_1}^2)(1 + \lambda t_{\theta_1}^2)} \right)
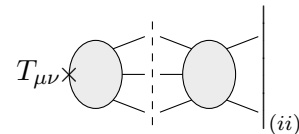\end{aligned} \qquad (20.15)$$

This concludes the integration over (θ_1, ϕ_1), so next, we will integrate over (θ_2, ϕ_2), where now also the first bracket in Eq. (20.12) has to be included. We have observed that all the dependence on the phase drops out, making the ϕ_2 integral trivial to solve. The integral over θ_2 can be written in terms of elementary functions, giving

$$\begin{aligned}
\int \mathrm{dLIPS}_3 F^{(0)} \mathcal{A}^{(0)} &\propto -\frac{(1-\lambda)^2 \pi^2}{\lambda} \int_0^\pi d\theta_1 \, (1 + 3c_{4\theta_2}) \, s_{\theta_2} c_{\theta_2} \log\left(\frac{(\lambda-1)^2 t_{\theta_1}^2}{(\lambda + t_{\theta_1}^2)(1 + \lambda t_{\theta_1}^2)} \right) \\
&= -4\pi^2 \left(2 - \frac{\lambda+1}{\lambda-1} \log \lambda \right).
\end{aligned} \qquad (20.16)$$

Finally, we can solve the last integration for λ,

$$\int \mathrm{dLIPS}_3 F^{(0)} \mathcal{A}^{(0)} \propto -4\pi^2 \int_0^1 d\lambda \, (1-\lambda) \left(2 - \frac{\lambda+1}{\lambda-1} \log \lambda \right) = \pi^2. \qquad (20.17)$$

Finally, after putting back all factors from the phase space measure we dropped so far, we get the final result for the contributions from category (ii) of the three-particle cuts,

$$T_{\mu\nu} \times \left. \vcenter{\hbox{}} \right|_{(ii)} = \frac{y^4}{64\pi^3} T_{2,0}^{(0)}(1_\phi, 2_\phi). \qquad (20.18)$$

Summing all the contributions, we have

$$\begin{aligned}
\sum_X \int &\left[\mathrm{dLIPS}_2 \left(T_{2,0}^{(0)} \mathcal{A}^{(1)*} + T_{2,0}^{(1)} \mathcal{A}^{(0)} \right) + \mathrm{dLIPS}_3 \, T_{2,0}^{(0)} \mathcal{A}^{(0)} \right] \\
&= \frac{1}{64\pi^3} \left[4y^4 \log\left(\frac{s_{12}}{\mu^2} \right) - \frac{y^4}{\epsilon} - \frac{85}{6} y^4 + \frac{\lambda^2}{24} \right] T_{2,0}^{(0)}(1_\phi, 2_\phi).
\end{aligned} \qquad (20.19)$$

But this result is still divergent, which cannot be correct, since it would imply that either the beta function or the anomalous dimension are divergent, which they are not. The crucial piece of information to resolve this issue is that the RGE needs to be evaluated for renormalized amplitudes and form factors only. While, we used renormalized loop amplitudes in the two-particle cuts, this does not cover the entire renormalization needed. Instead, it contains only counterterms for the vertices and intermediate propagators within the loop amplitude, but

187
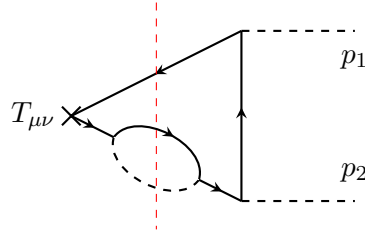
Figure 20.1: Diagram leading to a divergence in the three-particle cut. Scalars and fermions are denoted by dashed and solid lines with arrows, respectively. Crossed diagrams are not shown, but exhibit the same divergence in their three-particle cut.

does not account for divergences from external legs, which are left over in the field renormalization constants, even after amputation. These are precisely the counterterms needed, to render Eq. (20.19) finite. In particular, we will find that the divergence comes from two-loop diagrams with one-loop subdiagrams of the form of a fermion wave-function renormalization, with the corresponding cut going right through this loop, as shown in Fig. 20.1. Adding a diagram with the one-loop subdiagram replaced with the appropriate counterterm gives a contribution that exactly cancels this divergence.

In the light of on-shell methods, we need to include a cut of the form

$$2 \sum_{i=L,R} \delta_{\psi_i} \int \mathrm{dLIPS}_2^{(D)} T_{2,0}^{(0)}(1'_{\psi_i}, 2'_{\bar{\psi}_i}) \mathcal{A}^{(0)}(-2'_{\psi_i}, -1'_{\bar{\psi}_i}, 1_\phi, 2_\phi), \qquad (20.20)$$

with δ_{ψ_i} the divergent one-loop wave function counterterm for the fermion. We stress that it is important to perform the integration in D dimensions because a four-dimensional one is not sufficient to generate the correct finite terms from combining the divergence in δ_{ψ_i} with possible terms of $\mathcal{O}(\epsilon)$ that come out of the integral. Including this last counterterm, we finally arrive at our result for the sum of all the on-shell cuts necessary at the two-loop order

$$\sum_X \int \left[\mathrm{dLIPS}_2 \left(T_{2,0}^{(0)} \mathcal{A}^{(1)*} + T_{2,0}^{(1)} \mathcal{A}^{(0)} \right) + \mathrm{dLIPS}_3 \, T_{2,0}^{(0)} \mathcal{A}^{(0)} \right]$$
$$= \frac{1}{64\pi^3} \left[3y^4 \log \left(\frac{s_{12}}{\mu^2} \right) - \frac{23}{2} y^4 + \frac{\lambda^2}{24} \right] T_{2,0}^{(0)}(1_\phi, 2_\phi). \qquad (20.21)$$

At this point, we note that an alternative procedure would be to not use any renormalized amplitudes, perform all phase space integrals, in particular also the two-particle ones, in D dimensions and then replace bare couplings with the renormalized ones. Note also, there are no terms with a mixed dependence on the Yukawa and the scalar quartic coupling.

With this result, we are now ready to calculate the two-loop infrared anomalous dimension of the scalar in our theory. Of course, recalling Eq. (17.25), we also need the one-loop beta function. This can easily be calculated via the one-loop renormalization of the Yukawa vertex, which we will not reproduce here, instead we just quote the result,

$$\beta_y = \frac{5y^3}{16\pi^2}. \qquad (20.22)$$

For convenience, we also quote the projected and renormalized one-loop form factor here, as it is explicitly needed for the RGE, making the imaginary part explicit,

$$T_{2,0}^{(1)}(1_\phi, 2_\phi) = -T_{2,0}^{(0)}(1_\phi, 2_\phi) \frac{y^2}{16\pi^2} \left[2 \log \left(\frac{s_{12}}{\mu^2} \right) - 6 - 2i\pi \right]. \qquad (20.23)$$

Even though we already removed all imaginary parts in Eq. (17.25) on general grounds, we want to show the cancellation explicitly here. An intermediate step of the derivation of that equation contains an purely imaginary term built from only one-loop quantities, with the task to cancel the imaginary part of the one-loop form factor appearing in the RGE. Keeping this term explicitly at the cost of not taking the real part of the one-loop form factor amounts to calculating

$$\left(\gamma^{(1)} + \beta^{(1)}\partial\right) T_{2,0}^{(1)} + \frac{i\pi}{2}\left(\gamma^{(1)} + \beta^{(1)}\partial\right)^2 T_{2,0}^{(0)} = \frac{y^4}{64\pi^4}\left[9 - 3\log\left(\frac{s_{12}}{\mu^2}\right)\right] T_{2,0}^{(0)}. \tag{20.24}$$

This result shows explicitly how the higher-derivative terms are responsible for cancelling all imaginary terms, as required by the optical theorem. Further, recalling the extra factor of $-1/\pi$ the cuts have to be augmented with, we also see that all logarithms cancel, indicating that no soft divergences are present for the scalar in a Yukawa theory, even at two loops.

Finally, we can combine all of the above results to find the infrared anomalous dimension for the scalar, which comes out to be

$$\gamma_{\text{IR}}^{(\phi,2)} = -\frac{5y^4}{128\pi^4} + \frac{\lambda^2}{1536\pi^4}. \tag{20.25}$$

Before going to an alternative approach for calculating this anomalous dimension, we note that again, the infrared anomalous dimension coincides with that of the scalar field at two-loops [295], and we will come back to this shortly.

20.1.2 Feynman diagrammatic approach

Let us confirm this result by explicitly calculating the full two-loop form factor. The corresponding two-loop diagrams are shown in Fig. 20.2. There we recognize the first diagram to be the one giving a divergent three-particle cut. Further, the three-particle cut we could not straightforwardly integrate and had to use the residue theorem comes exclusively from the non-planar diagram.

After contracting the energy momentum tensor onto the desired form factor, we are left with only scalar products of external and loop momenta in the numerators of the loop integrals. These can further be reduced to scalar integrals by rewriting the scalar products in terms of inverse propagators such that they cancel parts of the denominator[2]. The resulting scalar integrals are, however, not linear independent and can be related to a basis of scalar integrals by using Integration-By-Parts (IBP) and Lorentz-Invariance (LI) identities. In practice, we use the software `Kira` [296], which fully automizes the reduction of scalar integrals to the basis integrals. For more details on the method, see App. IV.B

---

[2]At the two-loop level with two independent external momenta there are 7 independent scalar products including at least one loop momentum. In our case, the two-loop diagrams have at most six independent propagators, such that we have to include additional auxiliary propagators to be able to write all scalar products in terms of propagators.

$$p_{12} \bigcirc p_{12} \equiv A_3(d, p_{12}^2),$$

$$p_{12} \bigcirc\bigcirc p_{12} \equiv A_2(d, p_{12}^2), \qquad p_{12} \begin{array}{c} p_1 \\ p_2 \end{array} \equiv A_4(d, p_{12}^2), \qquad (20.26)$$

$$p_{12} \begin{array}{c} p_1 \\ p_2 \end{array} \equiv A_6(d, p_{12}^2).$$

We do not give the explicit analytic expressions of the integrals, as they are not particularly illuminating, but we refer the reader, e.g., [297, 298].

As usual, these two-loop integrals contain non-local divergences of the form of logarithms with divergent coefficients, originating from regions where only one of the two loop momenta becomes large at a time. These, being non-local, cannot be cancelled by any counterterms present in the Lagrangian, which can generate only local terms, i.e., polynomials of momenta. Instead, these will be cancelled by the same non-local divergences appearing in diagrams with insertions of one-loop counterterms. Conceptually, these are just one-loop diagrams, which can easily be solved using the standard methods. But note, that here, the one-loop basis integrals have to be expanded to $\mathcal{O}(\epsilon)$, to generate a rational term due to the $1/\epsilon$ factor from the counterterm.

Comparing this to the on-shell approach, including these one-loop counterterms is equivalent to using renormalized loop amplitudes in the two-particle cuts as well as adding Eq. (20.20), such that all divergences within the cuts cancel.

Then, adding the genuine two-loop diagrams and the one-loop counterterm diagrams as well as all other (tree-level) counterterms needed for renormalization, together with the one-loop and tree level form factors, we find

$$T_{2,0}(1_\phi, 2_\phi) = T_{2,0}^{(0)}(1_\phi, 2_\phi) \left\{ 1 + \delta_\phi^{(1)} + \delta_\phi^{(2)} + \left(\frac{y}{4\pi}\right)^2 \left[\frac{2}{\epsilon} + 2\log\left(-\frac{s_{12}}{\mu^2}\right) + 6\right] \right.$$
$$+ \left(\frac{y}{4\pi}\right)^4 \left[\frac{3}{\epsilon^2} - \frac{5}{2\epsilon} - 3\log^2\left(-\frac{s_{12}}{\mu^2}\right) + 23\log\left(-\frac{s_{12}}{\mu^2}\right) - \frac{547}{12} - \pi^2\right]$$
$$\left. + \frac{\lambda^2}{(4\pi)^4}\left[\frac{1}{24\epsilon} - \frac{1}{12}\log\left(-\frac{s_{12}}{\mu^2}\right) + \frac{65}{144}\right] + \ldots \right\},$$
(20.27)

with the ith loop counterterm $\delta^{(i)}$ and the ellipsis denote even higher-order contributions. We also explicitly kept the divergent piece, as well as the renormalization constant necessary to absorb it, such that the expression if finite, despite the explicit divergent term. Given this expression, it is easy to calculate the sum of all cuts by simply taking twice the imaginary part, yielding

$$2\text{Im}\left[T_{2,0}(1_\phi, 2_\phi)\right] = \frac{1}{64\pi^3}\left[3y^4\log\left(\frac{s_{12}}{\mu^2}\right) - \frac{23}{2}y^4 + \frac{\lambda^2}{24}\right] T_{2,0}^{(0)}(1_\phi, 2_\phi), \qquad (20.28)$$

in perfect agreement with Eq. (20.21), leading to the same anomalous dimension as in Eq. (20.25).

Because we left the divergences implicit, we can also use them to calculate the anomalous dimension. Using Eq. (16.3), we find the renormalization constant of the Green's function to be

$$Z_G^{(\phi)} = \left(1 + \delta_\phi^{(1)} + \delta_\phi^{(2)}\right)^{-1} = \left[1 + \left(\frac{y}{4\pi}\right)^2 \frac{2}{\epsilon} + \left(\frac{y}{4\pi}\right)^4 \left(\frac{5}{\epsilon^2} - \frac{7}{2\epsilon}\right) + \frac{\lambda^2}{6144\pi^4}\right]. \qquad (20.29)$$
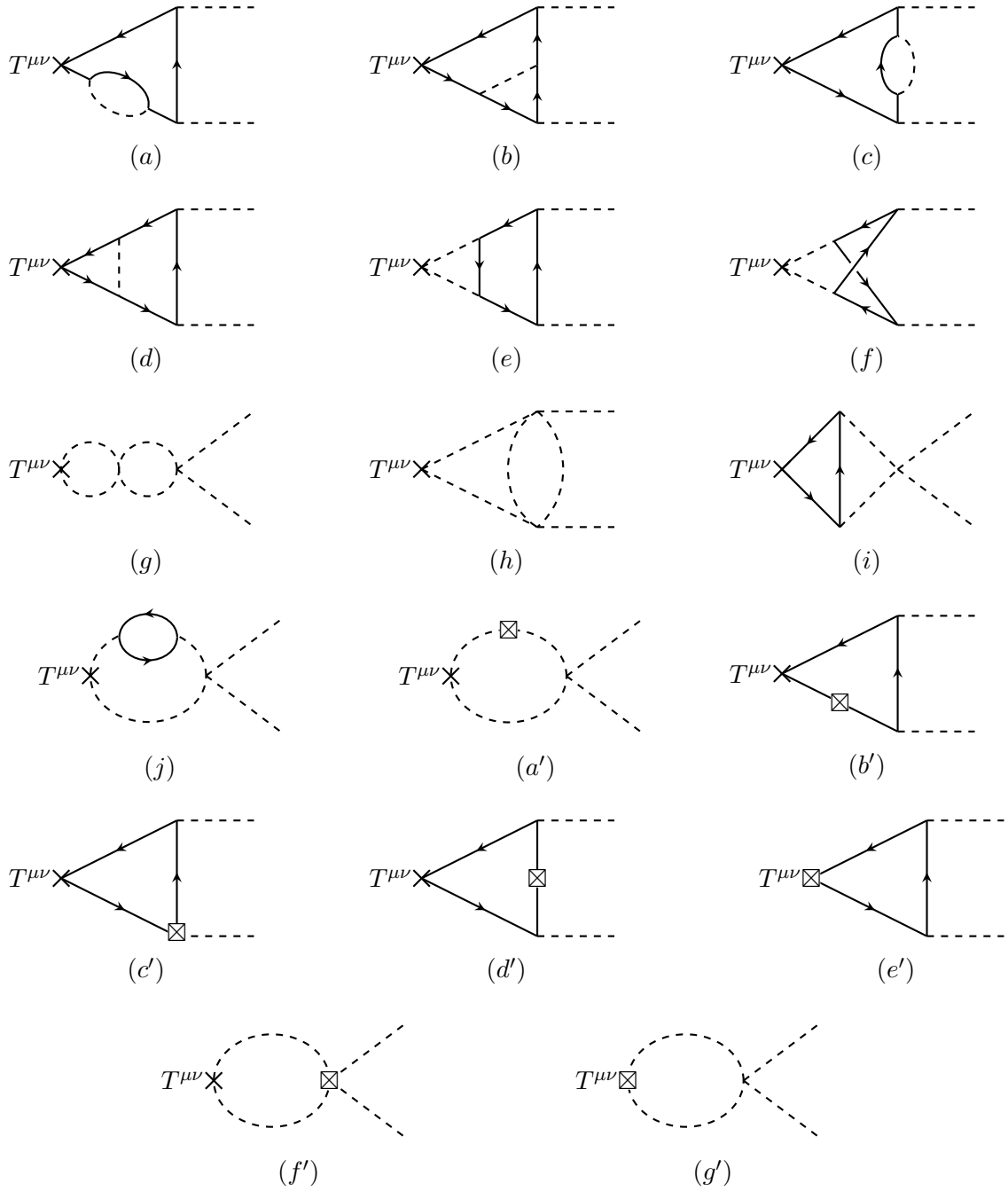
Figure 20.2: (a)–(f) Two-loop Feynman diagrams, up to symmetry operations, entering the computation of the two-loop corrections to the form factor $T_{2,0}(1_\phi, 2_\phi)$. (a')–(g') At the same order in perturbation theory, there are several one-loop diagrams with insertions of one-loop counterterms, which are needed for the cancellation of non-local sub divergences. As mentioned above, the double cut of (a'), precisely cancels the divergence of the three-particle phase space integral associated to the triple cut of (a), and cutting on either side of the counterterm vertex gives the factor of 2 in Eq. (20.20).

Taking the derivative according to Eq. (7.12), with the three level scalings of the couplings with μ given by $n(\lambda) = 2n(y) = 2$, we again arrive at Eq. (20.25). Further, the higher pole terms satisfy Eq. (7.13), as can be easily checked by direct computation.

20.1.3 Cancellation of Real Radiation

As a final cross-check, we calculate the cancellation divergences in real emission diagrams against those of loop amplitude, given the results of the previous sections. The precise amplitudes feeding into the squared amplitudes are in general not particularly illuminating, so we will not present them here, using a more diagrammatic approach to present equations, but explicitly show details, whenever necessary.

Starting, once more, at the one-loop level we have the diagrammatic relation

$$\left| \sim\!\!\bigotimes\!\!\prec \right|^2 \supset \sim\!\!\bigcirc\!\!=\!\!\bigcirc\!\!\sim + 2\,\mathrm{Re}\left(\sim\!\!\bigcirc\!\!=\!\!\bigcirc\!\!\sim \right) \overset{!}{=} \text{finite}. \tag{20.30}$$

Here, the textured ellipse on the left-hand side represents the all-order amplitude, while the number of inserted circles has the same meaning as before. Note, again, that the above equation implies the usage of UV renormalized amplitudes. But because the tree amplitude does not depend on any coupling (except for the gravitational coupling, but since all loop-amplitudes are of the same order in that coupling there is no need for renormalizing it), it is the same as the bare amplitude at this coupling order. However, since we are also interested in the two-loop expressions, we need to use the renormalized coupling in both the three- and two-particle cuts because the one-loop piece of the coupling in these cuts will contribute at the two-loop order.

The second term, being only a two-particle cut, on the right-hand side, is trivial to calculate, as explained in Chapter 18. Further, because the two-particle phase space is finite and we are interested only in the cancellation of the divergent terms, it suffices to use

$$\sim\!\!\bigcirc\!\!\prec = \left(\frac{1}{2\epsilon}\gamma_{\mathrm{IR}}^{(\phi,1)} + \mathcal{O}(\epsilon^0) \right) \times \sim\!\!\bigcirc\!\!\prec . \tag{20.31}$$

The three-particle cut, on the other hand, has to be integrated using Eq. (18.4) and the accompanying variable substitutions, which can be done in a straightforward fashion using computer algebra programs. In total, adding the two contributions and including symmetry factors wherever needed, we find that

$$\sim\!\!\bigcirc\!\!=\!\!\bigcirc\!\!\sim + 2\,\mathrm{Re}\left(\sim\!\!\bigcirc\!\!=\!\!\bigcirc\!\!\sim \right) = \frac{(P^2)^2}{96\pi^3\epsilon}\left(\gamma_{\mathrm{IR}}^{(\phi,1)} - \frac{y^2}{4\pi^2} \right), \tag{20.32}$$

with P the graviton momentum. This exactly vanishes after using the result in Eq. (20.6), providing an additional cross-check.

As expected, this calculation provides many insights concerning the structure of the infrared divergences. First, there find only a single pole in the individual contributions, showing once more the absence of divergences from soft divergences. Further, it explains, why the collinear anomalous dimension at this loop order is numerically the same as twice the field anomalous dimension. Performing the three-particle phase space integration diagram by diagram, we see that the only source of divergences are diagrams of the form shown in Fig. 20.3.
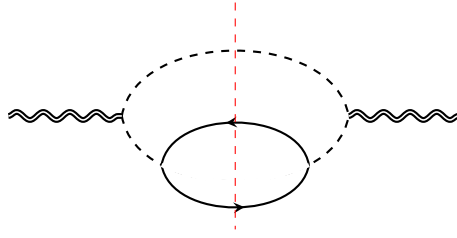
Figure 20.3: The only source of divergences from real radiation off the scalar legs.

This has a one-loop subdiagram with exactly the same form as the one-loop renormalization of the scalar field, so naturally the divergences look the same. Further, because the subdiagram can be inserted into either of the two scalars, we, in fact, get twice the divergence of a single scalar. Any diagram where the two fermions do not close onto the same scalar propagator is finite, just as in the on-shell calculation of the anomalous dimension, where very similar three-particle cuts appeared.

This seemingly straightforward calculation gets much more involved at the two-loop level. At this order, we have

$$
\left| \begin{array}{c}\includegraphics\end{array} \right|^2 \supset \begin{array}{c}\includegraphics\end{array} + 2\,\mathrm{Re}\left(\begin{array}{c}\includegraphics\end{array} \right)
$$
$$
+ \left| \begin{array}{c}\includegraphics\end{array} \right| + 2\,\mathrm{Re}\left(\begin{array}{c}\includegraphics\end{array} \right) \overset{!}{=} \text{finite.}
$$
(20.33)

Here we left implicit the contribution from the renormalized coupling in the three-particle cut between tree level amplitudes mentioned above. All these terms can be calculated using the results presented in Chapter 18. However, we will focus only on contributions generated by the scalar quartic coupling for simplicity. In this case, all three-particle phase space integrals vanish, as there are simply no amplitudes with an odd number of external states at this coupling order. Further, as we have seen before, also the one-loop amplitude for two scalars coupling to the graviton receives no contribution from the quartic coupling[3] This leaves only the four-particle phase space integral and the two-particle phase space containing the two-loop, two-scalar amplitude as the non-vanishing terms. We will focus on the former because we already calculated the latter in the previous section, and the calculation shows a few computational novelties.

As a first, naive try, we could use Eq. (18.5) and evaluate the phase-space integral in a rather brute-force way. While this works for the three-particle phase space because the integrands can factorize in the integration variables, this is highly non-trivial here because of the factor $\sqrt{\Delta}$ in the denominator. Instead, we will make use of the fact that a phase space integral can be seen as an on-shell cut of some higher loop integral. To explicitly see this, we can write [285]

$$
\int \mathrm{dLIPS}_4^{(D)} = \int \prod_k^4 \frac{dp_k}{(2\pi)^D} \frac{i}{D_k} (2\pi)^D \delta^D(P - p_1 - p_2 - p_3 - p_4),
$$
(20.34)

where the cut propagators are given as a difference of Feynman propagators with the opposite prescription for their imaginary part [271]

---

[3]Technically, we saw that the amplitude projected onto the $J = 2$ form factor vanishes in the absence of the Yukawa coupling. However, due to the traceless character of the graviton, convoluting the two two-point amplitudes and summing over the graviton polarizations is equivalent to projecting onto the traceless component.

$$\frac{1}{D_k} = 2\pi i \delta^+(p_k^2) = \frac{1}{p_k^2 + i\varepsilon} - \frac{1}{p_k^2 - i\varepsilon}. \tag{20.35}$$

Then, the phase-space integral is nothing more than a linear combination of the same loop integral, where the terms just differ by the imaginary parts of the individual propagators. But the Integration-by-Parts (IBP) identities presented in App. IV.B rely only on total derivatives of the integrands, so they do not depend on the prescription for the imaginary part. Hence, the application of the IBP identities commutes with cutting the loop integral [286]. In other words, in practice we can interpret the cut-propagators in Eq. (20.34) as actual Feynman propagators, reduce the loop integral to some set of easier to calculate (or already known) master integrals and finally perform the appropriate cuts on these master integrals. In the present case, we are interested in the four-particle cuts of three-loop self-energy diagrams. The corresponding master integrals are known to a sufficiently high order in ϵ [299,300]. In fact, of the six master integrals only three exhibit a four-particle cut, all of which were calculated in [285].

For the two-loop contribution generated by the scalar quartic coupling it turns out that only the two planar master integrals in [285] are needed and we find

$$\text{} = \lambda^2 \left[\frac{\epsilon(\epsilon+1)}{12(6\epsilon^2 - 13\epsilon + 6)} I_6 + \frac{18 - 33\epsilon + \mathcal{O}(\epsilon^2)}{36\epsilon(2\epsilon - 3)(2\epsilon - 1)(3\epsilon - 2)} I_4 \right] \Big|_{\text{4-cut}}, \tag{20.36}$$

where the master integrals are

$$\text{} \equiv I_4, \qquad \text{} \equiv I_6. \tag{20.37}$$

Because the four-particle cuts of both these master integrals are finite, we can also ignore the term proportional to I_6, as we are interested only in the divergent parts of the integral. Using the cut of I_4, which is nothing else than the volume of the four particle phase space, and adding the two-loop amplitude, we find

$$\text{} + 2\,\text{Re}\left(\text{} \right) = \frac{(P^2)^2}{192\pi\epsilon} \left(\gamma_{\text{IR},\lambda^2}^{(\phi,2)} - \frac{\lambda^2}{1536\pi^4} \right), \tag{20.38}$$

which exactly vanishes if we use the corresponding part of the anomalous dimension in Eq. (20.25), confirming our result obtained using the form factor of the energy-momentum tensor.

To conclude this section, we note that using this approach to calculating the infrared divergences makes it obvious that there are no contribution containing both the Yukawa and the quartic coupling because there are simply no amplitudes with additional external states at this coupling order, which can glue together in the phase-space integral.

20.2 Fermion Fields

20.2.1 Using the energy-momentum tensor

Let us continue with the fermion fields. The main difference compared to the scalar case is the projection we apply to the energy-momentum form factor because the external states now

carry helicity different from one. In this section, we will focus only on the case of left-handed fermion and its anti-particle in the final states, such that we need to consider $T_{2,-1}(1_{\psi_L}, 2_{\bar{\psi}_L})$. The results presented in this section are equally valid for the right-handed fermion if we use $T_{2,1}(1_{\psi_R}, 2_{\bar{\psi}_R})$ instead.

While the details of the computation, apart from the different projection needed, are of course different compared to the previous section, due to the different choice of external state, there are no additional conceptual complications. Thus, in this section we provide mostly the results without discussing them too much.

Starting again at the one-loop level, both the fermion and the scalar contribute in the cut and we find

$$T_{\mu\nu} \times \quad = \frac{y^2}{16\pi} T_{2,-1}^{(0)}(1_{\psi_L}, 2_{\bar{\psi}_L}), \tag{20.39}$$

directly giving

$$\gamma_{\text{IR}}^{(1)} = \frac{y^2}{16\pi^2}. \tag{20.40}$$

Again, this coincides with twice the one-loop field anomalous dimension. It being finite means that for the fermion, the correction term in Eq. (17.25) vanishes as well.

As for the scalar, also the two-particle cuts for the fermionic form factor pose no difficulties whatsoever, and can easily be integrated using the phase space parameterization from the previous sections. We find

$$T_{\mu\nu} \times \quad + \quad T_{\mu\nu} \times \quad = \frac{y^4}{1024\pi^3} \left[6 \log\left(\frac{s_{12}}{\mu^2}\right) - 51 \right] T_{2,-1}^{(0)}(1_{\psi_L}, 2_{\bar{\psi}_L}), \tag{20.41}$$

As for the scalar, the three-particle cuts can be separated into the same three categories, and we can use the same methods as described in the last section, such that we will just quote the sum of all cuts as

$$\sum_X \int \left[\text{dLIPS}_2 \left(T_{2,0}^{(0)} \mathcal{A}^{(1)*} + T_{2,0}^{(1)} \mathcal{A}^{(0)} \right) + \text{dLIPS}_3 \, T_{2,0}^{(0)} \mathcal{A}^{(0)} \right]$$
$$= \frac{y^4}{512\pi^3} \left[15 \log\left(\frac{s_{12}}{\mu^2}\right) - \frac{6}{\epsilon} - \frac{289}{6} \right] T_{2,-1}^{(0)}(1_{\psi_L}, 2_{\bar{\psi}_L}). \tag{20.42}$$

Once again, we find a divergent result. The resolution comes, once more, in the form of the one-loop propagator renormalization we did not include so far and which gets cut in the three-particle cuts. However, it turns out, that for the fermion form factor, not only the fermion renormalization, but also the scalar one contributes such that we have to add cuts of the form

$$\sum_{i=\psi_L, \psi_R, \phi} \delta_i \int \text{dLIPS}_2^{(D)} T_{2,-1}^{(0)}(1_i', 2_{\bar{i}}') \mathcal{A}^{(0)}(-2_i', -1_i', 1_{\psi_L}, 2_{\bar{\psi}_L}). \tag{20.43}$$

Including this contribution, we arrive at the final, finite expression for the sum of all cuts,

$$\sum_X \int \left[\text{dLIPS}_2 \left(T_{2,0}^{(0)} \mathcal{A}^{(1)*} + T_{2,0}^{(1)} \mathcal{A}^{(0)} \right) + \text{dLIPS}_3 \, T_{2,0}^{(0)} \mathcal{A}^{(0)} \right]$$
$$= \frac{y^4}{512\pi^3} \left[9 \log\left(\frac{s_{12}}{\mu^2}\right) - \frac{67}{2} \right] T_{2,-1}^{(0)}(1_{\psi_L}, 2_{\bar{\psi}_L}), \tag{20.44}$$

195

which we can use to calculate the IR anomalous dimension.

Because we need its explicit expression, we quote the full one-loop form factor

$$T_{2,-1}^{(1)}(1_{\psi_L}, 2_{\bar{\psi}_L}) = -\frac{y^2}{32\pi^2}\left[\log\left(\frac{s_{12}}{\mu^2}\right) - \frac{3}{2} - i\pi\right]T_{2,-1}^{(0)}(1_{\psi_L}, 2_{\bar{\psi}_L}). \tag{20.45}$$

Then, the terms containing only one-loop objects in the RGE give

$$\left(\gamma^{(1)} + \beta^{(1)}\partial\right)T_{2,-1}^{(1)} + \frac{i\pi}{2}\left(\gamma^{(1)} + \beta^{(1)}\partial\right)^2 T_{2,-1}^{(0)} = -\frac{y^4}{512\pi^4}\left[9\log\left(\frac{s_{12}}{\mu^2}\right) + \frac{27}{2}\right]T_{2,-1}^{(0)}. \tag{20.46}$$

Comparing to our results for the cuts, we see that all logarithms cancel, keeping in mind the extra factor of $-1/\pi$, confirming, that there are no soft divergences in a Yukawa theory, while for the two-loop collinear divergence of the fermion we find

$$\gamma_{\text{IR}} = -\frac{13y^4}{1024\pi^4}. \tag{20.47}$$

Notice that, as in the scalar case, this coincides with twice the field anomalous dimension [295]. To verify this result, we calculate the full two-loop form factor using the same method as for the scalar case for the diagrams shown in Fig. 20.4. The main difference is that after the integral reduction, only the planar integrals in Eq. (20.26) appear. The full result reads

$$\begin{aligned} T_{2,-1}(1_{\psi_L}, 2_{\bar{\psi}_L}) = T_{2,-1}^{(0)}(1_{\psi_L}, 2_{\bar{\psi}_L})\Bigg\{&1 + \delta^{(1)} + \delta^{(2)} + \frac{1}{2}\left(\frac{y}{4\pi}\right)^2\left[\frac{1}{\epsilon} - \log\left(-\frac{s_{12}}{\mu^2}\right) + 3\right] \\ &+ \left(\frac{y}{8\pi}\right)^4\left[\frac{18}{\epsilon^2} - \frac{13}{\epsilon} - 18\log^2\left(-\frac{s_{12}}{\mu^2}\right) + 134\log\left(-\frac{s_{12}}{\mu^2}\right) - \frac{519}{2} - 6\pi^2\right] + \dots\Bigg\}, \end{aligned} \tag{20.48}$$

Taking the imaginary part of this expression, we find

$$2\text{Im}\left[T_{2,0}(1_\phi, 2_\phi)\right] = \frac{y^4}{512\pi^3}\left[9\log\left(\frac{s_{12}}{\mu^2}\right) - \frac{67}{2}\right]T_{2,-1}^{(0)}(1_{\psi_L}, 2_{\bar{\psi}_L}), \tag{20.49}$$

which agrees perfectly with Eq. (20.44), therefore giving the same anomalous dimension.

Finally, let us briefly extract the renormalization constant for this form factor and we find

$$Z_G = \left(1 + \delta^{(1)} + \delta^{(2)}\right)^{-1} = \left[1 + \left(\frac{y}{4\pi}\right)^2\frac{1}{2\epsilon} + \left(\frac{y}{8\pi}\right)^4\left(\frac{22}{\epsilon^2} - \frac{13}{\epsilon}\right)\right]. \tag{20.50}$$

Using Eq. (7.12) once more, we recover both the one- and two-loop anomalous dimensions from above from the single pole terms, while the double pole term satisfies Eq. (7.13).

20.2.2 Using the charge current

Because the fermions are complex fields, there is yet another, non-trivial, cross-check we can perform. If we assign the fermions some auxiliary U(1) charge, there is one more conserved current next to the energy-momentum tensor, namely the vector charge current,

$$j_i^\mu = \bar{\psi}_i\gamma^\mu\psi_i. \tag{20.51}$$

As discussed in Sec. 3.2, this current, being conserved, has no suitable counterterm, provided there is no associated propagating gauge boson. This means that for Green's functions with an insertion of this current, we have $\Delta\gamma = -\gamma_{\text{IR}}$ and because the IR effects are universal for a
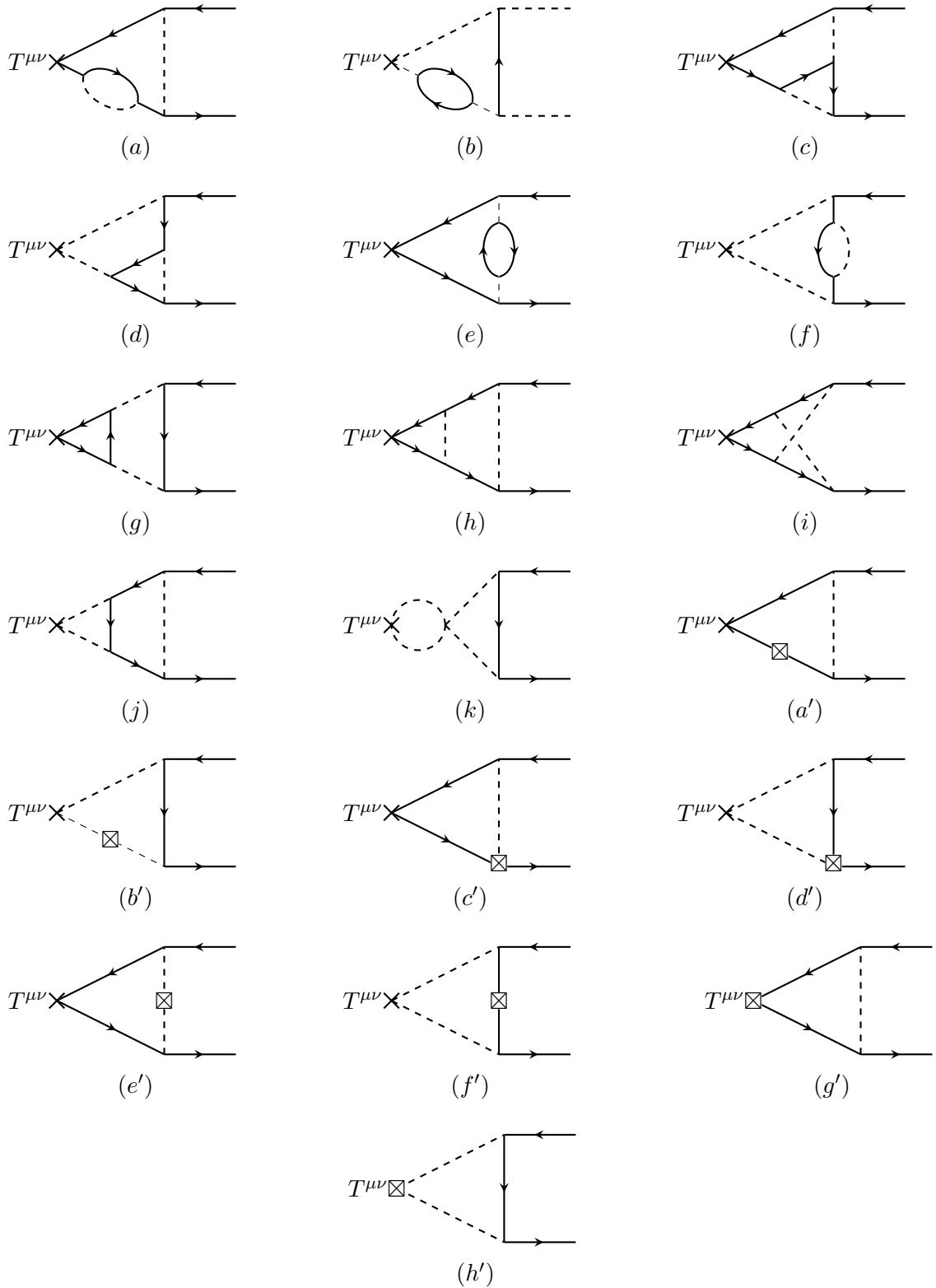
Figure 20.4: Two-loop Feynman diagrams and associated one-loop counterterm diagrams, up to symmetry operations, entering the computation of the two-loop corrections to the form factor $T_{2,-1}(1_{\psi_L}, 2_{\bar{\psi}_L})$. The diagrams needed for the two-loop form factor $j^\mu(1_{\psi_L}, 2_{\bar{\psi}_L})$ are the same after dropping all diagrams with operator insertions on a scalar leg.

197

given set of external states, we should be able to reproduce the results obtained in the previous section.

As for the energy-momentum tensor, it is convenient to perform a projection to remove all open indices. In general, we know that

$$j_\mu(1_{\psi_L}, 2_{\bar\psi_L}) = \bar v(p_2)\mathcal{F}_\mu P_L u(p_1) = F_L(s_{12})\bar v(p_2)\gamma^\mu P_L u(p_1), \tag{20.52}$$

where we used a notation similar to the previous sections to denote the Green's functions of the charge current. To extract the scalar form factor, we perform the projection as

$$F_L(s_{12}) = \frac{4}{(D-2)s_{12}^2}\mathrm{Tr}\left[\gamma^\mu \slashed{p}_2 \mathcal{F}_\mu P_L \slashed{p}_1\right], \tag{20.53}$$

and equivalently for the right-handed fermion.

While it is of course possible to perform the calculation using on-shell methods with no further complications compared to the case of the energy-momentum tensor, we choose to present only the Feynman diagrammatic calculation. The necessary diagrams are equivalent to those in Fig. 20.4, after replacing the energy-momentum tensor with the charge current and dropping all diagrams where the scalar couples directly to the current.

Following all the steps described in the previous sections, we find, up to two loops,

$$
\begin{aligned}
F_L(1_{\psi_L}, 2_{\bar\psi_L}) = F_L^{(0)}(1_{\psi_L}, 2_{\bar\psi_L})\Bigg\{ &1 + \delta^{(1)} + \delta^{(2)} + \frac12\left(\frac{y}{4\pi}\right)^2\left[\frac1\epsilon - \log\left(-\frac{s_{12}}{\mu^2}\right) + 1\right] \\
&+ \left(\frac{y}{8\pi}\right)^4\left[\frac{18}{\epsilon^2} - \frac{13}{\epsilon} - 18\log^2\left(-\frac{s_{12}}{\mu^2}\right) + 62\log\left(-\frac{s_{12}}{\mu^2}\right) - \frac{31}{2} - 6\pi^2\right] + \dots\Bigg\}.
\end{aligned} \tag{20.54}
$$

Notice the identical divergences as in Eq. (20.48), which directly leads to the same anomalous dimension using its definition Eq. (7.7), as it should be. In fact, while the single logarithmic term differs from that in Eq. (20.48)[4], the difference is such that it compensates for the different rational part in the one-loop expression if we chose to use the RGE in terms of the imaginary part or the on-shell cuts, respectively.

At this point, one might ask why we used the energy-momentum tensor to calculate the anomalous dimension instead of the vector current. Indeed, using the latter was computationally easier due to the reduced number of diagrams as well as the much simpler vertex rule for the current itself. However, usage of the current is limited to only external states that transform non-trivially under the global symmetry, in this case only the fermions. The energy-momentum tensor, on the other hand, covers every propagating degree of freedom, i.e., even those transforming trivially under every internal symmetry of the theory, in this case the scalar field. Further, we can only use the vector current to easily extract the IR anomalous dimension if the associated symmetry is a global one or, equivalently, the corresponding gauge boson is not allowed to propagate in the loops. Otherwise, we can find an identically conserved operator as a counterterm [293], such that the UV anomalous dimension is non-vanishing, making it necessary to disentangle UV and IR dynamics. In the end, for a local symmetry, the vector current cannot straightforwardly be used to extract contributions to the IR anomalous dimension proportional to the accompanying gauge coupling. However, these can be obtained using the energy-momentum tensor, provided we focus only on marginal couplings, as explained in Sec. 3.2. We will come back to these points in the next section, when considering a theory with multiple gauge symmetries.

---

[4]The coefficient of the double logarithmic term has to be the same, as it is fixed, through the RGE, in terms of the one-loop logarithm, which has to be the same as for the one-loop energy-momentum tensor because of the universality of the IR anomalous dimension.

Chapter 21

Infrared Divergences in an SM Toy Model

In the last chapter, we presented a detailed discussion of the main techniques necessary to calculate two-loop infrared anomalous dimensions in a simple toy model, which exhibits no soft divergences.

In this section, we will change gear and turn to a more realistic toy model of the Standard Model with multiple gauge groups. In this theory, soft divergences are expected to arise, which manifest themselves as non-local poles, even after removing subdivergences. In this chapter, we present only the Feynman diagrammatic calculation and discuss the subtleties arising from soft divergences. The calculation using purely on-shell methods is left for future work.

The theory we want to investigate has a $\mathrm{SU}(N_1) \times \mathrm{SU}(N_2) \times \mathrm{U}(1)_Y$ gauge symmetry and we will present all results for general N_1 and N_2, each group with its associated gauge boson, G, W and B. To make contact with the SM we can obviously just take $N_1 = 3$ and $N_2 = 2$. For the matter content, we have one complex scalar H, akin to the Higgs field, transforming as a $(\mathbf{1}, \mathbf{N_2})_{Y_H}$[1], a left-handed fermion ψ_L transforming as a $(\mathbf{N_1}, \mathbf{N_2})_{Y_L}$ and a right-handed fermion ψ_R, transforming as $(\mathbf{1}, \mathbf{N_2})_{Y_R}$. Using the Feynman diagrammatic approach, we also need to define a gauge fixing procedure and we use the well-known R_ξ gauge fixing with $\xi = 1$ for both non-Abelian gauge groups, also known as Feynman gauge. Of course, this introduces ghost fields, c_G and c_W, which transform in the adjoint representation under the group they are associated with and as singlets under the others. Including all possible marginal interactions between these fields, the theory can be summarized using the following Lagrangian

$$
\begin{aligned}
\mathcal{L} = & -\frac{1}{4} G^{A\mu\nu} G^A_{\mu\nu} - \frac{1}{4} W^{I\mu\nu} W^I_{\mu\nu} - \frac{1}{4} B^{\mu\nu} B_{\mu\nu} \\
& -\frac{1}{2}(\partial_\mu G^{A\mu})^2 - \frac{1}{2}(\partial_\mu W^{A\mu})^2 + (\partial_\mu \bar{c}_G)(D^\mu c_G) + (\partial_\mu \bar{c}_W)(D^\mu c_W) \\
& + (D_\mu H)^\dagger (D^\mu H) - i\bar{\psi}_L \slashed{D}\psi_L - i\bar{\psi}_R \slashed{D}\psi_R \\
& + y\bar{\psi}_L \psi_R H + y\bar{\psi}_R \psi_L H^\dagger - \frac{\lambda}{2}|H|^4,
\end{aligned}
\tag{21.1}
$$

where we defined the the covariant derivative to be of the form

$$
D_\mu \phi = \partial_\mu \phi - ig A^a T^a \phi,
\tag{21.2}
$$

---

[1]We denote the representation of the fields under the $\mathrm{SU}(N_1) \times \mathrm{SU}(N_2) \times \mathrm{U}(1)_Y$ group as $(R_{N_1}(\Phi), (R_{N_2}(\Phi))_Y$, where the subscript indicates the charge under the Abelian group.

and contractions of fundamental group indices are left implicit. Emulating the SM notations we use g_s, g_w and g_1 as names for the gauge couplings of the SU(N_1), SU(N_2) and U(1)$_Y$ groups, respectively

Note that here we did not include any explicit coupling to gravity, including the conformal coupling of the scalar field. In fact, when calculating the anomalous dimension of the scalar field by using the $J = 2$ projector defined in the previous chapter, we do so once without and once with the additional conformal coupling term, finding perfect agreement which serves as one non-trivial cross-check of the method.

Further, due to the many symmetries of this theory, there are, apart from the energy-momentum tensor, up to three conserved currents available for each of the matter fields, which we can use to cross-check at least partial results. In addition, since the symmetries are gauged, contrary to the charge symmetry from the last chapter, we can use our results of the infrared anomalous dimension to obtain the UV renormalization of all the currents, by computing the necessary counterterms. We will come back to this towards the end of this chapter.

Because we need them for the coupling renormalization, as well as the explicit computation of the anomalous dimension, we collect the D-dimensional beta functions of all the appearing couplings at this point:

$$\frac{\beta_{g_s}}{16\pi^2} = \frac{g_s^3}{3\pi^2}\left(C_{A,2} + 1 - 11C_{A,1}\right)$$

$$\frac{\beta_{g_w}}{16\pi^2} = \frac{g_w^3}{3}\left(C_{A,1} + \frac{1}{2} - 11C_{A,2}\right)$$

$$\frac{\beta_{g_1}}{16\pi^2} = \frac{g_1^3}{3}\left(2C_{A,1}C_{A,2}Y_L^2 + 2C_{A,1}Y_R^2 + C_{A,2}Y_H^2\right)$$

$$\frac{\beta_y}{16\pi^2} = \frac{y^3}{2}(C_{A,2} + 1 + 2C_{A_1}) - 3C_{F,2}g_w^2 y - 6C_{F,1}g_s^2 y - 3(Y_L^2 + Y_R^2)g_1^2 y$$

$$\frac{\beta_\lambda}{16\pi^2} = 2\lambda^2(C_{A,2} + 4) + 4C_{A,1}y^2\lambda - 12Y_H^2 g_1^2\lambda - 12C_{F,2}g_w^2\lambda$$

$$-4C_{A,1}y^4 + 12Y_H^2 g_1^4 + 12Y_H^2 g_1^2 g_w^2(1 - C_{A,2} + 2C_{F,2})$$

$$+3C_{F,2}g_w^4(C_{A,2}^2 + 5C_{A,2} - 13C_{F,2} - 4),$$

(21.3)

where subscripts denote the quadratic Casimirs in either the adjoint or fundamental representation for both the non-Abelian gauge groups. These beta functions were obtained from the respective coupling counterterms, the two of which are related as

$$\delta_i = \frac{\beta_i}{16\pi^2}\frac{1}{2\epsilon}.$$

(21.4)

We start this chapter by presenting the calculation of infrared anomalous dimensions of all the fields in the theory, using the two-loop energy-momentum tensor on-shell Green's functions. We use the same projection technique from the last chapter, but we expand on it to also remove all appearing gauge indices, such that the resulting form factor function does not carry any indices at all.

21.1 Two-loop Energy-Momentum Tensor

21.1.1 Gluon External States

We start by calculating the anomalous dimension of the "gluon" of the theory, that is, the $SU(N_1)$ gauge boson. Because it is not coupled to the scalar, we can cross-check a large part of the results with the literature on infrared divergences in QCD (see, e.g., [301, 302]). As discussed in 16, we can avoid using explicit counterterm diagrams by performing the UV and IR renormalization of any amplitude or form factor following Eq. (16.4). The crucial point is that for the last term in this equation to give finite contributions, it does not suffice to expand the one-loop amplitude only up to $\mathcal{O}(\epsilon^0)$. Instead, because it is multiplied by a divergent counterterm, we have to compute the higher-order terms such that it is possible to cancel the highest order pole in the counterterm, which, at one loop and in the presence of soft divergences, are of order $\mathcal{O}(\epsilon^2)$. Fortunately, we consider only three-point functions, hence only the scalar massless bubble and triangle master integrals are needed, which are known to all orders in ϵ

$$
\begin{aligned}
B_0(p^2) &= -\frac{(4\pi)^{\epsilon-2}}{\epsilon(2\epsilon-1)} \frac{\Gamma(1-\epsilon)^2\Gamma(\epsilon+1)}{\Gamma(1-2\epsilon)}(-p^2)^{-\epsilon}, \\
C_0(p^2) &= -\frac{2(4\pi)^{\epsilon-2}}{\epsilon}(2\epsilon-3)(2\epsilon-1)\frac{\Gamma(2-\epsilon)\Gamma(\epsilon+1)\Gamma(-\epsilon)}{\Gamma(4-2\epsilon)}(-p^2)^{-\epsilon-1}.
\end{aligned}
\tag{21.5}
$$

While the higher-order terms of the one-loop form factors are needed for the two-loop renormalization, they are not particularly illuminating. Hence, we will not present them at this point. Instead, we quote only terms up to order $\mathcal{O}(\epsilon^0)$ at this point and show the full form factor in terms of the one-loop master integrals in App. IV.A.

In the following we always normalize by the tree level form factor which, after contracting color indices, reads

$$
T_G^{(0)}(s_{12}) = 2C_{A,1}C_{F,1}.
\tag{21.6}
$$

Here we opted for a slightly decluttered notation for the form factor compared to the last chapter. While the superscript denotes the loop order, as usual, the subscript simply shows the chosen external states. Because in this chapter we only project onto the traceless component, matching this notation to the last chapter is unambiguous.

Then, up to one loop and up to $\mathcal{O}(\epsilon^{-1})$, we find for the renormalized form factor

$$
T_G^{(1)}(s_{12}) = \frac{1}{Z_{\mathrm{IR}}^G}\left\{1 + \left(-\frac{s_{12}}{\mu^2}\right)^{-\epsilon}\left(\frac{g_s}{4\pi}\right)^2\left[-\frac{2C_{A,1}}{\epsilon^2} + \frac{\beta_{g_s}}{g_s^3\epsilon} + \mathcal{O}(\epsilon^0)\right]\right\}
\tag{21.7}
$$

with the infrared renormalization constant of the gluon pair, Z_{IR}^G, yet to be specified. We chose to factor out the dependence on the kinematic variable to write the result in a more compact way. Because of this, the relevant information necessary for the one-loop anomalous dimension is contained entirely in the divergent terms, which generate logarithmic terms upon expanding the prefactor in ϵ.

Because the tree-level form factor does not depend on any couplings, this one-loop form factor is already free of UV divergences. However, the double pole generates non-local divergences of the form $\log/\epsilon$, contrary to the last chapter, where no higher order poles were present at this loop order. This is a direct consequence of non-zero soft divergences, which, as we will see shortly, also manifest themselves as logarithmic terms in the anomalous dimension.

We will, as discussed before, extract the anomalous dimension from both the divergent structure as well as the imaginary part using the RGE and optical theorem.

Starting with the former and requiring the finiteness of Eq. (16.4) at this loop order, we can easily solve for Z_{IR}^G, and we get

$$Z_{\text{IR}}^G = 1 - \left(\frac{g_s}{4\pi}\right)^2 \left[\frac{2C_{A,1}}{\epsilon^2} - \frac{\beta_{g_s}}{g_s^3\epsilon} - \frac{2C_{A,1}}{\epsilon}\log\left(-\frac{s_{12}}{\mu^2}\right)\right]. \tag{21.8}$$

With this, we can use its definition in terms of the renormalization constant Eq. (7.7) to easily calculate the anomalous dimension. Keeping in mind, that now Z_{IR} does not only implicitly depend on the renormalization scale through the couplings but also explicitly through the logarithm in the last term, we find

$$\gamma_{\text{IR}}^G = \left(\frac{g_s}{4\pi}\right)^2 \left[\frac{2\beta_{g_s}}{g_s^3} + 4C_{A_1}\log\left(-\frac{s_{12}}{\mu^2}\right)\right]. \tag{21.9}$$

Note that, while not constant, this is finite because the explicit dependence in the logarithmic term cancels the implicit one in the higher pole term.

Alternatively, following Eq. (17.22), we can immediately read of the (real part of the) anomalous dimension from the imaginary part of Eq. (21.7) (recall, that the tree level form factor is independent of any coupling, so the beta function term vanishes), which reads

$$\text{Im}\left[T_G^{(1)}(s_{12})\right] = -\frac{\pi}{2}\left(\frac{g_s}{4\pi}\right)^2 \left[-\frac{2\beta_{g_s}}{g_s^3} - 4C_{A_1}\log\left(\frac{s_{12}}{\mu^2}\right)\right]. \tag{21.10}$$

Multiplying this expression with the appropriate factor of $-2/\pi$ immediately gives the same result as in Eq. (21.9). Before comparing this result with the literature, we will first continue with the two-loop order. Up to the two-loop order, we find

$$T_G^{(2)}(s_{12}) = \frac{1}{Z_{\text{IR}}^G}\left\{(1 + 2\delta_{g_s})T_G^{(1)}(s_{12}) + \left(-\frac{s_{12}}{\mu^2}\right)^{-2\epsilon} t_2^G\right\}, \tag{21.11}$$

where we defined

$$\begin{aligned}
t_2^G &= \left(\frac{g_s}{4\pi}\right)^4 \left[\frac{2C_{A,1}^2}{\epsilon^4} - \frac{3C_{A,1}\beta_{g_s}}{2g_s\epsilon^3} - \frac{10C_{A,1}(C_{A,2}+1) + (\pi^2 - 113)C_{A,1}^2}{6\epsilon^2}\right.\\
&\quad + \frac{C_{A,1}\left((\pi^2 - 115)(C_{A,2}+1) - C_{A,1}(300\zeta(3) + 11\pi^2 - 1370)\right)}{36\epsilon}\\
&\quad \left. + \frac{C_{A_1}C_{F,1}(C_{A,2}+1)}{2\epsilon}\right]\\
&\quad + \left(\frac{g_s g_w}{16\pi^2}\right)^2 \frac{C_{A,2}C_{F,2}}{2\epsilon} + \left(\frac{g_s g_1}{16\pi^2}\right)^2 \frac{(C_{A,2}Y_L^2 + Y_R^2)}{2\epsilon} - \left(\frac{g_s y}{16\pi^2}\right)^2 \frac{C_{A,2}}{2\epsilon},,
\end{aligned} \tag{21.12}$$

In these expressions, the effects of the one-loop renormalized couplings are captured by δ_{g_s}, while t_2^G contains all the genuine two-loop contributions. As before, we factored the kinematic dependence and show only the divergent terms. Again, we can obtain Z_{IR}^G by requiring finiteness. Here, instead of presenting Z_{IR}^G itself, we will show its logarithm, as it exhibits a few interesting properties. We find

$$\log\left(Z_{\text{IR}}^G\right) = -\left(\frac{g_s}{4\pi}\right)^2 \left[\frac{2C_{A,1}}{\epsilon^2} - \frac{\beta_{g_s}}{g_s^3\epsilon} - \frac{2C_{A,1}}{\epsilon}\log\left(-\frac{s_{12}}{\mu^2}\right)\right]$$

$$+ \left(\frac{g_s}{4\pi}\right)^4 \left[-\frac{3C_{A,1}\beta_{g_s}}{2g_s^3\epsilon^3} \right.$$

$$+ \frac{\left(C_{A,2}^2 + C_{A,2}(2 - 17C_{A,1}) + 3\left(18 + \pi^2\right)C_{A,1}^2 - 17C_{A,1} + 1\right)}{18\epsilon^2}$$

$$- \frac{\left(3\pi^2 - 128\right)(C_{A,2} + 1)C_{A,1} - 54(C_{A,2} + 1)C_{F,1}}{108\epsilon} \tag{21.13}$$

$$+ \frac{C_{A,1}^2\left(108\zeta(3) + 33\pi^2 - 1384\right)}{108\epsilon}$$

$$\left. + \log\left(-\frac{s_{12}}{\mu^2}\right)\left(\frac{C_{A,1}\beta_{g_s}}{\epsilon^2} - \frac{C_{A,1}\left(5C_{A,2} + \left(3\pi^2 - 67\right)C_{A,1} + 5\right)}{9\epsilon}\right) \right]$$

$$+ \left(\frac{g_s g_w}{16\pi^2}\right)^2 \frac{C_{A,2}C_{F,2}}{2\epsilon} + \left(\frac{g_s g_1}{16\pi^2}\right)^2 \frac{\left(C_{A,2}Y_L^2 + Y_R^2\right)}{2\epsilon} - \left(\frac{g_s y}{16\pi^2}\right)^2 \frac{C_{A,2}}{2\epsilon}.$$

There are a few things to notice here. While the highest pole in Eq. (21.12) is of order $\mathcal{O}(\epsilon^{-4})$, the highest pole in Eq. (21.13) is only of $\mathcal{O}(\epsilon^{-3})$, as it should be [301]. Further, while Z_{IR}^G contains higher powers of logarithms, these cancel in Eq. (21.13) such that the anomalous dimension can contain at most linear logarithms, in accordance with the general results [273,274]. Finally, we see that all cross terms containing two different couplings have only a single pole, as required by the finiteness of the anomalous dimension, which tells that the highest order poles have to be related to lower loop ones. But since only g_s terms appear at one-loop, all higher pole mixed terms have to vanish at two-loops.

Then, to get the anomalous dimension, we simply take the total derivative with respect to the renormalization scale of Eq. (21.13), yielding

$$\gamma_{\text{IR}}^G = -\left(\frac{g_s}{4\pi}\right)^2 \left[\frac{2\beta_{g_s}}{g_s^3} + 4C_{A_1}\log\left(-\frac{s_{12}}{\mu^2}\right)\right]$$

$$- \left(\frac{g_s}{4\pi}\right)^4 \left\{ C_{A,1}^2 \left[\frac{1384}{27} - 4\zeta(3) - \frac{11\pi^2}{9}\right] - 2C_{F,1}(C_{A,2} + 1) \right.$$

$$+ C_{A,1}(C_{A,2} + 1)\left[\frac{\pi^2}{9} - \frac{128}{27}\right] \tag{21.14}$$

$$\left. + \frac{1}{3}\log\left(-\frac{s_{12}}{\mu^2}\right)\left[C_{A,1}^2\left(4\pi^2 - \frac{268}{3}\right) + \frac{20C_{A,1}(C_{A,2} + 1)}{3}\right]\right\}$$

$$+ 2\left(\frac{g_s g_w}{16\pi^2}\right)^2 C_{A,2}C_{F,2} + 2\left(\frac{g_s g_1}{16\pi^2}\right)^2\left(C_{A,2}Y_L^2 + Y_R^2\right) - 2\left(\frac{g_s y}{16\pi^2}\right)^2 C_{A,2}.$$

As it should be, this result is finite and contains at most linear logarithms, providing an excellent consistency check.

Of course, as required by the optical theorem, we can use the imaginary part of the renormalized two loop-form instead to arrive at the same result. We get

$$-\frac{2}{\pi}\text{Im}\left[T_G^{(2)}(s_{12})\right] = \left(\frac{g_s}{4\pi}\right)^4 \left\{ 4C_{A,1}^2 \log^3\left(-\frac{s_{12}}{\mu^2}\right) \right.$$

$$+ \frac{4}{3}\left[C_{A,1}(C_{A,2} + 1) - 22C_{A,1}C_{F,1} - 11\right]\log^2\left(-\frac{s_{12}}{\mu^2}\right)$$

$$+ \frac{1}{3}\left[C_{A,1}^2(46 - 10\pi^2) - 5C_{A,1}(C_{A,2} + 1)\right]\log\left(-\frac{s_{12}}{\mu^2}\right) \tag{21.15}$$

$$+ \frac{C_{A,1}^2}{27}\left(1384 - 108\zeta(3) + 99\pi^2\right) - 2C_{F,1}(C_{A,2} + 1)$$

$$- \frac{C_{A,1}(C_{A,1}+1)}{27} \left(128 + 9\pi^2\right) \Bigg\}$$
$$- 2\left(\frac{g_s g_w}{16\pi^2}\right)^2 C_{A,2}C_{F,2} - 2\left(\frac{g_s g_1}{16\pi^2}\right)^2 \left(C_{A,2}Y_L^2 + Y_R^2\right) + 2\left(\frac{g_s y}{16\pi^2}\right)^2 C_{A,2}.$$

Plugging this back into Eq. (17.25), we exactly recover the result in Eq. (21.14), as expected. At this point, we want to stress the importance of the last term on the left-hand side in Eq. (17.25). This term is crucial to get the correct terms with more powers of π^2, showing the need to appropriately include all higher derivative terms in the expansion of Eq. (17.16).

To conclude this section, we compare our result to the literature, see e.g., [273, 274, 301, 302]. To do so, we bring the anomalous dimension into the form [274]

$$\gamma_{\text{IR}} = \frac{1}{2} \log\left(-\frac{s_{12}}{\mu^2}\right) \sum_{i,j} \gamma_{\text{cusp}}^j C_i^j + \sum_i \gamma_{\text{coll}}^i, \tag{21.16}$$

where i runs over all external states, j enumerates all the gauge groups they are charged under, and C_j^i denotes the quadratic Casimir in the representation of the particle i corresponding to the gauge group j. We want to stress that the knowledge of the cusp and collinear anomalous dimensions is sufficient to derive the infrared divergences of any n-point amplitude in our theory, using the results in [273, 274, 303]. For this reason, we will only present the full result up to two loops by showing the values for the collinear anomalous dimension of the other fields as well as the cusp anomalous dimensions. Because the latter is independent of the external fields, we will only present it once when it is first encountered.

By extracting their values for $\gamma_{\text{cusp}}^{\text{SU}(3)}$ and γ_{coll}^g from our result for a pair of gluons, we find

$$\gamma_{\text{cusp}}^{\text{SU}(3)} = 4\left(\frac{g_s}{4\pi}\right)^2 + \left[\left(\frac{268}{9} - \frac{4\pi^2}{3}\right)C_{A,1} - \frac{20}{9}(C_{A_2}+1)\right]\left(\frac{g_s}{4\pi}\right)^4, \tag{21.17}$$

and

$$\gamma_{\text{coll}}^g = \frac{\beta_{g_s}}{g_s^3}\left(\frac{g_s}{4\pi}\right)^2 - \left\{C_{A,1}^2\left[\frac{692}{27} - 2\zeta(3) - \frac{11\pi^2}{18}\right] - C_{F,1}(C_{A,2}+1)\right.$$
$$\left. + C_{A,1}(C_{A,2}+1)\left[\frac{\pi^2}{18} - \frac{64}{27}\right]\right\}\left(\frac{g_s}{4\pi}\right)^4 \tag{21.18}$$
$$+ C_{A,2}C_{F,2}\left(\frac{g_s g_w}{16\pi^2}\right)^2 + \left(C_{A,2}Y_L^2 + Y_R^2\right)\left(\frac{g_s g_1}{16\pi^2}\right)^2 - C_{A,2}\left(\frac{g_s y}{16\pi^2}\right)^2.$$

The terms containing only g_s perfectly agree with the literature results [273, 274, 301, 302], after replacing $N_f \to (C_{A,2}+1)/2$, to correctly count the number of Weyl fermions in the theory charged under the SU(3) group.

21.1.2 W External States

We continue with the calculation of the infrared anomalous dimension for the case of an external pair of "W bosons", i.e., the gauge boson of the SU(N_2) gauge group. Conceptually, it is very similar to the gluon, as it is just another non-Abelian gauge boson, which allows for a considerable amount of possible cross-checks, after augmenting the counting of the number of contributing Weyl fermions. A new contribution, however, arises due to the presence of the charged scalar, which, as we will see, modifies both the cusp and collinear anomalous dimension.

We again normalize to the tree level form factor, which for the W boson reads

$$T_W^{(0)}(s_{12}) = 2C_{A,2}C_{F,2}. \tag{21.19}$$

Continuing up the loop orders, we get

$$T_W^{(1)}(s_{12}) = \frac{1}{Z_{\mathrm{IR}}^W} \left\{ 1 + \left(-\frac{s_{12}}{\mu^2} \right)^{-\epsilon} \left(\frac{g_w}{4\pi} \right)^2 \left[-\frac{2C_{A,2}}{\epsilon^2} + \frac{\beta_{g_w}}{g_w^3 \epsilon} + \mathcal{O}(\epsilon^0) \right] \right\}, \tag{21.20}$$

which is in perfect analogy to the result in Eq. (21.7), where the contribution of the scalar field is obviously included in the beta function for g_w. Hence, the renormalization constant is also equivalent to Eq. (21.8) after making the suitable replacements, leading to the one-loop anomalous dimension

$$\gamma_{\mathrm{IR}}^W = \left(\frac{g_w}{4\pi} \right)^2 \left[\frac{2\beta_{g_w}}{g_w} + 4C_{A_2} \log \left(-\frac{s_{12}}{\mu^2} \right) \right]. \tag{21.21}$$

Using the imaginary part, which again is completely analogous to the last section,

$$\mathrm{Im}\left[T_W^{(1)}(s_{12}) \right] = -\frac{\pi}{2} \left(\frac{g_w}{4\pi} \right)^2 \left[-\frac{2\beta_{g_w}}{g_w} - 4C_{A_2} \log \left(\frac{s_{12}}{\mu^2} \right) \right], \tag{21.22}$$

immediately gives the same result for the anomalous dimension.

Continuing to the two-loop order, we can split the two loop form factor into pieces originating from the one-loop renormalized couplings and from genuine two-loop diagrams, respectively,

$$T_W^{(2)}(s_{12}) = \frac{1}{Z_{\mathrm{IR}}^W} \left\{ (1 + 2\delta_{g_w}) \, T_W^{(1)}(s_{12}) + \left(-\frac{s_{12}}{\mu^2} \right)^{-2\epsilon} t_2^W \right\}, \tag{21.23}$$

with

$$\begin{aligned}
t_2^W = \left(\frac{g_s}{4\pi} \right)^4 &\left[\frac{2C_{A,2}^2}{\epsilon^4} - \frac{3\beta_{g_w} C_{A,2}}{2g_w^3 \epsilon^3} - \frac{C_{A,2}\left(\left(\pi^2 - 113 \right) C_{A,2} + 10C_{A,1} + 5 \right)}{6\epsilon^2} \right. \\
&\left. - \frac{C_{A,2}^2 \left(300\zeta(3) + 11\pi^2 - 1370 \right)}{36\epsilon} \right. \\
&\left. + \frac{C_{A,2}\left(2\left(\pi^2 - 115 \right) C_{A,1} + \pi^2 - 58 \right)}{72\epsilon} + \frac{(C_{A,1} + 2)C_{F,2}}{2\epsilon} \right] \\
+ \left(\frac{g_s g_w}{16\pi^2} \right)^2 &\frac{C_{A,3} C_{F,3}}{2\epsilon} + \left(\frac{g_w g_1}{16\pi^2} \right)^2 \frac{\left(C_{A,3} Y_L^2 + 2Y_H^2 \right)}{2\epsilon} - \left(\frac{g_w y}{16\pi^2} \right)^2 \frac{C_{A,3}}{4\epsilon}.
\end{aligned} \tag{21.24}$$

Note that because the scalar couples directly to the W boson, the form factor will, in general, be more sensitive to how the scalar is coupled to gravity. In fact, while the term containing the one-loop form factor is independent of if the scalar is coupled minimally or conformally, at least at this order, t_2^W is not. This dependence, however, will cancel in the calculation of the anomalous dimension, as it should, so we chose not to show it explicitly here. The cancellation, in the end, comes from the higher-order terms in $T_W^{(1)}$, which are such that already the renormalization constant Z_{IR}^W is already independent of the scalar-gravity coupling. Here, the logarithm of Z_{IR}^W

then turns out to be

$$
\begin{aligned}
\log\left(Z_{\mathrm{IR}}^{W}\right) = & -\left(\frac{g_w}{4\pi}\right)^2\left[\frac{2C_{A,2}}{\epsilon^2} - \frac{\beta_{g_w}}{g_w^3\epsilon} - \frac{2C_{A,2}}{\epsilon}\log\left(-\frac{s_{12}}{\mu^2}\right)\right] \\
& + \left(\frac{g_w}{4\pi}\right)^4\left[-\frac{3\beta_{g_w}C_{A,2}}{2g_w^3\epsilon^3}\right. \\
& + \frac{12\pi^2 C_{A,2}^2 - 4C_{A,2}(17C_{A,1} - 108C_{F,2} + 7)}{72\epsilon^2} \\
& + \frac{4C_{A,1}(C_{A,1} + 1) + 217}{72\epsilon^2} \\
& + \frac{C_{A,2}^2\left(108\zeta(3) + 33\pi^2 - 1384\right) + 54(C_{A,1} + 2)C_{F,2}}{108\epsilon} \\
& + \frac{C_{A,2}\left(-6\pi^2 C_{A,1} + 256C_{A,1} - 3\pi^2 + 176\right)}{216\epsilon} \\
& \left. + C_{A,2}\log\left(-\frac{s_{12}}{\mu^2}\right)\left(\frac{\beta_{g_w}}{g_w^3\epsilon^2} - \frac{\left(3\pi^2 - 67\right)C_{A,2} + 5C_{A,1} + 4}{9\epsilon}\right)\right] \\
& + \left(\frac{g_s g_w}{16\pi^2}\right)^2\frac{C_{A,3}C_{F,3}}{2\epsilon} + \left(\frac{g_w g_1}{16\pi^2}\right)^2\frac{\left(C_{A,3}Y_L^2 + 2Y_H^2\right)}{2\epsilon} - \left(\frac{g_w y}{16\pi^2}\right)^2\frac{C_{A,3}}{4\epsilon}.
\end{aligned}
\tag{21.25}
$$

As mentioned above, this expression is valid, regardless of how we choose to couple the scalar field to gravity. Notice that, again, the highest pole is of order $\mathcal{O}(\epsilon^{-3})$, meaning lower than the highest pole in the form factor and that all higher powers of logarithms exactly cancel. Taking the total derivative with respect to the renormalization scale and directly extracting the SU(2) cusp anomalous as well as collinear anomalous dimension of the W, we find

$$
\gamma_{\mathrm{cusp}}^{\mathrm{SU(2)}} = 4\left(\frac{g_w}{4\pi}\right)^2 + \left[\left(\frac{268}{9} - \frac{4\pi^2}{3}\right)C_{A,2} - \frac{20}{9}(C_{A_3} + 1) + \frac{4}{9}\right]\left(\frac{g_w}{4\pi}\right)^4,
\tag{21.26}
$$

and

$$
\begin{aligned}
\gamma_{\mathrm{coll}}^{W} = & \frac{\beta_{g_w}}{g_w^3}\left(\frac{g_w}{4\pi}\right)^2 - \left(\frac{g_s}{4\pi}\right)^4\left\{C_{A,2}^2\left[\frac{692}{27} - 2\zeta(3) - \frac{11\pi^2}{18}\right] - C_{F,1}(C_{A,2} + 2)\right. \\
& \left. + C_{A,1}\left[(2C_{A,3} + 1)\frac{\pi^2}{36} - \frac{64C_{A,1} + 44}{27}\right]\right\} \\
& + C_{A,1}C_{F,2}\left(\frac{g_s g_w}{16\pi^2}\right)^2 + \left(C_{A,1}Y_L^2 + 2Y_H^2\right)\left(\frac{g_w g_1}{16\pi^2}\right)^2 - \frac{C_{A,1}}{2}\left(\frac{g_w y}{16\pi^2}\right)^2.,
\end{aligned}
\tag{21.27}
$$

Note the similarities between these results and the gluonic cases. The coefficients of terms containing only the adjoint Casimir are equivalent – they can arise only from diagrams with the non-Abelian triple gauge vertices – the other terms are modified by the presence of a charged scalar field for the SU(2).

We conclude this section by mentioning that this result can, of course, be also obtained by using the imaginary part of the form factor and the optical theorem. While we checked this explicitly, we do not show it here, as it does not provide any further insight.

21.1.3 B External States

At this point, the only gauge boson left is the Abelian one. Due to its Abelian nature, we expect it to be the easiest case for calculating the infrared anomalous dimension. Because it is not

charged under any of the gauge groups, the tree level form factor is trivial

$$T_B^{(0)}(s_{12}) = 1. \tag{21.28}$$

Since it couples only to matter field directly, also the one-loop form factor has a particularly simple form,

$$T_B^{(1)}(s_{12}) = \frac{1}{Z_{\text{IR}}^B} \left\{ 1 + \left(-\frac{s_{12}}{\mu^2} \right)^{-\epsilon} \left(\frac{g_1}{4\pi} \right)^2 \frac{\beta_{g_1}}{g_1^3 \epsilon} + \mathcal{O}(\epsilon^0) \right\}. \tag{21.29}$$

Note, that this result does not exhibit any higher than single poles, such that the renormalization constant will not contain logarithms. In fact, we easily obtain

$$Z_{\text{IR}}^B = 1 + \left(\frac{g_1}{4\pi} \right)^2 \frac{\beta_{g_1}}{g_1^3 \epsilon}, \tag{21.30}$$

immediately giving

$$\gamma_{\text{IR}}^B = 2 \left(\frac{g_1}{4\pi} \right)^2 \frac{\beta_{g_1}}{g_1^3}. \tag{21.31}$$

Indeed, this result is constant and contains no logarithms. However, recalling Eq. (21.16) this is to be expected. The logarithmic term is conjectured to be proportional to the Casimirs of the external states, but because the B boson is a singlet under all gauge groups, its corresponding Casimirs vanish, such that there cannot be a logarithmic term in the infrared anomalous dimension. As we will see shortly, this also applies to the two-loop result.

As before, the two-loop form factor can be written as

$$T_B^{(2)}(s_{12}) = \frac{1}{Z_{\text{IR}}^B} \left\{ (1 + 2\delta_{g_1}) T_B^{(1)}(s_{12}) + \left(-\frac{s_{12}}{\mu^2} \right)^{-2\epsilon} t_2^B \right\}, , \tag{21.32}$$

and

$$\begin{aligned} t_2^B &= \left(\frac{g_1}{4\pi} \right)^4 \frac{C_{A,1}C_{A,2}Y_L^4 + C_{A,1}Y_R^4 + 2C_{A,2}Y_H^4}{\epsilon} + \left(\frac{g_1^2 g_s^2}{16\pi^2} \right)^2 \frac{C_{A,1}C_{F,1}(C_{A,2}Y_L^2 + Y_R^2)}{\epsilon} \\ &+ \left(\frac{g_1^2 g_w^2}{16\pi^2} \right)^2 \frac{C_{A,2}C_{F,2}(C_{A,1}Y_L^2 + 2Y_H^2)}{\epsilon} - \left(\frac{g_1^2 y^2}{16\pi^2} \right)^2 \frac{C_{A,1}C_{A,2}(Y_L^2 + Y_R^2)}{2\epsilon}. \end{aligned} \tag{21.33}$$

As expected, the highest pole at the two-loop order is of order $\mathcal{O}(\epsilon^{-2})$ and originates purely from the one-loop renormalized couplings. Indeed, as a consequence, the renormalization constant does not contain any logarithms and for the infrared anomalous dimension we find

$$\begin{aligned} \gamma_{\text{coll}}^B &= \frac{\beta_{g_1}}{g_1^3} \left(\frac{g_1}{4\pi} \right)^2 + 2(C_{A,1}C_{A,2}Y_L^4 + C_{A,1}Y_R^4 + 2C_{A,2}Y_H^4) \left(\frac{g_1}{4\pi} \right)^4 \\ &+ 2C_{A,1}C_{F,1}(C_{A,2}Y_L^2 + Y_R^2) \left(\frac{g_1^2 g_s^2}{16\pi^2} \right)^2 + 2C_{A,2}C_{F,2}(C_{A,1}Y_L^2 + 2Y_H^2) \left(\frac{g_1^2 g_w^2}{16\pi^2} \right)^2 \\ &- C_{A,1}C_{A,2}(Y_L^2 + Y_R^2) \left(\frac{g_1^2 y^2}{16\pi^2} \right)^2. \end{aligned} \tag{21.34}$$

Naively, the absence of logarithmic terms might suggest a vanishing U(1) cusp anomalous dimension. However, recalling Eq. (21.16), the logarithmic terms are proportional to the quadratic

207

Casimirs of the external states. But the Abelian gauge boson itself is not charged under any gauge group; hence it's corresponding Casimirs vanish, eliminating the logarithmic terms in the anomalous dimension, even for a non-vanishing cusp anomalous dimension.

As for the other gauge bosons, we checked explicitly that the same result can be obtained by using the imaginary part of Eq. (21.32).

21.1.4 Left-handed Fermion External States

Now that we have discussed all the gauge bosons in the theory, we can move on to the matter fields, starting with the left-handed fermion. Because it couples to all three gauge groups, as well as to the scalar field, this is the most computationally intensive field in the theory. However, because it transforms in the fundamental representation of all the (non-Abelian) gauge groups, there will be a lot of overlap between this calculation and the ones for the right-handed fermion and the scalar, which also transform only in the fundamental representation of their respective gauge group. Looking again at Eq. (21.16), this particularly applies to the logarithmic terms in the infrared anomalous dimension, which will the same for all particles at a given coupling order.

As usual, normalizing to the tree level form factor

$$T_{\psi_L}^{(0)}(s_{12}) = C_{A,1}C_{A,2}, \tag{21.35}$$

the one-loop expression we find is given by

$$
\begin{aligned}
T_{\psi_L}^{(1)}(s_{12}) = \frac{1}{Z_{\mathrm{IR}}^{\psi_L}} \Bigg\{ 1 - \left(-\frac{s_{12}}{\mu^2}\right)^{-\epsilon} \Bigg[& C_{F,1}\left(\frac{g_s}{4\pi}\right)^2\left(\frac{2}{\epsilon^2}+\frac{3}{\epsilon}\right) \\
& + C_{F,2}\left(\frac{g_w}{4\pi}\right)^2\left(\frac{2}{\epsilon^2}+\frac{3}{\epsilon}\right) \\
& + Y_L^2\left(\frac{g_1}{4\pi}\right)^2\left(\frac{2}{\epsilon^2}+\frac{3}{\epsilon}\right) - \left(\frac{y}{4\pi}\right)^2\frac{1}{2\epsilon} \Bigg] + \mathcal{O}(\epsilon^0) \Bigg\}.
\end{aligned}
\tag{21.36}
$$

We will postpone presenting the one-loop result for relevant the anomalous dimension to a later point, when also the two-loop term is computed.

As already mentioned, the calculation for ψ_L is the most computationally demanding, generating rather large results. To make them more readable, we will collect various terms by their respective coupling order, such that we can bring the two-loop form factor into the following form

$$
\begin{aligned}
T_{\psi_L}^{(2)}(s_{12}) = \frac{1}{Z_{\mathrm{IR}}^{\psi_L}} \Bigg\{ & [1 + 2(\delta_{g_s} + \delta_{g_w} + \delta_{g_1} + \delta_y)]\, T_{\psi_L}^{(1)}(s_{12}) \\
& + \left(-\frac{s_{12}}{\mu^2}\right)^{-2\epsilon}\left[\left(\frac{g_s}{4\pi}\right)^4 t_{g_s^4}^{\psi_L} + \left(\frac{g_w}{4\pi}\right)^4 t_{g_w^4}^{\psi_L} + \left(\frac{g_1}{4\pi}\right)^4 t_{g_1^4}^{\psi_L} + \left(\frac{y}{4\pi}\right)^4 t_{y^4}^{\psi_L} + t_{\mathrm{mixed}}^{\psi_L}\right] \Bigg\},
\end{aligned}
\tag{21.37}
$$

where the individual two-loop contributions read

$$
\begin{aligned}
t^{\psi_L}_{g_s^4} = &\frac{2C_{F,1}}{\epsilon^4} + \frac{C_{F,1}}{\epsilon^3}\left[\frac{\beta_{g_s}}{2g_s^3} + 6C_{F,1}\right] \\
&+ \frac{C_{F,1}}{6\epsilon^2}\left[\frac{14(C_{A,2}+1) + \left(3\pi^2 - 166\right)C_{A,1}}{3} - \left(2\pi^2 - 147\right)C_{F,1}\right] \\
&+ \frac{C_{F,1}}{12\epsilon}\left[\frac{\left(425 + 3\pi^2\right)\left(C_{A,2}+1\right) + C_{A,1}\left(1404\zeta(3) - 33\pi^2 - 4921\right)}{9}\right] \\
&- \frac{C_{F,1}^2}{12\epsilon}\left(256\zeta(3) - 927\right),
\end{aligned}
\tag{21.38}
$$

$$
\begin{aligned}
t^{\psi_L}_{g_w^4} = &\frac{2C_{F,2}}{\epsilon^4} + \frac{C_{F,2}}{\epsilon^3}\left[\frac{\beta_{g_w}}{2g_w^3} + 6C_{F,2}\right] \\
&+ \frac{C_{F,2}}{6\epsilon^2}\left[\frac{\left(\left(6\pi^2 - 332\right)C_{A,2} + 28C_{A,1} + 17\right)}{6} - \left(2\pi^2 - 147\right)C_{F,2}\right] \\
&+ \frac{C_{F,2}}{12\epsilon}\left[\frac{C_{A,2}\left(2808\zeta(3) - 66\pi^2 - 9842\right) + \left(850 + 6\pi^2\right)C_{A,1} + 3\pi^2 + 527}{18}\right] \\
&- \frac{C_{F,2}^2}{12\epsilon}\left(256\zeta(3) - 927\right),
\end{aligned}
\tag{21.39}
$$

$$
\begin{aligned}
t^{\psi_L}_{g_1^4} = &\frac{2Y_L^4}{\epsilon^4} + \frac{Y_L^2}{\epsilon^3}\left[\frac{\beta_{g_1}}{2g_1^3} + 6Y_L^2\right] \\
&+ \frac{Y_L^2}{18\epsilon^2}\left[17C_{A,2}Y_H^2 + 28C_{A,1}Y_R^2 + Y_L^2\left(28C_{A,1}C_{A,2} + 441 - 6\pi^2\right)\right] \\
&+ \frac{Y_L^2}{108\epsilon}\left[\left(527 + 3\pi^2\right)C_{A,2}Y_H^2 + 2\left(425 + 3\pi^2\right)C_{A,1}Y_R^2\right] \\
&- \frac{Y_L^4}{108\epsilon}\left[\left(2\left(425 + 3\pi^2\right)C_{A,2}C_{A,1} - 2304\zeta(3) + 8343\right)\right],
\end{aligned}
\tag{21.40}
$$

$$
t^{\psi_L}_{y^4} = -\frac{(C_{A,2} + 2C_{A,1})}{8\epsilon^2} - \frac{(13C_{A,2} + 30C_{A,1})}{16\epsilon},
\tag{21.41}
$$

and finally, the mixed terms,

$$
\begin{aligned}
t^{\psi_L}_{\text{mixed}} = &\left[C_{F,1}C_{F,2}\left(\frac{g_s^2 g_w^2}{16\pi^2}\right)^2 + C_{F,1}Y_L^2\left(\frac{g_s^2 g_1^2}{16\pi^2}\right)^2 + C_{F,2}Y_L^2\left(\frac{g_1^2 g_w^2}{16\pi^2}\right)^2\right] \times \\
&\left[\frac{4}{\epsilon^4} + \frac{12}{\epsilon^3} - \frac{2\pi^2 - 147}{3\epsilon^2} - \frac{256\zeta(3) - 927}{6\epsilon}\right] \\
&- C_{F,1}\left(\frac{g_s^2 y^2}{16\pi^2}\right)^2\left[\frac{1}{\epsilon^3} + \frac{3}{\epsilon^2} + \frac{17}{2\epsilon}\right] \\
&- C_{F,2}\left(\frac{g_w^2 y^2}{16\pi^2}\right)^2\left[\frac{1}{\epsilon^3} + \frac{15}{4\epsilon^2} + \frac{77}{8\epsilon}\right] \\
&- \left(\frac{g_1^2 y^2}{16\pi^2}\right)^2\left[\frac{Y_L^2}{\epsilon^3} + \frac{3(5Y_L^2 - Y_R^2)}{4\epsilon^2} - \frac{22Y_H^2 - 99Y_L^2 + 31Y_R^2}{8\epsilon}\right].
\end{aligned}
\tag{21.42}
$$

Using these lengthy expressions, we can easily compute the renormalization constant $Z_{\text{IR}}^{\psi_L}$ to get the collinear anomalous dimension the fermion, as well as the U(1) cusp term

$$\gamma_{\text{cusp}}^{\text{U}(1)} = 4\left(\frac{g_1}{4\pi}\right)^2 - \left[\frac{32}{9}C_{A,2}Y_H^2 + \frac{40}{9}C_{A,1}(C_{A_2}Y_L^2 + Y_R^2)\right]\left(\frac{g_1}{4\pi}\right)^4, \tag{21.43}$$

and

$$\begin{aligned}
\gamma_{\text{coll}}^{\psi_L} = {} & -3C_{F,1}\left(\frac{g_s}{4\pi}\right)^2 - 3C_{F,2}\left(\frac{g_w}{4\pi}\right)^2 - 3Y_L^2\left(\frac{g_1}{4\pi}\right)^2 + \frac{1}{2}\left(\frac{y}{4\pi}\right)^2 \\
& + \left[C_{F,1}^2\left(2\pi^2 - 24\zeta(3) - \frac{3}{2}\right) + C_{F,1}(C_{A,2}+1)\left(\frac{65}{54} + \frac{\pi^2}{6}\right)\right. \\
& \left. + C_{F,1}C_{A,1}\left(26\zeta(3) - \frac{11\pi^2}{6} - \frac{961}{54}\right)\right]\left(\frac{g_s}{4\pi}\right)^4 \\
& + \left[C_{F,2}^2\left(2\pi^2 - 24\zeta(3) - \frac{3}{2}\right) + C_{F,2}C_{A,1}\left(\frac{65}{54} + \frac{\pi^2}{6}\right)\right. \\
& \left. + C_{F,2}\left(\frac{167}{54} + \frac{\pi^2}{6}\right) + C_{F,2}C_{A,2}\left(26\zeta(3) - \frac{11\pi^2}{6} - \frac{961}{54}\right)\right]\left(\frac{g_w}{4\pi}\right)^4 \\
& + \left[Y_L^2 Y_H^2\left(\frac{167}{54} + \frac{\pi^2}{6}\right) + Y_L^2 Y_R^2\left(\frac{130}{54} + \frac{\pi^2}{3}\right)\right. \\
& \left. - Y_L^4\left(\frac{\pi^2}{3}C_{A,2}C_{A,1} + \frac{65C_{A,2}C_{A,1}}{27} - 24\zeta(3) + 2\pi^2 - \frac{3}{2}\right)\right]\left(\frac{g_1}{4\pi}\right)^4 \\
& - \frac{C_{A,2} + 6C_{A,1}}{8}\left(\frac{y}{4\pi}\right)^4 - \frac{C_{F,1}(6+\pi^2)}{3}\left(\frac{g_s^2 y^2}{16\pi^2}\right)^2 + \frac{C_{F,2}(57-4\pi^2)}{12}\left(\frac{g_w^2 y^2}{16\pi^2}\right)^2 \\
& - \frac{66Y_H^2 + (4\pi^2 - 123)Y_L^2 - 117Y_R^2}{12}\left(\frac{g_1^2 y^2}{16\pi^2}\right)^2 \\
& - \left[3 + 48\zeta(3) - 4\pi^2\right]\left[C_{F,1}C_{F,2}\left(\frac{g_s^2 g_w^2}{16\pi^2}\right)^2 + C_{F,1}Y_L^2\left(\frac{g_s^2 g_1^2}{16\pi^2}\right)^2 + C_{F,2}Y_L^2\left(\frac{g_1^2 g_w^2}{16\pi^2}\right)^2\right]
\end{aligned}$$

21.1.5 Right-handed Fermion External States

Compared to the previous section, the case of the right-handed fermion is much easier to calculate, as it is a singlet under the $\text{SU}(N_2)$ gauge group, eliminating a large portion of diagrams and associated contributions. In addition, the $\text{SU}(N_1)$ sector is blind to whether we use the left- or the right-handed fermion, so all terms containing only g_s will be very similar to those in the last section. Then, normalizing, as always, to the tree level expression

$$T_{\psi_L}^{(0)}(s_{12}) = C_{A,1}C_{A,2}, \tag{21.44}$$

the only contribution at the one-loop level, we have not computed before is

$$T_{\psi_R}^{(1)}(s_{12}) \supset \frac{1}{Z_{\text{IR}}^{\psi_R}}\left\{1 - \left(-\frac{s_{12}}{\mu^2}\right)^{-\epsilon}\left[Y_R^2\left(\frac{g_1}{4\pi}\right)^2\left(\frac{2}{\epsilon^2} + \frac{3}{\epsilon}\right) - \left(\frac{y}{4\pi}\right)^2\frac{C_{A,2}}{2\epsilon}\right] + \mathcal{O}(\epsilon^0)\right\}. \tag{21.45}$$

Note that we could have derived this result without the need of any computation from the Eq. (21.36). The term proportional to g_1^2 is the same after replacing $Y_L \to Y_R$, while the $C_{A,2}$ comes from the fact that all $\mathrm{SU}(N_2)$ indices have to be contracted for ψ_R and not for ψ_L, effectively just counting the number of components in the fundamental $\mathrm{SU}(N_2)$ multiplet running in the loop.

Continuing to the two-loop order, we can write

$$
T_{\psi_R}^{(2)}(s_{12}) = \frac{1}{Z_{\mathrm{IR}}^{\psi_R}} \Bigg\{ \left[1 + 2(\delta_{g_s} + \delta_{g_1} + \delta_y)\right] T_{\psi_R}^{(1)}(s_{12}) \tag{21.46}
$$
$$
+ \left(-\frac{s_{12}}{\mu^2}\right)^{-2\epsilon} \left[\left(\frac{g_s}{4\pi}\right)^4 t_{g_s^4}^{\psi_L} + \left(\frac{g_1}{4\pi}\right)^4 t_{g_1^4}^{\psi_R} + \left(\frac{y}{4\pi}\right)^4 t_{y^4}^{\psi_R} + t_{\mathrm{mixed}}^{\psi_R}\right] \Bigg\},
$$

where we already used the fact that the $\mathrm{SU}(N_1)$ sector is blind to the chirality of the fermions. The remaining contributions read

$$
\begin{aligned}
t_{g_1^4}^{\psi_R} =& \frac{2Y_R^4}{\epsilon^4} + \frac{Y_R^2}{\epsilon^3}\left[\frac{\beta_{g_1}}{2g_1^3} + 6Y_R^2\right] \\
&+ \frac{Y_R^2}{18\epsilon^2}\left[17 C_{A,2}Y_H^2 + 28 C_{A,1}C_{A,2}Y_L^2 + Y_R^2\left(28 C_{A,1} + 441 - 6\pi^2\right)\right] \\
&+ \frac{Y_R^2}{108\epsilon}\left[\left(527 + 3\pi^2\right)C_{A,2}Y_H^2 + 2\left(425 + 3\pi^2\right)C_{A,1}C_{A,2}Y_L^2\right] \\
&- \frac{Y_R^4}{108\epsilon}\left[\left(2\left(425 + 3\pi^2\right)C_{A,1} - 2304\zeta(3) + 8343\right)\right],
\end{aligned} \tag{21.47}
$$

$$
t_{y^4}^{\psi_R} = -\frac{C_{A,2}(2C_{A,1} + 1)}{8\epsilon^2} - \frac{C_{A,2}(30C_{A,1} + 13)}{16\epsilon}, \tag{21.48}
$$

$$
\begin{aligned}
t_{\mathrm{mixed}}^{\psi_R} =& C_{F,1}Y_L^2\left(\frac{g_s^2 g_1^2}{16\pi^2}\right)^2\left[\frac{4}{\epsilon^4} + \frac{12}{\epsilon^3} - \frac{2\pi^2 - 147}{3\epsilon^2} - \frac{256\zeta(3) - 927}{6\epsilon}\right] \\
&- C_{A,2}C_{F,1}\left(\frac{g_s^2 y^2}{16\pi^2}\right)^2\left[\frac{1}{\epsilon^3} + \frac{3}{\epsilon^2} + \frac{17}{2\epsilon}\right] \\
&+ C_{A,2}C_{F,2}\left(\frac{g_w^2 y^2}{16\pi^2}\right)^2\left[\frac{3}{4\epsilon^2} + \frac{53}{8\epsilon}\right] \\
&- C_{A,2}\left(\frac{g_1^2 y^2}{16\pi^2}\right)^2\left[\frac{Y_R^2}{\epsilon^3} + \frac{3(5Y_L^2 - Y_R^2)}{4\epsilon^2} - \frac{22Y_H^2 - 99Y_L^2 + 31Y_R^2}{8\epsilon}\right].
\end{aligned} \tag{21.49}
$$

Interestingly, even though ψ_R does not couple directly to the chiral $\mathrm{SU}(N_2)$ sector, its form factor does acquire divergent terms proportional to g_w, mediated through the scalar field and the Yukawa coupling.

Because we have computed all the cusp anomalous dimensions in this theory, we only need to extract the collinear anomalous dimension of the right-handed fermion, reading

$$
\gamma_{\text{coll}}^{\psi_R} = -3C_{F,1}\left(\frac{g_s}{4\pi}\right)^2 - 3Y_R^2\left(\frac{g_1}{4\pi}\right)^2 + \frac{C_{A,2}}{2}\left(\frac{y}{4\pi}\right)^2
$$

$$
+ \left[C_{F,1}^2\left(2\pi^2 - 24\zeta(3) - \frac{3}{2}\right) + C_{F,1}(C_{A,2}+1)\left(\frac{65}{54} + \frac{\pi^2}{6}\right) \right.
$$

$$
\left. + C_{F,1}C_{A,1}\left(26\zeta(3) - \frac{11\pi^2}{6} - \frac{961}{54}\right) \right] \left(\frac{g_s}{4\pi}\right)^4
$$

$$
+ \left[Y_R^2 Y_H^2 C_{A,2}\left(\frac{167}{54} + \frac{\pi^2}{6}\right) + Y_L^2 Y_R^2 C_{A,2}\left(\frac{65}{27} + \frac{\pi^2}{3}\right) \right.
$$

$$
\left. - Y_R^4\left(\frac{\pi^2}{3}C_{A,2}C_{A,1} + \frac{65C_{A,2}C_{A,1}}{27} - 24\zeta(3) + 2\pi^2 - \frac{3}{2}\right) \right]\left(\frac{g_1}{4\pi}\right)^4
$$

$$
- \frac{C_{A,2}(1+6C_{A,1})}{8}\left(\frac{y}{4\pi}\right)^4 - \frac{C_{A,2}C_{F,1}(6+\pi^2)}{3}\left(\frac{g_s^2 y^2}{16\pi^2}\right)^2 + \frac{17C_{A,2}C_{F,2}}{4}\left(\frac{g_w^2 y^2}{16\pi^2}\right)^2
$$

$$
+ \frac{66Y_H^2 - (4\pi^2+9)Y_R^2 - 15Y_L^2}{12}\left(\frac{g_1^2 y^2}{16\pi^2}\right)^2 - C_{F,1}Y_L^2\left[3 + 48\zeta(3) - 4\pi^2\right]\left(\frac{g_s^2 g_1^2}{16\pi^2}\right)^2
$$

21.1.6 Scalar External State

At this point, the scalar field is the last one we need to consider in this theory.

Calculating the form factors order by order, as for all other previous fields, and normalizing to

$$
T_H^{(0)}(s_{12}) = C_{A,2}, \tag{21.50}
$$

we find at the one-loop order

$$
T_H^{(1)}(s_{12}) = \frac{1}{Z_{\text{IR}}^H}\left\{ 1 - \left(-\frac{s_{12}}{\mu^2}\right)^{-\epsilon} C_{A,2}\left[C_{F,2}\left(\frac{g_w}{4\pi}\right)^2\left(\frac{2}{\epsilon^2} + \frac{4}{\epsilon}\right) \right.\right. \tag{21.51}
$$

$$
\left.\left. + Y_H^2\left(\frac{g_1}{4\pi}\right)^2\left(\frac{2}{\epsilon^2} + \frac{4}{\epsilon}\right) - \left(\frac{y}{4\pi}\right)^2 \frac{C_{A,1}}{\epsilon} \right] + \mathcal{O}(\epsilon^0) \right\}.
$$

Next, the two-loop form factor can be written as

$$
T_H^{(2)}(s_{12}) = \frac{1}{Z_{\text{IR}}^H}\left\{ [1 + 2(\delta_{g_w} + \delta_{g_1} + \delta_y)] T_H^{(1)}(s_{12}) \right. \tag{21.52}
$$

$$
\left. + \left(-\frac{s_{12}}{\mu^2}\right)^{-2\epsilon}\left[\left(\frac{g_w}{4\pi}\right)^4 t_{g_w^4}^H + \left(\frac{g_1}{4\pi}\right)^4 t_{g_1^4}^H + \left(\frac{y}{4\pi}\right)^4 t_{y^4}^H + \left(\frac{\lambda}{16\pi^2}\right)^2 t_{\lambda^2}^H + t_{\text{mixed}}^H \right] \right\},
$$

with the individual, genuine two-loop contributions given by

$$
\begin{aligned}
t_{g_w^4}^H =& \frac{2C_{F,2}}{\epsilon^4} + \frac{C_{F,2}}{\epsilon^3} \left[\frac{\beta_{g_w}}{2g_w^3} + 8C_{F,2} \right] \\
&+ \frac{C_{F,2}}{3\epsilon^2} \left[\frac{\left(\left(3\pi^2 - 199\right) C_{A,2} + 17C_{A,1} + 10 \right)}{6} - \left(\pi^2 - 96\right) C_{F,2} \right] \\
&+ \frac{C_{F,2}}{12\epsilon} \left[\frac{C_{A,2} \left(2808\zeta(3) - 66\pi^2 - 12869\right) + 2\left(545 + 3\pi^2\right) C_{A,1} + 3\pi^2 + 665}{18} \right] \\
&- \frac{C_{F,2}^2}{12\epsilon} \left(256\zeta(3) - 1269\right),
\end{aligned}
\tag{21.53}
$$

$$
\begin{aligned}
t_{g_1^4}^H =& \frac{2Y_H^4}{\epsilon^4} + \frac{Y_L^2}{\epsilon^3} \left[\frac{\beta_{g_1}}{2g_1^3} + 8Y_H^2 \right] \\
&+ \frac{Y_L^2}{9\epsilon^2} \left[17C_{A,2}C_{A,1}Y_L^2 + C_{A,1}Y_R^2 + Y_H^2 \left(10C_{A,2} + 288 - 3\pi^2\right) \right] \\
&+ \frac{Y_H^2}{54\epsilon} \left[\left(545 + 3\pi^2\right) C_{A,1}(C_{A,2}Y_L^2 + Y_R^2) \right] \\
&+ \frac{Y_H^4}{108\epsilon} \left[\left(\left(665 + 3\pi^2\right) C_{A,2} - 2304\zeta(3) + 11421 \right) \right],
\end{aligned}
\tag{21.54}
$$

$$
t_{y^4}^H = -\frac{C_{A,2}(2C_{A,1} + 1)}{4\epsilon} \left(\frac{1}{\epsilon} + \frac{15}{2} \right), \quad t_{\lambda^2}^H = \frac{C_{A,2} + 1}{4\epsilon},
\tag{21.55}
$$

$$
\begin{aligned}
t_{\text{mixed}}^H =& C_{F,2}Y_H^2 \left(\frac{g_1^2 g_w^2}{16\pi^2} \right)^2 \left[\frac{4}{\epsilon^4} + \frac{16}{\epsilon^3} - \frac{2\pi^2 - 96}{3\epsilon^2} - \frac{256\zeta(3) - 1269}{6\epsilon} \right] \\
& C_{A,1}C_{F,1} \left(\frac{g_s^2 y^2}{16\pi^2} \right)^2 \left[\frac{3}{\epsilon^2} + \frac{41}{2\epsilon} \right] \\
&- C_{A,1}C_{F,2} \left(\frac{g_w^2 y^2}{16\pi^2} \right)^2 \left[\frac{2}{\epsilon^3} + \frac{17}{2\epsilon^2} + \frac{111}{4\epsilon} \right] \\
& \left(\frac{g_1^2 y^2}{16\pi^2} \right)^2 \left[\frac{2Y_H^2}{\epsilon^3} + \frac{17Y_L^2 - 40Y_LY_R + 17Y_R^2}{2\epsilon^2} - \frac{111Y_L^2 - 304Y_LY_R + 111Y_R^2}{4\epsilon} \right].
\end{aligned}
\tag{21.56}
$$

Note that, similarly to the g_w^2 contribution to the ψ_R anomalous dimension, we see that, for the scalar, a contribution proportional to g_s^2 is generated even though it is not charged under the respective gauge group, using the Yukawa coupling as a mediator.

Having said this, we are now in the position to finally compute the last missing infrared anomalous dimension, the collinear one of the scalar field

$$
\begin{aligned}
\gamma_{\text{coll}}^{H} = {} & \left[C_{F,2}^2 \left(\frac{8\pi^2}{3} - 24\zeta(3) + \frac{7}{2} \right) + C_{F,2}C_{A,1} \left(\frac{113}{54} + \frac{\pi^2}{6} \right) \right. \\
& \left. + C_{F,2} \left(\frac{233}{108} + \frac{\pi^2}{12} \right) + C_{F,2}C_{A,2} \left(26\zeta(3) - \frac{11\pi^2}{6} - \frac{3365}{108} \right) \right] \left(\frac{g_w}{4\pi} \right)^4 \\
& + \left[Y_H^2 C_{A,1}(C_{A,2}Y_L^2 + Y_R^2) \left(\frac{113}{27} + \frac{\pi^2}{3} \right) \right. \\
& \left. + Y_L^4 \left(\frac{\pi^2}{6} C_{A,2}C_{A,1} + \frac{223 C_{A,2}}{54} - 24\zeta(3) + \frac{8\pi^2}{3} + \frac{7}{2} \right) \right] \left(\frac{g_1}{4\pi} \right)^4 \\
& - \frac{(3C_{A,2}+1)C_{A,1}}{4} \left(\frac{y}{4\pi} \right)^4 + \frac{C_{A,1}+1}{2} \left(\frac{\lambda}{16\pi^2} \right)^2 + 5 C_{A,1}C_{F,1} \left(\frac{g_s^2 y^2}{16\pi^2} \right)^2 \\
& + \frac{C_{A,1}C_{F,2}(15 - 4\pi^2)}{6} \left(\frac{g_w^2 y^2}{16\pi^2} \right)^2 + \frac{Y_H^2}{3} \left(21 - 144\zeta(3) + 16\pi^2 \right) \left(\frac{g_1^2 g_w^2}{16\pi^2} \right)^2 \\
& - \frac{C_{A,1}}{6} \left[4\pi^2 Y_H^2 - 15(Y_L^2 + Y_R^2) \right] \left(\frac{g_1^2 y^2}{16\pi^2} \right)^2 .
\end{aligned}
\tag{21.57}
$$

This completes the computation of all the relevant, infrared anomalous dimensions for every particle in our SM toy model.

To conclude this section, we want to mention that this theory naturally allows for cross-checking large parts of the results because all matter fields are charged under at least one internal symmetry group. As explained in Sec. 20.2.2, we can calculate the matrix elements of the spin-1 currents, and the anomalous dimension obtained should coincide with the IR anomalous dimension due to their non-conservation property. However, care has to be taken when considering contributions containing the gauge coupling corresponding to the spin-1 current, as these terms potentially contain UV pieces with counterterms of the form $\partial_\nu F^{\nu\mu}$. So, to not having to deal with these complications, we use the spin-1 currents only to cross-check the terms not containing these couplings, i.e., we use the $SU(N_1)$ current to check all terms free of g_s in the fermion anomalous dimensions.

21.2   UV Renormalization of the $U(1)$ Current

Of course, there are many useful applications for the results from the previous section, take e.g., the UV running of some higher-dimensional operators, which we could embed into our toy model in a way reminiscent of the SMEFT. In this section, we want to present an application that neatly fits into the discussion of conserved currents beyond tree level and does not require the addition of any extra operators or similar. Instead, we want to calculate the UV renormalization of a conserved current and for simplicity we will consider the one associated to the $U(1)$ gauge symmetry in our toy theory and we will closely follow the discussion in [293] on the general features.

As mentioned in Chapter 19, the charge current does not renormalize if the accompanying symmetry is not gauged, while there exists a potential counterterm in the presence of a gauge field, given by

$$
\partial_\nu F^{\nu\mu}.
\tag{21.58}
$$
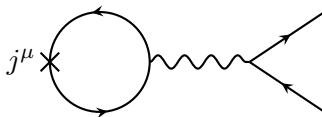
Figure 21.1: The non-1PI, one-loop diagram, contributing to the matrix element of the charge current. Shrinking the loop, it is obvious why the operator $\partial_\nu F^{\nu\mu}$ is needed as a counterterm.

But this operator does not come with its own, independent renormalization constant, as is usually the case for composite operators, but it is related to the wave function renormalization of the gauge field. This can easily be seen by looking at the equation of motion for the renormalized gauge field itself [293]

$$0 = \frac{\delta S}{\delta B_\mu} = g_1 Z_\psi \bar\psi \gamma^\mu \psi + Z_B \partial_\nu F^{\nu\mu}, \tag{21.59}$$

where the counterterm operator simply arises from the kinetic term of the gauge field after using the antisymmetry of the field strength tensor as well as integrating by parts once. We also ignored the term coming from the gauge fixing term, as it vanishes in physical matrix elements [293] as well as the overall scaling dimension of the coupling in dimensional regularization. In total, we get that the full, renormalized current is given by

$$j^\mu = Z_\psi \bar\psi \gamma^\mu \psi + \frac{Z_B - 1}{g_1} \partial_\nu F^{\nu\mu} = \bar\psi_0 \gamma^\mu \psi_0 + \frac{1 - Z_B^{-1}}{g_{1,0}} \partial_\nu F_0^{\nu\mu}, \tag{21.60}$$

where in the last term we have rewritten everything in terms of bare fields and couplings, using the relation between the coupling and gauge field renormalization as dictated by the Ward identity. The above equation directly shows that to obtain finite matrix elements, it does not suffice to just use the current as it is obtained from the Noether procedure, but also the the gauge counterterm has to be included. In fact, diagrammatically, it is clear why exactly this additional term is needed by considering the possible divergent loop diagrams obtained from a single insertion of the Noether current. The particularly relevant diagram at the one-loop order is shown in Fig. 21.1. While all the divergences from irreducible diagrams with an internal gauge field would be cancelled by the Noether current operator itself, we know that they contribute only to the IR divergences due to the non-renormalization. The reducible diagram, Fig. 21.1, on the other hand, cannot be renormalized by the Noether current, and it is clear that the operator $\partial_\nu F^{\nu\mu}$ is needed instead. Note that this also diagrammatically confirms the expectation that the needed renormalization constant is just given by the field renormalization constant, as coupling the gauge field back to the current, the diagram is just the one-loop self energy attached to the tree level vertex.

Following the general discussion, we expect that this holds also at higher loops and that the UV divergence originates from reducible diagrams corresponding to the self energy diagrams of the respective gauge field. We will check this explicitly in the following. Here, for simplicity, we choose to present the results using ψ_R as external states because this greatly reduces the number of diagrams to be calculated. We comment on different choices for the external states towards the end of this chapter. Using the same projection procedure as in Sec. 20.2.2 as well as contracting all color indices, we find that the current form factor up to two-loops and normalized to the tree-level form factor of the Noether current is given by

$$F_R(s_{12}) = \left(Z_{\mathrm{IR}}^{\psi_R} \right)^{-1} \left[1 + F_R^{(1)} + F_R^{(2)} + \frac{1 - Z_B^{-1}}{g_{1,0}} \left(-g_{1,0} + F_{\partial F}^{(1)} \right) \right] \tag{21.61}$$

Here $F_R^{(i)}$ and $F_{\partial F}^{(i)}$ are the bare form factors of the Noether current and counterterm operator at the i-loop order, respectively, and the effect of the renormalized couplings is already included in F_R^2.

At the one-loop order, we then have

$$
\begin{aligned}
F_R(s_{12}) &= \left(Z_{\text{IR}}^{\psi_R}\right)^{-1} \left[F_R^{(1)} + Z_B^{-1}\right] \\
&= -\left(\frac{g}{4\pi}\right)^2 \frac{2C_{A,2}C_{A,1}Y_L^2 + C_{A,2}Y_H^2 + 2C_{A,1}Y_R^2}{3\epsilon} - \delta_B^{(1)} + \mathcal{O}(\epsilon^0),
\end{aligned}
\tag{21.62}
$$

immediately giving the needed one-loop UV counterterm. In fact, its value matches perfectly the one-loop renormalization of the gauge field, as expected.

Using this result and continuing to the two-loop order, we find

$$
\begin{aligned}
F_R(s_{12}) &= \left(Z_{\text{IR}}^{\psi_R}\right)^{-1} \left[1 + F_R^{(1)} + F_R^{(2)} + \frac{1 - Z_B^{-1}}{g_{1,0}}\left(-g_{1,0} + F_{\partial F}^{(1)}\right)\right] \\
&= -\left(\frac{g_1}{4\pi}\right)^4 \frac{C_{A,1}C_{A,2}Y_L^4 + C_{A,1}Y_R^4 + C_{A,2}Y_H^4}{\epsilon} - \left(\frac{g_1^2 g_w^2}{16\pi^2}\right)^2 \frac{C_{A,1}Y_L^2 + 2Y_H^2}{\epsilon} \\
&\quad - \left(\frac{g_1^2 g_s^2}{16\pi^2}\right)^2 \frac{C_{A,2}Y_L^2 + Y_R^2}{\epsilon} + \left(\frac{g_1^2 y^2}{16\pi^2}\right)^2 \frac{C_{A,1}C_{A,3}(Y_L^2 + 2Y_R^2)}{2\epsilon} - \delta_B^{(2)} + \mathcal{O}(\epsilon^0).
\end{aligned}
\tag{21.63}
$$

Then, the total UV renormalization constant is given by

$$
\begin{aligned}
Z_B &= 1 + \delta_B^{(1)} + \delta_B^{(2)} = 1 - \left(\frac{g}{4\pi}\right)^2 \frac{2C_{A,2}C_{A,1}Y_L^2 + C_{A,2}Y_H^2 + 2C_{A,1}Y_R^2}{3\epsilon} - \\
&\quad - \left(\frac{g_1}{4\pi}\right)^4 \frac{C_{A,1}C_{A,2}Y_L^4 + C_{A,1}Y_R^4 + C_{A,2}Y_H^4}{\epsilon} - \left(\frac{g_1^2 g_w^2}{16\pi^2}\right)^2 \frac{C_{A,1}Y_L^2 + 2Y_H^2}{\epsilon} \\
&\quad - \left(\frac{g_1^2 g_s^2}{16\pi^2}\right)^2 \frac{C_{A,2}Y_L^2 + Y_R^2}{\epsilon} + \left(\frac{g_1^2 y^2}{16\pi^2}\right)^2 \frac{C_{A,1}C_{A,3}(Y_L^2 + 2Y_R^2)}{2\epsilon}.
\end{aligned}
\tag{21.64}
$$

This result is just the field renormalization of the Abelian gauge field, as we have checked explicitly by computing the corresponding off-shell two-point function. Interestingly, it has only single poles, even at two-loops. To conclude this section, we want to stress that for this calculation, we did not have to worry about disentangling UV and IR divergences at any intermediate steps. Instead, we simply computed the full divergent structure carrying it through the calculation and simply subtracting all IR poles using the factor $Z_{\text{IR}}^{\psi_R}$, which we already know from the energy-momentum matrix element. Notice also that the infrared subtraction was particularly easy because the external states are exactly the ones we used for the energy-momentum tensor, such that we did not have to worry about the combinatorics of the infrared divergences from different numbers and species of fields.

Finally, we want to mention that due to its universal character of being the field renormalization of the external gauge boson, the same result should be reproduced for any of the three matter fields. In fact, we checked this explicit by a direct computation, finding perfect agreement, which serves as yet another non-trivial cross-check of the IR divergences calculated in the previous section. For the scalar, we contracted the Lorentz index by multiplying the matrix elements with

$$
P_H^\mu = -\frac{1}{s_{12}}(p_1 - p_2)^\mu,
\tag{21.65}
$$

to project onto the respective scalar form factor. Note that this projector does not explicitly depend on the number of spacetime dimensions, simply because no traces of metrics will appear during the projection.

Chapter 22

Conclusions

In this part of the thesis, we have addressed the problem of disentangling IR and UV divergences in loop amplitudes. Of course, this can easily be done by simply using different regulators for both regimes, such that the different divergences have a different analytic form. However, in practice it is often more convenient to use the same regulator, in particular dimensional regularization, but this mixes UV and IR dynamics and from the result of a loop calculation alone it cannot be determined from which regime they arise.

We showed that conserved currents comprise a special class of operators, which, apart from a few well-understood exceptions, are UV finite, such that divergences arising in their matrix element are of infrared nature. In fact, we showed that the traceless energy-momentum tensor is always UV finite, provided we consider only theories of marginal couplings, making it a perfect candidate for studying infrared divergences in any given theory. This also presents a great opportunity for any higher loop calculation to be done, since the infrared divergences are fixed by the external states of an amplitude rather than by the details of the operators involved in the scattering. This means, if one has calculated the infrared divergences, in a given theory, for each kind of particle in the theory, using e.g., the energy momentum tensor, subtracting them from any other amplitude in the theory is trivial.

We apply this fact by calculating the infrared divergences and associated anomalous dimensions up to two loops in two toy models, which greatly differ in complexity, one containing a Dirac fermion and a real scalar with a Yukawa like coupling and a scalar quartic and the other being a miniature SM, with one left- and one right-handed quark, the Higgs and the same gauge groups as the SM. We studied the first one in great detail, also highlighting the rather modern on-shell methods to calculate the infrared anomalous dimension directly from on-shell cuts between lower-loop amplitudes. In the calculation we encounter divergences in certain phase space integrals, but we find that they are spurious and cancel if the correct one-loop renormalization of the theory is properly accounted for. In the end, we found the cancellation of all divergences as well as logarithmic terms, explicitly showing that in this simple toy model only collinear and no soft divergences arise, even at the two-loop order. In this theory, we also found a one-to-one correspondence between the on-shell cuts and the full two-loop Feynman diagrammatic approach, we used to cross-check all our results. As a further non-trivial cross-check, we used a physical approach for infrared divergences, in that they have to cancel in any physical observable, like total cross-sections. We found that, as dictated by the KLN theorem, the infrared divergences in the two-loop matrix elements are exactly such that they cancel the divergences arising from the soft and collinear regions of phase-space integrals with matrix elements with additional final states.

While being much closer to a realistic theory, our SM toy model is also much more compli-

cated due to the presence of many fields and couplings. In particular, we expect the presence of gauge field to lead to a much richer infrared divergent structure, including soft divergences. While this leaves a lot to discover, especially in the context of computing the infrared anomalous dimension in such theories using on-shell methods, we use only the standard diagrammatic approach here, leaving the development of the on-shell methods for future work. We found excellent agreement of our results with the literature, as far as they are available, like the pure QCD like sector of our model, but also augmented them with to our knowledge, so far unknown contributions, in particular terms with mixed interactions as well as effects from a scalar transforming non-trivially under a non-Abelian gauge group. The results for the cusp anomalous dimensions are shown in Eq. (21.17), Eq. (21.26) and Eq. (21.43) while the collinear anomalous dimensions of all fields are given in Eq. (21.18), Eq. (21.27), Eq. (21.34), Eq. (21.44), Eq. (21.50) and Eq. (21.57).

Looking ahead, not only can these results be used, as mentioned, whenever the higher loop running of operators or couplings needs to be computed, the presented method in general can be straightforwardly applied to any theory that comes to mind. While we leave all these applications for future investigation, we want to propose a few potential directions. The first, and probably phenomenologically most interesting, is the computation of the loop running of higher-dimensional operators, as the ones in the SMEFT, which will provide the theoretical precision needed to match current and especially future experiments. Second, the UV finiteness of conserved currents is only given under certain assumptions, like the absence of gauge fields for spin-1 currents, or the limitation to only marginal couplings for the energy-momentum tensor. Using the methods presented in this part of the thesis, the renormalization of currents can be performed in a general setting, by simply subtracting the known IR structure. This has already been started in this thesis, by renormalizing the current associated to the Abelian gauge symmetry of our SM toy model, confirming the result expected from general considerations. However, it would be interesting to use this also directly for the energy-momentum tensor if a propagating graviton is included in the theory.

Appendices part IV

IV.A All Order Form Factor for the SM Toy Model

In this appendix, we gather all the one-loop form factors needed for the computation of the infrared divergences presented in 21. We chose to present them as all order expression in ϵ by giving them in terms of the scalar one-loop basis integrals 21.5. Using a slight abuse of notation, we do only present the one-loop piece, ignoring the tree-level part and the multiplied infrared renormalization constant. They are

$$T_G^{(1)} = -\left(\frac{g_s}{4\pi}\right)^2 \left[\frac{(C_{A,2} - 1)(4\epsilon^2 - 9\epsilon + 4) - 4C_{A,1}(2\epsilon^4 + 6\epsilon^2 - 23\epsilon + 11)}{2(\epsilon - 1)(2\epsilon - 3)(3\epsilon - 2)} B_0(p^2) \right.$$
$$\left. + 2C_{A,3}\ p^2 C_0(p^2) \right], \tag{IV.A.1}$$

$$T_W^{(1)} = -\left(\frac{g_w}{4\pi}\right)^2 \left[\frac{4C_{A,2}\left(2\epsilon^4 + 6\epsilon^2 - 23\epsilon + 11\right)}{2(\epsilon - 1)(2\epsilon - 3)(3\epsilon - 2)} B_0(p^2) \right.$$
$$- \frac{C_{A,1}\left(4\epsilon^2 - 9\epsilon + 4\right) + 4\epsilon^3 + 4\epsilon^2 - 4\epsilon + 2}{2(\epsilon - 1)(2\epsilon - 3)(3\epsilon - 2)} B_0(p^2) \tag{IV.A.2}$$
$$\left. + 2C_{A,3}\ p^2 C_0(p^2) \right],$$

$$T_B^{(1)} = -\left(\frac{g_1}{4\pi}\right)^2 \left[\frac{C_{A,1}(C_{A,2}Y_L^2 + Y_R^2)\left(4\epsilon^2 - 9\epsilon + 4\right)}{2(\epsilon - 1)(2\epsilon - 3)(3\epsilon - 2)} \right.$$
$$\left. + \frac{C_{A,2}Y_H^2\left(4\epsilon^3 - 4\epsilon^2 - 4\epsilon + 2\right)}{2(\epsilon - 1)(2\epsilon - 3)(3\epsilon - 2)}\right] B_0(p^2), \tag{IV.A.3}$$

$$T_{\psi_L}^{(1)} = \left[C_{F,1}\left(\frac{g_s}{4\pi}\right)^2 + C_{F,2}\left(\frac{g_w}{4\pi}\right)^2 + Y_L^2\left(\frac{g_1}{4\pi}\right)^2\right] \times$$
$$\left[\frac{\epsilon + 3}{\epsilon - 1} B_0(p^2) - 2p^2 C_0(p_2)\right] - \left(\frac{y}{4\pi}\right)^2 \frac{B_0(p^2)}{2(\epsilon - 1)}, \tag{IV.A.4}$$

$$T_{\psi_R}^{(1)} = \left[C_{F,1}\left(\frac{g_s}{4\pi}\right)^2 + Y_R^2\left(\frac{g_1}{4\pi}\right)^2\right]\left[\frac{\epsilon + 3}{\epsilon - 1} B_0(p^2) - 2p^2 C_0(p_2)\right] - \left(\frac{y}{4\pi}\right)^2 \frac{B_0(p^2)}{2(\epsilon - 1)}, \tag{IV.A.5}$$

$$T_H^{(1)} = \left[C_{F,2}\left(\frac{g_w}{4\pi}\right)^2 + Y_H^2\left(\frac{g_1}{4\pi}\right)^2\right]\left[\frac{4B_0(p^2)}{\epsilon - 1} - 2p^2 C_0(p_2)\right] - \left(\frac{y}{4\pi}\right)^2 \frac{C_{A,1}B_0(p^2)}{(\epsilon - 1)}. \tag{IV.A.6}$$

IV.B   Loop Integral Reduction

In general, Feynman integrals are complicated functions of momenta, which we can write, at any loop order L, to be of the form

$$\int \prod_{l=1}^{L} d^D k_l \; \frac{S_1^{a_1} \cdots S_n^{a_n}}{D_1^{b_1} \cdots D_m^{b_m}}, \tag{IV.B.1}$$

where S_i and D_i denote scalar products of momenta and propagators, respectively, and both can depend on external and loop momenta. Evaluating them in this form turns out to be a complicated task, so it will be beneficial to find ways of simplifying them.

A large complication arises from the non-trivial numerator. However, we have to realize that the denominator, i.e., the propagators are just linear combinations of momenta and masses. This allows to express the numerator in terms of propagators, cancelling those already present or introducing new ones,

$$S_i = S_i(\{D_i\}), \tag{IV.B.2}$$

so we can always turn a loop integral into one containing only (possibly non-positive) powers of propagators and no additional scalar products,

$$I = \int \prod_{l=1}^{L} d^D k_l \; \frac{1}{D_1^{b_1} \cdots D_m^{b_m}}. \tag{IV.B.3}$$

Even though scalar integrals are already easier to evaluate than their tensorial counterparts, we can still try to simplify them even further. In fact, not all scalar integrals are linearly independent, and one possibility to generate relations among them is to use so-called IBP identities. To derive them, we use the fact that Feynman integrals are convergent in D dimensions, such that the integrands vanish at the boundaries and so it directly follows that, using integration by parts on the integrand,

$$\int \prod_{l=1}^{L} d^D k_l \; \frac{\partial}{\partial k_\mu} \left(\frac{v_\mu}{D_1^{b_1} \cdots D_m^{b_m}} \right) = 0, \tag{IV.B.4}$$

with v_μ either a loop or external momentum.

This allows us to relate different scalar Feynman integrals already at the integrand level, with the hope that we generate ones that can be evaluated more easily. To demonstrate this explicitly, we show the easiest example of one-loop tadpole integrals,

$$I(n) = \int d^D k \; \frac{v_\mu}{(k^2 + m^2)^n}, \tag{IV.B.5}$$

where we used a massive propagator, such that the integral is not scaleless and vanishes, and we already performed a Wick rotation. Then, choosing $v_\mu = k_\mu$ the IBP identity reads

$$\int d^D k \; \frac{\partial}{\partial k_\mu} \left(\frac{k_\mu}{(k^2 + m^2)^n} \right) = 0. \tag{IV.B.6}$$

Using the derivatives

$$\frac{\partial}{\partial k_\mu} k_\mu = D, \quad \frac{\partial}{\partial k_\mu} \frac{1}{(k^2 + m^2)^n} = -\frac{-2n}{(k^2 + m^2)^{n+1}} k_\mu, \tag{IV.B.7}$$

as well as the relation

$$\frac{k^2}{(k^2+m^2)^{n+1}} = \frac{1}{(k^2+m^2)^n} - \frac{m^2}{(k^2+m^2)^{n+1}}, \tag{IV.B.8}$$

we find

$$\int d^D k \, \frac{\partial}{\partial k_\mu} \left(\frac{k_\mu}{(k^2+m^2)^n} \right) = \int d^D k \, \frac{D-2n}{(k^2+m^2)^n} + \frac{2nm^2}{(k^2+m^2)^{n+1}} = 0. \tag{IV.B.9}$$

But the two terms in the integrand are again just tadpole integrals, but with different exponents, such that we find the recursion relation

$$I(n+1) = \frac{2n-D}{2nm^2} I(n), \tag{IV.B.10}$$

which allows us to calculate any tadpole integral in terms of the $n = 1$ case, which is the easiest to evaluate.

While the one-loop tadpole integrals can easily be evaluated using the standard methods like the Feynman parameterization for any n, the above procedure works equivalently for any number of propagators at any loop order.

Another set of relations can be derived by imposing Lorentz invariance. Scalar integrals being scalar have to be invariant under any Lorentz transformation of the E external momenta

$$p^\mu \to p^\mu + \delta p^\mu = p^\mu + \delta\epsilon_\nu^\mu p^\mu, \tag{IV.B.11}$$

where $\delta\epsilon_\nu^\mu$ represents the infinitesimal generators of the Lorentz group.

$$I(p_i + \delta p_i) = I(p_i) + \delta\epsilon_\nu^\mu \sum_{j=1}^{E} p_j^\nu \frac{\partial}{\partial p_j^\mu} I(p_i) \stackrel{!}{=} I(p_i), \tag{IV.B.12}$$

such that

$$\sum_{j=1}^{E} \left(p_j^\nu \frac{\partial}{\partial p_j^\mu} - p_j^\mu \frac{\partial}{\partial p_j^\nu} \right) I(p_i) \stackrel{!}{=} 0, \tag{IV.B.13}$$

where we used the fact that $\delta\epsilon_\nu^\mu$ is antisymmetric. Because the integration in $I(p_i)$ is independent of the external momenta, we can let the derivatives act directly on the integrand, just like for the IBP identities. To obtain scalar relations, the above equation can be projected using antisymmetric combinations of the external momenta, e.g., for calculating the renormalization of the energy-momentum tensor we have two independent external momenta from which we can construct a single antisymmetric combination such that there exists a single Lorentz-invariance relation.

While it can be shown, that Lorentz-invariance and IBP identities are not linearly independent, using both in unison can help to find all integral relations, as is implemented in the computer program `Kira` [296].

IV.C Derivations of Important Formulas

IV.C.1 Imaginary Part of Logarithms and their Derivatives

Provided the generic complex logarithm of the form

$$\log\left(-\frac{s_i}{\mu^2}\right) \equiv \log\left(\frac{s_i}{\mu^2}\right) + ik\pi, \quad s_i > 0, \ \ k \in \mathbb{Z}, \tag{IV.C.1}$$

we want to prove the relation between the imaginary part of an arbitrary power of the logarithm and a series of its derivatives,

$$2\mathrm{Im}\left[\log^n\left(-\frac{s_i}{\mu^2}\right)\right] = i\left(e^{ik\pi\mu\partial_\mu} - 1\right)\log^n\left(-\frac{s_i}{\mu^2}\right), \tag{IV.C.2}$$

which gives Eq. (17.14) for the choice $k = -1$.

We start by using the series expression of the exponential function,

$$\left(e^{ik\pi\mu\partial_\mu} - 1\right)\log^n\left(-\frac{s_i}{\mu^2}\right) = \left[\sum_{j=1}^n \frac{(ki\pi)^j}{j!}(\mu\partial_\mu)^j\right]\log^n\left(-\frac{s_i}{\mu^2}\right), \tag{IV.C.3}$$

where we already used the fact that applying the derivative more than n times trivially gives zero.

We then define $-2x \equiv \log(-s_i/\mu^2)$ such that the derivative is just $\mu\partial_\mu = \partial_x$. This very much simplifies taking the derivatives and we find

$$\left[\sum_{j=1}^n \frac{(ik\pi)^j}{j!}(\mu\partial_\mu)^j\right]\log^n\left(-\frac{s_i}{\mu^2}\right) = (-2)^n \sum_{j=1}^n \frac{n!}{j!(n-j)!}(ik\pi)^j x^{n-j}. \tag{IV.C.4}$$

Using the definition of the binomial coefficient, we can identify the above sum as the binomial sum, up to the fact that our sum starts at $j = 1$ instead of $j = 0$. However, we can trivially recover the binomial sum by just adding and subtracting the $j = 0$ term such that

$$(-2)^n \sum_{j=1}^n \frac{n!}{j!(n-j)!}(ik\pi)^j x^{n-j} = \left(\log^n\left(\frac{s}{\mu^2}\right) + ik\pi\right)^n - \left(\log\left(\frac{s}{\mu^2}\right) - ik\pi\right)^n$$
$$= \left(\log^n\left(-\frac{s}{\mu^2}\right)\right)^* - \log^n\left(-\frac{s}{\mu^2}\right), \tag{IV.C.5}$$

where in the last line we used Eq. (IV.C.1) for the logarithm and its complex conjugate. This concludes the proof of Eq. (17.14), as can be easily seen by plugging the above result back in and using the definition of the imaginary part.

Given a choice of branch, it is clear from Eq. (IV.C.1) that the analogous relation for the complex conjugate logarithm can be obtained by just setting $k \to -k$.

IV.C.2 Loop Parameterization and Phase Space Integrals

We start by expressing the integral over the phase space of two particles as an integral over only angular variables. We will work in arbitrary D dimensions and we will assume one of the two particles to be massive. This will be useful for the computation of the three-particle phase space later, and the massless limit can be taken straightforwardly in the end.

We start with the expression

$$\int \mathrm{dLIPS}_2^{(D)} = \int d^D p_1 d^D p_2 \delta^D(P - p_1 - p_2)\delta^+(p_1^2 - m^2)\delta^+(p_2^2), \tag{IV.C.6}$$

where for now we ignored factors of (2π), which we will reconstruct in the final result. P is the momentum that is injected into the $\{p_1, p_2\}$ system; for $2 \to 2$ scattering, it would correspond to the total momentum of the initial states.

Then, using

$$\delta^+(p_1^2 - m^2) = \frac{1}{2E_1}\delta(p_1^0 - E_1), \tag{IV.C.7}$$

with the usual relation $E_1^2 = \boldsymbol{p}^2 + m^2$. We use this to evaluate the integral over the temporal component of p_1,

$$\int \mathrm{dLIPS}_2^{(D)} = \int \frac{d^{D-1}\boldsymbol{p}_1}{2E_1}\delta^+((P - p_1)^2), \tag{IV.C.8}$$

where we also used the overall momentum conserving delta function to get rid of the integration over p_2. Expanding the argument of the delta function and expressing the integral over spatial components in D-dimensional spherical coordinates, we arrive at

$$\int \mathrm{dLIPS}_2^{(D)} = \int d\Omega_{D-1}dp_1 \frac{p_1^{D-2}}{2E_1}\delta^+\left(P^2 + m^2 - 2\sqrt{P^2}\sqrt{p_1^2 + m^2}\right), \tag{IV.C.9}$$

where in a slight abuse of notation we will denote the absolute value of $\boldsymbol{p}_1$ with just p_1 in the rest of this calculation. To get to this form of the argument in the delta function, we also assumed the rest frame of P. The differential solid angle is given by

$$d\Omega_D = \prod_{i=0}^{D-2} \sin^i(\phi_{i+1})d\phi_{i+1}, \tag{IV.C.10}$$

with the azimuthal angle $0 \leq \phi_1 \leq 2\pi$ and polar angles $0 \leq \phi_{i>1} \leq \pi$. Integrating this expression gives the surface area of a D-dimensional unit ball,

$$\Omega_D = \int d\Omega_D = \frac{2\pi^{d/2}}{\Gamma(d/2)}. \tag{IV.C.11}$$

From the definition of the differential solid angle, it is clear that we can factor out the integration over the lower-dimensional sphere surface, keeping only the integrals of high dimensional ones. Then, after simplifying the delta function as

$$\delta^+\left(P^2 + m^2 - 2\sqrt{P^2}\sqrt{p_1^2 + m^2}\right) = \frac{\sqrt{q^2 + m^2}}{2\sqrt{P^2}q}\delta(p_1 - q), \quad q = \frac{P^2 - m^2}{2\sqrt{P^2}}, \tag{IV.C.12}$$

and after reconstructing the appropriate factors of (2π), we arrive at our final expression:

$$\int \mathrm{dLIPS}_2^{(D)} = \frac{4^{2-D}\sqrt{\pi}^{1-D}}{\Gamma(\frac{D-3}{2})} \frac{1}{\sqrt{P^2}} \left(\frac{P^2 - m^2}{\sqrt{P^2}}\right)^{D-3} \int d\phi d\theta \ \sin^{D-3}\theta \sin^{D-4}\phi. \tag{IV.C.13}$$

We already suggestively renamed the angular variables and, in fact, in the limit $D \to 4$ we recover the usual integral over angles in spherical coordinates,

$$\int \mathrm{dLIPS}_2 = \frac{1}{32\pi^2} \frac{P^2 - m^2}{P^2} \int_0^{2\pi} \int_0^\pi d\theta \sin\theta = \frac{1}{8\pi^2} \frac{P^2 - m^2}{P^2} \int_0^{2\pi} \int_0^{\frac{\pi}{2}} d\theta \cos\theta \sin\theta. \tag{IV.C.14}$$

Note that an additional factor of $1/2$ has to be included in the $D \to 4$ limit to compensate for the fact that in this limit ϕ becomes the azimuthal angle and therefore has to be integrated up to 2π instead of just π. In the last equality we changed variables as $\theta \to \theta/2$ and used the relevant double angle identity. The $m \to 0$ limit of the above phase space integral exactly reproduces Eq. (17.23), corresponding to the rotation of loop momentum spinors given in Eq. (17.24).

The reason we kept one of the momenta to be massive is that this way we can reuse the result to easily calculate the three-particle phase space. First, we need to realize that the three-particle phase space can be simplified by factoring into two two-particle phase space factors, one of two massless and one of one massless and one massive momentum, as well as an integral over the energy at which the separation of the two factors takes place. Operationally, this can be achieved by inserting factors of unity in the right form at the correct places. We will show this explicitly now. Again, we will ignore factors of (2π) for now and reconstruct them only at the end of the calculation.

We start with

$$
\begin{aligned}
\int \mathrm{dLIPS}_3^{(D)} &= \int d^D p_1 d^D p_2 d^D p_3 \; \delta^D(P - p_1 - p_2 - p_3) \prod_{i=1}^3 \delta^+(p_i^2) \\
&= \int d^D p_1 d^D p_2 d^D p_3 \int d^D q \; \delta^{(D)}(q - p_1 - p_2) \delta^D(P - q - p_3) \prod_{i=1}^3 \delta^+(p_i^2),
\end{aligned}
\tag{IV.C.15}
$$

where we introduced the momentum q with the additional constraint $q = p_1 + p_2$. Collecting all terms containing p_1 or p_2, we see that they form an integral like in Eq. (IV.C.6) with $P \to q$ and $m \to 0$, while the remaining terms do not allow for such an identification yet, since q is not constrained to be on-shell so far. We can, however, introduce such a constraint at the cost of also introducing one more integration variable like

$$
\int \mathrm{dLIPS}_3^{(D)} = \int_0^{P^2} ds_{12} \int \mathrm{dLIPS}_{(1;2)}^{(D)} \mathrm{dLIPS}_{(12;3)}^{(D)},
\tag{IV.C.16}
$$

where we defined

$$
\begin{aligned}
\mathrm{dLIPS}_{(1;2)}^{(D)} &= d^D p_1 d^D p_2 \; \delta^D(q - p_1 - p_2) \delta^+(p_1^2) \delta^+(p_2^2), \\
\mathrm{dLIPS}_{(12;3)}^{(D)} &= d^D q \, d^D p_3 \; \delta^D(P - q - p_2) \delta^+(q^2 - s_{12}) \delta^+(p_3^2).
\end{aligned}
\tag{IV.C.17}
$$

We also already used that even though, formally, s_{12} has to be integrated over the entire real axis, the momentum conserving delta function forces it to lie in the interval $[0, P^2]$.

Before we continue, a few comments are in order. First, we note that this factorization of the phase space has a clear physical interpretation. If we interpret P as the momentum of a massive particle, we can treat it as decaying, in its rest frame, into an on-shell, massless particle characterized by p_3, as well as an intermediate, off-shell particle with momentum q. The way the energy is distributed among p_3 and q is governed by s_{12}. Then, because of Lorentz invariance, we can boost ourselves into the rest frame of q, where it further decays into two massless particles with momenta p_1 and p_2. To capture all possible ways this two-step decay can happen, we have to integrate over all possible ways to distribute P in the first decay, i.e., we integrate over s_{12}. This also explains the integration boundaries. If p_3 inherits all of P then nothing is left over for q and therefore $s_{12} = 0$ and vice versa in the case of $s_{12} = P^2$. Second, the procedure of dividing the n-particle phase space into phase spaces with lower phase spaces can straightforwardly be

generalized to any n. E.g, the four-particle phase space can be factored into a three- and a two-particle, which can be further decomposed into only two-particle expressions.

Using Eq. (IV.C.13) and reconstructing all factors of (2π) we finally arrive at

$$
\begin{aligned}
\int \mathrm{dLIPS}_3^{(D)} =& \frac{2^{7-4D}\pi^{-D}}{\Gamma(\frac{D-3}{2})^2}(P^2)^{D-3}\int_0^1 d\lambda \; \lambda^{D/2-2}(1-\lambda)^{D-3} \\
& \times \int_0^\pi d\theta d\phi \; \sin^{D-3}\theta \sin^{D-4}\phi \int_0^\pi d\theta' d\phi' \; \sin^{D-3}\theta' \sin^{D-4}\phi',
\end{aligned}
\tag{IV.C.18}
$$

where (θ, ϕ) and (θ', ϕ') are the angles between p_1 and p_2, as well as between $(p_1 + p_2)$ and p_3, respectively. In addition, we changed the variables from s_{12} to the dimensionless variable λ, defined as

$$
\lambda = \frac{s_{12}}{P^2}.
\tag{IV.C.19}
$$

In the limit $D \to 4$, this reduces to

$$
\int \mathrm{dLIPS}_3 = \frac{P^2}{2048\pi^5}\int_0^1 d\lambda \; (1-\lambda)\int_0^{2\pi} d\phi d\phi' \int_0^\pi d\theta d\theta' \; \sin\theta \sin\theta',
\tag{IV.C.20}
$$

where we included an additional factor of $1/2$ for both ϕ and ϕ' for the same reason as in Eq. (IV.C.14).

IV.D   Projection Procedure for $T_{\mu\nu}$

In this appendix, we show how to effectively project onto the scalar form factors in Eq. (20.3). We will treat each case of external states separately:

Scalars:

For external scalars, no polarization vectors or spinors are necessary, such that the energy-momentum tensor can be written purely in terms of momenta and we can write, using the decomposition Eq. (20.3),

$$
\mathcal{S}_{\mu\nu} = T_{2,i}(s_{12}) \; T_{\mu\nu,2}(1_\phi, 2_\phi) + T_{0,i}(s_{12}^2) \; T_{\mu\nu,0}(1_\phi, 2_\phi),
\tag{IV.D.1}
$$

where $\mathcal{S}_{\mu\nu}$ is an a priori general tensor built from only momenta and scalar products. In practice, it will be a linear combination of some tensor loop integrals.

Requiring symmetry in the Lorentz indices and the mass dimension of the energy-momentum tensor, we can find explicit expressions for the $J = 2$ and $J = 0$ pieces,

$$
\begin{aligned}
T_{\mu\nu,2}(1_\phi, 2_\phi) =& \; p_{1\mu}p_{2\nu} - \frac{1}{4}g_{\mu\nu} \; s_{12} + \frac{D-2}{2(D-1)}\left(\frac{1}{2}g_{\mu\nu} \; s_{12} - p_{1\mu}p_{2\nu} - p_{1\mu}p_{1\nu}\right) + (p_1 \leftrightarrow p_2), \\
T_{\mu\nu,0}(1_\phi, 2_\phi) =& \; -\frac{D-2}{2(D-1)}\left(\frac{1}{2}g_{\mu\nu} \; s_{12} - p_{1\mu}p_{2\nu} - p_{1\mu}p_{1\nu}\right) + (p_1 \leftrightarrow p_2).
\end{aligned}
\tag{IV.D.2}
$$

Note that the $J = 0$ piece, or in other words the trace, is precisely the one generated by the additional conformal coupling term in Eq. (20.1) and it is precisely what is subtracted from the minimal coupling piece to get the traceless $J = 2$ part. Then, we define some projectors $P_{\mu\nu}^{(i)}$

$$P^{(2)}_{\phi,\mu\nu} = 4\frac{D-1}{(D-2)s_{12}^2}\,T_{\mu\nu,2}(1_\phi, 2_\phi), \qquad P^{(0)}_{\phi,\mu\nu} = 4\frac{D-1}{(D-2)^2 s_{12}^2}\,T_{\mu\nu,0}(1_\phi, 2_\phi), \qquad \text{(IV.D.3)}$$

such that the scalar form factors can easily be obtained by projecting with

$$T_{i,0}(s_{12}) = P^{(i)}_{\phi,\mu\nu}\,\mathcal{S}^{\mu\nu}. \qquad \text{(IV.D.4)}$$

Fermions:

We start by discussing the case of a left-handed fermion with its anti-particle as an external state. The right-handed fermion can then be readily obtained from it. Again, using the symmetry of the energy-momentum tensor and the fixed mass dimension, we find that in general

$$T_{\mu\nu}(1_{\psi_L}, 2_{\bar{\psi}_L}) = \bar{v}(p_2)\mathcal{F}_{\mu\nu}u(p_1) = T_{2,-1}(s_{12})\left[(p_1 - p_2)_\mu \bar{v}(p_2)\gamma_\nu P_L u(p_1) + (\mu \leftrightarrow \nu)\right]. \qquad \text{(IV.D.5)}$$

Note that this is already traceless after using the Dirac equation, so there is no $J = 0$ piece for fermions. To extract the scalar form factor, we use an approach analogous to the projection of the QED vertex function. To do so, we multiply the above equation by complex conjugate spinors, sum over spins and trace over fermion indices. In the end, we find

$$T_{2,-1}(s_{12}) = \frac{4}{(D-2)s_{12}^2}(p_1 - p_2)^\mu\,\text{Tr}\left[\gamma^\nu \slashed{p}_2 \mathcal{F}_{\mu\nu} P_L \slashed{p}_1\right]. \qquad \text{(IV.D.6)}$$

Notice that the prefactor depends on the number of space-time dimensions to cancel the dependence arising from the fermion trace. For the right-handed fermion, the projection procedure is the same after replacing the helicity projector accordingly.

Vectors:

For external vector bosons, we do not distinguish between the different helicity states, as these correspond to the same particle and therefore the two helicity states couple in the same way. This is not the case for fermions, where left- and right-handed fermions are entirely different particles, that can couple differently to other particles. Using the same arguments as before, we can write

$$\begin{aligned}
T_{\mu\nu}(1_V, 2_V) &= \epsilon^\alpha(p_1)\epsilon^\beta(p_2)\mathcal{V}_{\mu\nu\alpha\beta} \\
&= T_{2,2}(s_{12})\epsilon^\alpha(p_1)\epsilon^\beta(p_2)\Big[\frac{1}{2}s_{12}\left(g_{\mu\alpha}g_{\nu\beta} + g_{\mu\beta}g_{\nu\alpha} - g_{\mu\nu}g_{\alpha\beta}\right) \\
&\qquad + p_{1\nu}(p_{2\mu}g_{\alpha\beta} - p_{2\alpha}g_{\mu\beta}) + p_{1\mu}(p_{2\nu}g_{\alpha\beta} - p_{2\alpha}g_{\nu\beta}) \qquad \text{(IV.D.7)} \\
&\qquad + p_{1\beta}(p_{2\alpha}g_{\mu\nu} - p_{2\nu}g_{\mu\alpha} - p_{2\mu}g_{\alpha\nu}) \\
&\equiv T_{2,2}(s_{12})\epsilon^\alpha(p_1)\epsilon^\beta(p_2)T_{\mu\nu\alpha\beta}\Big].
\end{aligned}$$

Again, this is traceless on its own, indicating the absence of a $J = 0$ term. Then, to extract the scalar form factor, it is enough to focus only on the four index tensor, which, as in the scalar case, are built from only scalar products and momenta. Then, a suitable projection is

$$T_{2,2}(s_{12}) = \frac{4}{3D^2 - 14D + 16}T_{\mu\nu\alpha\beta}\mathcal{V}^{\mu\nu\alpha\beta} \qquad \text{(IV.D.8)}$$

Part V

Conclusions

Despite irrefutable observations that cannot be explained by the Standard Model, signalling its incompleteness, physics beyond it has yet to be discovered. As already mentioned in the introduction, there exist hints at for new physics at various scales, and not only at those scales inaccessible to current experiments. In this thesis, we chose three benchmark experiments at vastly different energy scales and investigated their potential for probing physics beyond the SM: Starting at high energies, we explored the phenomenology of CH models in the limit of a fully composite, right-handed top quark at both current and future colliders in a model-independent EFT approach. Continuing down the energy ladder, we investigated, again in an EFT approach, how CP-violating new physics can generate contributions to the EDMs of the neutron and leptons both at tree level and beyond. In particular, we performed the full 1-loop computation in the second part. In the third part, we arrived at the lowest scale considered in this thesis, where we used the non-relativistic torsion balance experiment to constrain massive higher-spin fields coupling directly to matter. Finally, we presented a method to efficiently extract IR divergences at high loops in massless theories in the fourth part, by exploiting the non-renormalization property of conserved current.

In part I we studied generic CH models that feature partial compositeness, such that not only the Higgs, but potentially also the fermions are composite states. In fact, the degree of compositeness, or equivalently the mixing angle between the elementary fermions and the massive resonances from the new strong sector, is closely related to the measured fermion mass or Yukawa coupling. Further, we took the left- and right-handed chiralities of the fermions to carry different degrees of compositeness, which are, however, not unrelated as their product has to reproduce the Yukawa coupling, modulo a factor of the new strong coupling. In particular, we assume that, due to its large mass compared to all other fermions, only the top quark contains a significant admixture of the composite resonances, while all other fermions are taken to be practically elementary. Further, we assume that the the right-handed top quark is fully composite, leaving its left-handed counterpart only the minimal degree of compositeness, as this is favored by fine-tuning arguments.

Because, eventually, we wanted to rely on the least number of assumptions on the CH model itself, we adopted the EFT point of view, where integrating out the massive resonances generates many higher-dimensional operators built from SM states. Performing naive dimensional analysis, the relative expected size of these operators can be estimated, such that the dominant operators in a given process can easily be determined. While the sizes of operators containing fermions depend on the respective mixing angles, in the limit of a fully composite right-handed top quark we find that one of the most dominant for strong couplings is a four-fermion operator of the form $O_{tt} = (\bar{t}_R \gamma_\mu t_R)(\bar{t}_R \gamma_\mu t_R)$. While this is not the only operator with its scaling with the strong coupling and resonance mass, g_* and m_*, all but a four-Higgs operator either experience inferior experimental sensitivities or their power counting estimates have to be corrected by additional loop factors for most realistic models.

Then, we started chapter 3 by focussing on the production of four top quarks at hadron colliders, from which we set constraints on the $g_* - m_*$ plane. We find that already at the LHC, the scale suppressing the four-top operator has to be $\Lambda/\sqrt{|c_{tt}|} > 0.73\,\text{TeV}$, compatible with the value coming from Higgs measurements constraining the aforementioned four-Higgs operator. Taking this as an exciting glance at the potential reach of four top operators at hadron colliders, we performed realistic analyses of the four-top production process at the FCC-hh, mainly leptonic decay channels. Because of the strong energy growth of the top scattering induced by O_{tt}, we expect a great improvement at the 100 TeV collider compared with the LHC, if we appropriately focus the analysis on high-energy events. Indeed, these expectations were satisfied and we find $\Lambda/\sqrt{|c_{tt}|} > 6.5\,\text{TeV}$, increasing the reach of the LHC by an order of

magnitude and providing a superior probe of the relevant parameter space compared to the Higgs measurements at the same collider and even including the leptonic phase of the FCC. Further, we found that, against expectations, even future lepton colliders show a significant reach into the CH parameter space, even though four-top production at such machines is kinematically disfavored if not completely forbidden. Instead, O_{tt} enters the top pair-production process through its RG mixing with semi-leptonic four fermion operators and due to its power counting size, this contribution dominates over the tree level one despite it being only a one-loop effect. Further, in accordance with the energy growth of the operator, we find that the highest-energy runs of the respective colliders give the highest sensitivity, e.g., at a CLIC-like collider we find $\Lambda/\sqrt{|c_{tt}|} > 7.7\,\mathrm{TeV}$.

But even though these results look very promising, we believe that they can still be improved and there is much still to be learned. For instance, we focused mainly on the leptonic decay channels of the four-top system, but the fully hadronic final state might offer unique chances for discovery as well. On the one hand, it has the largest branching ratios of all the decay channels of the four tops, but due to the high multiplicities of jets and other particles, it is also a very busy one. Nevertheless, this can also be of an advantage, since there are very few other SM processes that can generate this many particles in the final state, making a targeted study of the fully hadronic signature worthwhile, also with the growing popularity of machine learning methods for high-energy applications. Finally, we want to mention that the analysis presented in the first part of this thesis does not rely directly on the helicity of the top quarks, but only on their high-energy behavior such that in principle the same constraint on the scale of the operator with left-handed quarks would have been obtained. So one way to further improve the bounds is to incorporate the condition of chirality into the analysis itself, in principle allowing for a significant reduction of the non-four-top background processes.

In part II we decreased the energy of interest all the way down to the mass of the electron, at which its electric moment is measured. Because EDMs in general are CP violating and possess only tiny SM backgrounds, they pose as an excellent point to look for new physics. In chapter 8 we performed the full 1-loop calculation of both lepton as well as the neutron EDM in the dimension-6 Warsaw basis of the SMEFT. Apart from showing the conceptual details of the theory, such as removing the appearing redundant operators with the appropriate field redefinitions, our main focus lies on the completeness of the result, i.e., also keeping all the terms beyond the RG logarithms, which have not been considered in the previous literature. We found that by including these not only rational but also non-rational, but finite and renormalization scale independent, contributions, we can set constraints on operator coefficients through the dipole, which are not seen by only their RG mixing. Further, assuming that the scale at which new physics has to set in is ~ 5 TeV, the bounds on operators which do not contribute already at tree level are changed by $10 - 20\%$.

Then, in part III, we arrive at the final destination of our journey through the energy ranges, the non-relativistic torsion balance experiments. However, before we get to those, we discuss general features of the gravitational EFT that contains higher dimensional operators built only from Riemann tensors on top of the leading term corresponding to the classical theory of GR. Up to dimension eight and with up to four Riemann structures, this EFT generates contributions to both the triple-graviton vertex as well as the four-graviton scattering amplitude. Further, we showed, how a tower of massive new fields with increasing spin $S > 2$ can be used to generate an gravitational EFT by integrating out these massive fields, already at tree level in the four-graviton amplitude. By explicitly performing the matching onto the EFT we find that only operators with at least four Riemann tensors are generated, while the cubic operator does not acquire any contributions. Having explicit expressions for the EFT coefficients in terms of the

higher-spin couplings and masses, we directly plug them into the causality constraints they have to obey [258]. We find that the lowest-spin field trivially satisfies a positivity constraint, while higher-spin parameters can be related to this lowest-spin one using other bounds.

Next, we investigated how this tower of higher-spin particles can be used to cure the bad high-energy behavior of the four-graviton scattering in the presence of higher-dimensional modifications of the triple-graviton vertex [244]. We explicitly took the $m_S \to 0$ limit, which is equivalent to the high-energy limit, and matched the relevant structure of Mandelstam invariant to the one generated by an R^3 insertion. Indeed, we found a closed form for a certain class of terms in the amplitude with vanishing total helicity, collecting contributions from all spins in the infinite tower of states, see Eq. (12.38). Using this expression, we straightforwardly found an infinite set of equations, which both relates the Wilson coefficient of the cubic operator to a linear combination of the couplings and masses of all particles with an even spin, as well as these parameters with each other by requiring the cancellation of the acausal high-energy behavior of R^3 and spurious higher-order terms individually. However, we think that it is worthwhile to investigate further the complete structure of Eq. (12.37), as this would allow us to map out the full pattern of relations between all the infinite degrees of freedom in the tower of states with $S > 4$. Further, an analogous study of the remaining two inequivalent helicity configurations of the four gravitons has yet to be performed. We have also seen that precisely specifying the UV limit is crucial, as the naive $E \to \infty$ would imply a vanishing of all higher spin couplings.

Finally, we turned to probing these higher-spin particles at extremely low energies using a torsion balance experiment, looking for deviations from the Newtonian potential. To do so, we modelled the experimental test masses as massive neutral scalars, interacting through an exchange of a massive higher-spin particle. We obtained the scattering amplitude in the t-channel in a closed form for an arbitrary exchanged spin, from which we found a Yukawa-like interaction potential by Fourier-transforming the amplitude into position space. While we are confident in our result, as it reproduces the relevant results in the literature on massive on-shell amplitudes, there is still some discrepancy with the known potentials for explicit values of S. While we believe the source of these differences to lie in the prescription chosen for the symmetrization of the little group indices appearing in calculations with massive spinor helicity variables, showing this explicitly is left for future work. Nevertheless, we use our result for the potential to constrain the new fields, which can trivially done by comparing with experimental results due to the analytic form of the potential. While the quantitative results presented might change based on the resolution of the aforementioned discrepancy, we believe that the qualitative statements remain largely unchanged. We found that for an increasing value of S the bound becomes both weaker and the features of the boundary of the exclusion region get flattened out more and more. While the latter is true for any S, the former is only true up to a maximum S, which we find is around $S \sim 100$, at which point the growth of the combinatorial factors in the potential overtake the suppression with a growing power of the scale, such that the constraints become stronger again.

In the final part, part IV, we stepped away from experimental probes at different scales and introduced a method to effectively calculate infrared divergences and the accompanying anomalous dimensions in massless theories. What allows us to do so is the fact that conserved currents do not get UV-renormalized apart from a few exceptions in the presence of identically conserved counterterms for scalar and gauge theories, as shown in chapter 19. But to start this part, we first used the optical theorem in chapter 17 to show how the renormalization of amplitudes can be performed by using on-shell cuts or equivalently the imaginary part of the amplitude itself. We also explicitly applied the method up to two loops, showing various ways of parameterizing the appearing phase space integrals to simplify the calculation as far as possible.

We then presented the calculation in two different toy models, vastly varying in complexity, highlighting the various aspects of the computation.

In chapter 20, we considered a simple theory of a neutral scalar with both a quartic self-coupling as well as a Yukawa-like coupling to a Dirac fermion. We first employed the on-shell approach to directly calculate the infrared anomalous dimension from on-shell cuts of two-loop matrix elements of the energy-momentum tensor. We found that while most of the phase-space integrals were straightforward to evaluate and gave finite results, another subset of diagrams was divergent in four dimensions. However, we found that performing the calculation in D dimensions and including all relevant lower-loop counterterm diagrams, these divergences exactly cancelled, as required by the finiteness of the anomalous dimension. In the end, we found that this theory does not have any soft divergences, as expected in a theory without gauge bosons, and the collinear anomalous dimension coincides with twice the field anomalous dimension for both the scalar and the fermion. Further, we performed the same calculation using the standard Feynman diagrammatic approach, confirming the result of the on-shell computation. Finally, for the scalar, we computed a subset of the squared matrix elements up to the two-loop order including real radiation diagrams, where we found that the infrared divergences cancel only if those in the loop-amplitudes are exactly the ones we calculated with Feynman diagrams or on-shell cuts.

Finally, in chapter 21, we considered a much more realistic model with all the SM gauge groups, a Higgs-like scalar and two fermions mimicking a left-handed quark doublet and a right-handed down quark. While this theory exhibits a much richer infrared structure, the loop integrals become much more complicated. We used only a Feynman diagrammatic approach because for this the methods are more refined and worked out and leave the computation from the on-shell side for a future work. The gauge bosons generate soft divergences in amplitudes with either matter or non-Abelian gauge fields and we confirmed the general structure of the infrared anomalous dimension, i.e., terms with at most one power of logarithms. For the QCD-like sector of the theory, we recovered the well-known results, and we also presented the contributions of a charged scalar in the weak-like sector as well as the mixed contributions to the collinear anomalous dimensions of all fields. We cross-checked a large part of the results by calculating the IR anomalous dimensions using the equally conserved gauge currents. However, due to the existence of identically conserved currents already with marginal couplings, the contributions to the IR divergences with certain coupling dependencies cannot straightforwardly be extracted from the poles of the matrix elements. This highlights one main advantage of using the energy-momentum tensor: It couples equally to every propagating degree of freedom in the theory, even those neutral under any symmetry group. In addition, because there are no counterterms with only marginal couplings, its matrix elements will always capture all possible coupling orders in a single computation. We then concluded this last part by applying the results to the full two-loop computation of the $U(1)$ gauge current matrix element. Since we already computed the universal IR divergences, we can easily subtract them, such that all remaining poles must necessarily correspond to UV ones. In fact, by doing so, we confirmed the general result that the renormalization of this current is simply the field renormalization of the associated gauge boson. At last, we want to mention that this strategy can be used for any massless theory at a priory any loop order: i) Compute all the cusp and collinear anomalous dimensions using the energy-momentum tensor at the desired loop order ii) Compute the matrix element of the operator we want to renormalize at the same loop order iii) Subtract the IR divergences by constructing them from the cusp and collinear anomalous dimension iv) The remaining divergences can only be of UV nature. Interesting applications would be, e.g., the higher-loop renormalization of the SMEFT or of the energy-momentum tensor in the presence of a propagating graviton through

an identically conserved counterterm operator.

Acknowledgements

First and foremost, I want like to thank my supervisor, Andreas Weiler, for giving me the opportunity to pursue my doctoral studies in his group. I want to thank him for his constant support, advice, and guidance as well as his encouragement to explore different directions during my PhD. This definitely made me a better physicist.

I want to thank Javi Serra for the countless discussions that we had. Without your constant guidance, I would not be the physicist I am.

During my PhD, I had the pleasure of collaborating and discussing with many excellent scientists, including Reuven Balkin, Elena Kaiser, Konstantin Springmann, Michael Stadlbauer, Stefan Stelzl, Ennio Salvioni, Maximilian Ruhdorfer, Jonathan Kley. I would like to thank all of them for the amazing work atmosphere and the inspiring discussions.

My whole PhD would not have been as much fun without my colleagues, fellow PhD students and office mates Konstantin Springmann, Reuven Balkin, Max Ruhdorfer, Michael Stadlbauer, Elena Kaiser, Dominik Haslehner, Kai Bartnick, and many others at TUM. It was really an amazing time and I hope we can keep up some of our traditions, like the (almost) yearly Weihnachtsmarkt crawl.

I want to thank my friends for always being there for me. You made this time special to me.

I want to thank my girlfriend, Jessi. Thank you for all your love and support.

Finally, I want to thank my parents, Hans and Margot, and my sister Tina for their constant support along this journey. Without you, this would not have been possible.

Bibliography

[1] R.D. Peccei and H.R. Quinn, *CP Conservation in the Presence of Instantons*, *Phys. Rev. Lett.* **38** (1977) 1440.

[2] R.D. Peccei and H.R. Quinn, *Constraints imposed by* CP *conservation in the presence of pseudoparticles*, *Phys. Rev. D* **16** (1977) 1791.

[3] S. Weinberg, *A New Light Boson?*, *Phys. Rev. Lett.* **40** (1978) 223.

[4] F. Wilczek, *Problem of Strong P and T Invariance in the Presence of Instantons*, *Phys. Rev. Lett.* **40** (1978) 279.

[5] G. Banelli, E. Salvioni, J. Serra, T. Theil and A. Weiler, *The Present and Future of Four Top Operators*, *JHEP* **02** (2021) 043 [`arXiv:2010.05915`].

[6] J. Kley, T. Theil, E. Venturini and A. Weiler, *Electric dipole moments at one-loop in the dimension-6 SMEFT*, *Eur. Phys. J. C* **82** (2022) 926 [`arXiv:2109.15085`].

[7] P. Baratella, S. Maggio, M. Stadlbauer and T. Theil, *Two-Loop Infrared Renormalization with On-shell Methods*, `arXiv:2207.08831`.

[8] E. Kaiser, J. Serra, T. Theil and A. Weiler, "Testing Massive Higher Spins with Torsion Balance Experiments." in preparation.

[9] P. Baratella, M. Stadlbauer, T. Theil and A. Weiler, "The Energy-Momentum Tensor as a Tool for Higher Loop Renormalization." in preparation.

[10] ATLAS collaboration, *Observation of a new particle in the search for the Standard Model Higgs boson with the ATLAS detector at the LHC*, *Phys. Lett. B* **716** (2012) 1 [`arXiv:1207.7214`].

[11] CMS collaboration, *Observation of a New Boson at a Mass of 125 GeV with the CMS Experiment at the LHC*, *Phys. Lett. B* **716** (2012) 30 [`arXiv:1207.7235`].

[12] R. Contino, *The Higgs as a Composite Nambu-Goldstone Boson*, in *Theoretical Advanced Study Institute in Elementary Particle Physics: Physics of the Large and the Small*, pp. 235–306, 2011, DOI [`arXiv:1005.4269`].

[13] B. Bellazzini, C. Csáki and J. Serra, *Composite Higgses*, *Eur. Phys. J. C* **74** (2014) 2766 [`arXiv:1401.2457`].

[14] G. Panico and A. Wulzer, *The Composite Nambu-Goldstone Higgs*, vol. 913, Springer (2016), 10.1007/978-3-319-22617-0, [`arXiv:1506.01961`].

[15] S. Coleman, J. Wess and B. Zumino, *Structure of phenomenological lagrangians. i*, *Phys. Rev.* **177** (1969) 2239.

[16] C.G. Callan, S. Coleman, J. Wess and B. Zumino, *Structure of phenomenological lagrangians. ii*, *Phys. Rev.* **177** (1969) 2247.

[17] P. Sikivie, L. Susskind, M.B. Voloshin and V.I. Zakharov, *Isospin Breaking in Technicolor Models*, *Nucl. Phys. B* **173** (1980) 189.

[18] K. Agashe, R. Contino and A. Pomarol, *The Minimal composite Higgs model*, *Nucl. Phys. B* **719** (2005) 165 [`arXiv:hep-ph/0412089`].

[19] B. Gripaios, A. Pomarol, F. Riva and J. Serra, *Beyond the Minimal Composite Higgs Model*, *JHEP* **04** (2009) 070 [`arXiv:0902.1483`].

[20] M. Frigerio, A. Pomarol, F. Riva and A. Urbano, *Composite Scalar Dark Matter*, *JHEP* **07** (2012) 015 [`arXiv:1204.2808`].

[21] D. Marzocca and A. Urbano, *Composite Dark Matter and LHC Interplay*, *JHEP* **07** (2014) 107 [`arXiv:1404.7419`].

[22] R. Balkin, M. Ruhdorfer, E. Salvioni and A. Weiler, *Charged Composite Scalar Dark Matter*, *JHEP* **11** (2017) 094 [`arXiv:1707.07685`].

[23] ATLAS collaboration, *Combination of the searches for pair-produced vector-like partners of the third-generation quarks at $\sqrt{s} = 13$ TeV with the ATLAS detector*, *Phys. Rev. Lett.* **121** (2018) 211801 [`arXiv:1808.02343`].

[24] CMS collaboration, *Search for vector-like quarks in events with two oppositely charged leptons and jets in proton-proton collisions at $\sqrt{s} = 13$ TeV*, *Eur. Phys. J. C* **79** (2019) 364 [`arXiv:1812.09768`].

[25] D.B. Kaplan, *Flavor at SSC energies: A New mechanism for dynamically generated fermion masses*, *Nucl. Phys. B* **365** (1991) 259.

[26] G.F. Giudice, C. Grojean, A. Pomarol and R. Rattazzi, *The Strongly-Interacting Light Higgs*, *JHEP* **06** (2007) 045 [`arXiv:hep-ph/0703164`].

[27] A. Pomarol and J. Serra, *Top Quark Compositeness: Feasibility and Implications*, *Phys. Rev. D* **78** (2008) 074026 [`arXiv:0806.3247`].

[28] G. 't Hooft, *Naturalness, chiral symmetry, and spontaneous chiral symmetry breaking*, *NATO Sci. Ser. B* **59** (1980) 135.

[29] L. Susskind, *Dynamics of Spontaneous Symmetry Breaking in the Weinberg-Salam Theory*, *Phys. Rev. D* **20** (1979) 2619.

[30] S. Dimopoulos and L. Susskind, *Mass Without Scalars*, *Nucl. Phys. B* **155** (1979) 237.

[31] G.F. Giudice, *Naturally Speaking: The Naturalness Criterion and Physics at the LHC*, `arXiv:0801.2562`.

[32] R. Barbieri, *Electroweak theory after the first Large Hadron Collider phase*, *Phys. Scripta T* **158** (2013) 014006 [`arXiv:1309.3473`].

[33] S. Dimopoulos and J. Preskill, *Massless Composites With Massive Constituents*, *Nucl. Phys. B* **199** (1982) 206.

[34] D.B. Kaplan and H. Georgi, *SU(2) x U(1) Breaking by Vacuum Misalignment*, *Phys. Lett. B* **136** (1984) 183.

[35] D.B. Kaplan, H. Georgi and S. Dimopoulos, *Composite Higgs Scalars*, *Phys. Lett. B* **136** (1984) 187.

[36] T. Banks, *CONSTRAINTS ON SU(2) x U(1) BREAKING BY VACUUM MISALIGNMENT*, *Nucl. Phys. B* **243** (1984) 125.

[37] H. Georgi and D.B. Kaplan, *Composite Higgs and Custodial SU(2)*, *Phys. Lett. B* **145** (1984) 216.

[38] M.J. Dugan, H. Georgi and D.B. Kaplan, *Anatomy of a Composite Higgs Model*, *Nucl. Phys. B* **254** (1985) 299.

[39] C. Csáki, S. Lombardo and O. Telem, *TASI Lectures on Non-supersymmetric BSM Models*, in *Proceedings, Theoretical Advanced Study Institute in Elementary Particle Physics : Anticipating the Next Discoveries in Particle Physics (TASI 2016): Boulder, CO, USA, June 6-July 1, 2016*, R. Essig and I. Low, eds., pp. 501–570, WSP (2018), DOI [`arXiv:1811.04279`].

[40] S. Weinberg, *Implications of Dynamical Symmetry Breaking*, *Phys. Rev. D* **13** (1976) 974.

[41] S. Weinberg, *Implications of dynamical symmetry breaking: An addendum*, *Phys. Rev. D* **19** (1979) 1277.

[42] K. Lane, *Two Lectures on Technicolor*, `arXiv:hep-ph/0202255`.

[43] R. Contino, T. Kramer, M. Son and R. Sundrum, *Warped/composite phenomenology simplified*, *JHEP* **05** (2007) 074 [`arXiv:hep-ph/0612180`].

[44] CMS collaboration, *Search for the production of four top quarks in the single-lepton and opposite-sign dilepton final states in proton-proton collisions at $\sqrt{s}$ = 13 TeV*, *JHEP* **11** (2019) 082 [`arXiv:1906.02805`].

[45] C. Englert, G.F. Giudice, A. Greljo and M. McCullough, *The $\hat{H}$-Parameter: An Oblique Higgs View*, *JHEP* **09** (2019) 041 [`arXiv:1903.07725`].

[46] K. Agashe, R. Contino, L. Da Rold and A. Pomarol, *A custodial symmetry for $Zb\bar{b}$*, *Phys. Lett. B* **641** (2006) 62 [`arXiv:hep-ph/0605341`].

[47] J. Mrazek, A. Pomarol, R. Rattazzi, M. Redi, J. Serra and A. Wulzer, *The Other Natural Two Higgs Doublet Model*, *Nucl. Phys. B* **853** (2011) 1 [`arXiv:1105.5403`].

[48] D. Liu, A. Pomarol, R. Rattazzi and F. Riva, *Patterns of Strong Coupling for LHC Searches*, *JHEP* **11** (2016) 141 [`arXiv:1603.03064`].

[49] C. Degrande, J.-M. Gérard, C. Grojean, F. Maltoni and G. Servant, *Non-resonant New Physics in Top Pair Production at Hadron Colliders*, *JHEP* **03** (2011) 125 [`arXiv:1010.6304`].

[50] B. Lillie, J. Shu and T.M. Tait, *Top Compositeness at the Tevatron and LHC*, *JHEP* **04** (2008) 087 [`arXiv:0712.3057`].

[51] M. Farina, C. Mondino, D. Pappadopulo and J.T. Ruderman, *New Physics from High Energy Tops*, *JHEP* **01** (2019) 231 [`arXiv:1811.04084`].

[52] K. Kumar, T.M. Tait and R. Vega-Morales, *Manifestations of Top Compositeness at Colliders*, *JHEP* **05** (2009) 022 [`arXiv:0901.3808`].

[53] D. Liu and R. Mahbubani, *Probing top-antitop resonances with $t\bar{t}$ scattering at LHC14*, *JHEP* **04** (2016) 116 [`arXiv:1511.09452`].

[54] R. Barbieri, A. Pomarol, R. Rattazzi and A. Strumia, *Electroweak symmetry breaking after LEP-1 and LEP-2*, *Nucl. Phys. B* **703** (2004) 127 [`arXiv:hep-ph/0405040`].

[55] G. Panico, M. Riembau and T. Vantalon, *Probing light top partners with CP violation*, *JHEP* **06** (2018) 056 [`arXiv:1712.06337`].

[56] G. Panico, A. Pomarol and M. Riembau, *EFT approach to the electron Electric Dipole Moment at the two-loop level*, *JHEP* **04** (2019) 090 [`arXiv:1810.09413`].

[57] ATLAS collaboration, *Search for pair production of up-type vector-like quarks and for four-top-quark events in final states with multiple b-jets with the ATLAS detector*, *JHEP* **07** (2018) 089 [`arXiv:1803.09678`].

[58] ATLAS collaboration, *Search for four-top-quark production in the single-lepton and opposite-sign dilepton final states in pp collisions at $\sqrt{s}$ = 13 TeV with the ATLAS detector*, *Phys. Rev. D* **99** (2019) 052009 [`arXiv:1811.02305`].

[59] CMS collaboration, *Search for physics beyond the Standard Model in events with two leptons of same sign, missing transverse momentum, and jets in proton–proton collisions at $\sqrt{s}$ = 13 TeV*, *Eur. Phys. J. C* **77** (2017) 578 [`arXiv:1704.07323`].

[60] CMS collaboration, *Search for Standard Model production of four top quarks with same-sign and multilepton final states in proton–proton collisions at $\sqrt{s}$ = 13 TeV*, *Eur. Phys. J. C* **78** (2018) 140 [`arXiv:1710.10614`].

[61] ATLAS collaboration, *Search for new phenomena in events with same-charge leptons and b-jets in pp collisions at $\sqrt{s}$ = 13 TeV with the ATLAS detector*, *JHEP* **12** (2018) 039 [`arXiv:1807.11883`].

[62] CMS collaboration, *Search for production of four top quarks in final states with same-sign or multiple leptons in proton-proton collisions at $\sqrt{s}$ = 13 TeV*, *Eur. Phys. J. C* **80** (2020) 75 [`arXiv:1908.06463`].

[63] ATLAS collaboration, *Evidence for $t\bar{t}t\bar{t}$ production in the multilepton final state in proton–proton collisions at $\sqrt{s}$ = 13 TeV with the ATLAS detector*, *Eur. Phys. J. C* **80** (2020) 1085 [`arXiv:2007.14858`].

[64] M. Cepeda, S. Gori, P. Ilten, M. Kado, F. Riva et al., *Report from Working Group 2: Higgs Physics at the HL-LHC and HE-LHC*, `arXiv:1902.00134`.

[65] J. Ellis, C.W. Murphy, V. Sanz and T. You, *Updated Global SMEFT Fit to Higgs, Diboson and Electroweak Data*, *JHEP* **06** (2018) 146 [`arXiv:1803.03252`].

[66] O. Domènech, A. Pomarol and J. Serra, *Probing the SM with Dijets at the LHC*, *Phys. Rev. D* **85** (2012) 074030 [`arXiv:1201.6510`].

[67] ATLAS collaboration, *Search for new phenomena in dijet events using 37 fb^{-1} of pp collision data collected at $\sqrt{s} = 13$ TeV with the ATLAS detector*, *Phys. Rev. D* **96** (2017) 052004 [`arXiv:1703.09127`].

[68] S. Alioli, M. Farina, D. Pappadopulo and J.T. Ruderman, *Precision Probes of QCD at High Energies*, *JHEP* **07** (2017) 097 [`arXiv:1706.03068`].

[69] M. Farina, G. Panico, D. Pappadopulo, J.T. Ruderman, R. Torre and A. Wulzer, *Energy helps accuracy: electroweak precision tests at hadron colliders*, *Phys. Lett. B* **772** (2017) 210 [`arXiv:1609.08157`].

[70] ATLAS collaboration, *Modelling of rare top quark processes at $\sqrt{s} = 13$ TeV in ATLAS*, .

[71] CMS collaboration, *Using associated top quark production to probe for new physics within the framework of effective field theory*, .

[72] CMS collaboration, *Observation of four top quark production in proton-proton collisions at $\sqrt{s} = 13$ TeV*, .

[73] ATLAS collaboration, *Observation of four-top-quark production in the multilepton final state with the ATLAS detector*, `arXiv:2303.15061`.

[74] CMS collaboration, *Measurement of the Higgs boson production rate in association with top quarks in final states with electrons, muons, and hadronically decaying tau leptons at $\sqrt{s} = 13$ TeV*, `arXiv:2011.03652`.

[75] J.A. Dror, M. Farina, E. Salvioni and J. Serra, *Strong tW Scattering at the LHC*, *JHEP* **01** (2016) 071 [`arXiv:1511.03674`].

[76] ATLAS collaboration, *Analysis of $t\bar{t}H$ and $t\bar{t}W$ production in multilepton final states with the ATLAS detector*, .

[77] CMS collaboration, *Measurement of top quark pair production in association with a Z boson in proton-proton collisions at $\sqrt{s} = 13$ TeV*, *JHEP* **03** (2020) 056 [`arXiv:1907.11270`].

[78] ATLAS collaboration, *Measurements of the inclusive and differential production cross sections of a top-quark-antiquark pair in association with a Z boson at $\sqrt{s} = 13$ TeV with the ATLAS detector*, .

[79] CMS collaboration, *Measurement of the cross section for top quark pair production in association with a W or Z boson in proton-proton collisions at $\sqrt{s} = 13$ TeV*, *JHEP* **08** (2018) 011 [`arXiv:1711.02547`].

[80] ATLAS collaboration, *Measurement of the $t\bar{t}Z$ and $t\bar{t}W$ cross sections in proton-proton collisions at $\sqrt{s} = 13$ TeV with the ATLAS detector*, *Phys. Rev. D* **99** (2019) 072009 [`arXiv:1901.03584`].

[81] R. Frederix, D. Pagani and M. Zaro, *Large NLO corrections in $t\bar{t}W^{\pm}$ and $t\bar{t}t\bar{t}$ hadroproduction from supposedly subleading EW contributions*, *JHEP* **02** (2018) 031 [`arXiv:1711.02116`].

[82] LHC Higgs Cross Section Working Group, *Handbook of LHC Higgs Cross Sections: 4. Deciphering the Nature of the Higgs Sector*, `arXiv:1610.07922`.

[83] CMS collaboration, *Measurement of top quark-antiquark pair production in association with a W or Z Boson in pp collisions at $\sqrt{s} = 8$ TeV*, *Eur. Phys. J. C* **74** (2014) 3060 [`arXiv:1406.7830`].

[84] A. Broggio, A. Ferroglia, R. Frederix, D. Pagani, B.D. Pecjak and I. Tsinikos, *Top-quark pair hadroproduction in association with a heavy boson at NLO+NNLL including EW corrections*, *JHEP* **08** (2019) 039 [`arXiv:1907.04343`].

[85] A. Kulesza, L. Motyka, D. Schwartländer, T. Stebel and V. Theeuwes, *Associated top quark pair production with a heavy boson: differential cross sections at NLO+NNLL accuracy*, *Eur. Phys. J. C* **80** (2020) 428 [`arXiv:2001.03031`].

[86] R. Frederix and I. Tsinikos, *Subleading EW corrections and spin-correlation effects in $t\bar{t}W$ multi-lepton signatures*, *Eur. Phys. J. C* **80** (2020) 803 [`arXiv:2004.09552`].

[87] G. Bevilacqua, H.-Y. Bi, H.B. Hartanto, M. Kraus and M. Worek, *The simplest of them all: $t\bar{t}W^{\pm}$ at NLO accuracy in QCD*, *JHEP* **08** (2020) 043 [`arXiv:2005.09427`].

[88] A. Denner and G. Pelliccioli, *NLO QCD corrections to off-shell $t\bar{t}W^+$ production at the LHC*, *JHEP* **11** (2020) 069 [`arXiv:2007.12089`].

[89] S. von Buddenbrock, R. Ruiz and B. Mellado, *Anatomy of inclusive $t\bar{t}W$ production at hadron colliders*, *Phys. Lett. B* **811** (2020) 135964 [`arXiv:2009.00032`].

[90] Q.-H. Cao, S.-L. Chen and Y. Liu, *Probing Higgs Width and Top Quark Yukawa Coupling from $t\bar{t}H$ and $t\bar{t}t\bar{t}$ Productions*, *Phys. Rev. D* **95** (2017) 053004 [`arXiv:1602.01934`].

[91] J. Alwall et al., *The automated computation of tree-level and next-to-leading order differential cross sections, and their matching to parton shower simulations*, *JHEP* **07** (2014) 079 [`arXiv:1405.0301`].

[92] A. Alloul, N.D. Christensen, C. Degrande, C. Duhr and B. Fuks, *FeynRules 2.0 - A complete toolbox for tree-level phenomenology*, *Comput. Phys. Commun.* **185** (2014) 2250 [`arXiv:1310.1921`].

[93] NNPDF collaboration, *Parton distributions with QED corrections*, *Nucl. Phys. B* **877** (2013) 290 [`arXiv:1308.0598`].

[94] T. Sjöstrand et al., *An introduction to PYTHIA 8.2*, *Comput. Phys. Commun.* **191** (2015) 159 [`arXiv:1410.3012`].

[95] J. de Favereau et al., *DELPHES 3, A modular framework for fast simulation of a generic collider experiment*, *JHEP* **02** (2014) 057 [`arXiv:1307.6346`].

[96] M. Cacciari, G.P. Salam and G. Soyez, *The anti-k_t jet clustering algorithm*, *JHEP* **04** (2008) 063 [`arXiv:0802.1189`].

[97] M. Cacciari, G.P. Salam and G. Soyez, *FastJet User Manual*, *Eur. Phys. J. C* **72** (2012) 1896 [`arXiv:1111.6097`].

[98] R. Röntsch and M. Schulze, *Constraining couplings of top quarks to the Z boson in $t\bar{t}$ + Z production at the LHC*, *JHEP* **07** (2014) 091 [`arXiv:1404.1005`].

[99] O. Bessidskaia Bylund, F. Maltoni, I. Tsinikos, E. Vryonidou and C. Zhang, *Probing top quark neutral couplings in the Standard Model Effective Field Theory at NLO in QCD*, *JHEP* **05** (2016) 052 [`arXiv:1601.08193`].

[100] C. Degrande, G. Durieux, F. Maltoni, K. Mimasu, E. Vryonidou and C. Zhang, *Automated one-loop computations in the SMEFT*, `arXiv:2008.11743`.

[101] F. Maltoni, L. Mantani and K. Mimasu, *Top-quark electroweak interactions at high energy*, *JHEP* **10** (2019) 004 [`arXiv:1904.05637`].

[102] FCC collaboration, *FCC Physics Opportunities: Future Circular Collider Conceptual Design Report Volume 1*, *Eur. Phys. J. C* **79** (2019) 474.

[103] G. Salam and A. Weiler, "Collider Reach." `http://collider-reach.web.cern.ch`.

[104] E. Alvarez, D.A. Faroughy, J.F. Kamenik, R. Morales and A. Szynkman, *Four Tops for LHC*, *Nucl. Phys. B* **915** (2017) 19 [`arXiv:1611.05032`].

[105] J.H. Kim, K. Kong, S.J. Lee and G. Mohlabeng, *Probing TeV scale Top-philic Resonances with Boosted Top-tagging at the HL-LHC*, *Phys. Rev. D* **94** (2016) 035023 [`arXiv:1604.07421`].

[106] K. Rehermann and B. Tweedie, *Efficient Identification of Boosted Semileptonic Top Quarks at the LHC*, *JHEP* **03** (2011) 059 [`arXiv:1007.2221`].

[107] R. Contino et al., *Physics at a 100 TeV pp collider: Higgs and EW symmetry breaking studies*, *CERN Yellow Rep.* (2017) 255 [`arXiv:1606.09408`].

[108] P. Torrielli, *Rare Standard Model processes for present and future hadronic colliders*, `arXiv:1407.1623`.

[109] D. Curtin, J. Galloway and J.G. Wacker, *Measuring the $t\bar{t}h$ coupling from same-sign dilepton +2b measurements*, *Phys. Rev. D* **88** (2013) 093006 [`arXiv:1306.5695`].

[110] M. Czakon and A. Mitov, *Top++: A Program for the Calculation of the Top-Pair Cross-Section at Hadron Colliders*, *Comput. Phys. Commun.* **185** (2014) 2930 [`arXiv:1112.5675`].

[111] M. Mangano et al., *Physics at a 100 TeV pp Collider: Standard Model Processes*, *CERN Yellow Rep.* (2017) 1 [`arXiv:1607.01831`].

[112] J. de Blas et al., *Higgs Boson Studies at Future Particle Colliders*, *JHEP* **01** (2020) 139 [`arXiv:1905.03764`].

[113] J. Doyle, "*Search for the Electric Dipole Moment of the Electron with Thorium Monoxide – The ACME Experiment.*" Talk at the KITP, September 2016.

[114] CMS collaboration, *Top Tagging with New Approaches*, .

[115] C. Helsens, D. Jamin, M.L. Mangano, T.G. Rizzo and M. Selvaggi, *Heavy resonances at energy-frontier hadron colliders*, *Eur. Phys. J. C* **79** (2019) 569 [`arXiv:1902.11217`].

[116] G. Kasieczka, T. Plehn et al., *The Machine Learning Landscape of Top Taggers*, *SciPost Phys.* **7** (2019) 014 [`arXiv:1902.09914`].

[117] S. Marzani, G. Soyez and M. Spannowsky, *Looking inside jets: an introduction to jet substructure and boosted-object phenomenology*, Springer (2019), 10.1007/978-3-030-15709-8, [arXiv:1901.10342].

[118] CLIC, CLICDP collaboration, P. Burrows, N. Catalan Lasheras, L. Linssen, M. Petriˇ c, A. Robson, D. Schulte et al., eds., *The Compact Linear Collider (CLIC) - 2018 Summary Report*, arXiv:1812.06018.

[119] P. Bambade et al., *The International Linear Collider: A Global Project*, arXiv:1903.01629.

[120] G. Durieux and O. Matsedonskyi, *The top-quark window on compositeness at future lepton colliders*, JHEP **01** (2019) 072 [arXiv:1807.10273].

[121] G. Durieux, M. Perelló, M. Vos and C. Zhang, *Global and optimal probes for the top-quark effective field theory at future lepton colliders*, JHEP **10** (2018) 168 [arXiv:1807.02121].

[122] J. Elias-Miró, J. Espinosa, E. Massó and A. Pomarol, *Higgs windows to new physics through d=6 operators: constraints and one-loop anomalous dimensions*, JHEP **11** (2013) 066 [arXiv:1308.1879].

[123] A. Wulzer et al., "*Muon Collider Physics Potential.*" Letter of Interest, Snowmass 2021.

[124] D. Hanneke, S. Fogwell and G. Gabrielse, *New Measurement of the Electron Magnetic Moment and the Fine Structure Constant*, Phys. Rev. Lett. **100** (2008) 120801 [arXiv:0801.1134].

[125] X. Fan, T.G. Myers, B.A.D. Sukra and G. Gabrielse, *Measurement of the Electron Magnetic Moment*, arXiv:2209.13084.

[126] V. Andreev, *Improved limit on the electric dipole moment of the electron*, Nature **562** (2018) 355.

[127] MUON (G-2) collaboration, *An Improved Limit on the Muon Electric Dipole Moment*, Phys. Rev. D **80** (2009) 052008 [arXiv:0811.1207].

[128] A.G. Grozin, I.B. Khriplovich and A.S. Rudenko, *Electric dipole moments, from e to tau*, Phys. Atom. Nucl. **72** (2009) 1203 [arXiv:0811.1641].

[129] C. Abel, S. Afach, N.J. Ayres, C.A. Baker, G. Ban, G. Bison et al., *Measurement of the permanent electric dipole moment of the neutron*, Phys. Rev. Lett. **124** (2020) 081803.

[130] D. Buttazzo and P. Paradisi, *Probing the muon g-2 anomaly at a Muon Collider*, arXiv:2012.02769.

[131] N2EDM collaboration, *The design of the n2EDM experiment*, arXiv:2101.08730.

[132] M. Pospelov and A. Ritz, *CKM benchmarks for electron electric dipole moment experiments*, Phys. Rev. D **89** (2014) 056006 [arXiv:1311.5537].

[133] M.E. Pospelov and I.B. Khriplovich, *Electric dipole moment of the W boson and the electron in the Kobayashi-Maskawa model*, Sov. J. Nucl. Phys. **53** (1991) 638.

[134] M.J. Booth, *The Electric dipole moment of the W and electron in the Standard Model*, `arXiv:hep-ph/9301293`.

[135] I. Khriplovich and A. Zhitnitsky, *What is the value of the neutron electric dipole moment in the kobayashi-maskawa model?*, *Physics Letters B* **109** (1982) 490.

[136] A. Czarnecki and B. Krause, *Neutron electric dipole moment in the standard model: Valence quark contributions*, *Phys. Rev. Lett.* **78** (1997) 4339 [`arXiv:hep-ph/9704355`].

[137] Y. Yamaguchi and N. Yamanaka, *Large long-distance contributions to the electric dipole moments of charged leptons in the standard model*, *Phys. Rev. Lett.* **125** (2020) 241802 [`arXiv:2003.08195`].

[138] G.F. Giudice and A. Romanino, *Electric dipole moments in split supersymmetry*, *Phys. Lett. B* **634** (2006) 307 [`arXiv:hep-ph/0510197`].

[139] Y. Nakai and M. Reece, *Electric Dipole Moments in Natural Supersymmetry*, *JHEP* **08** (2017) 031 [`arXiv:1612.08090`].

[140] C. Cesarotti, Q. Lu, Y. Nakai, A. Parikh and M. Reece, *Interpreting the Electron EDM Constraint*, *JHEP* **05** (2019) 059 [`arXiv:1810.07736`].

[141] D. Aloni, P. Asadi, Y. Nakai, M. Reece and M. Suzuki, *Spontaneous CP Violation and Horizontal Symmetry in the MSSM: Toward Lepton Flavor Naturalness*, `arXiv:2104.02679`.

[142] B. Keren-Zur, P. Lodone, M. Nardecchia, D. Pappadopulo, R. Rattazzi and L. Vecchi, *On Partial Compositeness and the CP asymmetry in charm decays*, *Nucl. Phys. B* **867** (2013) 394 [`arXiv:1205.5803`].

[143] M. König, M. Neubert and D.M. Straub, *Dipole operator constraints on composite Higgs models*, *Eur. Phys. J. C* **74** (2014) 2945 [`arXiv:1403.2756`].

[144] I. Doršner, S. Fajfer, A. Greljo, J.F. Kamenik and N. Košnik, *Physics of leptoquarks in precision experiments and at particle colliders*, *Phys. Rept.* **641** (2016) 1 [`arXiv:1603.04993`].

[145] K. Fuyuto, M. Ramsey-Musolf and T. Shen, *Electric Dipole Moments from CP-Violating Scalar Leptoquark Interactions*, *Phys. Lett. B* **788** (2019) 52 [`arXiv:1804.01137`].

[146] W. Dekens, J. de Vries, M. Jung and K.K. Vos, *The phenomenology of electric dipole moments in models of scalar leptoquarks*, *JHEP* **01** (2019) 069 [`arXiv:1809.09114`].

[147] W. Altmannshofer, S. Gori, H.H. Patel, S. Profumo and D. Tuckler, *Electric dipole moments in a leptoquark scenario for the B-physics anomalies*, *JHEP* **05** (2020) 069 [`arXiv:2002.01400`].

[148] W. Altmannshofer, S. Gori, N. Hamer and H.H. Patel, *Electron EDM in the complex two-Higgs doublet model*, *Phys. Rev. D* **102** (2020) 115042 [`arXiv:2009.01258`].

[149] W.-S. Hou, G. Kumar and S. Teunissen, *Charged Lepton EDM with Extra Yukawa Couplings*, `arXiv:2109.08936`.

[150] H.E. Logan, S. Moretti, D. Rojas-Ciofalo and M. Song, *CP violation from charged Higgs bosons in the three Higgs doublet model*, *JHEP* **07** (2021) 158 [`arXiv:2012.08846`].

[151] K. Cheung, A. Jueid, Y.-N. Mao and S. Moretti, *Two-Higgs-doublet model with soft CP violation confronting electric dipole moments and colliders*, *Phys. Rev. D* **102** (2020) 075029 [`arXiv:2003.04178`].

[152] E.J. Chun, J. Kim and T. Mondal, *Electron EDM and Muon anomalous magnetic moment in Two-Higgs-Doublet Models*, *JHEP* **12** (2019) 068 [`arXiv:1906.00612`].

[153] H. Davoudiasl, I.M. Lewis and M. Sullivan, *Higgs Troika for Baryon Asymmetry*, *Phys. Rev. D* **101** (2020) 055010 [`arXiv:1909.02044`].

[154] H. Davoudiasl, I.M. Lewis and M. Sullivan, *Multi-TeV signals of baryogenesis in a Higgs troika model*, *Phys. Rev. D* **104** (2021) 015024 [`arXiv:2103.12089`].

[155] A. Abada and T. Toma, *Electric dipole moments in the minimal scotogenic model*, *JHEP* **04** (2018) 030 [`arXiv:1802.00007`].

[156] P. Fileviez Perez and A.D. Plascencia, *Electric dipole moments, new forces and dark matter*, *JHEP* **03** (2021) 185 [`arXiv:2008.09116`].

[157] G. Panico, A. Pomarol and M. Riembau, *Eft approach to the electron electric dipole moment at the two-loop level*, `arXiv:1810.09413`.

[158] J. Aebischer, W. Dekens, E.E. Jenkins, A.V. Manohar, D. Sengupta and P. Stoffer, *Effective field theory interpretation of lepton magnetic and electric dipole moments*, *JHEP* **07** (2021) 107 [`arXiv:2102.08954`].

[159] U. Haisch and A. Hala, *Bounds on cp-violating higgs-gluon interactions: the case of vanishing light-quark yukawa couplings*, `arXiv:1909.09373`.

[160] U. Haisch and G. Koole, *Beautiful and charming chromodipole moments*, *JHEP* **09** (2021) 133 [`arXiv:2106.01289`].

[161] J.F. Kamenik, M. Papucci and A. Weiler, *Constraining the dipole moments of the top quark*, *Phys. Rev. D* **85** (2012) 071501 [`arXiv:1107.3143`].

[162] J. Brod, U. Haisch and J. Zupan, *Constraints on CP-violating Higgs couplings to the third generation*, *JHEP* **11** (2013) 180 [`arXiv:1310.1385`].

[163] J. Brod and E. Stamou, *Electric dipole moment constraints on CP-violating heavy-quark Yukawas at next-to-leading order*, *JHEP* **07** (2021) 080 [`arXiv:1810.12303`].

[164] E. Fuchs, M. Losada, Y. Nir and Y. Viernik, *CP violation from τ, t and b dimension-6 Yukawa couplings - interplay of baryogenesis, EDM and Higgs physics*, *JHEP* **05** (2020) 056 [`arXiv:2003.00099`].

[165] K. Fuyuto and M. Ramsey-Musolf, *Top Down Electroweak Dipole Operators*, *Phys. Lett. B* **781** (2018) 492 [`arXiv:1706.08548`].

[166] V. Cirigliano, W. Dekens, J. de Vries and E. Mereghetti, *Is there room for CP violation in the top-Higgs sector?*, *Phys. Rev. D* **94** (2016) 016002 [`arXiv:1603.03049`].

[167] V. Cirigliano, A. Crivellin, W. Dekens, J. de Vries, M. Hoferichter and E. Mereghetti, *CP Violation in Higgs-Gauge Interactions: From Tabletop Experiments to the LHC*, *Phys. Rev. Lett.* **123** (2019) 051801 [`arXiv:1903.03625`].

[168] V. Cirigliano, W. Dekens, J. de Vries and E. Mereghetti, *Constraining the top-Higgs sector of the Standard Model Effective Field Theory*, Phys. Rev. D **94** (2016) 034031 [arXiv:1605.04311].

[169] W. Altmannshofer, J. Brod and M. Schmaltz, *Experimental constraints on the coupling of the Higgs boson to electrons*, JHEP **05** (2015) 125 [arXiv:1503.04830].

[170] Y.T. Chien, V. Cirigliano, W. Dekens, J. de Vries and E. Mereghetti, *Direct and indirect constraints on CP-violating Higgs-quark and Higgs-gluon interactions*, JHEP **02** (2016) 011 [arXiv:1510.00725].

[171] B. Grzadkowski, M. Iskrzynski, M. Misiak and J. Rosiek, *Dimension-six terms in the standard model lagrangian*, arXiv:1008.4884.

[172] E.E. Jenkins, A.V. Manohar and M. Trott, *Renormalization group evolution of the standard model dimension six operators i: Formalism and lambda dependence*, arXiv:http://arxiv.org/abs/1308.2627v4.

[173] E.E. Jenkins, A.V. Manohar and M. Trott, *Renormalization group evolution of the standard model dimension six operators ii: Yukawa dependence*, arXiv:http://arxiv.org/abs/1310.4838v3.

[174] R. Alonso, E.E. Jenkins, A.V. Manohar and M. Trott, *Renormalization group evolution of the standard model dimension six operators iii: Gauge coupling dependence and phenomenology*, arXiv:http://arxiv.org/abs/1312.2014v4.

[175] E.E. Jenkins, A.V. Manohar and P. Stoffer, *Low-energy effective field theory below the electroweak scale: Operators and matching*, JHEP 1803 (2018) 016 (2017) [arXiv:http://arxiv.org/abs/1709.04486v2].

[176] E.E. Jenkins, A.V. Manohar and P. Stoffer, *Low-energy effective field theory below the electroweak scale: Anomalous dimensions*, arXiv:http://arxiv.org/abs/1711.05270v2.

[177] W. Dekens and P. Stoffer, *Low-energy effective field theory below the electroweak scale: matching at one loop*, JHEP 1910 (2019) 197 (2019) [arXiv:1908.05295].

[178] J.S. Schwinger, *On Quantum electrodynamics and the magnetic moment of the electron*, Phys. Rev. **73** (1948) 416.

[179] B. Sekhar Chivukula and H. Georgi, *Composite-technicolor standard model*, Physics Letters B **188** (1987) 99.

[180] J. Fuentes-Martín, G. Isidori, J. Pagès and K. Yamamoto, *With or without U(2)? Probing non-standard flavor and helicity structures in semileptonic B decays*, Phys. Lett. B **800** (2020) 135080 [arXiv:1909.02519].

[181] R. Barbieri, D. Buttazzo, F. Sala and D.M. Straub, *Flavour physics from an approximate $U(2)^3$ symmetry*, JHEP **07** (2012) 181 [arXiv:1203.4218].

[182] G. D'Ambrosio, G.F. Giudice, G. Isidori and A. Strumia, *Minimal flavour violation: an effective field theory approach*, Nucl.Phys.B645:155-187,2002 (2002) [arXiv:hep-ph/0207036].

[183] G. Isidori and D.M. Straub, *Minimal flavour violation and beyond*, `arXiv:1202.0464`.

[184] C. Smith and S. Touati, *Edm with and beyond flavor invariants*, `arXiv:1707.06805`.

[185] C. Jarlskog, *Commutator of the quark mass matrices in the standard electroweak model and a measure of maximal* CP *nonconservation, Phys. Rev. Lett.* **55** (1985) 1039.

[186] Q. Bonnefoy, E. Gendy, C. Grojean and J.T. Ruderman, *Beyond Jarlskog: 699 invariants for CP violation in SMEFT, JHEP* **08** (2022) 032 [`arXiv:2112.03889`].

[187] M. Pospelov and A. Ritz, *Electric dipole moments as probes of new physics, Annals Phys.* **318** (2005) 119 [`arXiv:hep-ph/0504231`].

[188] R. Gupta, B. Yoon, T. Bhattacharya, V. Cirigliano, Y.-C. Jang and H.-W. Lin, *Flavor diagonal tensor charges of the nucleon from 2+1+1 flavor lattice qcd, Phys. Rev. D 98, 091501 (2018)* (2018) [`arXiv:1808.07597`].

[189] J. Engel, M.J. Ramsey-Musolf and U. van Kolck, *Electric dipole moments of nucleons, nuclei, and atoms: The standard model and beyond*, `arXiv:1303.2371`.

[190] J. Hisano, J.Y. Lee, N. Nagata and Y. Shimizu, *Reevaluation of neutron electric dipole moment with qcd sum rules, Phys.Rev.D85:114044,2012* (2012) [`arXiv:1204.2653`].

[191] J. de Vries, E. Mereghetti, R.G.E. Timmermans and U. van Kolck, *The Effective Chiral Lagrangian From Dimension-Six Parity and Time-Reversal Violation, Annals Phys.* **338** (2013) 50 [`arXiv:1212.0990`].

[192] JLQCD collaboration, *Nucleon charges with dynamical overlap fermions, Phys. Rev. D* **98** (2018) 054516 [`arXiv:1805.10507`].

[193] N. Yamanaka and E. Hiyama, *Weinberg operator contribution to the nucleon electric dipole moment in the quark model, Phys. Rev. D* **103** (2021) 035023 [`arXiv:2011.02531`].

[194] D.A. Demir, M. Pospelov and A. Ritz, *Hadronic EDMs, the Weinberg operator, and light gluinos, Phys. Rev. D* **67** (2003) 015007 [`arXiv:hep-ph/0208257`].

[195] U. Haisch and A. Hala, *Sum rules for CP-violating operators of Weinberg type, JHEP* **11** (2019) 154 [`arXiv:1909.08955`].

[196] S. Weinberg, *Larger higgs-boson-exchange terms in the neutron electric dipole moment, Physical Review Letters* **63** (1989) 2333.

[197] A. Hook, *TASI Lectures on the Strong CP Problem and Axions, PoS* **TASI2018** (2019) 004 [`arXiv:1812.02669`].

[198] M. Pospelov and A. Ritz, *Hadron electric dipole moments from cp-odd operators of dimension five via qcd sum rules: The vector meson, Phys.Lett. B471 (2000) 388-395* (1999) [`arXiv:hep-ph/9910273`].

[199] M. Pospelov and A. Ritz, *Neutron edm from electric and chromoelectric dipole moments of quarks, Phys.Rev. D63 (2001) 073015* (2000) [`arXiv:hep-ph/0010037`].

[200] J. Elias-Miro, J.R. Espinosa and A. Pomarol, *One-loop non-renormalization results in EFTs, Phys. Lett. B* **747** (2015) 272 [`arXiv:1412.7151`].

[201] Z. Bern, J. Parra-Martinez and E. Sawyer, *Nonrenormalization and Operator Mixing via On-Shell Methods*, Phys. Rev. Lett. **124** (2020) 051601 [`arXiv:1910.05831`].

[202] C. Cheung and C.-H. Shen, *Non-renormalization theorems without supersymmetry*, Phys. Rev. Lett. 115, 071601 (2015) (2015) [`arXiv:1505.01844`].

[203] N. Craig, M. Jiang, Y.-Y. Li and D. Sutherland, *Loops and trees in generic efts*, `arXiv:http://arxiv.org/abs/2001.00017v1`.

[204] A. Azatov, R. Contino, C.S. Machado and F. Riva, *Helicity selection rules and non-interference for bsm amplitudes*, Phys. Rev. D 95, 065014 (2017) (2016) [`arXiv:1607.05236`].

[205] C. Anastasiou, R. Britto, B. Feng, Z. Kunszt and P. Mastrolia, *Unitarity cuts and Reduction to master integrals in d dimensions for one-loop amplitudes*, JHEP **03** (2007) 111 [`arXiv:hep-ph/0612277`].

[206] S.D. Badger, *Direct Extraction Of One Loop Rational Terms*, JHEP **01** (2009) 049 [`arXiv:0806.4600`].

[207] N. Arkani-Hamed, T.-C. Huang and Y.-t. Huang, *Scattering amplitudes for all masses and spins*, JHEP **11** (2021) 070 [`arXiv:1709.04891`].

[208] F. Boudjema, K. Hagiwara, C. Hamzaoui and K. Numata, *Anomalous moments of quarks and leptons from nonstandardWWγcouplings*, Physical Review D **43** (1991) 2223.

[209] B. Gripaios and D. Sutherland, *On lhc searches for cp-violating, dimension-6 electroweak gauge boson operators*, Phys. Rev. D 89, 076004 (2014) (2013) [`arXiv:1309.7822`].

[210] P. Baratella, C. Fernandez and A. Pomarol, *Renormalization of higher-dimensional operators from on-shell amplitudes*, `arXiv:2005.07129`.

[211] M. Jiang, J. Shu, M.-L. Xiao and Y.-H. Zheng, *New selection rules from angular momentum conservation*, Phys. Rev. Lett. 126, 011601 (2021) (2020) [`arXiv:2001.04481`].

[212] H.H. Patel, *Package-x: A mathematica package for the analytic calculation of one-loop integrals*, `arXiv:http://arxiv.org/abs/1503.01469v2`.

[213] A. Alloul, N.D. Christensen, C. Degrande, C. Duhr and B. Fuks, *Feynrules 2.0 - a complete toolbox for tree-level phenomenology*, Comput.Phys.Commun. 185 (2014) 2250-2300 (2013) [`arXiv:1310.1921`].

[214] T. Hahn, *Generating feynman diagrams and amplitudes with feynarts 3*, Comput.Phys.Commun. 140 (2001) 418-431 (2000) [`arXiv:hep-ph/0012260`].

[215] T. Hahn and M. Perez-Victoria, *Automatized one-loop calculations in 4 and d dimensions*, `arXiv:http://arxiv.org/abs/hep-ph/9807565v1`.

[216] C. Hartmann and M. Trott, *On one-loop corrections in the standard model effective field theory; the $\Gamma(h \to \gamma\,\gamma)$ case*, JHEP **07** (2015) 151 [`arXiv:1505.02646`].

[217] F. Jegerlehner, *Facts of life with gamma(5)*, Eur.Phys.J.C18:673-679,2001 (2000) [`arXiv:hep-th/0005255`].

[218] G. t Hooft and M. Veltman, *Regularization and renormalization of gauge fields, Nuclear Physics B* **44** (1972) 189.

[219] P. Breitenlohner and D. Maison, *Dimensional renormalization and the action principle, Communications in Mathematical Physics* **52** (1977) 11.

[220] G. Bonneau, *Trace and axial anomalies in dimensional renormalization through zimmermann-like identities, Nuclear Physics B* **171** (1980) 477.

[221] C. Becchi, A. Rouet and R. Stora, *The abelian higgs kibble model, unitarity of the s-operator, Physics Letters B* **52** (1974) 344.

[222] C. Becchi, A. Rouet and R. Stora, *Renormalization of the abelian higgs-kibble model, Communications in Mathematical Physics* **42** (1975) 127.

[223] C. Becchi, A. Rouet and R. Stora, *Renormalization of gauge theories, Annals of Physics* **98** (1976) 287.

[224] T. Bhattacharya, V. Cirigliano, R. Gupta, E. Mereghetti and B. Yoon, *Dimension-5 cp-odd operators: Qcd mixing and renormalization*, `arXiv:1502.07325`.

[225] L. Abbott, *The background field method beyond one loop, Nuclear Physics B* **185** (1981) 189.

[226] L. Abbott, M. Grisaru and R. Schaefer, *The background field method and the s-matrix, Nuclear Physics B* **229** (1983) 372.

[227] A. Denner, S. Dittmaier and G. Weiglein, *Application of the background-field method to the electroweak standard model, Nucl.Phys. B440 (1995) 95-128* (1994) [`arXiv:hep-ph/9410338`].

[228] A. Denner, S. Dittmaier and G. Weiglein, *The background-field formulation of the electroweak standard model, Acta Phys.Polon.B27:3645-3660,1996* (1996) [`arXiv:hep-ph/9609422`].

[229] A. Helset, M. Paraskevas and M. Trott, *Gauge fixing the standard model effective field theory, Phys. Rev. Lett. 120, 251801 (2018)* (2018) [`arXiv:1803.08001`].

[230] T. Corbett, *The feynman rules for the smeft in the background field gauge*, `arXiv:2010.15852`.

[231] T. Corbett and M. Trott, *One loop verification of smeft ward identities*, `arXiv:2010.08451`.

[232] M. Jiang, N. Craig, Y.-Y. Li and D. Sutherland, *Complete one-loop matching for a singlet scalar in the Standard Model EFT, JHEP* **02** (2019) 031 [`arXiv:1811.08878`].

[233] V. Gherardi, D. Marzocca and E. Venturini, *Matching scalar leptoquarks to the SMEFT at one loop, JHEP* **07** (2020) 225 [`arXiv:2003.12525`].

[234] S. Weinberg, *Photons and Gravitons in S-Matrix Theory: Derivation of Charge Conservation and Equality of Gravitational and Inertial Mass, Phys. Rev.* **135** (1964) B1049.

[235] M.T. Grisaru, H.N. Pendleton and P. van Nieuwenhuizen, *Supergravity and the S Matrix*, *Phys. Rev. D* **15** (1977) 996.

[236] M.T. Grisaru and H.N. Pendleton, *Soft Spin 3/2 Fermions Require Gravity and Supersymmetry*, *Phys. Lett. B* **67** (1977) 323.

[237] S. Weinberg and E. Witten, *Limits on Massless Particles*, *Phys. Lett. B* **96** (1980) 59.

[238] M. Porrati, *Universal Limits on Massless High-Spin Particles*, *Phys. Rev. D* **78** (2008) 065016 [`arXiv:0804.4672`].

[239] D. Sorokin, *Introduction to the classical theory of higher spins*, *AIP Conf. Proc.* **767** (2005) 172 [`arXiv:hep-th/0405069`].

[240] X. Bekaert, N. Boulanger and P. Sundell, *How higher-spin gravity surpasses the spin two barrier: no-go theorems versus yes-go examples*, *Rev. Mod. Phys.* **84** (2012) 987 [`arXiv:1007.0435`].

[241] M. Porrati, *Old and New No Go Theorems on Interacting Massless Particles in Flat Space*, in *17th International Seminar on High Energy Physics*, 9, 2012 [`arXiv:1209.4876`].

[242] R. Rahman and M. Taronna, *From Higher Spins to Strings: A Primer*, `arXiv:1512.07932`.

[243] J. Bonifacio and K. Hinterbichler, *Universal bound on the strong coupling scale of a gravitationally coupled massive spin-2 particle*, *Phys. Rev. D* **98** (2018) 085006 [`arXiv:1806.10607`].

[244] X.O. Camanho, J.D. Edelstein, J. Maldacena and A. Zhiboedov, *Causality Constraints on Corrections to the Graviton Three-Point Coupling*, *JHEP* **02** (2016) 020 [`arXiv:1407.5597`].

[245] H. Elvang and Y.-t. Huang, *Scattering Amplitudes*, `arXiv:1308.1697`.

[246] C. Cheung, *TASI Lectures on Scattering Amplitudes*, in *Proceedings, Theoretical Advanced Study Institute in Elementary Particle Physics : Anticipating the Next Discoveries in Particle Physics (TASI 2016): Boulder, CO, USA, June 6-July 1, 2016*, R. Essig and I. Low, eds., pp. 571–623 (2018), DOI [`arXiv:1708.03872`].

[247] L.J. Dixon, *Calculating scattering amplitudes efficiently*, in *Theoretical Advanced Study Institute in Elementary Particle Physics (TASI 95): QCD and Beyond*, pp. 539–584, 1, 1996 [`arXiv:hep-ph/9601359`].

[248] L.J. Dixon, *A brief introduction to modern amplitude methods*, in *Theoretical Advanced Study Institute in Elementary Particle Physics: Particle Physics: The Higgs Boson and Beyond*, pp. 31–67, 2014, DOI [`arXiv:1310.5353`].

[249] H.K. Dreiner, H.E. Haber and S.P. Martin, *Two-component spinor techniques and Feynman rules for quantum field theory and supersymmetry*, *Phys. Rept.* **494** (2010) 1 [`arXiv:0812.1594`].

[250] G. Durieux, T. Kitahara, Y. Shadmi and Y. Weiss, *The electroweak effective field theory from on-shell amplitudes*, *JHEP* **01** (2020) 119 [`arXiv:1909.10551`].

[251] G. 't Hooft, *An algorithm for the poles at dimension four in the dimensional regularization procedure*, *Nucl. Phys. B* **62** (1973) 444.

[252] G. 't Hooft and M.J.G. Veltman, *One loop divergencies in the theory of gravitation*, *Ann. Inst. H. Poincare Phys. Theor. A* **20** (1974) 69.

[253] M.H. Goroff and A. Sagnotti, *The Ultraviolet Behavior of Einstein Gravity*, *Nucl. Phys. B* **266** (1986) 709.

[254] S. Deser and P. van Nieuwenhuizen, *Nonrenormalizability of the Quantized Dirac-Einstein System*, *Phys. Rev. D* **10** (1974) 411.

[255] S. Deser and P. van Nieuwenhuizen, *One Loop Divergences of Quantized Einstein-Maxwell Fields*, *Phys. Rev. D* **10** (1974) 401.

[256] S. Deser, H.-S. Tsao and P. van Nieuwenhuizen, *One Loop Divergences of the Einstein Yang-Mills System*, *Phys. Rev. D* **10** (1974) 3337.

[257] P. Bueno, P.A. Cano, J. Moreno and A. Murcia, *All higher-curvature gravities as Generalized quasi-topological gravities*, *JHEP* **11** (2019) 062 [arXiv:1906.00987].

[258] S. Caron-Huot, Y.-Z. Li, J. Parra-Martinez and D. Simmons-Duffin, *Causality constraints on corrections to Einstein gravity*, arXiv:2201.06602.

[259] K.S. Stelle, *Classical Gravity with Higher Derivatives*, *Gen. Rel. Grav.* **9** (1978) 353.

[260] J.F. Donoghue, *Leading quantum correction to the Newtonian potential*, *Phys. Rev. Lett.* **72** (1994) 2996 [arXiv:gr-qc/9310024].

[261] J.F. Donoghue, *Introduction to the effective field theory description of gravity*, in *Advanced School on Effective Theories*, 6, 1995 [arXiv:gr-qc/9512024].

[262] J.G. Lee, E.G. Adelberger, T.S. Cook, S.M. Fleischer and B.R. Heckel, *New Test of the Gravitational $1/r^2$ Law at Separations down to 52 μm*, *Phys. Rev. Lett.* **124** (2020) 101101 [arXiv:2002.11761].

[263] M. Accettulli Huber, A. Brandhuber, S. De Angelis and G. Travaglini, *Note on the absence of R^2 corrections to Newton's potential*, *Phys. Rev. D* **101** (2020) 046011 [arXiv:1911.10108].

[264] A. Falkowski and G. Isabella, *Matter coupling in massive gravity*, *JHEP* **04** (2020) 014 [arXiv:2001.06800].

[265] A. Addazi, Z. Berezhiani and Y. Kamyshkov, *Gauged $B − L$ number and neutron–antineutron oscillation: long-range forces mediated by baryophotons*, *Eur. Phys. J. C* **77** (2017) 301 [arXiv:1607.00348].

[266] J.A.R. Cembranos, A.L. Maroto and H. Villarrubia-Rojo, *Constraints on hidden gravitons from fifth-force experiments and stellar energy loss*, *JHEP* **09** (2017) 104 [arXiv:1706.07818].

[267] J.G. Lee, *A Fourier-Bessel Test of the Gravitational Inverse-Square Law*, Ph.D. thesis, U. Washington, Seattle (main), 2020.

[268] T. Cook, *A test of the gravitational inverse-square law at short distance*, Ph.D. thesis, U. Washington, Seattle (main), 2013.

[269] J.G. Lee, E.G. Adelberger, F.V. Marcoline, W.A. Terrano and B.R. Heckel, *The fourier–bessel expansion: application to experimental probes of gravity and feeble short-range interactions*, *Classical and Quantum Gravity* **38** (2021) 085020.

[270] P. Baratella, D. Haslehner, M. Ruhdorfer, J. Serra and A. Weiler, *RG of GR from on-shell amplitudes*, *JHEP* **03** (2022) 156 [`arXiv:2109.06191`].

[271] R.E. Cutkosky, *Singularities and discontinuities of Feynman amplitudes*, *J. Math. Phys.* **1** (1960) 429.

[272] G.F. Sterman and M.E. Tejeda-Yeomans, *Multiloop amplitudes and resummation*, *Phys. Lett. B* **552** (2003) 48 [`arXiv:hep-ph/0210130`].

[273] T. Becher and M. Neubert, *Infrared singularities of scattering amplitudes in perturbative QCD*, *Phys. Rev. Lett.* **102** (2009) 162001 [`arXiv:0901.0722`].

[274] T. Becher and M. Neubert, *On the Structure of Infrared Singularities of Gauge-Theory Amplitudes*, *JHEP* **06** (2009) 081 [`arXiv:0903.1126`].

[275] S. Caron-Huot and M. Wilhelm, *Renormalization group coefficients and the S-matrix*, *JHEP* **12** (2016) 010 [`arXiv:1607.06448`].

[276] B.I. Zwiebel, *From Scattering Amplitudes to the Dilatation Generator in N=4 SYM*, *J. Phys. A* **45** (2012) 115401 [`arXiv:1111.0083`].

[277] J. Elias Miró, J. Ingoldby and M. Riembau, *EFT anomalous dimensions from the S-matrix*, *JHEP* **09** (2020) 163 [`arXiv:2005.06983`].

[278] P. Baratella. Personal Communication.

[279] P. Baratella, C. Fernandez, B. von Harling and A. Pomarol, *Anomalous Dimensions of Effective Theories from Partial Waves*, *JHEP* **03** (2021) 287 [`arXiv:2010.13809`].

[280] P. Baratella, C. Fernandez and A. Pomarol, *Renormalization of Higher-Dimensional Operators from On-shell Amplitudes*, *Nucl. Phys. B* **959** (2020) 115155 [`arXiv:2005.07129`].

[281] T. Becher, A. Broggio and A. Ferroglia, *Introduction to Soft-Collinear Effective Theory*, vol. 896, Springer (2015), 10.1007/978-3-319-14848-9, [`arXiv:1410.1892`].

[282] F. Bloch and A. Nordsieck, *Note on the Radiation Field of the electron*, *Phys. Rev.* **52** (1937) 54.

[283] T. Kinoshita, *Mass singularities of Feynman amplitudes*, *J. Math. Phys.* **3** (1962) 650.

[284] T.D. Lee and M. Nauenberg, *Degenerate Systems and Mass Singularities*, *Phys. Rev.* **133** (1964) B1549.

[285] A. Gehrmann-De Ridder, T. Gehrmann and G. Heinrich, *Four particle phase space integrals in massless QCD*, *Nucl. Phys. B* **682** (2004) 265 [`arXiv:hep-ph/0311276`].

[286] C. Anastasiou and K. Melnikov, *Higgs boson production at hadron colliders in NNLO QCD*, *Nucl. Phys. B* **646** (2002) 220 [`arXiv:hep-ph/0207004`].

[287] M. Srednicki, *Quantum field theory*, Cambridge University Press (1, 2007).

[288] M.E. Peskin and D.V. Schroeder, *An Introduction to quantum field theory*, Addison-Wesley, Reading, USA (1995).

[289] G. Sterman, *An Introduction to Quantum Field Theory*, Cambridge University Press (1993), 10.1017/CBO9780511622618.

[290] S. Pokorski, *GAUGE FIELD THEORIES*, Cambridge University Press (1, 2005).

[291] J.C. Collins, *Renormalization: An Introduction to Renormalization, The Renormalization Group, and the Operator Product Expansion*, vol. 26 of *Cambridge Monographs on Mathematical Physics*, Cambridge University Press, Cambridge (1986), 10.1017/CBO9780511622656.

[292] C.G. Callan, Jr., S.R. Coleman and R. Jackiw, *A New improved energy - momentum tensor*, *Annals Phys.* **59** (1970) 42.

[293] J.C. Collins, A.V. Manohar and M.B. Wise, *Renormalization of the vector current in QED*, *Phys. Rev. D* **73** (2006) 105019 [`arXiv:hep-th/0512187`].

[294] J. Erdmenger and H. Osborn, *Conserved currents and the energy momentum tensor in conformally invariant theories for general dimensions*, *Nucl. Phys. B* **483** (1997) 431 [`arXiv:hep-th/9605009`].

[295] M.E. Machacek and M.T. Vaughn, *Two Loop Renormalization Group Equations in a General Quantum Field Theory. 1. Wave Function Renormalization*, *Nucl. Phys. B* **222** (1983) 83.

[296] P. Maierhöfer, J. Usovitsch and P. Uwer, *Kira—A Feynman integral reduction program*, *Comput. Phys. Commun.* **230** (2018) 99 [`arXiv:1705.05610`].

[297] T. Gehrmann, T. Huber and D. Maitre, *Two-loop quark and gluon form-factors in dimensional regularisation*, *Phys. Lett. B* **622** (2005) 295 [`arXiv:hep-ph/0507061`].

[298] T. Gehrmann and E. Remiddi, *Differential equations for two loop four point functions*, *Nucl. Phys. B* **580** (2000) 485 [`arXiv:hep-ph/9912329`].

[299] K.G. Chetyrkin and F.V. Tkachov, *Integration by Parts: The Algorithm to Calculate beta Functions in 4 Loops*, *Nucl. Phys. B* **192** (1981) 159.

[300] P.A. Baikov and K.G. Chetyrkin, *Four Loop Massless Propagators: An Algebraic Evaluation of All Master Integrals*, *Nucl. Phys. B* **837** (2010) 186 [`arXiv:1004.1153`].

[301] T. Gehrmann, E.W.N. Glover, T. Huber, N. Ikizlerli and C. Studerus, *Calculation of the quark and gluon form factors to three loops in QCD*, *JHEP* **06** (2010) 094 [`arXiv:1004.3653`].

[302] C. Gnendiger, A. Signer and D. Stöckinger, *The infrared structure of QCD amplitudes and $H \to gg$ in FDH and DRED*, *Phys. Lett. B* **733** (2014) 296 [`arXiv:1404.2171`].

[303] S. Catani, *The Singular behavior of QCD amplitudes at two loop order*, *Phys. Lett. B* **427** (1998) 161 [`arXiv:hep-ph/9802439`].